UNIVERSIDAD COMPLUTENSE DE MADRID

FACULTAD DE CIENCIAS FÍSICAS
DEPARTAMENTO DE FÍSICA TEÓRICA

TESIS DOCTORAL

Study of the electroweak symmetry breaking sector for the LHC
Estudio del sector de ruptura de simetría electrodébil para el LHC

MEMORIA PARA OPTAR AL GRADO DE DOCTOR

PRESENTADA POR

Rafael Delgado López

DIRECTORES

Antonio Dobado González
Felipe José Llanes Estrada

Madrid, 2017

Study of the Electroweak Symmetry Breaking Sector for the LHC

Estudio del Sector de Ruptura de Simetría Electrodébil para el LHC

Presented by

Rafael Delgado López

Directed by

Antonio Dobado González

Felipe J. Llanes Estrada

Dissertation submitted for the Degree of Doctor in Physics to the

Universidad Complutense de Madrid

Dep. Theoretical Physics I

MMXVI

Acknowledgements

First of all, I would like to acknowledge the contributions of my PhD supervisors, Profs. Antonio Dobado and Felipe J. Llanes-Estrada, to this work. I also acknowledge my coauthors Juan José Sanz Cillero and Maria José Herrero Solans, with whom I published the $\gamma\gamma$ computation, and who gave me very useful comments and advice while I was writing this thesis. And our collaborator Andrés Fernando Castillo, a PhD student from Bogotá who visited us to collaborate on the $\omega\omega$, $hh \to t\bar{t}$ scattering.

I am also indebt to Profs. Stefania de Curtis and Christophe Grojean, members of my thesis committee, and to Oscar Catà and Verónica Sanz, for their valuable comments and corrections.

I have also worked with Prof. Domènec Espriu, with whom I published a congress contribution. Moreover, his group at Barcelona made an independent study of the a_4-a_5 parameter space of the $\omega\omega \to \omega\omega$ computation, which is an interesting check of part of this work, and they provided me in full detail.

I also would like to thank Prof. Thomas Hahn and the Theoretical Physics Division group at the Max-Planck-Institute for Physics (Werner-Heisenberg-Institute, Germany), who kindly welcomed me during a stay there. Prof. Thomas Hahn taught me the deep details of the programs FeynArts and FormCalc, which he develops actively and that I use for this thesis, and gave me good advice.

I also remember Prof. Stefano Moretti, who supervised me during my earlier stay at the SHEP group in the University of Southampton (UK). He introduced me to the usage of the Monte Carlo tool MadGraph. The graphs where I compare, for the Standard Model and at leading order, the Equivalence Theorem computations versus the exact ones has been obtained in collaboration with Prof. Stefano Moretti. As a host PhD student in the SHEP group, I was allowed to use the facilities of both the NExT Institute and the South East Physics Network (SEPnet). As a result of this, I followed some PhD lectures from the institutions which participate on the NExT PhD School. Furthermore, I was allowed to contribute to both the NExT Meeting at Sussex and the UK HEP Forum 2014 "Future Collider" (STFC, Abingdon, Oxford).

As part of my Master and PhD program, I collaborated with Profs. Fernando Sols Lucia, Pedro Bargueño de Retes and José Alberto Ruiz Cembranos. These collaborations are not directly related to the EWSBS. However, the collaboration with José Alberto Ruiz Cembranos is centered on the phenomenological study of BSM models at the LHC, and it helped me gain many computational skills.

This thesis has been funded by the MINECO (Spain) predoctoral grant BES-2012-056054, and by MINECO projects Nos. FPA2011-27853-C02-01, FPA2014-53375-C2-1-P, FPA2016-75654-C2-1-P and FIS2013-41716-P. I would like to acknowledge the staff of the Theoretical Physics I department (UCM), where I concluded this work, as well as the staff of the University of Southampton (UK) and the Max-Planck-Institute for Physics, where I was kindly received during my short stays.

Some parts of this thesis required the computer resources, technical expertise, and assistance provided by the Barcelona Supercomputing Centre —Centro Nacional de Supercomputación— and the Tirant supercomputer support staff at Valencia.

I also acknowledge useful discussions with Profs. José Ramón Peláez and Ignazio Scimemi, as well as the help from Torbjörn Sjöstrand with the use of his program Pythia 8; from the developers of FORM at the Nikhef institute; from Olivier Mattelaer with the use of MadGraph 5; and very constructive and useful comments of an anonymous referee of the European Physical Journal C.

Finally, I would like to acknowledge all the people who helped me with this work but, unfortunatelly, I cannot remember at this time. And, of course, to all my friends, who have encouraged me during these years which I have dedicated to this PhD thesis. And to my parents, who gave me their support during these years as a PhD student.

Abstract

English version In this dissertation, a strongly interacting Electroweak Symmetry Breaking Sector is considered. We use the framework of Effective Field Theories (EFT) and unitarization procedures, successfully deployed to study resonances in low energy QCD in the last decades. The EFT amplitudes are computed at the Next to Leading order (NLO).

If new resonances were discovered at the LHC run-II, different theoretical approaches could be used to study them. However, the framework that we follow here has several advantages. For instance, it only contains a few parameters. Seven in the case of scattering within the Electroweak Symmetry Breaking Sector ($W_L^{\pm}$, Z_L and h); a few more if the $\gamma\gamma$ and $t\bar{t}$ states are included. And, even more important, the masses and widths of the resonances emerge as a consequence of the low-energy behaviour of the theory. They are not free parameters of the model, we will derive them from the Lagrangian.

The EFTs for longitudinal gauge bosons plus Higgs are being actively investigated, because of their direct application to the experimental program of the LHC run-II. However, they are frequently considered only as a useful parameterization of slight deviations from the Standard Model behaviour. In other cases, they are extended to implement new resonances in an explicit way. Our approach shares with these models the use of an EFT in the very first steps, as well as the experimental bounds over the parameters of the Effective Lagrangian.

If we used only the EFT, the perturbative expansion would break down because it is derivative. But in our work below, the EFT is efficiently extended to cover the regime of saturation of unitarity. This is achieved by dispersion relations, whose subtraction constants and left cut contribution can be approximately obtained in different ways giving rise to different unitarization procedures.

Several unitarization procedures have been considered. We have studied three of them in finer detail, since they have the best properties. These chosen methods are the Inverse Amplitude Method, one version of the N/D method and another improved version of the K-matrix. An extended version of the first two is used for the coupling with $\gamma\gamma$ and $t\bar{t}$. In all the cases we get partial waves which are unitary, analytical with the proper left and right cuts and in some cases poles in the second Riemann sheet that can be understood as dynamically generated resonances. A new numerical method has been developed in order to look for such poles.

We also point out that the unitarization formalisms are also extendable to coupled channels. This is a novelty, and implies the possibility that an hypothetical resonance comes from a strongly process like $VV \to hh \to VV$ (V stands for a longitudinal gauge boson). Such a resonance would be triggered by the coupling $VVhh$ (parameter b of the EFT), which is less constrained that the coupling VVh (parameter a).

Finally, all this work is given in a form that it could be implemented in a Monte Carlo (MC) simulation program, in order to generate MC events for the LHC Run-II or future

collider experiments.

Spanish vesion En esta disertación, consideramos un Sector de Ruptura de Simetría Electrodébil con interacciones fuertes, y utilizamos el marco teórico de las Teorías Efectivas (calculadas a primer orden en teoría de perturbaciones, NLO) y los métodos de unitarizaicón. Algunas décadas atrás, este marco explicó satisfactoriamente la aparición de resonancias a baja energía en QCD.

Si apareciesen nuevas resonancias en el run-II del LHC, habría varios modelos teóricos en el mercado para estudiarlas. Sin embargo, el nuestro tiene varias ventajas. Por ejemplo, sólo contiene unos pocos parámetros libres. Siete en el caso de procesos de dispersión en el Sector de Ruptura de Simetría Electrodébil ($W_L^{\pm}$, Z_L, y h). Unos pocos más si se incluye el acoplamiento con los estados $\gamma\gamma$ y $t\bar{t}$. E, incluso más importante, las masas y anchuras de las resonancias aparecen como consecuencia del comportamiento a baja energía de la teoría. No son parámetros libres del modelo, se derivan del Lagrangiano.

Las teorías efectivas para bosones gauge longitudinales y Higgs son objeto de investigación activa, debido a su aplicación directa al programa experimental del run-II de LHC. Pero suelen considerarse únicamente como una parametrización útil de pequeñas desviaciones del comportamiento del Modelo Estándar. En otros casos, son extendidas para incluir explícitamente nuevas resonancias. El vínculo entre todos estos modelos y el nuestro es la utilización de una teoría efectiva, así como las cotas experimentales sobre los parámetros de dicha teoría.

Si sólo utilizamos las teorías efectivas, la expansión perturbativa se rompe. En este trabajo, mostraremos que estas teorías efectivas pueden extenderse para cubrir el régimen de saturación de unitariedad. Esto se consigue mediante las relaciones de dispersión, cuyas constantes de substracción y contribuciones al corte izquierdo pueden obtenerse de forma aproximada de diferentes formas, dando lugar así a los diversos métodos de unitarización.

Se han considerado varios métodos de unitarización, y estudiado en detalle tres de ellos. Estos últimos son el método de la matriz inversa (IAM), una versión del N/D y una variación mejorada de la matriz-K (I-K). Para el estudio del acoplamiento a los canales $\gamma\gamma$ y $t\bar{t}$ se ha utilizado una modificación de los dos primeros métodos (IAM y N/D). En todos los casos obtenemos ondas parciales que son unitarias, analíticas, presentan los cortes izquierdo y derecho requeridos por la teoría relativista de procesos de dispersión, y en algunos casos muestran polos en la segunda hoja de Reimann que pueden interpretarse como resonancias generadas dinámicamente. Se ha desarrollado un nuevo método numérico para buscar la posición de tales polos.

También hemos extendido los procedimientos de unitarizaicón al caso de canales acoplados. Esto es una novedad, e implica la posibilidad de que una resonancia hipotética proceda de un proceso de dispersión fuerte como $VV \to hh \to hh$ (V denota un bosón gauge longitudinal). Tal resonancia estaría regulada por el acoplamiento $VVhh$ (parámetro b de la teoría efectiva), que está menos acotado experimentalmente que el acoplamiento VVh (parámetro a).

Por último, este trabajo está estructurado de una forma tal que podría ser implementado en un programa de simulación Monte Carlo (MC), para generar eventos MC para el run-II de LHC o futuros experimentos de colisionadores.

CV and Publication List

Dr. Rafael L. Delgado (born in 1989) received his PhD degree on June 2016, with his doctoral dissertation at the Complutense University of Madrid (UCM, Spain). A few months after that, he obtained his habilitation as Assistant Professor from the ANECA (National Agency for Quality Assessment and Accreditation of Spain). He completed his doctoral training with short research stays at the University of Southampton (UK), Max Planck Institut für Physik (Munich, Germany) and the Stanford Linear Acceleration Center (SLAC, Menlo Park, USA).

During his PhD work, he has collaborated with Profs. Maria José Herrero Solans and Juan José Sanz-Cillero from the IFT-UAM[1], and with Prof. Domènec Espriu from the Universitat de Barcelona. During his short stays, he collaborated with Prof. Stefano Moretti (Univ. Southampton), Thomas Hahn (MPI in Munich) and Stanley Brodsky (SLAC). Among his peers, he has worked with Dr. Andrés Fernando Castillo (from the UNAL, Colombia) while his short doctoral stays at the UCM.

The research activity performed in this thesis has lead to a contribution to the CERN's Yellow Report 4 of the LHCHXSWG[2], and to the peer-reviewed articles listed below:

[1] Andrés Castillo, Rafael L. Delgado, Antonio Dobado, Felipe J. Llanes-Estrada, *Top-antitop production from $W_L^+W_L^-$ and Z_LZ_L scattering under a strongly-interacting symmetry-breaking sector*,
e-Print: arXiv:1607.01158 [hep-ph], accepted for publication in Eur. Phys. J. C.

[2] Rafael L. Delgado, Antonio Dobado, and Felipe J. Llanes-Estrada, *Coupling WW, ZZ unitarized amplitudes to $\gamma\gamma$ in the TeV region*,
Eur. Phys. J. C 77, no.4, 205 (2017).

[3] Rafael L. Delgado, Antonio Dobado, and Felipe J. Llanes-Estrada, *Possible New Resonance from $W_LW_L - hh$ Interchannel Coupling*,
Phys. Rev. Lett. 114, 221803 (2015).

[4] Rafael L. Delgado, Antonio Dobado and Felipe J. Llanes-Estrada, *Strongly Interacting Electroweak Symmetry Breaking Sector with a Higgs-like light scalar*,
Phys. Rev. D 91, 075017 (2015).

[5] R.L. Delgado, A. Dobado, M.J. Herrero and J.J. Sanz-Cillero, *One-loop $\gamma\gamma \to W_L^+W_L^-$ and $\gamma\gamma \to Z_LZ_L$ from the Electroweak Chiral Lagrangian with a light Higgs-like scalar*,
JHEP 1407, 149 (2014).

[1] Prof. J.J. Sanz-Cillero has recently joined the UCM faculty.
[2] The Yellow Report 4 can be found in `https://inspirehep.net/record/1494411`.

[6] Rafael L. Delgado, Antonio Dobado and Felipe J. Llanes-Estrada,
One-loop W_LW_L and Z_LZ_L scattering from the electroweak Chiral Lagrangian with a light Higgs-like scalar,
JHEP 1402, 121 (2014).

[7] Rafael L. Delgado, Antonio Dobado and Felipe J. Llanes-Estrada,
Light 'Higgs', yet strong interactions,
J. Phys. G 41, 025002 (2014), chosen as one of the Journal's highlights of 2014.

[8] Jose A. R. Cembranos, Rafael L. Delgado and Antonio Dobado,
Brane-Worlds at the LHC: Branons and KK-gravitons,
Phys. Rev. D 88, 075021 (2013).

[9] Rafael L. Delgado, Carlos Hidalgo-Duque and Felipe J. Llanes-Estrada,
To What Extent is Gluon Confinement an Empirical Fact?,
Few Body Syst. 54, 1705-1717 (2013).

Additionally, the following contributions to conference proceedings have been prepared:

[10] Rafael L. Delgado,
Coupling of $t\bar{t}$ and $\gamma\gamma$ with a strongly interacting Electroweak Symmetry Breaking Sector,
Proceedings of the 12th Conference on Quark Confinement and the Hadron Spectrum, (Thessaloniki, Greece, 28/08 - 04/09, 2016),
EPJ Web Conf. 137 (2017) 10001.

[11] Antonio Dobado, Rafael L. Delgado, Felipe J. Llanes-Estrada, Domenec Espriu,
Comparing mesons and W_L W_L TeV-resonances,
Proceedings of the Bled miniworkshop *Exploring hadron resonances*, (Bled, Slovenia, July 5-11, 2015),
Bled Workshops Phys. 16 (2015), nº 1, 20-26.

[12] Antonio Dobado, Rafael L. Delgado, Felipe J. Llanes-Estrada,
Resonances in W_LW_L, Z_LZ_L and hh scattering from dispersive analysis of the non-linear Electroweak+Higgs Effective Theory,
Proceedings of The European Physical Society Conference on High Energy Physics, (Vienna, Austria, July 22-29, 2015),
PoS EPS-HEP2015 (2015) 173.

[13] Felipe J. Llanes-Estrada, Antonio Dobado, Rafael L. Delgado,
Describing 2-TeV scale W_LW_L resonances with Unitarized Effective Theory,
Proceedings of the XVIIIth workshop *What comes Beyond the Standard Model?*, (Bled, Slovenia, July 11-19, 2015),
Bled Workshops Phys. 16 (2015), nº 2, 78-86.

[14] Rafael L. Delgado, Antonio Dobado and Felipe J. Llanes-Estrada,
A Strongly Interacting Electroweak Symmetry Breaking Sector with a Higgs-like light scalar,
Proceedings of the XIth Quark Confinement and the Hadron Spectrum, (Saint-Petersburg, Russia, September 8-12, 2014),
AIP Conf.Proc. 1701 (2016) 090003.

[15] R.L. Delgado, A. Dobado, M.J. Herrero and J.J. Sanz-Cillero,
Electroweak chiral Lagrangian with a light Higgs and $\gamma\gamma \to Z_L Z_L$, $W_L^+ W_L^-$ scattering at one loop,
Proceedings of the 37th International Conference on High Energy Physics (ICHEP 2014), (Valencia, Spain, July 2-9, 2014),
Nucl.Part.Phys.Proc. 273-275 (2016) 703-709.

[16] Rafael L. Delgado, Antonio Dobado and Felipe J. Llanes-Estrada,
Strongly interacting $W_L W_L$, $Z_L Z_L$ and hh from unitarized one-loop computations,
Proceedings of the 37th International Conference on High Energy Physics (ICHEP 2014) (Valencia, Spain, July 2-9, 2014),
Nucl.Part.Phys.Proc. 273-275 (2016) 2436-2438.

[17] R.L. Delgado, A. Dobado, M.J. Herrero and J.J. Sanz-Cillero,
Electroweak Chiral Lagrangians and $\gamma\gamma \to Z_L Z_L$, $W_L^+ W_L^-$ at One Loop,
proceedings of the Second Annual Conference on Large Hadron Collider Physics - LCHP 2014, Columbia University (New York, U.S.A, June 2-7, 2014),
arXiv:1409.3983 [hep-ph],
`http://www.slac.stanford.edu/econf/C140602.2/` .

[18] Antonio Dobado, Rafael L. Delgado and Felipe J. Llanes-Estrada,
Strongly Interacting Electroweak Symmetry Breaking Sector with a Higgs-like light scalar,
delivered at the II Russian-Spanish Congress *Particle and Nuclear Physics at all Scales and Cosmology*, Institute of Cosmos Sciences (Saint-Petersburg, Russia, October 1-4, 2013),
AIP Conf. Proc. 1606, 151-158 (2014).

Finally, there is one article nrelated with the topic of this PhD thesis:

[19] R.L. Delgado, P. Bargueño, F. Sols,
Two-step condensation of the charged Bose gas,
Phys. Rev. E 86 (2012) 031102.

Contents

Chapter 1

Introduction

In this dissertation, we revisit the prospects of a strongly interacting theory for the Electroweak Symmetry Breaking Sector (EWSBS) of the Standard Model, after the discovery at the LHC of a Higgs-like boson at $\sim 125\,\mathrm{GeV}$ (refs. [1–3]). The tools of Effective Chiral Lagrangians and unitarization procedures will be used, and the old Higgsless Electroweak Chiral Lagrangian [4–21](EChL) will be extended to accommodate a Higgs-like boson at $\sim 125\,\mathrm{GeV}$. Since the discovery of the Higgs-like boson at the LHC, this field has received increasing attention [22–33]. I hope that this dissertation, besides our original results [34–39][1] that will be described, can be a useful introduction to the field of a strongly interacting EWSBS with a light Higgs but below the possible new-physics scale. To this end, several appendices with detailed computations have been included. And some of the sections, especially those containing the physical fundamentation of the computational procedures (secs. 3.3 and 4), are very detailed.

First of all, let us introduce the theory that has worked very well until now, becoming a *standard* in particle physics: the so–called Standard Model (SM)[2]. It became widely accepted from the late 60's on, and it describes all the known interactions but gravity, under a *Quantum Field Theory* (QFT) formalism. This is achieved in a way that it is compatible with all the experimental data until now. The SM describes three fundamental interactions, which are *gauge* interactions[3], mediated by spin–1 bosons[4]. The matter particles are spin–1/2 fermions, to which Pauli's exclusion principle applies, but for our purposes let us concentrate on the gauge sector.

The relativistic electromagnetic interaction is mediated by one massless photon (γ), and the corresponding gauge symmetry group is $U(1)_{\mathrm{em}}$. Indeed, the idea of gauge interaction comes from the classical Maxwell equations, which are invariant under some transformations of the electromagnetic four-potential vector. Note that Quantum Electrodynamics (QED), the theory which describes electromagnetic interaction, has produced some of the most precise and successful predictions in physics. The fact that the photon is massless, does not interact strongly with itself, and we live in 3 spatial dimensions + 1 temporal dimension, entails an interaction field strength decaying like r^{-1}.

The second force, the strong one, is mediated by eight massless gluons (g), and the corresponding gauge symmetry group is $SU(3)_C$. Note that the interaction of gluons among themselves is very strong. This leads to a theory that is *strongly coupled* at

[1] And unpublished work in sections 3 and 4 that will be made available in some form.

[2] Look up, for example, ref. [40–42], and ref. [43] for an updated review of the properties of the SM particles, besides some BSM searches.

[3] The Lagrangian which describes them is invariant under a continuous group of local transformations.

[4] That is, by particles that can share a quantum state.

low energies, but is *weakly-coupled* (or *pertubative*) at high energies. What does this mean? That at high energies, the perturbative methods for working with QFTs (that is, Feynman diagrams [40]) will work. But at low energies, the contributions of higher orders (NLO, NNLO, N3LO,...) will be so high that the series expansion is meaningless, so new methods will be needed: from the brute-force computing one, lattice-QCD [44], to effective approaches like chiral perturbation theory (χPT, see refs. [45–49]). Indeed, bound states appear, but no free coloured particle has been observed in the final state (*confinement*). As an introduction to my PhD program, I have collaborated on a study about the bound that the LHC sets over the presence of *unconfined* gluons [50].

Finally, we have the weak interaction, which is mediated by three *massive* gauge bosons: the charged $W^{\pm}$ ($M_W = 80.385 \pm 0.015\,\text{GeV}$), and the neutral Z ($M_W/M_Z = 0.8819 \pm 0.0012$). At the EW scale, this interaction is unified with the electromagnetic one, giving rise to an *electroweak* interaction, whose Lagrangian is invariant under a local $SU(2) \times U(1)_Y$ gauge group. However, having a gauge interaction mediated by massive gauge bosons is problematic. Both from a fundamental point of view, because the massive terms are not gauge invariant, and from a phenomenological one, since the theory is non-renormalizable. That is, the procedure for taking into account higher order corrections fails. Furthermore, the elastic scattering of longitudinal modes[5] of gauge bosons associated with the weak interactions would break unitarity bounds: the interaction probability would be higher than unity at some energy scale[6]; *at least* at leading order (LO) in perturbation theory. That means that the theory could not be described with perturbative theory. Could it perhaps be a strongly interacting one, like QCD at low energy? In that case, some kind of new physics would be necessary here, which also solves the theoretical issue of having a gauge theory with massive gauge bosons.

Either way, the solution which was developed for the Standard Model (SM) is the application of the so–called Higgs mechanism[7] [52–56]. This mechanism keeps the required $SU(2)_L \times U(1)_Y$ symmetry on the Electroweak Lagrangian. However, the lowest energy state would be $U(1)_{\text{em}}$ symmetric only (see fig. 1.1 for an illustration of this concept). Thus, the vacuum state of the theory, from which perturbation theory is obtained, is not symmetric under a local $SU(2)_L \times U(1)_Y$ symmetry group, but only under $U(1)_{\text{em}}$. In this way it is possible to fulfill both the mathematical requirements of renormalizable QFT and the experimental masses of gauge bosons. This Higgs mechanism gives rise to a spin-0 boson (*Higgs boson*) as a byproduct of the process.

The Higgs mechanism requires the EW sector of the SM to be coupled with a Symmetry Breaking Sector (SBS). In the standard model, the SBS contains a complex $SU(2)_L$ doublet with hypercharge $Y = +1/2$. In the limit $g = g' = 0$, the doublet potential is invariant under a global $SU(2)_L \times SU(2)_R$ symmetry group. However, due to the *Mexican-hat* shape potential (see fig. 1.1), its lowest energy state is invariant only under $SU(2)_{L+R}$ (custodial symmetry). The spontaneous symmetry breaking (SSB) $SU(2)_L \times SU(2)_R \to SU(2)_{L+R}$ gives rise to 3 massless scalars (the would-be Goldstone bosons), and another massive scalar (the Higgs particle). This global SSB triggers the breaking of the $SU(2)_L \times U(1)_Y$ gauge symmetry into the $U(1)_{\text{em}}$ gauge symmetry. Three gauge bosons acquire masses by absorbing the degrees of freedom of the would-be

[5]Note that these longitudinal modes come from the fact that these gauge bosons are massive.

[6]This also happens with some beyond *Standard Models* (BSM) proposals. See ref. [51].

[7]The *Higgs* mechanism was, indeed, developed by several theoretical physicists, including P.W. Anderson (for the non-relativistic case of superconductivity), F. Englert, R. Brout, P. Higgs, G.S. Guralnik, C.R. Hagen and T.W.B. Kibble.

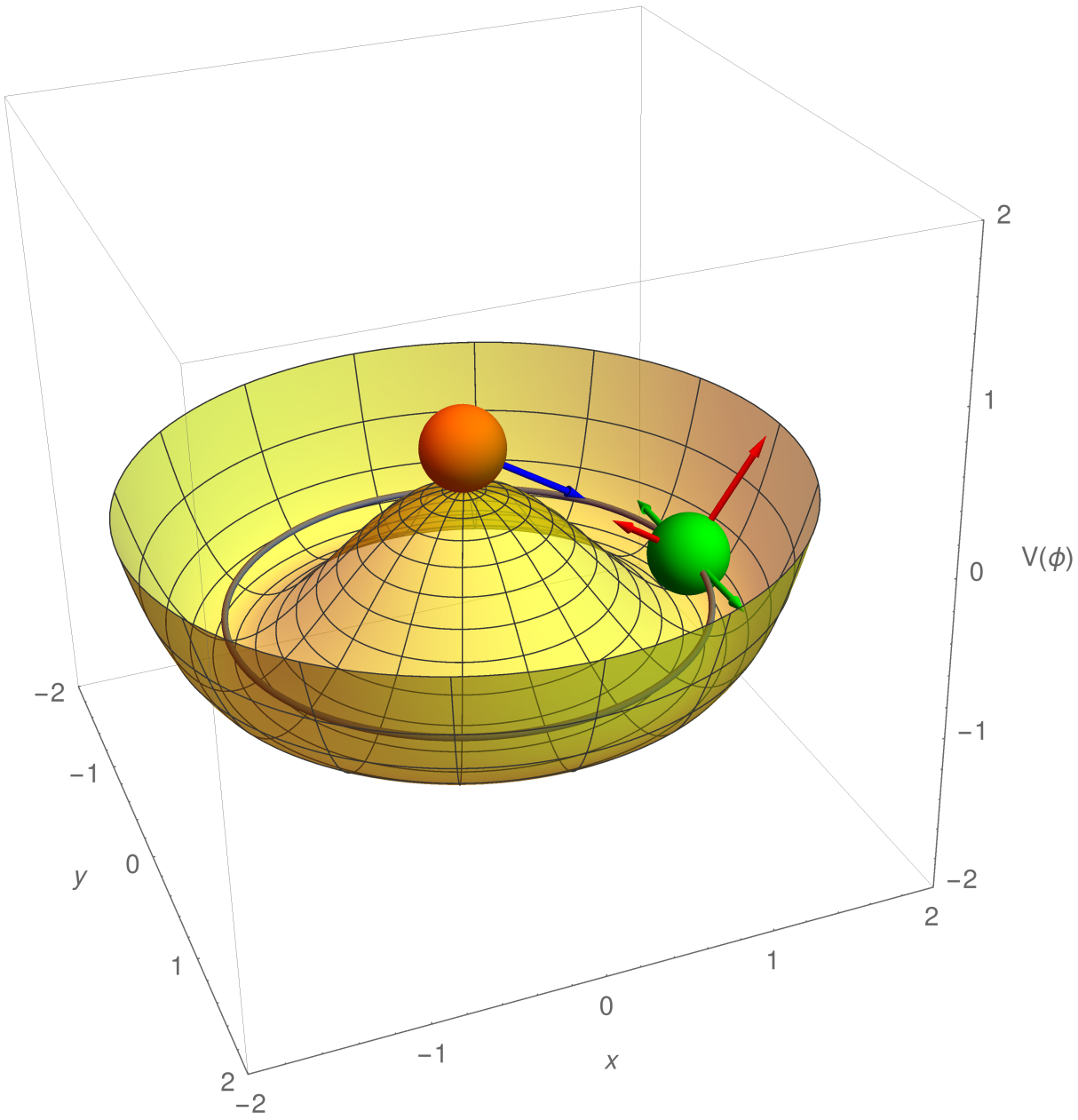

Figure 1.1: Illustration of the Higgs mechanism. We represent the Mexican-hat potential, $V(\phi) = -(1/2)\mu^2\phi^2 + (1/4)\lambda\phi^4$, where $\mu^2 = 2$, $\lambda = 1$ and ϕ^2 is the radial squared coordinate. Two stationary states are present: the unstable point $\phi = 0$ (red ball) and the ground state $|phi| = \mu/\sqrt{\lambda}$ (green ball). Note that such a ground state is degenerate, so it no longer respects the cylindrical symmetry of the original potential. The quantization of the excitations marked with green arrows will lead to the appearance of massless modes. Those marked with red arrows will produce massive modes. Such a mass comes from the curvature of the potential.

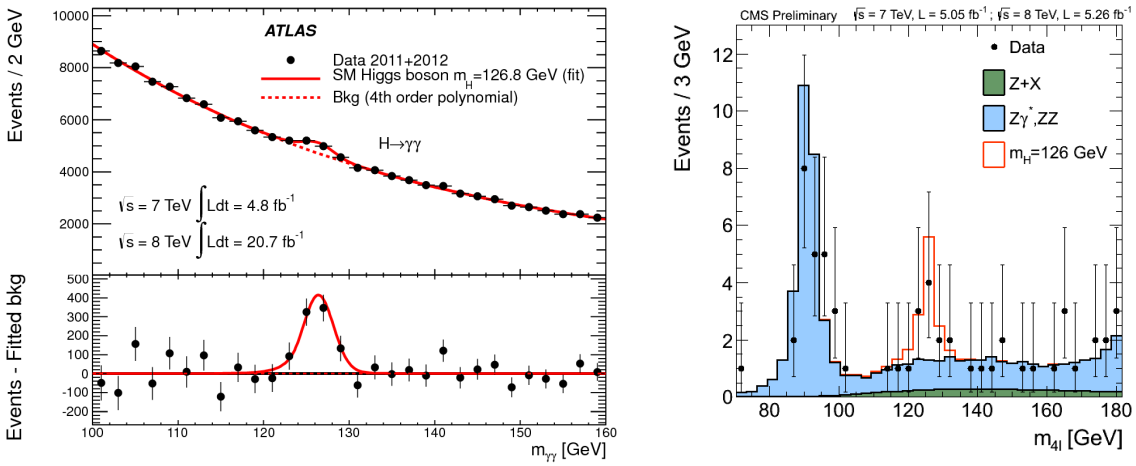

Figure 1.2: Discovery of the spin 0 boson at the LHC with the properties of the SM Higgs boson. Left: two photon decay channel with the ATLAS detector [1]. Right: four lepton decay $ZZ \to 4l$ with the CMS detector [3]. Both pictures are reproduced from the corresponding reference under the Creative Commons CC-BY-3.0 license.

Goldstone bosons (Higgs mechanism), letting a free massive boson (the Higgs one).

In 2003, the reanalysis of the LEP experiment at CERN [57, 58] found a lower bound of 107.9 GeV (at 95% confidence level) for the Higgs mass and, more interesting, its electroweak precision measurements allow to compute an upper bound for the SM Higgs boson mass of 193 GeV (also at 95% confidence level). Thus, LEP constrained the value of the SM Higgs mass inside a window of ≈ 85 GeV, provided that no new physics at the electroweak scale was involved and, thus, the electroweak precision measurements could be used in a reliable way.

After that, and more than 40 years after the proposal of the Higgs mechanism for the SM, the ATLAS and CMS experiments at the Large Hadron Collider (LHC) report a boson with a mass of nearly $M_h \simeq 125$ GeV, compatible with the properties of the SM Higgs boson [1–3]. A machine like LHC, able to study particle physics at the TeV scale[8], was necessary. At this scale, the LHC gives two pieces of information. The first one was the discovery of the new bosonic resonances. And the second one [59–61] is a mass gap for the presence of new physics up to an energy of about 600-700 GeV, or even higher for the presence of new vector resonances [59–61].

In fig. 1.3, the mass distribution of diphoton candidates of Higgs decay $H \to \gamma\gamma$ on the ATLAS detector can be seen [1, 2]. Both the $\sqrt{s} = 7$ TeV and the $\sqrt{s} = 8$ TeV data samples of the LHC Run-I have been combined. In a mass windows around $M_h = 126.5$ GeV, which contains 90% of the expected signal events, the expected background events is $N_B = 8284$; the expected signal ones, $N_S = 223$; and the observed ones, 8802. The background computation is based on studies on MC samples of $\gamma - \gamma$, $\gamma -$ jets and jet $-$ jet. They are modelled by polynomials and exponentials. The background line of fig. 1.2 (inclusive data background) is described by a fourth-order Bernstein polynomial, whose parameters come from a fit to data in the 100-160 GeV diphoton invariant mass range.

The CMS analysis [3] for the four-lepton invariant mass for the $ZZ \to 4l$ is shown in fig. 1.2 (right). This analysis looks for $H \to ZZ \to 4l$ events, and uses 5.1 fb^{-1} at

[8] With $\sqrt{s} \sim 7 - 8$ TeV at LHC Run-I.

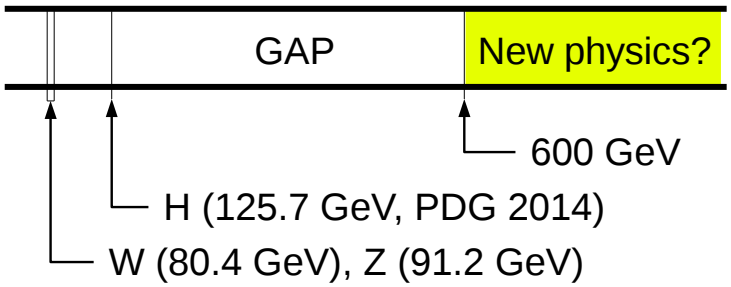

Figure 1.3: Image of the EWSBS physics discovered at the LHC Run-I. Note the presence of a mass gap until a scale of about 600-700 GeV, according to the ATLAS ancd CMS results [59–61]. The top quark is not represented here ($M_t \approx 173\,\text{GeV}$).

$7\,\text{TeV}$ and $5.3\,\text{fb}^{-1}$ at $8\,\text{TeV}$. The background sources have been computed by using Monte Carlo tools: direct ZZ production via $q\bar{q}$ and gluon-gluon, $Z + b\bar{b}$, $t\bar{t}$, $Z +$ jets and $WZ +$ jets. Three channels have been considered ($4e$, 4μ and $2e2\mu$). Adding all these channels, 7.54 ± 0.78 signal events and 3.8 ± 0.5 background ones were expected. And 9 events were observed.

So, is it all? The SM until the Planck scale? This, besides implying an extremely technical challenge for going beyond on our knowledge of the laws of highest energy physics, would present some problems. The first one, the explanation of the neutrino masses. Furthermore, if we try to explain gravity, it raises the so-called *naturalness problem*: where does the 16 orders of magnitude energy hierarchy come from? The SM does not explain the astrophysical signatures of dark matter and dark energy [62–65]nor the nature of neutrinos. And it appears that the model would be *metastable*, our electroweak vacuum being a *false vacuum* [66–73]. The instability would be triggered by the masses of the top quark and the Higgs-like boson found at the LHC, assuming the SM is correct until the Planck scale [74, 75].

The aim of this thesis is the study of some of the theoretical proposals, beyond the SM one (BSM). But, in any case, we look for signals which are detectable at the LHC or, at least, next to the TeV scale. Our tools will be the Effective Theories: a subset of the actual theory, developed with the tools of QFT, which is valid for a certain regime of energies. It has the advantage of abstracting the details of whatever full theory may be at work.

Let us first remember the Goldstone's theorem. Developed in the early 60's [76, 77], it states that[9], when a continuous symmetry is spontaneously broken, each broken degree of freedom produces the appearance of a massless *Goldstone boson*. If the symmetry is approximate, that is, if it is explicitly (besides spontaneously) broken, the generated bosons are massive (although usualy light). In the old Chiral Perturbation Theory (ChPT) (refs. [45–49]), the (global and approximate) spontaneously broken chiral-flavor symmetries of QCD give rise to the *pions* as pseudo Goldstone-bosons..

Regarding the EWSBS, which will be the topic of this PhD thesis, several BSM proposals have been put forward, like Supersymmetry (SUSY), different kinds of composite Higgs models (technicolor, $SO(5)/SO(4)$, dilatons,...) and more. Some of these

[9]Although it was inspired by the non-relativistic case of superconductivity, this formulation only works for relativistic theories

models consider that the EWSBS constituents are pseudo-Goldstone bosons coming from a global symmetry (like $SO(5)$ for the MCHM [78–81]) which breaks to a global $SO(4) \approx SU(2)_L \times SU(2)_R$. This last global symmetry undergoes a second breaking to $SU(2)_{L+R}$. Examples of this kind of models are the (Minimal) Composite Higgs Model (based on the coset SO(5)/SO(4) [78–81]), dilaton models [82, 83],.... This would explain, in a natural way, the presence of a mass gap between the electroweak scale (*light EWSBS constituents*) and the new physics scale which is shown in fig. 1.3. Note that *composite Higgs* would imply the EWSBS dynamics being a strongly interacting one.

We propose the study of an Effective Lagrangian via unitarization procedures [34–39, 84–89], based on the old ChPT for QCD [46–49]. Letting the EWSBS couplings free, we are able to study a wide range of theories. And, by using those unitarization procedures, we can deal with the strongly interacting regime. Indeed, in ref. [90], it was shown that the IAM works quite well for the strongly interacting regime of QCD (see the footnote of figs. 1.4 and 1.5, reprinted from ref. [91]).

Our far goal would be producing Monte Carlo simulations for signals of new physics coming from a strongly interacting EWSBS. This is still work in progress, as an extension of the collaboration of ref. [36]. In this dissertation however we can already provide all (chiral/EFT) scattering amplitudes. The channels studied are the most relevant ones in the exploration of the EWSBS at the LHC,

$$\omega\omega \to \omega\omega \qquad hh \to \omega\omega \qquad hh \to hh \tag{1.1a}$$

$$\omega\omega \to t\bar{t} \qquad hh \to t\bar{t} \qquad t\bar{t} \to t\bar{t} \tag{1.1b}$$

$$\gamma\gamma \to \omega\omega \qquad \gamma\gamma \to hh. \tag{1.1c}$$

Due to time reversal invariance (see sec. 4.7),

$$T(p_1p_2 \to k_1k_2) = T(k_1k_2 \to p_1p_2), \tag{1.2}$$

several other channels are implied. We are mainly interested in processes with $\omega\omega$ as initial state, and $\omega\omega$, hh, $\gamma\gamma$ and $t\bar{t}$ as final one. The reason is that $\gamma\gamma$ and $t\bar{t}$ will turn out to be perturbatively coupled (as $\alpha_{\rm EM} \ll 1$ and $M_t^2/s \ll 1$) to the strongly interacting sector if there is one, and the initial state (quarks and gluons within the proton) have a higher chance of emitting an $\omega\omega$ pair than a hh pair.

However, both in CMS and ATLAS, there are Forward Detector Facilities, which are designed to detect the elastically scattered forward protons from events with $\gamma\gamma$ as initial state at the TeV range. These are AFP in ATLAS [105] and TOTEM in CMS [106, 107]. This makes a study with a $\gamma\gamma$ initial state interesting as the Coulomb field of the charged beam is very boosted. Note that, even before TOTEM starts operation, there is a study from CMS (ref. [108], results quoted in fig. 1.6) where they look for scattering of $\gamma\gamma$ at the TeV scale, although only 2 events have been detected so far.

Furthermore, studying an initial $t\bar{t}$ state can be interesting since an important part of the SM and BSM physics at the TeV is initiated through a top quark triangle ($t\bar{t}$ in the initial state), including some processes of production of Higgs bosons in the SM.

The near-term goal that we have achieved within this dissertation is to have at hand amplitudes that can describe any resonances of the EWSBS discovered in the LHC in the $\frac{1}{2}$-3 TeV region. The EFT framework does not provide specific predictions of where such resonances may be. But should they be found, it becomes a powerful method to correlate observables, such as masses and widths, or line shapes in different channels. In this direction we provide the couplings of the $\gamma\gamma$ and $t\bar{t}$ channels to the EWSBS in sections 2.2.2 and 2.2.3.

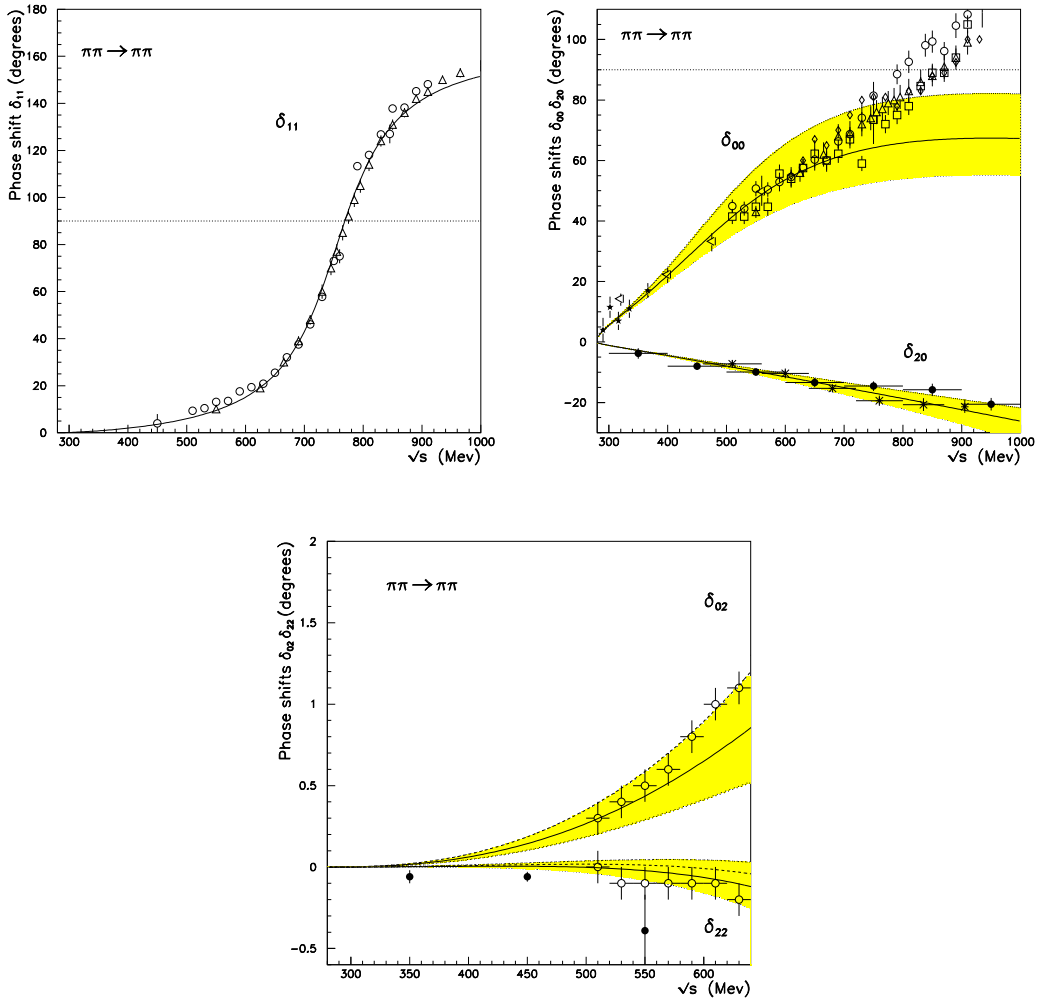

Figure 1.4: *Pion elastic scattering phase shifts δ_{IJ} obtained from the IAM fit imposing the correct M_ρ. The shaded areas cover the error bars of the fitted parameters with the constraint $\hat{l}_1 - \hat{l}_2 = -5.95 \pm 0.02$. The dotted straight lines stand at $\delta = 90^0$. Remember that the $J = 2$ partial waves have to be calculated in plain ChPT. Indeed, the dashed lines in those channels correspond to plain ChPT with the parameters in the first row of Table 2. The data come from: [92] ($\triangle$), [93] ($\Diamond$,$\square$), [94] ($\times$),[95] ($\circ$), [96] ($\triangleleft$), [97] ($\star$) and [98] ($\bullet$). The corresponding curves within $SU(3)$ ChPT would almost superimpose.*

Inverse Amplitude Method (IAM) applied to the $\pi\pi \to \pi\pi$ process, in the strongly interacting regime of QCD. Note the excellent agreement with the experimental data, excluding the δ_{00} channel above 800 MeV. In this dissertation, we will use a version of this IAM method to study a hypothetical strongly interacting regime of the EWSBS.

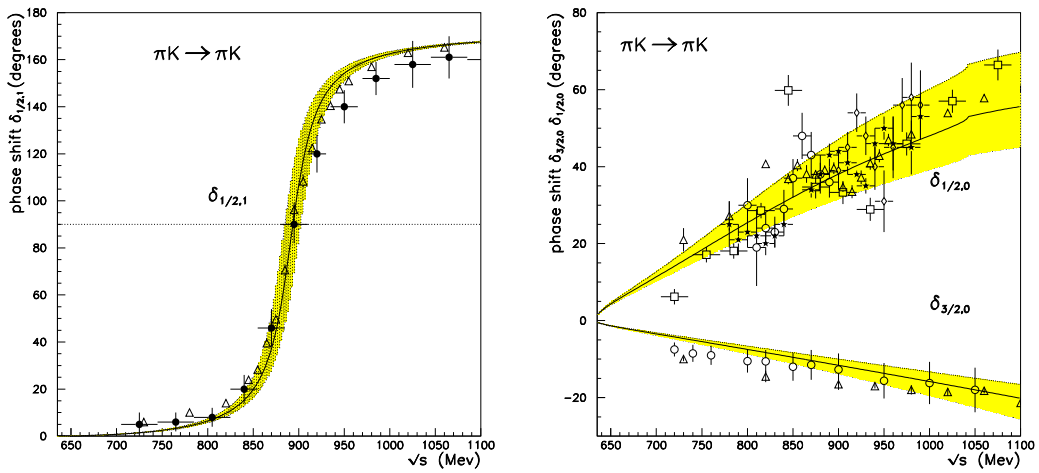

Figure 1.5: *πK elastic scattering phase shifts δ_{IJ} obtained from the IAM fit imposing the correct M_ρ and M_{K^*}. The shaded areas cover the error bars of the fitted parameters with the constraint $2\hat{L}_1^r + \hat{L}_3 - \hat{L}_2^r = (-3.11 \pm 0.01)10^{-3}$. The dotted straight line stands at $\delta = 90^0$. The experimental data come from: [99] (•), [100] (⋆), [101] (○), [102] (♢), [103] (□) and [104] (△).*

Reprinted Fig. 4 with permission from ref. ([91], A. Dobado, J.R. Pelaez., Physical Review D**56**, 3057-3073, 1997). Copyright 1997 by the American Physical Society.

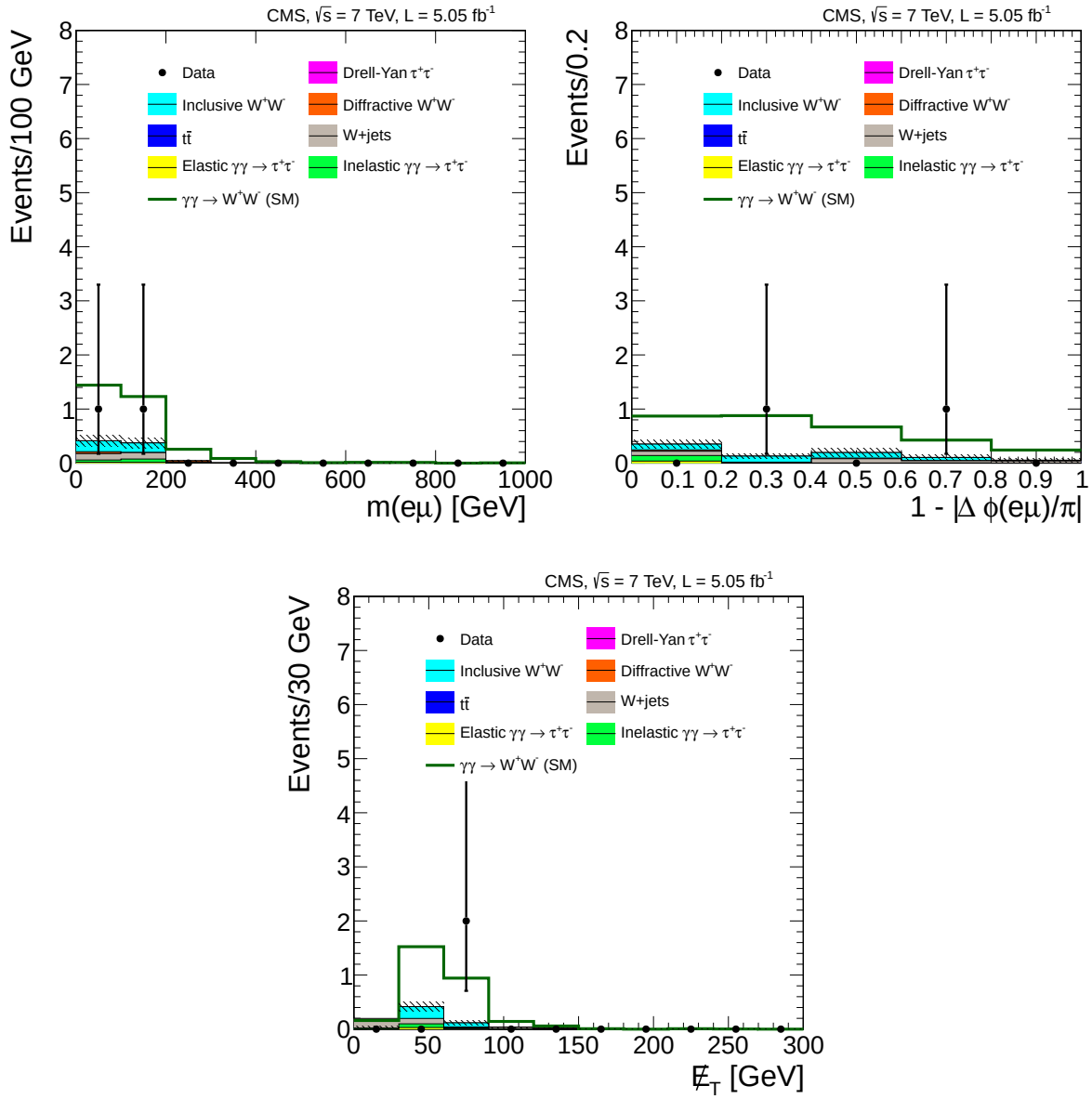

Figure 1.6: Only two events of inelastic scattering $\gamma\gamma \to \omega\omega$ have been found in CMS Run-I, with $\sqrt{s} = 7\,\text{TeV}$, and an integrated luminosity of $5.05\,\text{fb}^{-1}$ (ref. [108]; reproduced under the Creative Commons Attribution License). $\mu^{\pm}e^{\mp}$ invariant mass (top left), acoplanarity (top right) and missing transverse energy (bottom) distributions.

Chapter 2

Chiral EW Lagrangian

The ATLAS and CMS collaborations at LHC have found a new boson compatible with the SM Higgs [1, 2], with a mass of nearly[1] $M_h \simeq 125\,\text{GeV}$. Furthermore, the most probable J^P quantum numbers are 0^+, and couplings with other particles are in agreement with the SM Higgs, although with moderate precision. Moreover, there is a mass gap for the presence of new physics [59–61] until an energy of about 600-700 GeV, or even higher for the presence of new vector resonances.

However, the data is still compatible with either an elementary or a composite Higgs: this last possibility will be considered in this work. The mass gap between the M_W, M_Z and M_h masses, all of $\mathcal{O}(100\,\text{GeV})$, and the new physics scale (if there is one within reach), suggests that the Higgs boson and the would-be Goldstone bosons $\omega^\pm$ and z could be (pseudo) Goldstone Boson [111–118], related with a global spontaneous symmetry breaking extending the $SU(2)_L \times SU(2)_R \to SU(2)_{L+R}$ global symmetry breaking of the SM. There are several models with specific implementations for the relevant global symmetry breaking pattern: the (Minimal) Composite Higgs Model based on the coset SO(5)/SO(4) [78–81], dilaton models [82, 83] and others [119].

The old electroweak chiral Lagrangian (ECL) [4–21], based on standard chiral perturbation theory (ChPT) of QCD [46–49], assumed a Higgsless model, but solved the problems that the Higgs was intended for by supposing a strongly interacting regime for the EWSBS instead. In view that the h has been found, it can be extended to include the new Higgs-like particle found at the LHC (refs. [22–33]). One of the goals of this work will be to expose this extension, considering non-linear Electroweak Chiral Lagrangians as a low-energy ($M_W, M_h \ll \sqrt{s} \ll 3\,\text{TeV}$) parameterization of the new physics at the TeV scale.

2.1 Equivalence theorem

To simplify the computations, we will make use of the Equivalence Theorem (ET) [120–123], which states that, in the regime $s \gg M_h^2, M_W^2, M_Z^2 \simeq (100\,\text{GeV})^2$, we can identify the longitudinal modes of gauge bosons with the would-be Goldstones[2] (R_ξ gauge). For example,

$$T(W_L^a W_L^b \to W_L^c W_L^d) = T(\omega^a \omega^b \to \omega^c \omega^d) + O\left(\frac{M_W}{\sqrt{s}}\right), \tag{2.1}$$

[1] $M_h^{\text{ATLAS}} = 125.5 \pm 0.6\,\text{GeV}$ and $M_h^{\text{CMS}} = 125.7 \pm 0.4\,\text{GeV}$, according to [109] and [110], respectively.

[2] See app. D.5 for a brief historical review about the discussion concerning the hypothesis of the ET.

where T stands for the corresponding scattering amplitude. In fact, this theorem can be interpreted as if, at sufficiently large energies, the symmetry $SU(2)_L \times U(1)_Y$ was not spontaneously broken, so that the three would-be Goldstones coming from the broken $SU(2)_L \times U(1)_Y$ were directly observable as scalar physical particles, which indeed would correspond to the longitudinal modes of the gauge bosons. So, the non-gauged (but with the broken symmetry $SU(2)_L \times U(1)_Y$) Lagrangian can be used directly to compute the scattering amplitudes. At lower energies, these would-be Goldstones give rise to the longitudinal modes of gauge bosons through a rotation in the coordinates (gauge), according to the Higgs mechanism explained, for instance, in ref. [40] and section 1.

Let us illustrate the application of the ET. We will compare the (exact) tree level computation and the Equivalence Theorem for WW and ZZ scattering on the SM, which can be found in Refs. [124, 125]. The complete SM tree level matrix element for $W_L^+ W_L^- \to HH$ is

$$\begin{aligned}\mathcal{A} = \frac{g^2}{4-(1-4M_W^2/s)} \Bigg\{ & \frac{M_h^2}{M_W^2}\left[1+\frac{3M_h^2}{s-M_h^2}+M_h^2\left(\frac{1}{t-M_W^2}+\frac{1}{u-M_W^2}\right)\right] \\ & +2\left[1-\frac{9M_h^2}{s-M_h^2}+4\frac{M_W^2}{s}\left(1+\frac{3M_h^2}{s-M_h^2}\right)\right] \\ & +2\left[s-2M_h^2-4M_W^2+8\frac{M_W^4}{s}\right]\left(\frac{1}{t-M_W^2}+\frac{1}{u-M_W^2}\right)\Bigg\}, \end{aligned} \tag{2.2}$$

whereas, for the ET $\omega^+\omega^- \to HH$,

$$\begin{aligned}\tilde{\mathcal{A}} = \frac{g^2}{4} \Bigg\{ & \frac{M_h^2}{M_W^2}\left[1+\frac{3M_h^2}{s-M_h^2}+M_h^2\left(\frac{1}{t-M_W^2}+\frac{1}{u-M_W^2}\right)\right] \\ & +2\left[1+(s-M_h^2)\left(\frac{1}{t-M_W^2}+\frac{1}{u-M_W^2}\right)\right]\Bigg\}. \end{aligned} \tag{2.3}$$

Both eqs. 2.2 and 2.3, can be evaluated for certain values of the scattering angle θ and s. According to the Equivalence Theorem, both results should converge in the limit $(M_W^2/s) \to 0$. In order to recover $u = u(s,\theta)$ and $t = t(s,\theta)$ as a function of the scattering angle θ and the squared center of mass energy s, see the expressions of appendix A.

In collaboration with prof. Stefano Moretti (University of Southampton), we have tested the equivalence theorem in this way (see fig. 2.1). The aim of this test was to cross-check a modified version of the Monte Carlo (MC) program MadGraph [126]. According to this experience, when dealing with expressions from other authors or Monte Carlo (MC) programs, it is crucial that both the masses and the coupling are compatible. Sometimes, the Monte Carlo program accepts masses and couplings separately, without ensuring compatibility. Or you can develop a program for generating points in the phase space that, of course, will take the masses of gauge bosons as an input. It can also happen that the MC program uses the so–called *Complex Mass Scheme*, which would also require to modify the couplings. The fact is that the cancellation between diagrams which leads to a weakly interacting EWSBS on the SM can be very easily spoiled at TeV energies because of using incompatible values for the constants. Thus, the set of numerical values of the LO couplings should verify, with high precision, the well–known SM relations[3].

[3]See, for instance, ref. [43] or [40].

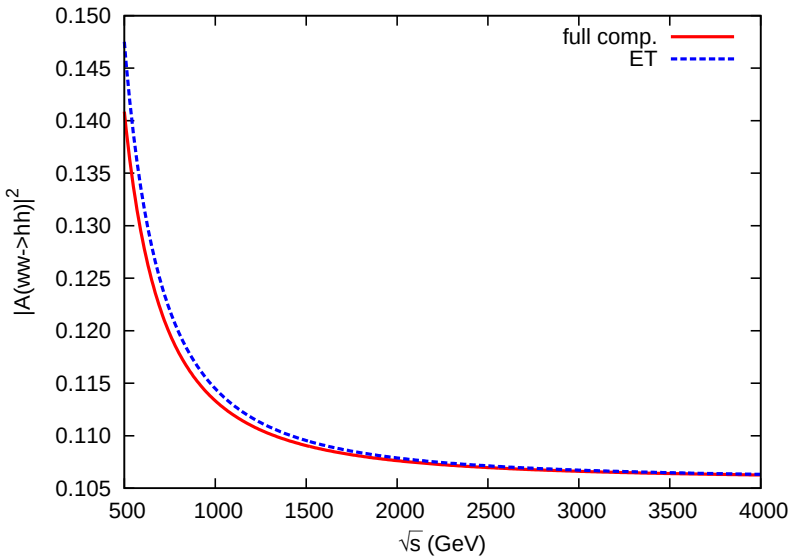

Figure 2.1: Comparison between the full LO scattering amplitude for $\omega\omega \to hh$ (eq. 2.2 and green dashed line on the plot) and that computed though the equivalence theorem (eq. 2.3 and red solid line on the plot). See ref. [124, 125] for the computation. $x = \cos\theta = 0.3$

2.2 The chiral Lagrangian and its parameterizations

In ref. [34] we present the effective Lagrangian describing the low-energy dynamics of four light modes: three would-be Goldstone Bosons ω^a (WBGBs) and the Higgs-like particle[4] h. This model is valid for the energy range $M_h, M_W, M_Z \simeq (100\,\text{GeV})^2 \ll s \ll 4\pi v \simeq 3\,\text{TeV}$. The effective Lagrangian is

$$\mathcal{L} = \frac{v^2}{4} g(h/f) \text{Tr}[(D_\mu U)^\dagger D^\mu U] + \frac{1}{2}\partial_\mu h \partial^\mu h - V(h), \tag{2.4}$$

where $v = 246\,\text{GeV}$ is the SM Higgs-doublet vacuum expectation value; f, a new dynamical energy scale; and $g(x)$, an arbitrary analytical funtion of the scalar field,

$$g(h/f) = 1 + \sum_{n=1}^{\infty} g_n \left(\frac{h}{f}\right)^n = 1 + 2\alpha\frac{h}{f} + \beta\left(\frac{h}{f}\right)^2 + \dots \tag{2.5}$$

Instead of using a power expansion over $1/f$, we could also choose $1/v$, v being the vacuum expectation value,

$$g(h/v) = 1 + 2a\frac{h}{v} + b\left(\frac{h}{v}\right)^2 + \dots . \tag{2.6}$$

V is an arbitrary analytical potential for the scalar field,

$$V(h) = \sum_{n=0}^{\infty} V_n h^n \equiv V_0 + \frac{M_h^2}{2}h^2 + \sum_{n=3}^{\infty} \lambda_n h^n \tag{2.7}$$

[4] Also called φ in some early works like [34].

U is a field taking values in the $SU(2)$ coset. In this work, unless otherwise stated, we will use the so–called *spherical parameterization*,

$$U = \sqrt{1 - \frac{\tilde{\omega}^2}{v^2}} + i\frac{\tilde{\omega}}{v}, \tag{2.8}$$

$\tilde{\omega} = \omega_a \tau^a$ being the would-be Goldstone bosons (WBGB) field and τ^a, the Pauli matrices. Note the presence of the non-linear term $\sqrt{1 - (\tilde{\omega}^2/v^2)}$. This is the main difference from linear approaches like [22–33].

The covariant derivative of the U field (eq. 2.8) is defined as

$$D_\mu U = \partial_\mu U + i\hat{W}_\mu U - iU\hat{B}_\mu, \tag{2.9}$$

where

$$\hat{W}_\mu = gW_{\mu,i}\frac{\tau^i}{2}, \qquad \hat{B}_\mu = g'B_\mu\frac{\tau^3}{2} \tag{2.10a}$$

$$\hat{W}_{\mu\nu} = \partial_\mu\hat{W}_\nu - \partial_\nu\hat{W}_\mu + i[\hat{W}_\mu, \hat{W}_\nu], \qquad \hat{B}_{\mu\nu} = \partial_\mu\hat{B}_\nu - \partial_\nu\hat{B}_\mu. \tag{2.10b}$$

We follow the chiral counting of refs. [19, 30, 46]. Alonso et al. [28] have also studied the counting of Electroweak Chiral Lagrangians, but from a different point of view. Note that the chiral counting which we use is explained in detail in our ref. [36], and is applied only once the approximation $M_h^2, M_W^2, M_Z^2 \ll s$ is taken into account.

Anyway, the 'chiral counting' involves organizing the invariant terms of the Effective Lagrangian by means of their *chiral dimension*. That is, a term $\mathcal{L}_d$ with *chiral dimension* d will contribute to $\mathcal{O}(p^d)$ in the corresponding power momentum expansion. The derivatives and the masses of the dynamical particles (when they are not neglected) are considered as soft scales of the Effective Theory, of order $\mathcal{O}(p)$. To sum up,

$$\partial_\mu,\ M_W,\ M_Z,\ M_h \sim \mathcal{O}(p) \tag{2.11a}$$

$$D_\mu U,\ V_\mu,\ g'v\mathcal{T},\ \hat{W}_\mu,\ \hat{B}_\mu \sim \mathcal{O}(p) \tag{2.11b}$$

$$\hat{W}_{\mu\nu}\,, \hat{B}_{\mu\nu} \sim \mathcal{O}(p^2) \tag{2.11c}$$

The parameters a and b can be adjusted to fit different theoretical models, and the NLO parameters will depend on the renormalization of the underlying theory. For instance,

- $a^2 = b = 0$ ..... Higgsless ECL (ruled out) [4, 6, 7],
- $a^2 = b = 1$ ..... SM,
- $a^2 = 1 - \frac{v^2}{f^2}$, $b = 1 - \frac{2v^2}{f^2}$ ..... $SO(5)/SO(4)$ MCHM [78–81],
- $a^2 = b = \frac{v^2}{\hat{f}^2}$ ..... Dilaton [82, 83].

There is no strong direct limit over the b parameter, because of the difficulty of measuring a 2-Higgs state. However, an indirect limit arises because of the coupling between the hh decay and the elastic $\omega\omega$ scattering, as we will show later (see ref. [39]). The direct limit over the a parameter, at a confidence level of 2σ ($\approx 95\%$), is

- CMS [128] ..... $a \in (0.87, 1.14)$

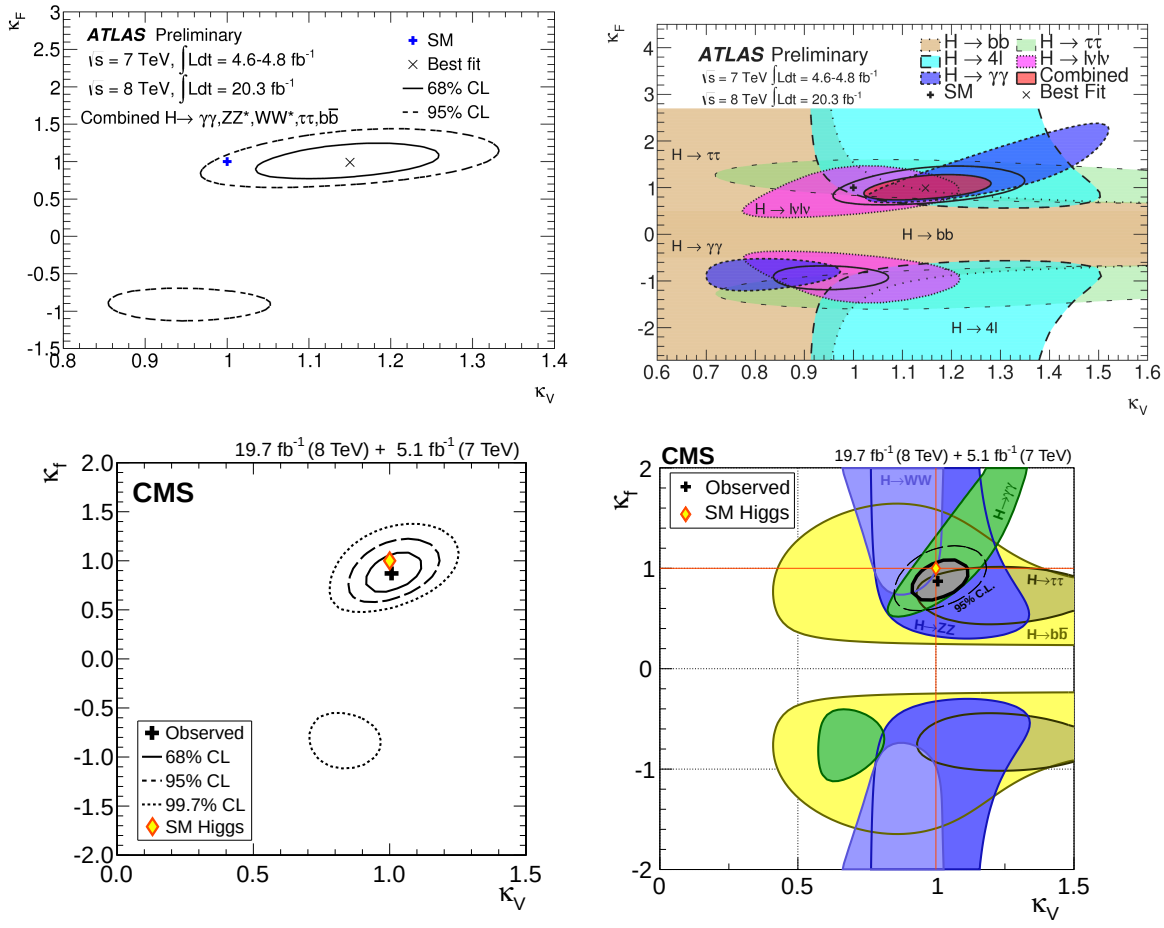

Figure 2.2: From top to bottom, bounds over the $a = k_V$ and k_F coming from ATLAS ([127]; reproduced under the CC-BY-3.0 license) and CMS ([128]; reproduced under the CC-BY-4.0 license).

- ATLAS [127] ..... $a \in (0.96,\ 1.34)$
- Fit of Buchalla et. al. [129] ..... $a \in (0.80,\ 1.16)$

The actual experimental results are shown in fig. 2.2. Anyway, note that these limits are continuously improving, because of the LHC data reanalysis. Ref. [129] uses the computer code Lilith-1.1.3 [130] for constraining the Effective Lagrangian. P.P. Giardino, in his PhD Thesis [131], studied in detail the LHC constraints over a huge range of SM extensions, including the a parameter. We quote it though the situation is changing quickly.

Now, let us consider the $U(\omega^a)$ coset. Since $U(\omega^a) \in SU(2)_L \times SU(2)_R/SU(2)_{L+R}$, it must be of the form

$$U = \mathbb{1} + \frac{i\omega^a \tau^a}{v} + \mathcal{O}(\omega^2), \tag{2.12}$$

whatever the non–linear term is. So, the covariant derivative can be expanded as [36]

$$D_\mu U = \frac{i\partial_\mu \omega_a \tau^a}{v} + i\frac{g}{2} W_{\mu,i}\tau^i - i\frac{g'}{2} B_\mu \tau^3 + \dots \tag{2.13}$$

However, specifying the parameterization of the $U \in SU(2)$ coset is necessary, since the non-linear terms will depend on it. One of the most usual elections is the exponential parameterization,

$$U(x) = \exp\left(i\frac{\tau^a \pi^a(x)}{v}\right), \tag{2.14}$$

τ^a ($a = 1,\ 2,\ 3$) being the Pauli matrices[5]. Working with this expression,

$$U = \begin{pmatrix} \cos\left(\frac{\pi}{v}\right) + i\frac{\pi^3}{\pi}\sin\left(\frac{\pi}{v}\right) & \frac{i\pi^1+\pi^2}{\pi}\sin\left(\frac{\pi}{v}\right) \\ \frac{i\pi^1-\pi^2}{\pi}\sin\left(\frac{\pi}{v}\right) & \cos\left(\frac{\pi}{v}\right) - i\frac{\pi^3}{\pi}\sin\left(\frac{\pi}{v}\right) \end{pmatrix} = \mathbb{1}\cos\left(\frac{\pi}{v}\right) + i\frac{\tau^a\pi^a}{\pi}\sin\left(\frac{\pi}{v}\right), \tag{2.15}$$

where $\pi^2 \equiv \pi^a\pi^a$. With this parameterization, it can be checked that, as expected,

$$U \in SU(2) \Rightarrow U^\dagger \cdot U = U \cdot U^\dagger = \mathbb{1} \tag{2.16}$$

Only if we can neglect both the masses of Goldstone modes and couplings with longitudinal modes (ET limit, $M_W^2 \ll s$), then $D^\mu = \partial^\mu$ in eq. 2.13. Otherwise, some of the couplings with $\hat{W}$ and $\hat{B}$ fields in eq. 2.13 must we kept. Anyway,

$$\mathrm{Tr}\left[\partial_\mu U^\dagger \cdot \partial^\mu U\right] = \frac{A^2}{2v^2\pi^2} + \frac{(4v^2\pi^2 B - Av^2)}{2v^2\pi^4}\sin\frac{\pi}{v}, \tag{2.17}$$

where

$$\pi^2 = \pi^a\pi^a \tag{2.18a}$$
$$A = (\partial_\mu \pi^2)^2 = 4\left(\pi^a\pi^b\partial_\mu\pi^a\partial^\mu\pi^b\right) \tag{2.18b}$$
$$B = \partial_\mu\pi^a\partial^\mu\pi^a. \tag{2.18c}$$

Thus, $\mathrm{Tr}(\partial_\mu U^\dagger \cdot \partial^\mu U)$ can be expressed as

$$\mathrm{Tr}\left[\partial_\mu U^\dagger \cdot \partial^\mu U\right] = \frac{2}{v^2}\left[\frac{v^2}{\pi^2}\sin^2\frac{\pi}{v}\left(\delta_{ab} - \frac{\pi^a\pi^b}{\pi^2}\right) + \frac{\pi^a\pi^b}{\pi^2}\right]\partial_\mu\pi^a\partial^\mu\pi^b \tag{2.19}$$

[5]Einstein's sum convention will be used unless otherwise stated.

However, as explained in [36], this is a good option for QCD Chiral Perturbation Theory (ChPT), where the $SU(3)$ coset is studied [46–49]. But we are dealing with an $SU(2)$ coset, which is isomorphic to S^3. Unless otherwise stated, the so–called *spherical parameterization* will be used (see eq. 2.8), since computations in this basis are much simpler for the particular case of the $SU(2)$ coset. Note the notation change between eqs. 2.8 and 2.14 ($\pi^a \leftrightarrow \omega^a$) in order to distinguish these two parameterizations. According to eq. 2.15, we can change the parameterization by using

$$U = \mathbb{1}\cos\frac{\pi}{v} + i\frac{\tau^a\pi^a}{\pi}\sin\frac{\pi}{v} = \mathbb{1}\sqrt{1-\frac{\omega^2}{v^2}} + i\frac{\tau^a\omega^a(x)}{v} \Rightarrow \frac{\omega^a}{v} = \frac{\pi^a}{\pi}\sin\frac{\pi}{v}. \tag{2.20}$$

By expanding this result,

$$\omega^a = \pi^a\left[1 - \frac{1}{6}\left(\frac{\pi}{v}\right)^2 + \frac{1}{120}\left(\frac{\pi}{v}\right)^4 - \frac{1}{5040}\left(\frac{\pi}{v}\right)^6 + \ldots\right]. \tag{2.21}$$

Let us study the spherical basis. If eq. 2.8 is expanded,

$$U = \begin{pmatrix} \sqrt{1-\frac{\omega^2}{v^2}} + \frac{i\omega^3}{v} & \frac{i\omega^1+\omega^2}{v} \\ \frac{i\omega^1-\omega^2}{v} & \sqrt{1-\frac{\omega^2}{v^2}} - \frac{i\omega^3}{v} \end{pmatrix}. \tag{2.22}$$

Eq. 2.16 can be also checked within the spherical parameterization (eq. 2.22). Now, computations are much simpler than with the exponential parameterization. For instance,

$$\mathrm{Tr}\left[\partial_\mu U_s^\dagger \cdot \partial^\mu U_s\right] = \frac{2}{v^2}\left[\delta_{ab} + \frac{\omega^a\omega^b}{v^2-\omega^2}\right]\partial_\mu\omega^a\partial^\mu\omega^b \tag{2.23}$$

For these fields ($\omega^a, \quad a = 1,2,3$) the spherical (or charge) basis is introduced,

$$\omega^\pm = \frac{\omega^1 \mp i\omega^2}{\sqrt{2}},\ \omega^0 = \omega^3, \tag{2.24}$$

which also implies

$$\omega^2 = 2\omega^+\omega^- + \omega^0\omega^0 \tag{2.25}$$

The same definition can be carried over to $\pi^\pm$ and π^0, which belongs to the exponential parameterization. On our ref. [36], we studied these two parameterizations (spherical and exponential), for $\gamma\gamma$ scattering. As expected, the physical S-matrix elements are identical (in terms of ω^a and π^a, respectively). However, the intermediate results (i.e., the Feynman diagrams) are different.

According to the Equivalence Theorem (sec. 2.1), if they are part of the physical initial or final states, and we have a high $\sqrt{s} \gg M_W$ (center of mass energy), the $\omega^\pm$, ω^0 (or $\pi^\pm$, π^0) can be identified with the longitudinal polarizations of gauge bosons $W^\pm$ and Z, up to an error $\mathcal{O}(M_W/\sqrt{s})$. The possible differences between parameterizations will be suppressed by a factor $\mathcal{O}(M_W/\sqrt{s})$. In the particular case of our ref. [36], since we consider $M_W, M_h = 0$, these differences cancel.

2.2.1 WBGB scattering

In ref. [35] we reported the one-loop computation for the $\omega\omega \to \omega\omega$, $\omega\omega \to hh$ and $hh \to hh$ processes. Here we expand the discussion. Since we are working with an

effective (non-renormalizable) theory, the following counterterms are needed in order to renormalize the scattering amplitudes,

$$\mathcal{L}_4 = a_4[\mathrm{Tr}(V_\mu V_\nu)][\mathrm{Tr}(V^\mu V^\nu)] + a_5[\mathrm{Tr}(V_\mu V^\mu)][\mathrm{Tr}(V_\nu V^\nu)] + \frac{\gamma}{f^4}(\partial_\mu\varphi\partial^\mu\varphi)^2 + \frac{\delta}{f^2}(\partial_\mu\varphi\partial^\mu\varphi)\,\mathrm{Tr}[(D_\nu U)^\dagger D^\nu U] + \frac{\eta}{f^2}(\partial_\mu\varphi\partial^\nu\varphi)\,\mathrm{Tr}[(D^\mu U)^\dagger D_\nu U] + \ldots, \quad (2.26)$$

where $V_\mu = (D_\mu U)U^\dagger$. The $\hat{W}_\mu U$ and $U\hat{B}_\mu$ terms of eq. 2.13 are neglected, so that $D_\mu U \equiv \partial_\mu U$. This approximation is valid because we are in the Equivalence Theorem regime (sec. 2.1) and we are dealing with couplings to neither photons nor transverse modes of gauge bosons. The spherical parameterization (see eqs. 2.8 and 2.22) is used.

In subsequent work [38, 39] we changed the notation in eq. 2.26, in order to adopt a recently agreed-upon standard. Thus, from now on, the next expressions will be used [36, 38]:

$$\mathcal{L}_0 = \frac{v^2}{4}\mathcal{F}(h)\,\mathrm{Tr}[(D_\mu U)^\dagger D^\mu U] + \frac{1}{2}\partial_\mu h\partial^\mu h - V(h) \quad (2.27)$$

$$\mathcal{L}_4 = a_4[\mathrm{Tr}(V_\mu V_\nu)][\mathrm{Tr}(V^\mu V^\nu)] + a_5[\mathrm{Tr}(V_\mu V^\mu)][\mathrm{Tr}(V_\nu V^\nu)] + \frac{g}{v^4}(\partial_\mu h\partial^\mu h)^2 + \frac{d}{v^2}(\partial_\mu h\partial^\mu h)\,\mathrm{Tr}[(D_\nu U)^\dagger D^\nu U] + \frac{e}{v^2}(\partial_\mu h\partial^\nu h)\,\mathrm{Tr}[(D^\mu U)^\dagger D_\nu U] + \ldots \quad (2.28)$$

$$\mathcal{F}(h) = 1 + 2a\frac{h}{v} + b\left(\frac{h}{v}\right)^2 + \ldots \quad (2.29)$$

$$V(h) = \sum_{n=0}^{\infty} V_n h^n = V_0 + \frac{1}{2}M_h^2 h^2 + d_3\frac{M_h^2}{2v}h^3 + d_4\frac{M_h^2}{8v^2}h^4 + \ldots \quad (2.30)$$

If we choose the spherical parameterization, according to [35, 38] and as follows from eqs. 2.27 and 2.28, the NLO phenomenological Lagrangian for the WBGB scattering can be written as

$$\mathcal{L} = \frac{1}{2}\mathcal{F}(h)\partial_\mu\omega^a\partial^\mu\omega^b\left(\delta_{ab} + \frac{\omega^a\omega^b}{v^2}\right) + \frac{1}{2}\partial_\mu h\partial^\mu h + \frac{4a_4}{v^4}\partial_\mu\omega^a\partial_\nu\omega^a\partial^\mu\omega^b\partial^\nu\omega^b + \frac{4a_5}{v^4}\partial_\mu\omega^a\partial^\mu\omega^a\partial_\nu\omega^b\partial^\nu\omega^b + \frac{g}{v^4}(\partial_\mu h\partial^\nu h)^2 + \frac{2d}{v^4}\partial_\mu h\partial^\mu h\partial_\nu\omega^a\partial^\nu\omega^a + \frac{2e}{v^4}\partial_\mu h\partial^\nu h\partial^\mu\omega^a\partial_\nu\omega^a. \quad (2.31)$$

Note that we have neglected the Higgs mass and self-couplings which appear on the potential $V(h)$ that was defined in eq. 2.30. This is valid on the regime $M_h \ll \sqrt{s}$, and provided that the strong dynamics is not triggered by unnaturally high d_i self-coupling parameters.

2.2.2 Coupling with $\gamma\gamma$

The effective Lagrangian (with the corresponding NLO counterterms) of eq. 2.31 is valid provided that only interactions between WBGBs are taken into account. According to the Equivalence Theorem (sec. 2.1), these WBGBs can be identified with the longitudinal modes of gauge bosons ($W^\pm$ and Z) and the Higgs-like scalar (H), as long as the CM

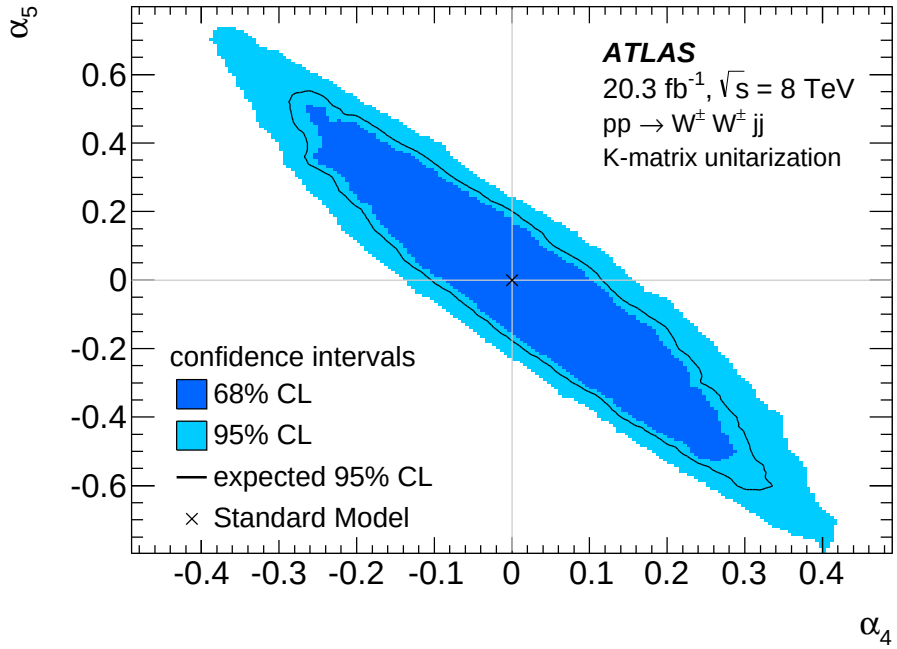

Figure 2.3: Direct constraint over the a_4 and a_5 parameters coming from ATLAS [132]. The constraint of CMS [133] are given in terms of the F_{S0}/Λ^4 and F_{S1}/Λ^4 parameters, which have no direct translation to the a_4 and a_5 ones [134]. Figure reproduced from ref. [132] under the CC-BY-3.0 license.

energy is $\sqrt{s} \gg M_h^2, M_W^2, M_Z^2 \approx (100\,\text{GeV})^2$. Thus, for the processes $\gamma\gamma \to zz$ and $\gamma\gamma \to \omega^+\omega^-$, aditional terms involving the photon field must be introduced.

First of all, we can now not turn eq. 2.13 into $D_\mu U = \partial_\mu U$ as in earlier works on the strong sector alone, because the couplings with the photon field A come from the couplings with $\hat{W}_{\mu\nu}$ and $\hat{B}_{\mu\nu}$ in eq. 2.13, once a rotation to the physical basis is performed,

$$-c_W \frac{h}{v}\hat{W}_{\mu\nu}\hat{W}^{\mu\nu} - c_B \frac{h}{v}\hat{B}_{\mu\nu}\hat{B}^{\mu\nu} = -\frac{c_\gamma}{2}\frac{h}{v}e^2 A_{\mu\nu}A^{\mu\nu} + \dots, \tag{2.32}$$

where $\hat{W}$ and $\hat{B}$ are defined in eqs. 2.10a and 2.10b. Thus, the $\mathcal{O}(p^2)$ Lagrangian [36] is, for the exponential parameterization,

$$\begin{aligned}\mathcal{L}_2(\pi, h, \gamma) = {} & \frac{1}{2}\partial_\mu h \partial^\mu h + \frac{1}{2}\mathcal{F}(h)(2\partial_\mu\pi^+\partial^\mu\pi^- + \partial_\mu\pi^0\partial^\mu\pi^0) \\ & + \frac{1}{6v^2}\mathcal{F}(h)\left[(\partial_\mu\pi^+\pi^- + \pi^+\partial_\mu\pi^- + \pi^0\partial_\mu\pi^0)^2 - \pi^2(2\partial_\mu\pi^+\partial^\mu\pi^- + \partial_\mu\pi^0\partial^\mu\pi^0)\right] \\ & + ie\mathcal{F}(h)A^\mu(\partial_\mu\pi^+\pi^- - \partial_\mu\pi^-\pi^+)\left(1 - \frac{\pi^2}{3v^2}\right) \\ & + e^2\mathcal{F}(h)A_\mu A^\mu\pi^+\pi^-\left(1 - \frac{\pi^2}{3v^2}\right).\end{aligned} \tag{2.33}$$

And, for the spherical one,

$$\begin{aligned}\mathcal{L}_2(\omega,h,\gamma) = &\frac{1}{2}\partial_\mu h\partial^\mu h + \frac{1}{2}\mathcal{F}(h)(2\partial_\mu\omega^+\partial^\mu\omega^- + \partial_\mu\omega^0\partial^\mu\omega^0)\\ &+ \frac{1}{2v^2}\mathcal{F}(h)(\partial_\mu\omega^+\omega^- + \omega^+\partial_\mu\omega^- + \omega^0\partial_\mu\omega^0)^2\\ &+ ie\mathcal{F}(h)A^\mu(\partial_\mu\omega^+\omega^- - \omega^+\partial_\mu\omega^-) + e^2\mathcal{F}(h)A_\mu A^\mu\omega^+\omega^-. \end{aligned} \quad (2.34)$$

In both cases, $\mathcal{F}(h) = 1 + 2a(h/v) + b(h/v)^2$, as defined in eq. 2.29. Furthermore, the next NLO extra counterterms are needed,

$$\mathcal{L}_{4'} = a_1\,\mathrm{Tr}(U\hat{B}_{\mu\nu}U^\dagger\hat{W}^{\mu\nu}) + ia_2\,\mathrm{Tr}(U\hat{B}_{\mu\nu}U^\dagger[V^\mu,V^\nu]) - ia_3\,\mathrm{Tr}(\hat{W}_{\mu\nu}[V^\mu,V^\nu]), \quad (2.35)$$

besides those required for the WBGBs scattering: a_4, a_5, g, d and e (see eq. 2.28). As for existing constraints on parameter values, ref. [130] quotes a constraint on the c_γ parameter, coming from LHC data. At a confidence level of 2σ, $c_\gamma \in (-0.98, 0.50)/16\pi^2$. Note the $1/16\pi^2$ factor, which comes from the normalization of ref. [130]. On the a_1, a_2 and a_3 parameters, there are only weaker constraints based on electroweak precision observables from LEP and purely SM one-loop calculations. See ref. [135] for a review of such constraints. To sum up, $a_1 = (1.0 \pm 0.7) \times 10^{-3}$, $a_2 \in (-0.26, 0.26)$, $a_3 \in (-0.10, 0.04)$. However, these constraints are highly model dependent.

2.2.3 Coupling with $t\bar{t}$

The effective Lagrangian of eq 2.31 models scattering processes between particles of the Electroweak Symmetry Breaking Sector. Thus, if we want to consider scattering processes between massive fermions, more terms (the so-called *Yukawa sector*) are required. Thus, as exposed in our ref. [136], the considered effective Lagrangian is

$$\mathcal{L} = \frac{v^2}{4}\mathcal{F}(h)\mathrm{Tr}[(D_\mu U)^\dagger D^\mu U] + \frac{1}{2}\partial_\mu h\partial^\mu h - V(h) + i\bar{Q}\partial Q - v\mathcal{G}(h)[\bar{Q}'_L U H_Q Q'_R + h.c.]. \quad (2.36)$$

In the Yukawa sector of eq. 2.36, the quark doublets are

$$Q' = \begin{pmatrix}\mathcal{U}'\\ \mathcal{D}'\end{pmatrix}, \quad (2.37)$$

where the two Q entries are made of the different up and down quark sectors

$$\mathcal{U}' = (u,c,t)', \qquad \mathcal{D}' = (d,s,b)'. \quad (2.38)$$

and the Yukawa-coupling matrix has the following form

$$H_Q = \begin{pmatrix}H_U & 0\\ 0 & H_D\end{pmatrix}. \quad (2.39)$$

This matrix can be diagonalized by tranforming independently the right and left handed up and down quarks as:

$$\mathcal{D}_{L,R} = V^D_{L,R}\mathcal{D}'_{L,R}, \qquad \mathcal{U}_{L,R} = V^U_{L,R}\mathcal{U}'_{L,R}. \quad (2.40)$$

where $V_{L,R}^{U,D}$ are four 3×3 unitary matrices. Thus, the Yukawa part of the Lagrangian can be written as

$$\begin{aligned}\mathcal{L}_Y = & -\mathcal{G}(h)\left\{\sqrt{1-\frac{\omega^2}{v^2}}\left(\bar{\mathcal{U}}M_U\mathcal{U}+\bar{\mathcal{D}}M_D\mathcal{D}\right)+\frac{i\omega^0}{v}\left(\overline{\mathcal{U}}M_U\gamma^5\mathcal{U}-\bar{\mathcal{D}}M_D\gamma^5\mathcal{D}\right)\right.\\ & +\frac{i\sqrt{2}\omega^+}{v}\left(\bar{\mathcal{U}}_L V_{CKM}M_D\mathcal{D}_R-\bar{\mathcal{U}}_R M_U V_{CKM}\mathcal{D}_L\right)\\ & \left.+\frac{i\sqrt{2}\omega^-}{v}\left(\bar{\mathcal{D}}_L V_{CKM}^\dagger M_U\mathcal{U}_R-\bar{\mathcal{D}}_R M_D V_{CKM}^\dagger\mathcal{U}_L\right)\right\},\end{aligned} \tag{2.41}$$

where (eq. 2.24) $\omega^\pm = (\omega^1 \mp i\omega^2)/\sqrt{2}$, $\omega^0 = \omega^3$ and the new quark fields are mass eigenstates, with M_U and M_D being the corresponding diagonal and real mass matrices. $V_{CKM} = V_L^U V_L^{D\dagger}$ is the Cabibbo-Kobayashi-Maskawa matrix. For the case of the heaviest quark generation (the only relevant one for this work), the matrix element V_{tb} has been omitted since it is very close to unity. Hence, we have the effective Yukawa sector

$$\begin{aligned}\mathcal{L}_Y = -\mathcal{G}(h)\left\{\sqrt{1-\frac{\omega^2}{v^2}}\left(M_t t\bar{t}+M_b b\bar{b}\right)+\frac{i\omega^0}{v}\left(M_t\bar{t}\gamma^5 t-M_b\bar{b}\gamma^5 b\right)\right.\\ \left.+\frac{i\sqrt{2}\omega^+}{v}\left(M_b\bar{t}_L b_R-M_t\bar{t}_R b_L\right)+\frac{i\sqrt{2}\omega^-}{v}\left(M_t\bar{b}_L t_R-M_b\bar{b}_R t_L\right)\right\}.\end{aligned} \tag{2.42}$$

As can be seen, the different couplings of the left and right chiral parts of top and bottom quarks are an effect of custodial symmetry breaking. The $\mathcal{F}$ and $\mathcal{G}$ appearing in the Lagrangian (eq. 2.36) are arbitrary analytical functions on the Higgs field h. $\mathcal{F}(h)$ is as defined in eq. 2.29 above, $\mathcal{F}(h) = 1 + 2a(h/v) + b(h/v)^2$, whereas the new $\mathcal{G}(h)$ is

$$\mathcal{G}(h) = 1 + c_1\frac{h}{v} + c_2\frac{h^2}{v^2} + \dots \tag{2.43}$$

For the computations presented in this work these functions are only needed up to the quartic terms $\mathcal{O}(h^4)$. Also we will consider the limit of massless botton quark ($M_b = 0$). Then we get the Yukawa Lagrangian:

$$\mathcal{L}_Y = -\mathcal{G}(h)\left[\left(1-\frac{\omega^2}{2v^2}\right)M_t t\bar{t}+\frac{i\omega^0}{v}M_t\bar{t}\gamma^5 t-\frac{i\sqrt{2}\omega^+}{v}M_t\bar{t}_R b_L+\frac{i\sqrt{2}\omega^-}{v}M_t\bar{b}_L t_R\right], \tag{2.44}$$

where we have kept only the would-be Goldstone boson fields up to order $\omega^2 = 2\omega^+\omega^- + (\omega^0)^2$ (eq. 2.25). Finally, the relevant Lagrangian for $\omega\omega \to t\bar{t}$ process in the regime[6] $M_h^2/v^2 \ll M_t^2/v^2 \ll s/v^2$ is given by

$$\begin{aligned}\mathcal{L} = -\mathcal{G}(h)\left[\left(1-\frac{\omega^2}{2v^2}\right)M_t t\bar{t}+\frac{i\sqrt{2}\omega^0}{v}M_t\bar{t}\gamma^5 t-\frac{i\sqrt{2}\omega^+}{v}M_t\bar{t}_R b_L+\frac{i\sqrt{2}\omega^-}{v}M_t\bar{b}_L t_R\right]\\ +\frac{1}{2}\mathcal{F}(h)\partial_\mu\omega^a\partial^\mu\omega_b\left(\delta_{ab}+\frac{\omega_a\omega_b}{v^2}\right)+\frac{1}{2}\partial_\mu h\partial^\mu h.\end{aligned} \tag{2.45}$$

[6]This regime verifies the Equivalence Theorem. See section 2.1.

Ref. [129] also gives a direct constraint $c_1 \in (1.15, 1.53)$, at 2σ-confidence level. The one-loop divergences appearing in the $\omega\omega$ and hh scattering amplitudes can be absorbed in the GB four-derivative and the following two-derivative top antitop couplings

$$\begin{aligned}\mathcal{L}_4 = &\frac{4a_4}{v^4}\partial_\mu\omega^a\partial_\nu\omega^a\partial^\mu\omega^b\partial^\nu\omega^b + \frac{4a_5}{v^4}\partial_\mu\omega^a\partial^\mu\omega^a\partial_\nu\omega^b\partial^\nu\omega^b \\ &+ \frac{2d}{v^4}\partial_\mu h\partial^\mu h\partial_\nu\omega^a\partial^\nu\omega^a + \frac{2e}{v^4}\partial_\mu h\partial^\nu h\partial^\mu\omega^a\partial_\nu\omega^a + \frac{g}{v^4}\left(\partial_\mu h\partial^\mu h\right)^2 \\ &+ g_t\frac{M_t}{v^4}\partial_\mu\omega^a\partial^\mu\omega^b t\bar{t} + g_t'\frac{M_t}{v^4}\partial_\mu h\partial^\mu h t\bar{t}. \end{aligned} \tag{2.46}$$

Chapter 3

Scattering amplitudes

3.1 Generic form of the WBGB scattering amplitude and the isospin basis

The chiral Lagrangian in eq. 2.31 is invariant under custodial symmetry $SU(2)_{L+R}$. Hence, for the process $\omega^a\omega^b \to \omega^c\omega^d$, the scattering amplitude can be written as [137]

$$\mathcal{A}_{abcd} = A(s,t,u)\delta_{ab}\delta_{cd} + A(t,s,u)\delta_{ac}\delta_{bd} + A(u,t,s)\delta_{ad}\delta_{bc} \tag{3.1}$$

Only one function, though with arguments exchanged $A(s,t,u)$, $A(t,s,u)$ and $A(u,t,s)$, and in no other combinations, appears. This is because of Bose symmetry, which makes A satisfy the relation

$$A(x,y,z) = A(x,z,y)\,\forall x,y,z. \tag{3.2}$$

This relation can also be checked on the actual computation of the scattering amplitude A. See eqs. 3.31-3.34.

According to eq. 2.24, $\omega^\pm = (\omega^1 \mp i\omega^2)/\sqrt{2}$ and $z = \omega^3$. Note that these relations apply for *fields*. In order to be consistent, the *states* should be

$$\left|\omega^\pm\right\rangle = \frac{1}{\sqrt{2}}\left(\left|\omega^1\right\rangle \pm i\left|\omega^2\right\rangle\right), \quad |z\rangle = \left|\omega^3\right\rangle \tag{3.3}$$

This is easily proven if we take into account that $\langle\emptyset\,|\,a_i(x)\,|\,a_{j,p}\rangle = e^{i\vec{p}\cdot\vec{x}}\delta_{i,j}$, where $|a_{j,p}\rangle$ is any quantum state; $a_i(x)$, its associated field; and $|\emptyset\rangle$, the vacuum quantum state. If we applied a_i over an orthonormal quantum state[1] $|a_j\rangle$, $|a_i\rangle \perp |a_j\rangle$, then $\langle\emptyset\,|\,a_i\,|\,a_j\rangle = 0$. Thus, applying the fields 2.24 over the states 3.3,

$$\begin{aligned}\left\langle\emptyset\,\middle|\,\omega^\pm(x)\,\middle|\,\omega^\pm_{\vec{p}}\right\rangle &= \frac{1}{2}\left\langle\emptyset\,\middle|\,\omega^1(x) \mp i\omega^2(x)\,\middle|\,\omega^1_{\vec{p}} \pm i\omega^2_{\vec{p}}\right\rangle \\ &= \frac{1}{2}\left(\left\langle\emptyset\,\middle|\,\omega^1(x)\,\middle|\,\omega^1_{\vec{p}}\right\rangle + \left\langle\emptyset\,\middle|\,\omega^2(x)\,\middle|\,\omega^2_{\vec{p}}\right\rangle\right) = e^{i\vec{p}\cdot\vec{x}},\end{aligned} \tag{3.4}$$

and $\langle\emptyset\,|\,z(x)\,|\,z_{\vec{p}}\rangle = \left\langle\emptyset\,\middle|\,\omega^3(x)\,\middle|\,\omega^3_{\vec{p}}\right\rangle = e^{i\vec{p}\cdot\vec{x}}$. For simplicity, we will take the notation $|a+b\rangle = |a\rangle + |b\rangle$ and $|ab\rangle \equiv |a\rangle \otimes |b\rangle$. Hence, the physical amplitudes (provided that the

[1] i and j are indices which describe an internal degree of freedom of the particle. This fact will allow us to decompose composite states by using tensor products. Otherwise, the full definition of a quantum field, $\phi(x) = \int \frac{d^3p}{(2\pi)^3}\frac{1}{\sqrt{2\omega_{\vec{p}}}}\left(a_{\vec{p}} + a^\dagger_{-\vec{p}}\right)e^{i\vec{p}\cdot\vec{x}}$, should be taken into account. Note that $a_{\vec{p}}$ and $a^\dagger_{-\vec{p}}$ are, respectively, annihilation and creation operators. See ref. [40] for an introduction to the QFT formalism.

ET is applicable) can be computed in the following way. For the $\omega^+\omega^- \to zz$ process,

$$\begin{aligned} A^{+-zz} &= \langle zz \,|\, A \,|\, \omega^+\omega^- \rangle = \left\langle \omega^3\omega^3 \,\middle|\, A \,\middle|\, \frac{\omega^1 + i\omega^2}{\sqrt{2}} \frac{\omega^1 - i\omega^2}{\sqrt{2}} \right\rangle \\ &= \frac{1}{2} \left[\langle \omega^3\omega^3 \,|\, A \,|\, \omega^1\omega^1 \rangle + \langle \omega^3\omega^3 \,|\, A \,|\, \omega^2\omega^2 \rangle + \cancel{i\langle \omega^3\omega^3 \,|\, A \,|\, \omega^2\omega^1 \rangle} - \cancel{i\langle \omega^3\omega^3 \,|\, A \,|\, \omega^1\omega^2 \rangle} \right] \\ &= \frac{1}{2} \left\{ 2 \left[A(s,t,u) \right] \right\} = A(s,t,u). \end{aligned} \tag{3.5}$$

First of all, because of eq. 3.2, A^{+-zz} is symmetric under interchange of t and u. That is, under the change of the scattering angle $\theta \to \pi - \theta$.

Besides, note the usage of the sesquilinear form, since we are dealing with a relativistic version of Quantum Mechanics[2]. For the $zz \to zz$ process,

$$\begin{aligned} A^{zzzz} &= \langle zz \,|\, A \,|\, zz \rangle = \langle \omega^3\omega^3 \,|\, A \,|\, \omega^3\omega^3 \rangle \\ &= A(s,t,u) + A(t,s,u) + A(u,t,s), \end{aligned} \tag{3.6}$$

which is also invariant under t and u interchange, according to eq. 3.2. For the $\omega^+\omega^- \to \omega^+\omega^-$ process,

$$\begin{aligned} A^{+-+-} &= \langle \omega^+\omega^- \,|\, A \,|\, \omega^+\omega^- \rangle = \left\langle \frac{\omega^1 + i\omega^2}{\sqrt{2}} \frac{\omega^1 - i\omega^2}{\sqrt{2}} \,\middle|\, A \,\middle|\, \frac{\omega^1 + i\omega^2}{\sqrt{2}} \frac{\omega^1 - i\omega^2}{\sqrt{2}} \right\rangle \\ &= \frac{1}{4} \left[\langle \omega^1\omega^1 \,|\, A \,|\, \omega^1\omega^1 \rangle + \langle \omega^1\omega^1 \,|\, A \,|\, \omega^2\omega^2 \rangle + \cancel{i\langle \omega^1\omega^1 \,|\, A \,|\, \omega^2\omega^1 \rangle} - \cancel{i\langle \omega^1\omega^1 \,|\, A \,|\, \omega^1\omega^2 \rangle} \right. \\ &\quad + \langle \omega^2\omega^2 \,|\, A \,|\, \omega^1\omega^1 \rangle + \langle \omega^2\omega^2 \,|\, A \,|\, \omega^2\omega^2 \rangle + \cancel{i\langle \omega^2\omega^2 \,|\, A \,|\, \omega^2\omega^1 \rangle} - \cancel{i\langle \omega^2\omega^2 \,|\, A \,|\, \omega^1\omega^2 \rangle} \\ &\quad - \cancel{i\langle \omega^2\omega^1 \,|\, A \,|\, \omega^1\omega^1 \rangle} - \cancel{i\langle \omega^2\omega^1 \,|\, A \,|\, \omega^2\omega^2 \rangle} + \langle \omega^2\omega^1 \,|\, A \,|\, \omega^2\omega^1 \rangle - \langle \omega^2\omega^1 \,|\, A \,|\, \omega^1\omega^2 \rangle \\ &\quad \left. + \cancel{i\langle \omega^1\omega^2 \,|\, A \,|\, \omega^1\omega^1 \rangle} + \cancel{i\langle \omega^1\omega^2 \,|\, A \,|\, \omega^1\omega^1 \rangle} - \langle \omega^1\omega^2 \,|\, A \,|\, \omega^2\omega^1 \rangle + \langle \omega^1\omega^2 \,|\, A \,|\, \omega^1\omega^2 \rangle \right] \\ &= \frac{1}{4} \left\{ 2 \left[A(s,t,u) + A(t,s,u) + A(u,t,s) \right] + 2A(s,t,u) + 2A(t,s,u) - 2A(u,t,s) \right\} \\ &= A(s,t,u) + A(t,s,u) \end{aligned} \tag{3.7}$$

You could also consider the clasically non-equivalent process

$$\begin{aligned} A^{+--+} &= \langle \omega^-\omega^+ \,|\, A \,|\, \omega^+\omega^- \rangle = \left\langle \frac{\omega^1 - i\omega^2}{\sqrt{2}} \frac{\omega^1 + i\omega^2}{\sqrt{2}} \,\middle|\, A \,\middle|\, \frac{\omega^1 + i\omega^2}{\sqrt{2}} \frac{\omega^1 - i\omega^2}{\sqrt{2}} \right\rangle \\ &= \frac{1}{4} \left[\langle \omega^1\omega^1 \,|\, A \,|\, \omega^1\omega^1 \rangle + \langle \omega^1\omega^1 \,|\, A \,|\, \omega^2\omega^2 \rangle - \cancel{i\langle \omega^1\omega^1 \,|\, A \,|\, \omega^1\omega^2 \rangle} + \cancel{i\langle \omega^1\omega^1 \,|\, A \,|\, \omega^2\omega^1 \rangle} \right. \\ &\quad + \langle \omega^2\omega^2 \,|\, A \,|\, \omega^1\omega^1 \rangle + \langle \omega^2\omega^2 \,|\, A \,|\, \omega^2\omega^2 \rangle - \cancel{i\langle \omega^2\omega^2 \,|\, A \,|\, \omega^1\omega^2 \rangle} + \cancel{i\langle \omega^2\omega^2 \,|\, A \,|\, \omega^2\omega^1 \rangle} \\ &\quad - \cancel{i\langle \omega^1\omega^2 \,|\, A \,|\, \omega^1\omega^1 \rangle} - \cancel{i\langle \omega^1\omega^2 \,|\, A \,|\, \omega^2\omega^2 \rangle} - \langle \omega^1\omega^2 \,|\, A \,|\, \omega^1\omega^2 \rangle + \langle \omega^1\omega^2 \,|\, A \,|\, \omega^2\omega^1 \rangle \\ &\quad \left. + \cancel{i\langle \omega^2\omega^1 \,|\, A \,|\, \omega^1\omega^1 \rangle} + \cancel{i\langle \omega^2\omega^1 \,|\, A \,|\, \omega^2\omega^2 \rangle} + \langle \omega^2\omega^1 \,|\, A \,|\, \omega^1\omega^2 \rangle - \langle \omega^2\omega^1 \,|\, A \,|\, \omega^2\omega^1 \rangle \right] \\ &= \frac{1}{4} \left\{ 2 \left[A(s,t,u) + A(t,s,u) + A(u,t,s) \right] + 2A(s,t,u) - 2A(t,s,u) + 2A(u,t,s) \right\} \\ &= A(s,t,u) + A(u,t,s). \end{aligned} \tag{3.8}$$

But Bose symmetry, eq. 3.2, yields $A^{+--+}(s,t,u) = A(s,t,u) + A(u,t,s) = A(s,u,t) + A(u,s,t) = A^{+-+-}(s,u,t)$. Thus, A^{+-+-} is recovered through an interchange of t and u, as expected.

[2]This sesquilinear form verifies the properties $\langle aA \,|\, bB \rangle = a^* b \langle A \,|\, B \rangle$ and $\langle A + B \,|\, C + D \rangle = \langle A \,|\, C \rangle + \langle A \,|\, D \rangle + \langle B \,|\, C \rangle + \langle B \,|\, D \rangle$.

The coupled channels $\omega^a\omega^b \to hh$ and $hh \to \omega^a\omega^b$ have the same amplitude due to time reversal invariance. Because h is an isospin singlet ($I = 0$), the amplitude can be written as

$$M_{ab}(s,t,u) = M(s,t,u)\delta_{ab} \tag{3.9}$$

We also compute the amplitude $hh \to hh$,

$$A(hh \to hh) \equiv T(s,t,u) \tag{3.10}$$

For studying unitarity, using the isospin and spin-projected partial waves is easier. For the state of a single particle ω^a, we use the following correspondence, where the notation $|I, M_I\rangle$ (I being the isospin and M_I its projection) has been used[3]:

$$|1,1\rangle \equiv |+\rangle \equiv -\omega^+ = -\frac{|\omega^1\rangle + i\,|\omega^2\rangle}{\sqrt{2}} \tag{3.11a}$$

$$|1,0\rangle \equiv |0\rangle \equiv \omega^0 = \left|\omega^3\right\rangle \tag{3.11b}$$

$$|1,-1\rangle \equiv |-\rangle \equiv \omega^- = \frac{|\omega^1\rangle - i\,|\omega^2\rangle}{\sqrt{2}} \tag{3.11c}$$

Anyway, we are dealing with 2-particle states. Since we assume that the Lagrangian has custodial symmetry, states with different isospin do not mix. Thus, we have to compute eigenvectors of the isospin operator I^2. We will employ the usual definition of the Clebsch-Gordan coefficients[4], so that, using the notation $|I, M_I\rangle$ for the 2-particles states, the correspondence between the one-particle state basis and the isospin basis can be found on table 3.1.

In either case, every choice which satisfied $\hat{I}^2\,|I, M_I\rangle = I(I+1)\,|I, M_I\rangle$ and $\hat{I}_z\,|I, M_I\rangle = M_I\,|I, M_I\rangle$ would have been valid. In particular, multiplying the states by any complex phase factor does not change even the orthonormality of the basis. As well known in quantum mechanics [43], the $\hat{I}^2$ and $\hat{I}_z$ operators, for the 2–particle state, are given by

$$\hat{I}^2 = \hat{I}_x^2 + \hat{I}_y^2 + \hat{I}_z^2, \quad \hat{I}_{x,y,z} = \mathbb{1}_{3\times3} \otimes J_{1,2,3} + J_{1,2,3} \otimes \mathbb{1}_{3\times3}, \tag{3.12}$$

where the representation of $SU(2)$ is

$$J_1 = \frac{1}{\sqrt{2}}\begin{pmatrix} 0 & 1 & 0 \\ 1 & 0 & 1 \\ 0 & 1 & 0 \end{pmatrix}, \quad J_2 = \frac{i}{\sqrt{2}}\begin{pmatrix} 0 & -1 & 0 \\ 1 & 0 & -1 \\ 0 & 1 & 0 \end{pmatrix}, \quad J_3 = \begin{pmatrix} 1 & 0 & 0 \\ 0 & 0 & 0 \\ 0 & 0 & -1 \end{pmatrix}, \tag{3.13}$$

the basis being $|+\rangle = e_1$, $|0\rangle = e_2$, $|-\rangle = e_3$. On the one-particle state basis, the 2-particle states are written as

$$|ab\rangle = |a\rangle \otimes |b\rangle\,, \text{ where } a, b \in \{+, 0, -\}. \tag{3.14}$$

These relations allow to check the validity of the Clebsch-Gordan coefficients from table 3.1.

[3]These definitions are the usual ones in the literature. For instance, see refs. [90, 137–140]. Eq. 2.24 (page 17) shows the relation between $\omega^\pm$ and ω^1, ω^2.

[4]See ref. [43] and the contained references. Only exception: we have taken a sign change for the $|0,0\rangle$ isospin singlet state.

$\lvert I, M_I\rangle$	$\{\lvert\pm\rangle, \lvert 0\rangle\}$	$\{\lvert\omega^{\pm}\rangle, \lvert z\rangle\}$	$\{\omega^{1,2,3}\}$
$\lvert 0,0\rangle$	$\frac{1}{\sqrt{3}}\left(\lvert+-\rangle - \lvert 00\rangle + \lvert -+\rangle\right)$	$-\frac{1}{\sqrt{3}}\left(\lvert\omega^+\omega^-\rangle + \lvert\omega^-\omega^+\rangle + \lvert zz\rangle\right)$	$-\frac{1}{\sqrt{3}}\left(\lvert\omega^1\omega^1\rangle + \lvert\omega^2\omega^2\rangle + \lvert\omega^3\omega^3\rangle\right)$
$\lvert 1,1\rangle$	$\frac{1}{\sqrt{2}}\left(\lvert+0\rangle - \lvert 0+\rangle\right)$	$\frac{1}{\sqrt{2}}\left(\lvert z\omega^+\rangle - \lvert\omega^+ z\rangle\right)$	$\frac{1}{2}\left(i\lvert\omega^3\omega^2\rangle + \lvert\omega^3\omega^1\rangle - \lvert\omega^1\omega^3\rangle - i\lvert\omega^2\omega^3\rangle\right)$
$\lvert 1,0\rangle$	$\frac{1}{\sqrt{2}}\left(\lvert+-\rangle - \lvert -+\rangle\right)$	$\frac{1}{\sqrt{2}}\left(\lvert\omega^-\omega^+\rangle - \lvert\omega^+\omega^-\rangle\right)$	$\frac{i}{\sqrt{2}}\left(\lvert\omega^1\omega^2\rangle - \lvert\omega^2\omega^1\rangle\right)$
$\lvert 1,-1\rangle$	$\frac{1}{\sqrt{2}}\left(\lvert 0-\rangle - \lvert -0\rangle\right)$	$\frac{1}{\sqrt{2}}\left(\lvert z\omega^-\rangle - \lvert\omega^- z\rangle\right)$	$\frac{1}{2}\left(i\lvert\omega^2\omega^3\rangle - \lvert\omega^1\omega^3\rangle + \lvert\omega^3\omega^1\rangle - i\lvert\omega^3\omega^2\rangle\right)$
$\lvert 2,2\rangle$	$\lvert++\rangle$	$\lvert\omega^+\omega^+\rangle$	$\frac{1}{2}\left(\lvert\omega^1\omega^1\rangle - \lvert\omega^2\omega^2\rangle + i\lvert\omega^1\omega^2\rangle + i\lvert\omega^2\omega^1\rangle\right)$
$\lvert 2,1\rangle$	$\frac{1}{\sqrt{2}}\left(\lvert+0\rangle + \lvert 0+\rangle\right)$	$-\frac{1}{\sqrt{2}}\left(\lvert\omega^+ z\rangle + \lvert z\omega^+\rangle\right)$	$-\frac{1}{2}\left(\lvert\omega^1\omega^3\rangle + \lvert\omega^3\omega^1\rangle + i\lvert\omega^2\omega^3\rangle + i\lvert\omega^3\omega^2\rangle\right)$
$\lvert 2,0\rangle$	$\frac{1}{\sqrt{6}}\left(\lvert+-\rangle + 2\lvert 00\rangle + \lvert -+\rangle\right)$	$\frac{1}{\sqrt{6}}\left(2\lvert zz\rangle - \lvert\omega^+\omega^-\rangle - \lvert\omega^-\omega^+\rangle\right)$	$-\frac{1}{\sqrt{6}}\left(\lvert\omega^1\omega^1\rangle + \lvert\omega^2\omega^2\rangle - 2\lvert\omega^3\omega^3\rangle\right)$
$\lvert 2,-1\rangle$	$\frac{1}{\sqrt{2}}\left(\lvert 0-\rangle + \lvert -0\rangle\right)$	$\frac{1}{\sqrt{2}}\left(\lvert\omega^- z\rangle + \lvert z\omega^-\rangle\right)$	$\frac{1}{2}\left(\lvert\omega^1\omega^3\rangle + \lvert\omega^3\omega^1\rangle - i\lvert\omega^2\omega^3\rangle - i\lvert\omega^3\omega^2\rangle\right)$
$\lvert 2,-2\rangle$	$\lvert--\rangle$	$\lvert\omega^-\omega^-\rangle$	$\frac{1}{2}\left(\lvert\omega^1\omega^1\rangle - \lvert\omega^2\omega^2\rangle - i\lvert\omega^1\omega^2\rangle - i\lvert\omega^2\omega^1\rangle\right)$

Table 3.1: Clebsch-Gordan coefficients for the two-(spin-1) particle states. Take into account that $\lvert ab\rangle \equiv \lvert a\rangle \otimes \lvert b\rangle$. See refs. [43, 138].

3.1.1 Decomposition of elastic scattering $\omega\omega \to \omega\omega$

Let us express the scattering amplitude $\mathcal{A}(s,t,u)$ in term of the $|I, M_I\rangle$ basis. Because of the isospin symmetry,

$$A_I(s,t,u) = \langle I, M_J \,|\, A \,|\, I, M_J \rangle \,,\ \forall M_J = -I, -I+1, \ldots, I-1, I, \tag{3.15}$$

$$\langle I - M_J \,|\, A \,|\, I', M'_J \rangle = 0,\ \forall (I, M_I) \neq (I', M'_I) \tag{3.16}$$

These relations are guaranteed even under a change of the phases of the vectors, because of the sesquilinear product. So, computing only the elastic matrix element for one state for each I will be enough.

For the unique $\omega\omega$ isovector with $I = 0$,

$$\begin{aligned} A_0(s,t,u) =\ & \langle I = 0 \,|\, A \,|\, I = 0 \rangle = \frac{1}{3} \left\langle \omega^1\omega^1 + \omega^2\omega^2 + \omega^3\omega^3 \,\middle|\, A \,\middle|\, \omega^1\omega^1 + \omega^2\omega^2 + \omega^3\omega^3 \right\rangle \\ &= \frac{1}{3} \left\{ 3[A(s,t,u) + A(t,s,u) + A(u,t,s)] + 6[A(s,t,u)] \right\} \\ &= 3A(s,t,u) + A(t,s,u) + A(u,t,s) \end{aligned} \tag{3.17}$$

For the $A_1(s,t,u)$, we will take the $|1,0\rangle$ state,

$$\begin{aligned} A_1(s,t,u) =\ & \langle 1,0 \,|\, A \,|\, 1,0 \rangle = \left\langle \frac{i}{\sqrt{2}}(\omega^1\omega^2 - \omega^2\omega^1) \,\middle|\, A \,\middle|\, \frac{i}{\sqrt{2}}(\omega^1\omega^2 - \omega^2\omega^1) \right\rangle \\ &= \frac{1}{2} \left\langle \omega^1\omega^2 - \omega^2\omega^1 \,\middle|\, A \,\middle|\, \omega^1\omega^2 - \omega^2\omega^1 \right\rangle = \frac{1}{2} \left[2A(t,s,u) - 2A(u,t,s) \right] \\ &= A(t,s,u) - A(u,t,s) \end{aligned} \tag{3.18}$$

And, for the $A_2(s,t,u)$, the $|2,0\rangle$ one gives

$$\begin{aligned} A_2(s,t,u) =\ & \langle 2,0 \,|\, A \,|\, 2,0 \rangle \\ &= \left\langle -\frac{1}{\sqrt{6}}(\omega^1\omega^1 + \omega^2\omega^2 - 2\omega^3\omega^3) \,\middle|\, A \,\middle|\, -\frac{1}{\sqrt{6}}(\omega^1\omega^1 + \omega^2\omega^2 - 2\omega^3\omega^3) \right\rangle \\ &= \frac{1}{6} \left\{ 6[A(s,t,u) + A(t,s,u) + A(u,t,s)] - 6[A(s,t,u)] \right\} \\ &= A(t,s,u) + A(u,t,s) \end{aligned} \tag{3.19}$$

We can also obtain $A(s,t,u)$, $A(t,s,u)$ and $A(u,t,s)$ as a function of A_0, A_1 and A_2. This will be useful for recovering the physical amplitudes from the unitarized partial waves, in order to perform phenomenological studies. So, rearranging eqs. 3.17, 3.18 and 3.19,

$$A(s,t,u) = \frac{1}{3}[A_0(s,t,u) - A_2(s,t,u)] \tag{3.20a}$$

$$A(t,s,u) = \frac{1}{2}[A_2(s,t,u) + A_1(s,t,u)] \tag{3.20b}$$

$$A(u,t,s) = \frac{1}{2}[A_2(s,t,u) - A_1(s,t,u)] \tag{3.20c}$$

Of course, eqs. 3.20 are not independent, due to the crossing symmetry for four identical particles (i.e., the values of A can be permuted). Substituting these eqs. 3.20 in eqs. 3.5,

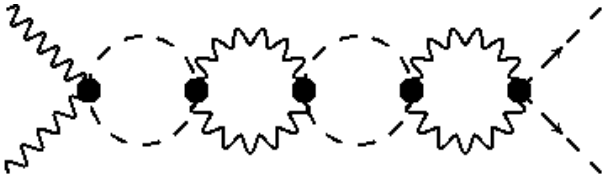

Figure 3.1: Typical Feynman diagram mixing the $\omega\omega$ (wiggled lines) and the hh (dashed lines) channels. Taken from Ref. [39].

3.6 and 3.7 we can compute the scattering amplitudes for physical states $\omega^{\pm}$ and z,

$$\begin{aligned}
\mathcal{A}(\omega^+\omega^- \to \omega^+\omega^-) &= A(s,t,u) + A(t,s,u) \\
&= \frac{1}{3}A_0(s,t,u) + \frac{1}{2}A_1(s,t,u) + \frac{1}{6}A_2(s,t,u) && \text{(3.21a)} \\
\mathcal{A}(\omega^+\omega^- \to \omega^-\omega^+) &= A(s,t,u) + A(u,t,s) \\
&= \frac{1}{3}A_0(s,t,u) - \frac{1}{2}A_1(s,t,u) + \frac{1}{6}A_2(s,t,u) && \text{(3.21b)} \\
\mathcal{A}(\omega^+\omega^- \to zz) &= \mathcal{A}(zz \to \omega^+\omega^-) = A(s,t,u) \\
&= \frac{1}{3}\left[A_0(s,t,u) - A_2(s,t,u)\right] && \text{(3.21c)} \\
\mathcal{A}(zz \to zz) &= A(s,t,u) + A(t,s,u) + A(u,t,s) \\
&= \frac{1}{3}\left[A_0(s,t,u) + 2A_2(s,t,u)\right] && \text{(3.21d)}
\end{aligned}$$

3.1.2 Higgs-Higgs cross-channel: $\omega\omega \to hh$ and $hh \to hh$ amplitudes

Due to the fact that hh is an isospin singlet, it only couples to $|I, M_i\rangle = |0,0\rangle$. The coupling is

$$M_0(s,t,u) = \left\langle hh \left| M \right| -\frac{1}{\sqrt{3}}\left(\omega^1\omega^1 + \omega^2\omega^2 + \omega^3\omega^3\right) \right\rangle = -\sqrt{3}M(s,t,u) \qquad (3.22)$$

Note that when we deal with $\omega\omega$ scattering, without couplings to photons, in our refs. [34, 35, 38, 39, 84, 85, 87–89], the signs of $|0,0\rangle$ and $M_0(s,t,u)$ are changed. However, this fact does not modify the cross sections, even when using unitarization procedures with crossed channels, since the election of a complex phase for $|0,0\rangle$ is arbitrary. We changed this sign in order to be consequent with the usual election of the Clebsch-Gordan coefficients (see ref. [43]), which was also followed by our collaborators M.J. Herrero and J.J. Sanz-Cillero, with whom we computed the $\gamma\gamma$ scattering (sec. 3.2.2).

The $hh \to hh$ is an elastic scattering process between isospin singlet states, so that computation of isospin projections is trivial. However, it is necessary when studying the unitarity of elastic $\omega\omega$ scattering taking into account coupling with hh states. In fig. 3.1 you can see the kind of processes that is necessary to consider, and which could eventually involve a $hhhh$ vertex.

3.1.3 Other channels: $\omega^{\pm}z \to \omega^{\pm}z$

For this kind of process, taking into account eq. 2.24 and 3.1,

$$\begin{aligned}\mathcal{A}(\omega^{\pm}z \to \omega^{\pm}z) &= \left\langle \frac{1}{\sqrt{2}}[(\omega^1 \pm i\omega^2)\omega^3] \,\middle|\, A \,\middle|\, \frac{1}{\sqrt{2}}[(\omega^1 \pm i\omega^2)\omega^3] \right\rangle \\ &= \frac{1}{2}\left[\langle \omega^1\omega^3 \,|\, A \,|\, \omega^1\omega^3\rangle + \langle \omega^2\omega^3 \,|\, A \,|\, \omega^2\omega^3\rangle \right. \\ &\quad \cancel{\pm i\langle \omega^1\omega^3 | A | \omega^2\omega^3\rangle} \cancel{\mp i\langle \omega^2\omega^3 | A | \omega^1\omega^3\rangle}\Big] \\ &= A(t,s,u) \end{aligned} \tag{3.23}$$

If we exchange the particles in the final state,

$$\begin{aligned}\mathcal{A}(\omega^{\pm}z \to z\omega^{\pm}) &= \left\langle \frac{1}{\sqrt{2}}[\omega^3(\omega^1 \pm i\omega^2)] \,\middle|\, A \,\middle|\, \frac{1}{\sqrt{2}}[(\omega^1 \pm i\omega^2)\omega^3] \right\rangle \\ &= \frac{1}{2}\left[\langle \omega^3\omega^1 \,|\, A \,|\, \omega^1\omega^3\rangle + \langle \omega^3\omega^2 \,|\, A \,|\, \omega^2\omega^3\rangle \right. \\ &\quad \cancel{\pm i\langle \omega^3\omega^1 | A | \omega^2\omega^3\rangle} \cancel{\mp i\langle \omega^3\omega^2 | A | \omega^1\omega^3\rangle}\Big] \\ &= A(u,t,s). \end{aligned} \tag{3.24}$$

Note that, taking into account eq. 3.2, $\mathcal{A}(\omega^{\pm}z \to z\omega^{\pm}) = A(u,t,s) = A(u,s,t)$, thus $\mathcal{A}(\omega^{\pm}z \to \omega^{\pm}z)$ is recovered through an interchange of u and t, as expected. Also, from eqs. 3.20b and 3.20c,

$$\mathcal{A}(\omega^{\pm}z \to \omega^{\pm}z) = \frac{1}{2}\left[A_2(s,t,u) + A_1(s,t,u)\right] \tag{3.25a}$$

$$\mathcal{A}(\omega^{\pm}z \to z\omega^{\pm}) = \frac{1}{2}\left[A_2(s,t,u) - A_1(s,t,u)\right] \tag{3.25b}$$

3.2 LO and NLO computation of invariant scattering amplitudes

The computations with the Chiral Lagrangian at tree level was reported for the channels $\omega\omega \to \omega\omega$, $\omega\omega \to hh$ and $hh \to hh$, in Ref. [34]. Soon thereafter, in Ref. [35] we provided the Next to Leading Order (NLO) computation. The masses M_h and M_W were neglected. Actually, the error introduced by doing so is of the same order as that of using the Equivalence Theorem[5],

$$T(W_L^a W_L^b \to W_L^c W_L^d) = T(\omega^a\omega^b \to \omega^c\omega^d) + O\left(\frac{M_W}{\sqrt{s}}\right),$$

since this requires $M_h, M_W \ll \sqrt{s}$. Independently, Ref. [141] also performed some of the computations with a slightly different formulation, keeping finite masses M_h and M_W. The good agreement with their results is a reassuring test for this approach.

3.2.1 $\omega\omega$ scattering

In ref. [34], we reported the LO scattering amplitudes for $\omega\omega$, hh at tree-level, keeping a finite value for the mass M_h of the Higgs-like scalar. See fig. 3.2 for the Feynman

[5] See chapter 2.1 and eq. 2.1.

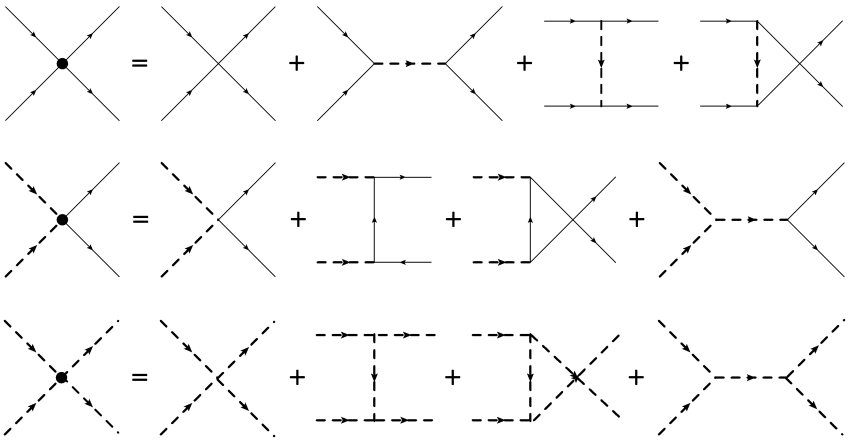

Figure 3.2: LO diagrams for the $\omega\omega \to \omega\omega$, $\omega\omega \to hh$ and $hh \to hh$ processes. ω in solid lines and h in dashed ones. Fig. taken from Ref. [34]. The NLO diagrams for $\omega\omega$ scattering can be found in Appendix F.

diagrams considered. The scattering amplitudes are

$$A^{2\omega 2\omega}(s,t,u) = \frac{s}{v^2}\left(1 + \frac{a^2 s}{M_h^2 - s}\right) \tag{3.26a}$$

$$M^{2\omega 2h}(s,t,u) = -\frac{1}{v^2}\left[bs + a^2\frac{(t-M_h^2)^2}{t} + a^2\frac{(u-M_h^2)^2}{u} + \frac{6a\lambda_3 vs}{s-M_h^2}\right] \tag{3.26b}$$

$$T^{2h2h}(s,t,u) = -24\lambda_4 - 36\lambda_3^2\left[\frac{1}{s-M_h^2} + \frac{1}{t-M_h^2} + \frac{1}{u-M_h^2}\right] \tag{3.26c}$$

Here, λ_3 and λ_4 stand for the Higgs self-coupling constants, which come from the analytic potential of the scalar field h in eq. 2.7,

$$V(\varphi) = \sum_{n=0}^{\infty} V_n h^n \equiv V_0 + \frac{M_h^2}{2}h^2 + \sum_{n=3}^{\infty}\lambda_n h^n$$

In the SM, they would be $M_h^2 = 2\lambda v^2$, $\lambda_3 = \lambda v = M_h^2/2v$, $\lambda_4 = \lambda/4 = M_h^2/8v^2$. Taking into account that the SM also implies $a^2 = b = 1$, eqs. 3.26 turn into

$$A^{2\omega 2\omega}(s,t,u) = \frac{M_h^2}{v^2}\frac{s}{M_h^2 - s} \tag{3.27a}$$

$$M^{2\omega 2h}(s,t,u) = \frac{M_h^2}{v^2}\left[2 + \frac{3s}{M_h^2 - s} - M_h^2\left(\frac{1}{t} + \frac{1}{u}\right)\right] \tag{3.27b}$$

$$T^{2h2h}(s,t,u) = \frac{M_h^2}{v^2}\left[9M_h^2\left(\frac{1}{M_h^2 - s} + \frac{1}{M_h^2 - t} + \frac{1}{M_h^2 - u}\right) - 3\right] \tag{3.27c}$$

These amplitudes do not grow as $\mathcal{O}(s)$ at the TeV scale. Even worse, if we compare with eqs. 2.2 and 2.3 we will see a different. At high energy ($s \sim 1\,\text{TeV}^2$), the difference is a constant. This is due to the fact that we have neglected the couplings with the transverse modes of $W^{\pm}$ and Z, which should appear even when using the Equivalence Theorem. They give additional Feynman diagrams which account for the interchange of these virtual transverse modes. We have omitted them because their contribution at high energy is negligible, since it does not grow with $\mathcal{O}(s)$. Anyway, the scattering amplitudes 3.27

give a sensible order of magnitude of the effects that we have neglected, so that they will be used in sec. 3.3.4 for constraining the validity of our simplified effective Lagrangians (eqs. 2.31, 2.33, 2.34, 2.45 and 2.46).

Hence, at very high energies ($M_h \ll \sqrt{s}$), and when the amplitudes do grow with $\mathcal{O}(s)$ or $\mathcal{O}(s^2)$, the λ_3 and λ_4 couplings are weak, and the mass M_h is negligible. We will neglect them in this work. Thus, in the massless limit, and taking λ_3, $\lambda_4 \to 0$, eqs. 3.26 reduce to

$$A(s,t,u) = \frac{1-a^2}{v^2}s \tag{3.28}$$

$$M(s,t,u) = \frac{a^2-b}{v^2}s \tag{3.29}$$

$$T(s,t,u) = 0 \tag{3.30}$$

The complete NLO amplitude for the elastic scattering $\omega\omega \to \omega\omega$ has been reported by us in Ref. [35], with the LO plus tree-level NLO counterterms yielding

$$A^{(0)}(s,t,u) + A^{(1)}_{\text{tree}}(s,t,u) = (1-a^2)\frac{s}{v^2} + \frac{4}{v^4}\left[2a_5 s^2 + a_4(t^2+u^2)\right]. \tag{3.31}$$

The one-loop computation, rather lengthy because of the number of Feynman diagrams, was automated with the Mathematica programs FeynRules [142], FeynArts [143] and FormCalc [144, 145], which take a Lagrangian as input and give as output an analytical expression for the one-loop scattering amplitudes in terms of the Passarino-Veltman functions. For a proper definition of these functions, please see Appendix C. The NLO Feynman Diagrams for all the studied processes are in Appendix F. The value of the NLO scattering amplitude $\omega\omega \to \omega\omega$ is

$$A^{(1)}_{\text{loop}}(s,t,u) = \frac{1}{36(4\pi)^2 v^4}[f(s,t,u)s^2 + (1-a^2)^2(g(s,t,u)t^2 + g(s,u,t)u^2)] \tag{3.32}$$

with auxiliary functions

$$\begin{aligned} f(s,t,u) := {} & 4[9(a^2-b)^2 + 5(1-a^2)^2] + 6[3(a^2-b)^2 + 2(1-a^2)^2]N_\varepsilon \\ & - 18[(a^2-b)^2 + (1-a^2)^2]\log\left(\frac{-s}{\mu^2}\right) \\ & + 3(a^2-1)^2\left[\log\left(\frac{-t}{\mu^2}\right) + \log\left(\frac{-u}{\mu^2}\right)\right] \end{aligned} \tag{3.33}$$

$$g(s,t,u) := 26 + 12N_\varepsilon - 9\log\left(-\frac{t}{\mu^2}\right) - 3\log\left(-\frac{u}{\mu^2}\right) \tag{3.34}$$

where in dimensional regularization the $1/\epsilon = 1/(4-D)$ pole is contained in[6]

$$N_\epsilon = \frac{2}{\epsilon} + \log 4\pi - \gamma\ . \tag{3.35}$$

For the $\omega\omega \to hh$ scattering amplitude we find,

$$M^{(0)}_{\text{tree}}(s,t,u) + M^{(1)}_{\text{tree}}(s,t,u) = (a^2-b)\frac{s}{v^2} + \frac{2d}{v^4}s^2 + \frac{e}{v^4}(t^2+u^2) \tag{3.36}$$

[6]See Appendix C for an explanation.

that takes a one-loop correction:

$$M^{(1)}_{\text{loop}}(s,t,u) = \frac{a^2-b}{576\pi^2 v^2}\left[f'(s,t,u)\frac{s^2}{v^2} + \frac{a^2-b}{v^2}[g(s,t,u)t^2 + g(s,u,t)u^2]\right] \tag{3.37}$$

where

$$\begin{aligned} f'(s,t,u) = &-8[2(a^2-b) - 9(1-a^2)] - 6N_\varepsilon[(a^2-b) - 6(1-a^2)] \\ &+ 36(a^2-1)\log\left(-\frac{s}{\mu^2}\right) + 3(a^2-b)\left[\log\left(-\frac{t}{\mu^2}\right) + \log\left(-\frac{u}{\mu^2}\right)\right], \end{aligned} \tag{3.38}$$

and the function g is as defined in Eq. (3.34).

Finally, the $hh \to hh$ elastic amplitude is, at tree-level and keeping only the operator necessary to renormalize the one-loop part,

$$T^{(0)}(s,t,u) + T^{(1)}_{\text{tree}}(s,t,u) = \frac{2g}{v^4}(s^2+t^2+u^2)\ , \tag{3.39}$$

while the one-loop piece may be written in terms of only one function

$$T(s) = 2 + N_\varepsilon - \log\left(-\frac{s}{\mu^2}\right) \tag{3.40}$$

as

$$T^{(1)}_{\text{loop}}(s,t,u) = \frac{3(a^2-b)^2}{2(4\pi)^2 v^4}\left[T(s)s^2 + T(t)t^2 + T(u)u^2\right]\ . \tag{3.41}$$

The divergences N_ϵ from the one-loop amplitudes are unphysical and appear while we employ the unrenormalized parameters. We use the $\overline{\text{MS}}$ scheme to eliminate them and introduce the renormalized couplings as

$$a_4^r = a_4 + \frac{N_\epsilon}{192\pi^2}(1-a^2)^2 \tag{3.42a}$$

$$a_5^r = a_5 + \frac{N_\epsilon}{768\pi^2}[3(a^2-b)^2 + 2(1-a^2)^2] \tag{3.42b}$$

$$g^r = g + \frac{3N_\epsilon}{64\pi^2}(a^2-b)^2 \tag{3.42c}$$

$$d^r = d - \frac{N_\epsilon}{192\pi^2}(a^2-b)[(a^2-b) - 6(1-a^2)] \tag{3.42d}$$

$$e^r = e + \frac{N_\epsilon}{48\pi^2}(a^2-b)^2 \tag{3.42e}$$

Since the physical amplitudes cannot depend on the arbitrary scale μ,

$$\frac{d\,A_i}{d\,\mu} = 0 \quad \forall \text{ channel } i, \tag{3.43}$$

which is a renormalization-group evolution equation that determines the running of the NLO parameters with the scale. Interestingly, these evolution equations are decoupled

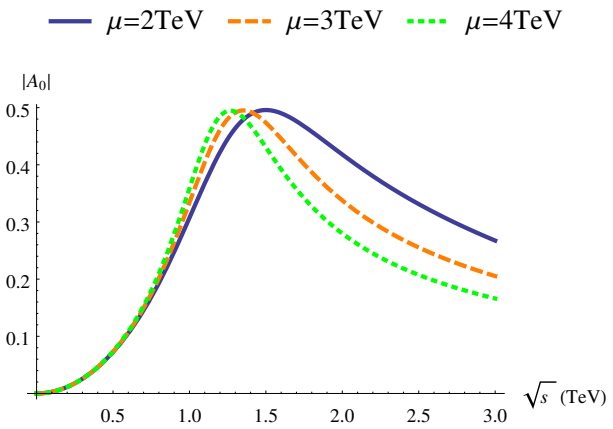

Figure 3.3: Dependence of the isoscalar elastic scattering amplitude on the renormalization parameter μ. Process $\omega\omega \to \omega\omega$, $I = J = 0$. Parameters $a^2 = 1$, $b = 2$ and all the other parameters set to zero. For $\sqrt{s} \lesssim 1.5\,\text{TeV}$, the amplitude is independent of μ. For higher energies, there is a slight dependence on μ.

(at NLO), and give the relations

$$a_4^r(\mu) = a_4^r(\mu_0) - \frac{1}{192\pi^2}(1-a^2)^2 \log\frac{\mu^2}{\mu_0^2} \tag{3.44a}$$

$$a_5^r(\mu) = a_5^r(\mu_0) - \frac{1}{768\pi^2}[3(a^2-b)^2 + 2(1-a^2)^2] \log\frac{\mu^2}{\mu_0^2} \tag{3.44b}$$

$$g^r(\mu) = g^r(\mu_0) - \frac{3}{64\pi^2}(a^2-b)^2 \log\frac{\mu^2}{\mu_0^2} \tag{3.44c}$$

$$d^r(\mu) = d^r(\mu_0) + \frac{1}{192\pi^2}(a^2-b)[(a^2-b) - 6(1-a^2)] \log\frac{\mu^2}{\mu_0^2} \tag{3.44d}$$

$$e^r(\mu) = e^r(\mu_0) - \frac{1}{48\pi^2}(a^2-b)^2 \log\frac{\mu^2}{\mu_0^2} \tag{3.44e}$$

In this work, unless otherwise stated, we have taken all the NLO parameters to the value at a scale $\mu = 3\,\text{TeV}$. This is motivated by the $\sqrt{s}/(4\pi v)$ expansion factor of the effective theory, which gives the maximum energy at which the predictions of the effective theory are reliable. v is the vacuum expectation value ($v \approx 246\,\text{GeV}$). See fig. 3.3 for a comparison of three different renormalization scales μ fixing all NLO couplings to zero. Putting all the parts together, the final NLO amplitudes for $\omega\omega \to \omega\omega$ scattering are

$$\begin{aligned} A(s,t,u) = {} & \frac{1}{v^2}(1-a^2)s + \frac{4}{v^4}\left[2a_5^r(\mu)s^2 + a_4^r(\mu)(t^2+u^2)\right] \\ & + \frac{1}{864\pi^2 v^4}\Big\{6[9(a^2-b)^2 + 5(1-a^2)^2]s^2 + 39(1-a^2)^2(t^2+u^2) \\ & - 27[(a^2-b)^2 + (1-a^2)^2]s^2 \log\frac{-s}{\mu^2} \\ & + 4(1-a^2)^2(s^2-3t^2-u^2)\log\frac{-t}{\mu^2} \\ & + 4(1-a^2)^2(s^2-t^2-3u^2)\log\frac{-u}{\mu^2}\Big\} \end{aligned} \tag{3.45}$$

For $\omega\omega \to hh$,

$$\begin{aligned} M(s,t,u) = &\frac{1}{v^2}(a^2-b)s + \frac{2}{v^4}d^r(\mu)s^2 + \frac{1}{v^4}e^r(\mu)(t^2+u^2) \\ &+ \frac{1}{576\pi^2 v^4}\left\{8[-2(a^2-b)+9(1-a^2)](a^2-b)s^2 + 26(a^2-b)^2(t^2+u^2)\right. \\ &- 36(a^2-b)(1-a^2)s^2\log\frac{-s}{\mu^2} \\ &+ 3(a^2-b)^2(s^2-3t^2-u^2)\log\frac{-t}{\mu^2} \\ &\left.+ 3(a^2-b)^2(s^2-t^2-3u^2)\log\frac{-u}{\mu^2}\right\} \end{aligned} \tag{3.46}$$

And, for the $hh \to hh$ amplitude,

$$\begin{aligned} T(s,t,u) = &\frac{2}{v^4}g^r(\mu)(s^2+t^2+u^2) + \frac{3}{32\pi^2 v^4}(a^2-b)^2\left[2(s^2+t^2+u^2)\right. \\ &\left.-s^2\log\frac{-s}{\mu^2} - t^2\log\frac{-t}{\mu^2} - u^2\log\frac{-u}{\mu^2}\right]. \end{aligned} \tag{3.47}$$

Finally, by crossing in eq. 3.46, we can also quote the $\omega h \to \omega h$ amplitude,

$$[T(\omega^a h \to \omega^b h)](s,t,u) = [T(\omega^a\omega^b \to hh)](t,s,u) = M(t,s,u)\delta_{a,b} \equiv M'(s,t,u)\delta_{a,b}, \tag{3.48}$$

where we have used that the would-be Goldstones $\omega^{a,b}$ are in the isospin basis (so that they are their own antiparticle). $M'(s,t,u)$ is the crossed $M(s,t,u)$ in eq. 3.46,

$$\begin{aligned} M'(s,t,u) = &\frac{1}{v^2}(a^2-b)t + \frac{2}{v^4}d^r(\mu)t^2 + \frac{1}{v^4}e^r(\mu)(s^2+u^2) \\ &+ \frac{1}{576\pi^2 v^4}\left\{8[-2(a^2-b)+9(1-a^2)](a^2-b)t^2 + 26(a^2-b)^2(s^2+u^2)\right. \\ &- 36(a^2-b)(1-a^2)t^2\log\frac{-t}{\mu^2} \\ &+ 3(a^2-b)^2(t^2-3s^2-u^2)\log\frac{-s}{\mu^2} \\ &\left.+ 3(a^2-b)^2(t^2-s^2-3u^2)\log\frac{-u}{\mu^2}\right\}. \end{aligned} \tag{3.49}$$

Thus,

$$T(\omega^a h \to \omega^b h) = M'(s,t,u)\delta_{a,b}, \tag{3.50}$$

where $M'(s,t,u)$ is defined in eq. 3.49.

3.2.2 $\gamma\gamma$ scattering

The amplitudes for $\gamma\gamma$ scattering, computed by us in ref. [36], provide a good example of the equivalence between the two parameterizations considered for the $SU(2)$ coset (spherical and exponential) as they are equal. In both $\gamma\gamma \to zz$ and $\gamma\gamma \to \omega^+\omega^-$ cases, the amplitudes can be decomposed as

$$\mathcal{M} = iT = ie^2\left(\epsilon_1^\mu\epsilon_2^\nu T_{\mu\nu}^{(1)}\right)A + ie^2\left(\epsilon_1^\mu\epsilon_2^\nu T_{\mu\nu}^{(2)}\right)B, \tag{3.51}$$

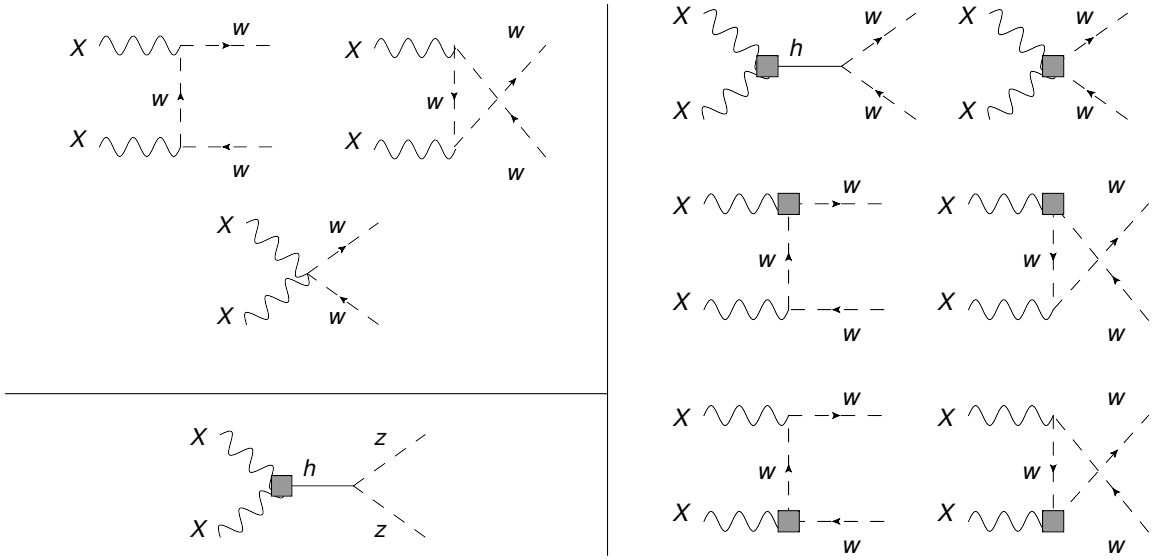

Figure 3.4: Up and middle left, three LO diagrams for $\gamma\gamma \to \omega^+\omega^-$ at order $\mathcal{O}(e^2)$. On the right, diagrams for the same process at order $\mathcal{O}(e^2p^2)$. Lowest left, unique LO diagram for process $\gamma\gamma \to zz$, order $\mathcal{O}(e^2p^2)$. Figures taken from Ref. [36]. The NLO diagrams for $\gamma\gamma$ scattering can be found in Appendix F.

the two Lorentz structures being

$$\left(\epsilon_1^\mu \epsilon_2^\nu T^{(1)}_{\mu\nu}\right) = \frac{s}{2}(\epsilon_1\epsilon_2) - (\epsilon_1 k_2)(\epsilon_2 k_1) \tag{3.52}$$

$$\begin{aligned}\left(\epsilon_1^\mu \epsilon_2^\nu T^{(2)}_{\mu\nu}\right) &= 2s(\epsilon_1\Delta)(\epsilon_2\Delta) - (t-u)^2(\epsilon_1\epsilon_2) \\ &\quad - 2(t-u)[(\epsilon_1\Delta)(\epsilon_2 k_1) - (\epsilon_1 k_2)(\epsilon_2\Delta)].\end{aligned} \tag{3.53}$$

Here, $e = \sqrt{\alpha/4\pi} \approx 0.303$ is the electric charge; ϵ_i and k_i, the polarization state and the 4-momentum of each photon $i = 1, 2$; p_i, the 4-momenta of the Gauge boson $i = 1, 2$; and $\Delta^\mu = p_1^\mu - p_2^\mu$.

For the $\gamma\gamma \to zz$ process, at order $\mathcal{O}(e^2)$ in the chiral expansion, we have a vanishing leading order amplitude,

$$\mathcal{M}(\gamma\gamma \to zz)_{\rm LO} = 0. \tag{3.54}$$

The NLO contribution [order $\mathcal{O}(p^2e^2)$] is

$$A(\gamma\gamma \to zz)_{\rm NLO} = \frac{2ac^r_\gamma}{v^2} + \frac{a^2-1}{4\pi^2 v^2} \tag{3.55a}$$

$$B(\gamma\gamma \to zz)_{\rm NLO} = 0. \tag{3.55b}$$

For $\gamma\gamma \to \omega^+\omega^-$ (the other process allowed by charge conservation), at order $\mathcal{O}(e^2)$,

$$A(\gamma\gamma \to \omega^+\omega^-)_{\rm LO} = 2sB(\gamma\gamma \to \omega^+\omega^-) = -\frac{1}{t} - \frac{1}{u}, \tag{3.56}$$

whereas, at order $\mathcal{O}(p^2e^2)$ (NLO),

$$A(\gamma\gamma \to \omega^+\omega^-)_{\rm NLO} = \frac{8(a_1^r - a_2^r + a_3^r)}{v^2} + \frac{2ac^r_\gamma}{v^2} + \frac{a^2-1}{8\pi^2 v^2} \tag{3.57a}$$

$$B(\gamma\gamma \to \omega^+\omega^-)_{\rm NLO} = 0. \tag{3.57b}$$

It is very interesting that for both channels and in dimensional regularization, the UV divergences cancel in the end, so that no renormalization is required at all. Although this is a feature of the NLO computation, in ref. [146] an explanation in terms of a projection of Effective Field Theories (EFTs) to SUSY formalism can be found. Thus,

$$c_\gamma^r = c_\gamma \tag{3.58a}$$
$$a_i^r = a_i \quad \forall i = 1,\, 2,\, 3 \tag{3.58b}$$

As for $\omega\omega$ scattering, the NLO diagrams for the $\gamma\gamma$ scattering can be found on app. F. We will use the following notation for the parameterization of the initial and final states,

$$[\gamma(\epsilon_1^\pm, k_1), \gamma(\epsilon_2^\pm, k_2)] \to [\omega/h(p_1), \omega/h(p_2)], \tag{3.59}$$

where $\epsilon_i^\pm$ $(i = 1,\, 2)$ are the polarization vectors; k_i, the 4-momenta of the incoming photons; and p_i the 4-momenta of the outgoing WBGBs. Without loss of generality, we can choose the next parameterization for the momenta,

$$k_1 = (E, 0, 0, E) \quad k_2 = (E, 0, 0, -E) \tag{3.60a}$$
$$p_1 = (E, \vec{p}) \quad p_2 = (E, -\vec{p}) \quad \Delta = p_1 - p_2 \tag{3.60b}$$
$$\vec{p} = (p_x, p_y, p_z) = (\sin\theta\cos\varphi, \sin\theta\sin\varphi, \cos\theta). \tag{3.60c}$$

The 4-dimensional polarization states $\epsilon_i^\pm$ are transverse, that is,

$$\epsilon_i^\pm \cdot k_i = 0, \quad i = 1,\, 2. \tag{3.61}$$

Note also that, because we are taking $\vec{k}_1 \parallel \vec{k}_2$,

$$\epsilon_1^\pm \cdot k_2 = \epsilon_2^\pm \cdot k_1 = 0. \tag{3.62}$$

With these conditions, the Lorentz structure of eq. 3.52 becomes

$$\left(\epsilon_1^\mu \cdot \epsilon_2^\nu T_{\mu\nu}^{(1)}\right) = \frac{s}{2}\epsilon_1 \cdot \epsilon_2. \tag{3.63}$$

And the one of eq. 3.53,

$$\left(\epsilon_1^\mu \cdot \epsilon_2^\nu T_{\mu\nu}^{(2)}\right) = 2s(\epsilon_1 \cdot \Delta)(\epsilon_2 \cdot \Delta) - (t-u)^2\epsilon_1 \cdot \epsilon_2. \tag{3.64}$$

Provided that the WBGBs can be considered to be massless, taking into account eqs. A.16 and A.17,

$$(t-u)^2 = \left[-\frac{s}{2}(1-\cos\theta) + \frac{s}{2}(1+\cos\theta)\right]^2 = s^2\cos^2\theta, \tag{3.65}$$

so that eq. 3.64 becomes

$$\left(\epsilon_1^\mu \cdot \epsilon_2^\nu T_{\mu\nu}^{(2)}\right) = 2s(\epsilon_1 \cdot \Delta)(\epsilon_2 \cdot \Delta) - s^2(\cos\theta)^2(\epsilon_1 \cdot \epsilon_2). \tag{3.66}$$

The final election for the polarization states $\epsilon_i^\pm$, following ref. [138], is

$$\epsilon_1^\pm = \frac{1}{\sqrt{2}}(0, \mp 1, -i, 0) \tag{3.67a}$$
$$\epsilon_2^\pm = \frac{1}{\sqrt{2}}(0, \mp 1, i, 0)\ . \tag{3.67b}$$

By using eqs. 3.67, the following orthogonality relations are obtained,

$$\epsilon_1^+ \cdot \epsilon_2^+ = \frac{1}{2}(0-1-1+0) = -1 \tag{3.68a}$$

$$\epsilon_1^- \cdot \epsilon_2^- = \frac{1}{2}(0-1-1+0) = -1 \tag{3.68b}$$

$$\epsilon_1^+ \cdot \epsilon_2^- = \frac{1}{2}(0+1-1+0) = 0 \tag{3.68c}$$

$$\epsilon_1^- \cdot \epsilon_2^+ = \frac{1}{2}(0+1-1+0) = 0\ . \tag{3.68d}$$

If eqs. 3.60 are also considered,

$$\epsilon_1^+ \cdot \Delta = \sqrt{2}(p_x + ip_y) = \sqrt{2}E\sin\theta e^{i\varphi} \tag{3.69a}$$

$$\epsilon_1^- \cdot \Delta = \sqrt{2}(-p_x + ip_y) = -\sqrt{2}E\sin\theta e^{-i\varphi} \tag{3.69b}$$

$$\epsilon_2^+ \cdot \Delta = \sqrt{2}(p_x - ip_y) = \sqrt{2}E\sin\theta e^{-i\varphi} \tag{3.69c}$$

$$\epsilon_2^- \cdot \Delta = \sqrt{2}(-p_x - ip_y) = -\sqrt{2}E\sin\theta e^{i\varphi}\ . \tag{3.69d}$$

Thus, taking into account that $s = 4E^2$ (app. A.3), the Lorentz structures (eqs. 3.63 and 3.66) become those shown on table 3.2.

$(\lambda_1\lambda_2)$	$(++)$	$(+-)$	$(-+)$	$(--)$
$\epsilon_1^\mu \cdot \epsilon_2^\nu T_{\mu\nu}^{(1)}$	$-s/2$	0	0	$-s/2$
$\epsilon_1^\mu \cdot \epsilon_2^\nu T_{\mu\nu}^{(2)}$	s^2	$-s^2(\sin\theta)^2 e^{2i\varphi}$	$-s^2(\sin\theta)^2 e^{-2i\varphi}$	s^2

Table 3.2: Lorentz structures $\epsilon_1^\mu \cdot \epsilon_2^\nu T_{\mu\nu}^{(1)}$ and $\epsilon_1^\mu \cdot \epsilon_2^\nu T_{\mu\nu}^{(2)}$ (eqs. 3.63 and 3.66).

For simplicity, we introduce the notation

$$T_{N,C}^{\lambda_1\lambda_2} = e^2 e^{i(\lambda_1-\lambda_2)\varphi} H_{\lambda_1\lambda_2}^{N,C}(s,t), \tag{3.70}$$

where N and C indicate, respectively, zz (neutral) and $\omega^+\omega^-$ (charged) final states. Note that both Lorentz structures $\epsilon_1^\mu \cdot \epsilon_2^\nu T_{\mu\nu}^{(1)}$ and $\epsilon_1^\mu \cdot \epsilon_2^\nu T_{\mu\nu}^{(2)}$ (table 3.2) and the LO and NLO coefficients $A(s,t,u)$, $B(s,t,u)$, which correspond to $\gamma\gamma \to \omega^+\omega^-$ (eqs. 3.56 and 3.57) are invariant under the permutation of t and u. That is, under the transformation $\theta \to \pi - \theta$. Thus, $\mathcal{M}(\gamma\gamma \to \omega^+\omega^-)_{\mathrm{LO,NLO}} = \mathcal{M}(\gamma\gamma \to \omega^-\omega^+)_{\mathrm{LO,NLO}}$.

With this notation, and considering both eq. 3.51 and table 3.2,

$$H_{N,C}^{++} = H_{N,C}^{--} = -\frac{s}{2}A_{\mathrm{LO+NLO},N,C}(s,t,u) + s^2 B_{\mathrm{LO+NLO},N,C}(s,t,u) \tag{3.71}$$

$$H_{N,C}^{+-} = H_{N,C}^{-+} = -s^2(\sin\theta)^2 B_{\mathrm{LO+NLO},N,C}(s,t,u), \tag{3.72}$$

where LO + NLO has been used to denote the sum of both the LO and the NLO terms. For the zz state (N), $A_{\mathrm{LO},N} = B_{\mathrm{LO},N} = 0$ (eq. 3.54). Thus, if we define (eq. 3.55a)

$$A_N \equiv A_{\mathrm{NLO},N}(s,t,u) = \frac{2ac_\gamma^r}{v^2} + \frac{a^2-1}{4\pi^2 v^2}, \tag{3.73}$$

and take into account that $B_{\mathrm{NLO},N}(s,t,u) = 0$ (eq. 3.55b), then

$$H_N^{++} = H_N^{--} = -\frac{s}{2}A_N, \quad H_N^{+-} = H_N^{-+} = 0 \tag{3.74}$$

Now, let us take eq. 3.56 and compute the LO contribution to $H_C^{++} = H_C^{--}$ (eq. 3.71) with the Lorentz structures of table 3.2,

$$H_{\mathrm{LO},C}^{++} = H_{\mathrm{LO},C}^{--} = -\frac{s}{2}A_{\mathrm{LO},C}(s,t,u) + s^2 B_{\mathrm{LO},C}(s,t,u)$$
$$= -\frac{s}{2}\left(-\frac{1}{t}-\frac{1}{u}\right) + s^2\frac{1}{2s}\left(-\frac{1}{t}-\frac{1}{u}\right) = 0. \quad (3.75)$$

Thus, taking into account that $B_{\mathrm{NLO},C}(s,t,u) = 0$ (eq. 3.57b, and defining (eq. 3.55a)

$$A_C \equiv A_{\mathrm{NLO},C}(s,t,u) = \frac{8(a_1^r - a_2^r + a_3^r)}{v^2} + \frac{2ac_\gamma^r}{v^2} + \frac{a^2-1}{8\pi^2 v^2}, \quad (3.76)$$

we have that

$$H_C^{++} = H_C^{--} = -\frac{s}{2}A_C. \quad (3.77)$$

Finally, let us compute $H_C^{+-} = H_C^{-+}$. Considering eqs. 3.72, 3.56 and 3.57b, and table 3.2, it can be seen that only the LO contribution survives. Thus,

$$H_C^{+-} = H_C^{-+} = -s^2(\sin\theta)^2\frac{1}{2s}\left(-\frac{1}{t}-\frac{1}{u}\right) = \frac{s}{2}\frac{t+u}{tu}\sin^2\theta \quad (3.78)$$

Now, because the initial state particles (photons) are massless (eqs. A.16 and A.17),

$$\frac{t+u}{tu} = \frac{-s}{\frac{s^2}{4}(1-\cos^2\theta)} = -\frac{4}{s}\frac{1}{\sin^2\theta}. \quad (3.79)$$

Substituting in eq. 3.78,

$$H_C^{+-} = H_C^{-+} = -2. \quad (3.80)$$

Now, let us take the isospin basis $|I, M_I\rangle$ of table 3.1 for the final $\omega\omega$ state. Because of both charge conservation (only $\omega^+\omega^-$, $\omega^-\omega^+$ and zz are possible in the final state) and the invariance of the matrix element under permutation of the final state particles (Bose symmetry), only 2 states give a non-vanishing contribution,

$$|0,0\rangle = -\frac{1}{\sqrt{3}}\left(\left|\omega^+\omega^-\right\rangle + \left|\omega^-\omega^+\right\rangle + |zz\rangle\right) \quad (3.81)$$

$$|2,0\rangle = \frac{1}{\sqrt{6}}\left(2\,|zz\rangle - \left|\omega^+\omega^-\right\rangle - \left|\omega^-\omega^+\right\rangle\right). \quad (3.82)$$

If we take the definition

$$T_I^{\lambda_1\lambda_2} \equiv \langle I, 0\,|\,T\,|\,\lambda_1\lambda_2\rangle\,, \quad (3.83)$$

then

$$T_0^{\lambda_1\lambda_2} = -\frac{1}{\sqrt{3}}\left(2T_C^{\lambda_1\lambda_2} + T_N^{\lambda_1\lambda_2}\right) \quad (3.84)$$

$$T_2^{\lambda_1\lambda_2} = \frac{2}{\sqrt{6}}\left(T_N^{\lambda_1\lambda_2} - T_C^{\lambda_1\lambda_2}\right). \quad (3.85)$$

Taking into account ecs. 3.70, 3.74, 3.77 and 3.80,

$$T_0^{++} = T_0^{--} = \frac{e^2 s}{2\sqrt{3}}\,(2A_C + A_N) \tag{3.86a}$$

$$T_0^{+-} = (T_0^{-+})^* = \frac{4e^2}{\sqrt{3}} e^{2i\varphi} \tag{3.86b}$$

$$T_2^{++} = T_2^{--} = \frac{e^2 s}{\sqrt{6}}\,(A_C - A_N) \tag{3.86c}$$

$$T_2^{+-} = (T_2^{-+})^* = \frac{4e^2}{\sqrt{6}} e^{2i\varphi} \tag{3.86d}$$

And, for the crossed-channel $\gamma\gamma \to hh$ scattering amplitude $R(\gamma\gamma \to hh)$, also required for the unitarization below in subsec. 4.4,

$$R(\gamma\gamma \to hh) = -\frac{e^2}{8\pi^2 v^2}(a^2 - b)(\epsilon_1 \cdot \epsilon_2). \tag{3.87}$$

This is an NLO scattering amplitude. The LO one vanishes. According to eqs. 3.68, for the polarization states of eq. 3.67, this scattering amplitude turns into

$$R(\gamma\gamma \to hh) = \frac{e^2}{8\pi^2 v^2}(a^2 - b)\delta_{\lambda_1,\lambda_2}. \tag{3.88}$$

Thus, the final state is $|hh\rangle$, which is an isospin singlet state,

$$R_0^{++} = R_0^{--} = \langle hh\,|\,R(\gamma\gamma \to hh)\,|\,{+}{+}\rangle = \frac{e^2}{8\pi^2 v^2}(a^2 - b) \tag{3.89}$$

Lastly, it is also worth to remark that the one-loop contributions in our final results show up in the form $(1-a^2)E^2/(16\pi^2 v^2)$. Since the present fits to LHC data [127, 128] suggest a value of a close to one, these corrections are surprisingly suppressed with respect to the naively expected $E^2/(16\pi^2 v^2)$ contributions, typically occurring from chiral loops of chiral effective field theories. We believe that the origin of the simplicity of our results in eqs. 3.86 and 3.89 could be relying on the custodially symmetric structure of the theory and an enlarged symmetry of the dynamical boson sector (h, $w^\pm$ z) that arises in the relevant Lagrangian for $\gamma\gamma \to w^a w^b$ in the massless Higgs limit. This simplicity may also be related to the fact that, when using dimensional regularization, the UV divergences cancel for all the channels, $\gamma\gamma \to zz$, $\omega\omega$, hh.

3.2.3 $t\bar{t}$ in the final state

In this section, which expands our ref. [136], we are interested in the processes $V_L V_L \to t\bar{t}$ ($V = W, Z$) and $hh \to t\bar{t}$, at high energies compared with M_Z, M_W and M_h. In this case, we can use the ET and concentrate only in the GB, h and the b and t quarks. At TeV energies the top quark mass is small. More specifically, we will consider the regime $M_t^2/v^2 \ll \sqrt{s}M_t/v^2 \ll s/v^2$. Then, it is not difficult to see that this is equivalent to neglecting diagrams with internal top lines at the one-loop level. At tree level (see fig. 3.5), the scattering amplitude is given by:

$$\mathcal{Q}_{\rm LO}\left(\omega^a\omega^b \to t^{\lambda_1}\bar{t}^{\lambda_2}\right) = \sqrt{3}\left(1 - ac_1 + \frac{g_t}{2}\frac{s}{v^2}\right)\frac{M_t}{v^2}\bar{u}^{\lambda_1}(p_1)v^{\lambda_2}(p_2)\delta_{ab} \tag{3.90}$$

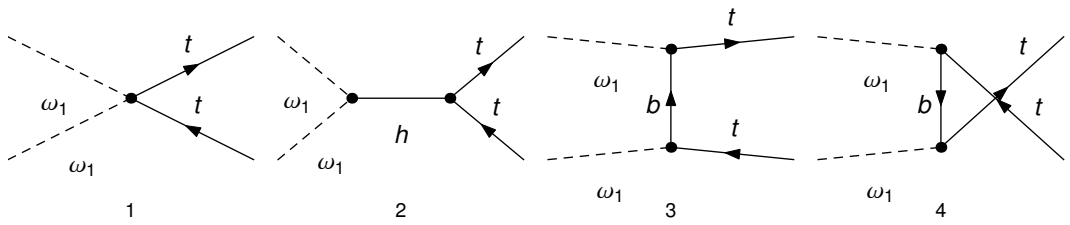

Figure 3.5: LO contributions to the process $\omega\omega \to t\bar{t}$

where a and b are the custodial isospin indices of the incoming GB p_1 and p_2 and λ_1 and λ_2 are top and antitop momenta and helicities respectively.

Note that the $\sqrt{3}$ factor included in eq. 3.90 is a color factor. Taking into account that the initial state is a color singlet, the $t\bar{t}$ final state must be also a color singlet,

$$|t\bar{t}\rangle = \frac{1}{\sqrt{3}} \sum_{c=1}^{3} |t_c \bar{t}_c\rangle \,. \tag{3.91}$$

This $\sqrt{3}$ color factor can be exposed with a redefinition of $\mathcal{T}$,

$$\mathcal{T} \, |t\bar{t}\rangle \equiv \sqrt{3}\mathcal{T}' \, |t_1 \bar{t}_1\rangle \,, \tag{3.92}$$

and it will be explicit in all of the next equations.

Next, we consider the one-loop contributions. The Feynmann diagrams contributing to this order can be found in appendix F.3.1. By using dimensional regularization (see appendix C) the result is:

$$\mathcal{Q}^{\mathrm{NLO}} \left(\omega^a \omega^b \to t^{\lambda_1} \bar{t}^{\lambda_2}\right) = \sqrt{3} \frac{s}{(4\pi)^2 v^2} \left[(1 - ac_1)(1 - a^2) + c_2(b - a^2)\right] \cdot \\ \cdot \left(N_\varepsilon + 2 - \log \frac{-s}{\mu^2}\right) \frac{M_t}{v^2} \bar{u}^{\lambda_1} v^{\lambda_2} \delta_{ab}, \tag{3.93}$$

where, as usual,

$$N_\varepsilon = \frac{2}{\varepsilon} + \log 4\pi - \gamma, \tag{3.94}$$

and μ is an arbitrary renormalization scale. Hence, the sum of the two contributions is

$$\mathcal{Q}\left[\omega^a \omega^b \to t^{\lambda_1} \bar{t}^{\lambda_2}\right] = \sqrt{3} \left[Q_{\mathrm{LO}}(s) + Q_{\mathrm{NLO}}(s)\right] \frac{M_t}{v^2} \bar{u}^{\lambda_1} v^{\lambda_2} \delta_{ab}, \tag{3.95}$$

where

$$Q_{\mathrm{LO}}(s) = 1 - ac_1 + \frac{g_t}{2} \frac{s}{v^2} \tag{3.96}$$

$$Q_{\mathrm{NLO}}(s) = \frac{s}{(4\pi)^2 v^2} C_t \left(N_\varepsilon + 2 - \log \frac{-s}{\mu^2}\right), \tag{3.97}$$

and

$$C_t = (1 - ac_1)(1 - a^2) + c_2(b - a^2). \tag{3.98}$$

The divergence in this amplitude can be absorbed by renormalizing the g_t coupling. Using the $\overline{MS}$ renormalization scheme, we define

$$g_t^r = g_t + \frac{C_t}{8\pi^2} N_\epsilon \tag{3.99}$$

and consequently

$$Q_{\rm LO}(s) + Q_{\rm NLO}(s) = 1 - ac_1 + \frac{s}{v^2}\left[\frac{g_t^r}{2} + \frac{C_t}{(4\pi)^2}\left(2 - \log\frac{-s}{\mu^2}\right)\right]. \tag{3.100}$$

Moreover, in the absence of wave or mass renormalization, amplitudes must be observable, and hence μ-independent; so we require that total derivatives of the amplitude with respect to $\log\mu^2$ vanish,

$$\frac{d\left[Q_{\rm LO}(s) + Q_{\rm NLO}(s)\right]}{d\log\mu^2} = \frac{s}{v^2}\left[\frac{1}{2}\frac{dg_t^r}{d\log\mu^2} + \frac{C_t}{(4\pi)^2}\right] = 0. \tag{3.101}$$

Then, the renormalization equation for g_t^r reads

$$\frac{dg_t^r}{d\log\mu^2} = -\frac{C_t}{8\pi^2}, \tag{3.102}$$

which can be integrated to give

$$g_t^r(\mu) = g_t^r(\mu_0) - \frac{C_t}{8\pi^2}\log\left(\frac{\mu^2}{\mu_0^2}\right). \tag{3.103}$$

On the other hand, the different spinor helicity combinations appearing in the amplitudes in eq. 3.95 are[7]

$$\bar{u}^+(p_1)\, v^+(p_2) = +\sqrt{s - 4M_t^2} = +\sqrt{s} + \mathcal{O}\left(\frac{M_t^2}{s}\right). \tag{3.104a}$$

$$\bar{u}^+(p_1)\, v^-(p_1) = 0. \tag{3.104b}$$

$$\bar{u}^-(p_1)\, v^+(p_2) = 0. \tag{3.104c}$$

$$\bar{u}^-(p_1)\, v^-(p_2) = -\sqrt{s - 4M_t^2} = -\sqrt{s} + \mathcal{O}\left(\frac{M_t^2}{s}\right). \tag{3.104d}$$

Therefore, the tree level amplitude is of order of $\sqrt{s}M_t/v^2$, and the one-loop is of order $s\sqrt{s}M_t/v^4$, where we have neglected higher order powers on M_t^2/s. Thus, the amplitude $\omega^a\omega^b \to t\bar{t}$ is given by

$$\mathcal{Q}\left(\omega^a\omega^b \to t^+\bar{t}^+\right) = \sqrt{3}\left[Q_{\rm LO}(s) + Q_{\rm NLO}(s)\right]\frac{M_t\sqrt{s}}{v^2}\delta_{ab} \tag{3.105a}$$

$$\mathcal{Q}\left(\omega^a\omega^b \to t^-\bar{t}^-\right) = -\mathcal{Q}\left(\omega^a\omega^b \to t^+\bar{t}^+\right) \tag{3.105b}$$

$$\mathcal{Q}\left(\omega^a\omega^b \to t^-\bar{t}^+\right) = \mathcal{Q}\left(\omega^a\omega^b \to t^+\bar{t}^-\right) = 0, \tag{3.105c}$$

where

$$\begin{aligned}\mathcal{Q}\left(\omega^a\omega^b \to t^+\bar{t}^+\right) =& \sqrt{3}\left[Q_{\rm LO}(s) + Q_{\rm NLO}(s)\right]\frac{M_t\sqrt{s}}{v^2}\delta_{ab} \\ =& \sqrt{3}\frac{M_t\sqrt{s}}{v^2}(1 - ac_1)\delta_{ab} \\ &+ \sqrt{3}\frac{s\sqrt{s}M_t}{v^4}\left[\frac{g_t^r(\mu)}{2} + \frac{C_t}{16\pi^2}\left(2 - \log\frac{-s}{\mu^2}\right)\right]\delta_{ab}\end{aligned} \tag{3.106}$$

[7] See appendix B.1 for a proof of these relations.

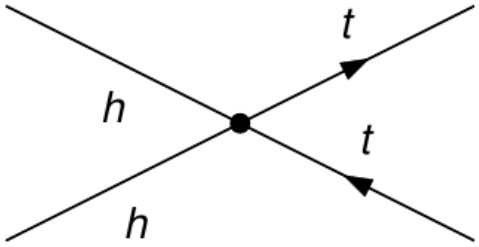

Figure 3.6: Contribution at LO to $hh \to t\bar{t}$ annihilation

In a similar way the $hh \to t\bar{t}$ annihilation can be considered. Note also the introduction of a $\sqrt{3}$ color factor and, since our final state is also $t\bar{t}$, the validity of eqs. 3.104 applied to $hh \to t\bar{t}$ scattering.

The diagramatic contribution (direct vertex) to the LO $hh \to t\bar{t}$ amplitude is depicted in fig. 3.6. Then, it is easy to verify that the tree level amplitude $hh \to t\bar{t}$, $\mathcal{N}_{\text{LO}}$, is

$$\mathcal{N}_{\text{LO}}\left(hh \to t^{\lambda_1}\bar{t}^{\lambda_2}\right) = \sqrt{3}\left(-\frac{2c_2 M_t}{v^2} + \frac{g_t' s M_t}{2v^4}\right)\bar{u}^{\lambda_1}(p_1)\, v^{\lambda_2}(p_2) \tag{3.107}$$

At the one loop level the scattering amplitude, $\mathcal{N}_{\text{NLO}}$, is given by the diagrams in appendix F.3.2, which amount to

$$\begin{aligned}\mathcal{N}_{\text{NLO}}\left(hh \to t^{\lambda_1}\bar{t}^{\lambda_2}\right) = \\ -\sqrt{3}\frac{3sM_t}{32\pi^2 v^4}(b-a^2)(1-ac_1)\left(N_\varepsilon + 2 - \log\frac{-s}{\mu^2}\right)\bar{u}^{\lambda_1}(p_1)\, v^{\lambda_2}(p_2)\end{aligned} \tag{3.108}$$

Then the tree plus the one-loop amplitude is

$$\begin{aligned}\mathcal{N}\left(hh \to t^{\lambda_1}\bar{t}^{\lambda_2}\right) =& \sqrt{3}\left\{-2c_2 + \frac{s}{v^2}\left[\frac{g_t'}{2} - \frac{3}{32\pi^2}(b-a^2)(1-ac_1)\left(N_\varepsilon + 2 - \log\frac{-s}{\mu^2}\right)\right]\right\}\cdot \\ & \cdot \bar{u}^{\lambda_1}(p_1)\, v^{\lambda_2}(p_2) \\ =& \sqrt{3}\left\{-2c_2 + \frac{s}{v^2}\left[\frac{g_t'^r}{2} - \frac{3}{32\pi^2}(b-a^2)(1-ac_1)\left(2 - \log\frac{-s}{\mu^2}\right)\right]\right\}\cdot \\ & \cdot \bar{u}^{\lambda_1}(p_1)\, v^{\lambda_2}(p_2)\end{aligned} \tag{3.109}$$

The renormalized coupling $g_t'^r$ is obviously defined as:

$$g_t'^r = g_t' - \frac{3C_t'}{(4\pi)^2}N_\varepsilon \tag{3.110}$$

where

$$C_t' = (b-a^2)(1-ac_1). \tag{3.111}$$

Again, the lack of wave function renormalization at this level requires this amplitude to be scale independent. Thus the coupling dependence on μ is given by:

$$\frac{dg_t'^r}{d\log\mu^2} = \frac{3C_t'}{(4\pi)^2}. \tag{3.112}$$

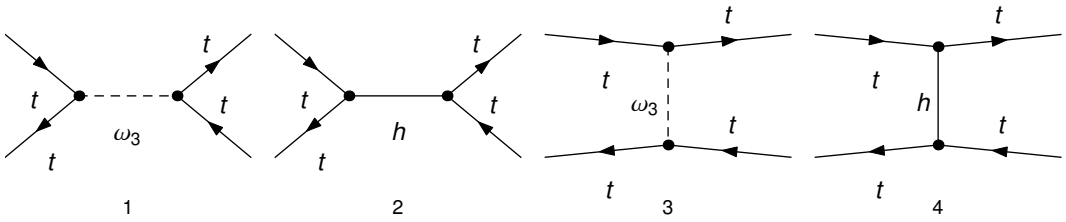

Figure 3.7: LO contribution to $t\bar{t} \to t\bar{t}$ elastic scattering.

By integrating (3.112), the renormalized coupling evolves with the scale as

$$g_t'^r(\mu) = g_t'^r(\mu_0) + \frac{3C_t'}{(4\pi)^2} \log\left(\frac{\mu^2}{\mu_0^2}\right). \tag{3.113}$$

In a way similar to that in the would-be GB case (eq. 3.105b), we get for the amplitudes in eq. 3.109,

$$\mathcal{N}\left(hh \to t^-\bar{t}^-\right) = -\mathcal{N}\left(hh \to t^+\bar{t}^+\right) \tag{3.114}$$

$$\mathcal{N}\left(hh \to t^-\bar{t}^+\right) = \mathcal{N}\left(hh \to t^+\bar{t}^-\right) = 0, \tag{3.115}$$

where

$$\mathcal{N}\left(hh \to t^+\bar{t}^+\right) = -2\sqrt{3}c_2\frac{M_t\sqrt{s}}{v^2} + \sqrt{3}\frac{s}{v^2}\left[\frac{g_t'^r(\mu)}{2} - \frac{3C_t'}{32\pi^2}\left(2 - \log\frac{-s}{\mu^2}\right)\right]\frac{M_t\sqrt{s}}{v^2}. \tag{3.116}$$

The final state $t\bar{t}$ will be in a helicity state

$$|S=1, S_z=0\rangle = \frac{1}{\sqrt{2}}\left(\left|t^+\bar{t}^+\right\rangle - \left|t^-\bar{t}^-\right\rangle\right), \tag{3.117}$$

having taken into account that the only non-vanishing contributions to the scattering amplitude come from the polarizations $\lambda_1\lambda_2 = ++$ and $--$, and that the substitution $++ \to --$ produces a change of sign in the scattering amplitude, just as in eqs. 3.105b and 3.114. Note that we have no $t\bar{b}$ or $\bar{t}b$ on the final state, according to the LO and NLO computations. Actually, these vertices are supressed by a factor which is proportional to the mass of the bottom quark, $M_b \approx 4.18\,\text{GeV} \ll M_t, M_h, v \sim 10^2\,\text{GeV}$.

3.2.4 $t\bar{t} \to t\bar{t}$ scattering amplitude

For completeness, though not strictly needed to order $\mathcal{O}(M_t/v)$ in the $(M_t, \sqrt{s})$ counting, we compute the elastic $t\bar{t}$ process, at least at the LO (see fig. 3.7 for the Feynman diagrams). By using the obvious notation $u^{\lambda_i}(p_i) = u_i$ and $v^{\lambda_i}(p_i) = u_i$ with $i = 1, 2, 3, 4$ the amplitude $1, 2 \to 3, 4$ is given by

$$\mathcal{S}(t\bar{t} \to t\bar{t}) = -3c_1^2\frac{M_t^2}{v^2 s}\bar{u}_3 v_4 \bar{v}_2 u_1 - 3c_1^2\frac{M_t^2}{v^2 t}\bar{u}_3 u_1 \bar{v}_2 v_4 + 3\frac{M_t^2}{v^2 s}\bar{u}_3\gamma^5 v_4 \bar{v}_2\gamma^5 u_1 + 3\frac{M_t^2}{v^2 t}\bar{u}_3\gamma^5 u_1 \bar{v}_2\gamma^5 v_4. \tag{3.118}$$

Note the color factor 3 introduced on eq. 3.118; it is easily computed considering that both the initial and final $t\bar{t}$ states are color singlets. The spinor chains which appear

in eq. 3.118 are in turn computed on appendix B.2. Once substituted in eq. 3.118, and taking into account the limit $s \gg M_t^2$, eq. 3.118 turns into

$$\mathcal{S}(t^+\bar{t}^+ \to t^+\bar{t}^+) = -\frac{3M_t^2(1+c_1^2)}{v^2} \tag{3.119a}$$

$$\mathcal{S}(t^-\bar{t}^- \to t^-\bar{t}^-) = \mathcal{S}(t^+\bar{t}^+ \to t^+\bar{t}^+) \tag{3.119b}$$

$$\mathcal{S}(t^+\bar{t}^- \to t^-\bar{t}^+) = \frac{3M_t^2(1+c_1^2)}{v^2} e^{2i\phi} \tag{3.119c}$$

$$\mathcal{S}(t^-\bar{t}^+ \to t^+\bar{t}^-) = \left[\mathcal{S}(t^+\bar{t}^- \to t^-\bar{t}^+)\right]^* . \tag{3.119d}$$

All the other helicity combinations give a vanishing scattering amplitude. Note the subleading order of this amplitude [$\mathcal{S} \sim \mathcal{O}(M_t^2/v^2)$]; thus this is confirmed by explicit calculation. Even more, because of eq. 3.119b, if we consider the $|S=1, S_z=0\rangle$ helicity state (eq. 3.117), the scattering amplitude vanishes.

3.3 Partial wave decomposition

We will study the partial wave decomposition of the matrix elements described in sections 3.1 and 3.2, with normalization

$$F_{IJ}^{\lambda_1\lambda_2}(s) = \frac{1}{64\pi^2 K}\sqrt{\frac{4\pi}{2J+1}} \int d\Omega\, A_I^{\lambda_1\lambda_2}(s,\Omega) Y_{J,\Lambda}^*(\Omega), \tag{3.120}$$

where $\Lambda = \lambda_1 - \lambda_2$ is the difference between the polarizations of the initial (or final) state particles, and $K = 1$, 2 for distinguishable and indistinguishable particles in the initial state, respectively. $Y_{J,J_z}(\Omega)$ is a spherical-harmonic function[8]. The inverse of eq. 3.120 reconstructs the amplitude,

$$A_I^{\lambda_1\lambda_2}(s,\Omega) = 64\pi^2 K \sum_{J,\Lambda} \sqrt{\frac{2J+1}{4\pi}} Y_{J,\Lambda}(\Omega) F_{IJ}^{\lambda_1\lambda_2}(s). \tag{3.121}$$

If we were in the general case where both the initial and final state particles have polarization, then the Wigner D-functions should be used (see ref. [149]). But, in this particular case, where one of the two particles states has no polarization, the Wigner D-function reduces to eq. 3.120.

In the case of particles without polarization, as in the case of the WBGBs scattering processes without coupling with γ and fermions, then $\Lambda = 0$. Taking into account the definition of spherical harmonics,

$$Y_{J,J_z}(\theta,\varphi) = \sqrt{\frac{2J+1}{4\pi}}\sqrt{\frac{(J-J_z)!}{(J+J_z)!}} P_J^{J_z}(\cos\theta) e^{iJ_z\varphi}, \tag{3.122}$$

where $P_l^m(x)$ is the *associated Legendre Polynomial*, if azimuthal symmetry is present, then eq. 3.120 reduces to

$$F_{IJ,0}(s) \equiv A_{IJ}(s) = \frac{1}{32\pi K}\int_{-1}^{1} d\,x\, P_J(x) A_I[s, t(s,x), u(s,x)], \tag{3.123}$$

[8] See, for example, ref. [138, 147, 148].

$P_J(x)$ being the Legendre polynomials [note that $P_l^0(x) = P_l(x)$] and $x = \cos\theta$, the cosine of the scattering angle θ, that can be computed from (s,t,u) by using the relations from app. A. In particular, eqs. A.12 for the most general case (all the four particles have different masses); eq. A.15, if $m_1 = m_2$ (initial state particles) and $m_3 = m_4$ (final state particles); and eq. A.18, for the massless case. Now, the inverse of eq. 3.123 reconstructs the amplitude,

$$A_I(s,t,u) = 16\pi K \sum_{J=0}^{\infty} (2J+1) P_J[x(s,t)] A_{IJ}(s), \tag{3.124}$$

which is the spinless version of eq. 3.121. Integrating the modulus of eq. 3.124 over x,

$$\frac{1}{32\pi}\int_{-1}^{1} d\,x |A_I[s,t(s,x),u(s,x)]|^2 = 64\pi \sum_{J=0}^{\infty} (2J+1)|A_{IJ}(s)|^2. \tag{3.125}$$

Provided that the initial states can be considered massless, because they are photons or we are taking the WBGBs as massless[9], then

$$x = 1 - \frac{2t}{s},\ u = -(s+t). \tag{3.126}$$

Our final goal would be computing differential and total cross sections. According to [40], considering a $2 \to 2$ scattering processes

$$\left(\frac{d\,\sigma}{d\,\Omega}\right)_{\text{CM}} = \frac{1}{2E_{\mathcal{A}} 2E_{\mathcal{B}} |v_{\mathcal{A}} - v_{\mathcal{B}}|} \frac{|\vec{p}_1|}{(2\pi)^2 4E_{\text{CM}}} |\mathcal{M}(p_{\mathcal{A}}, p_{\mathcal{B}} \to p_1, p_2)|^2, \tag{3.127}$$

with $|v_{\mathcal{A}} - v_{\mathcal{B}}|$ the Galilean relative velocity of the beams as viewed in the laboratory frame. However, if we deal with massless particles (or we can use $M_W, M_h \ll \sqrt{s}$), then this last formula simplifies to

$$\left(\frac{d\,\sigma}{d\,\Omega}\right)_{\text{CM}} = \frac{|\mathcal{M}|^2}{64\pi^2 s}, \tag{3.128}$$

where we have used that $s = E_{\text{CM}}^2$. To obtain the total cross section, because of the definition of spherical angle[10],

$$\sigma = \frac{1}{32\pi s}\int_{-1}^{1} d\,x |\mathcal{M}[s,t(s,x),u(s,x)]|^2 \tag{3.129}$$

3.3.1 $\omega\omega$ scattering

For the $\omega\omega$ scattering, we take the particles as massless (and without polarization), and $K = 2$ in eq. 3.123 (indistinguishable particles). First of all, let us compute the partial waves corresponding to the matrix elements without neglecting the couplings λ_3, λ_4 and

[9] $M_W, M_h \ll \sqrt{s}$, limit of applicability of the ET.

[10] This holds when the φ variable is trivial and, if spin is present, for averaged cross sections.

M_h (see our ref. [34]). Some of the corresponding amplitudes t_{IJ} for eqs. 3.26 are

$$t_{00}^{2\omega 2\omega}(s) = \frac{s}{32\pi v^2}\left[2 - a^2\left(\frac{3s}{s-M_h^2} - 1\right) - 2\frac{M_h^2 a^2}{s} + \frac{2M_h^4 a^2}{s^2}\log\left(1+\frac{s}{M_h^2}\right)\right] \tag{3.130a}$$

$$t_{00}^{2\omega 2h}(s) = -\frac{\sqrt{3}s}{32\pi v^2}\left[(a^2-b) + \frac{6a\lambda_3 v}{M_h^2-s} + \frac{2M_h^2 a^2}{s} - \frac{2M_h^4 a^2}{s^2\sigma}\log\left(\frac{2M_h^2 - s(1-\sigma)}{2M_h^2 - s(1+\sigma)}\right)\right] \tag{3.130b}$$

$$t_{00}^{2h2h}(s) = -\frac{1}{16\pi}\left(12\lambda_4 - \frac{18\lambda_3^2}{M_h^2-s}\right) - \frac{9\lambda_3^2}{4\pi s\sigma^2}\log\left(\frac{M_h^2}{s-3M_h^2}\right) \tag{3.130c}$$

$$t_{11}^{2\omega 2\omega}(s) = \frac{s}{32\pi v^2}\left[\frac{1}{3}(1-a^2) - \frac{4M_h^4 a^2}{s^2} + \frac{2M_h^4 a^2}{s^3}(2M_h^2+s)\log\left(1+\frac{s}{M_h^2}\right)\right], \tag{3.130d}$$

where $\sigma = \sqrt{1-4M_h^2/s}$. Thus, for the SM ($a^2 = b = 1$, $\lambda_3 = M_h^2/2v$, $\lambda_4 = M_h^2/8v^2$), eqs. 3.130 turn into

$$t_{00}^{2\omega 2\omega} = \frac{s}{32\pi v^2}\left[3 - \frac{3s}{s-M_h^2} - 2\frac{M_h^2}{s} + \frac{2M_h^4}{s^2}\log\left(1+\frac{s}{M_h^2}\right)\right] \tag{3.131a}$$

$$t_{00}^{2\omega 2h} = \frac{\sqrt{3}s}{32\pi v^2}\left[-\frac{2M_h^2}{s} + \frac{3M_h^2}{s-M_h^2} + \frac{2M_h^4}{s^2\sigma}\log\left(\frac{2M_h^2 - s(1-\sigma)}{2M_h^2 - s(1+\sigma)}\right)\right] \tag{3.131b}$$

$$t_{00}^{2h2h} = -\frac{3M_h^2}{32\pi v^2}\left[1 + \frac{3M_h^2}{s-M_h^2} + \frac{6M_h^2}{s-4M_h^2}\log\left(\frac{M_h^2}{s-3M_h^2}\right)\right] \tag{3.131c}$$

$$t_{11}^{2\omega 2\omega} = \frac{1}{32\pi v^2}\left[-\frac{4M_h^4}{s} + \frac{2M_h^4}{s^2}(2M_h^2+s)\log\left(1+\frac{s}{M_h^2}\right)\right]. \tag{3.131d}$$

However, as explained on sec. 3.2.1, we have kept λ_3, λ_4 and M_h^2 only for testing purposes[11], and we will neglect them in all our work except in sec. 3.3.4. Thus, once λ_3, λ_4 and M_h are neglected, for the elastic channels $\omega\omega \to \omega\omega$, these partial waves accept a chiral expansion just as the full amplitude in subsec. 3.2,

$$A_{IJ}^{(0)}(s) = Ks \tag{3.132a}$$

$$A_{IJ}^{(1)}(s) = \left(B(\mu) + D\log\frac{s}{\mu^2} + E\log\frac{-s}{\mu^2}\right)s^2. \tag{3.132b}$$

These constants will depend on the IJ parameters of the considered channel. For the coupled channels $\omega\omega \to hh$, the inelastic amplitude expanded in partial waves is

$$M_J(s) = K's + \left(B'(\mu) + D'\log\frac{s}{\mu^2} + E'\log\frac{-s}{\mu^2}\right)s^2 + \cdots \tag{3.133}$$

and, for the elastic $hh \to hh$, a similar expression holds,

$$T_J(s) = K''s + \left(B''(\mu) + D''\log\frac{s}{\mu^2} + E''\log\frac{-s}{\mu^2}\right)s^2 + \cdots \tag{3.134}$$

In all three cases, and in general in all the partial waves of the form of eq. 3.132, because the final result must be independent of the scale μ, the dependence with μ of B (or, equivalently, B' and B'') follows

$$B(\mu) = B(\mu_0) + (D+E)\log\frac{\mu^2}{\mu_0^2}. \tag{3.135}$$

[11] Actually, eqs. 3.131 are not the result of applying the equivalence theorem to the full SM, because the couplings with the transverse modes of gauge bosons have been neglected.

Thus, from the partial-wave definition of eq. 3.123, the isospin projection relations of eqs. 3.20 and the results of sec. 3.2.1, we can compute the partial waves associated with $\omega\omega$ scattering, which take the form of eq. 3.132. We take $K = 2$ in eq. 3.123, since the $\omega\omega$ states are made of indistinguishable particles. So, for the scalar-isoscalar channel $I = J = 0$,

$$\begin{aligned}
K_{00} &= \frac{1}{16\pi v^2}(1-a^2) \\
B_{00}(\mu) &= \frac{1}{9216\pi^3 v^4}\left[101(1-a^2)^2 + 68(a^2-b)^2 + 768\{7a_4(\mu) + 11a_5(\mu)\}\pi^2\right] \\
D_{00} &= -\frac{1}{4608\pi^3 v^4}\left[7(1-a^2)^2 + 3(a^2-b)^2\right] \\
E_{00} &= -\frac{1}{1024\pi^3 v^4}\left[4(1-a^2)^2 + 3(a^2-b)^2\right].
\end{aligned} \tag{3.136}$$

For the vector-isovector $IJ = 11$ amplitude,

$$\begin{aligned}
K_{11} &= \frac{1}{96\pi v^2}(1-a^2) \\
B_{11}(\mu) &= \frac{1}{110592\pi^3 v^4}\left[8(1-a^2)^2 - 75(a^2-b)^2 + 4608\{a_4(\mu) - 2a_5(\mu)\}\pi^2\right] \\
D_{11} &= \frac{1}{9216\pi^3 v^4}\left[(1-a^2)^2 + 3(a^2-b)^2\right] \\
E_{11} &= -\frac{1}{9216\pi^3 v^4}(1-a^2)^2.
\end{aligned} \tag{3.137}$$

For the scalar-isotensor $IJ = 20$:

$$\begin{aligned}
K_{20} &= -\frac{1}{32\pi v^2}(1-a^2) \\
B_{20}(\mu) &= \frac{1}{18432\pi^3 v^4}\left[91(1-a^2)^2 + 28(a^2-b)^2 + 3072\{2a_4(\mu) + a_5(\mu)\}\pi^2\right] \\
D_{20} &= -\frac{1}{9216\pi^3 v^4}\left[11(1-a^2)^2 + 6(a^2-b)^2\right] \\
E_{20} &= -\frac{1}{1024\pi^3 v^4}(1-a^2)^2
\end{aligned} \tag{3.138}$$

and for the tensor-isoscalar $IJ = 02$,

$$\begin{aligned}
K_{02} &= 0 \\
B_{02}(\mu) &= \frac{1}{921600\pi^3 v^4}\left[320(1-a^2)^2 + 77(a^2-b)^2 + 15360\{2a_4(\mu) + a_5(\mu)\}\pi^2\right] \\
D_{02} &= -\frac{1}{46080\pi^3 v^4}\left[10(1-a^2)^2 + 3(a^2-b)^2\right] \\
E_{02} &= 0.
\end{aligned} \tag{3.139}$$

Next we quote a calculation of the tensor-isotensor $I = J = 2$ partial wave which is not

usually considered in the literature[12],

$$\begin{aligned} K_{22} &= 0 \\ B_{22}(\mu) &= \frac{1}{921600\pi^3 v^4}\left[71(1-a^2)^2 + 77(a^2-b)^2 + 7680\{a_4(\mu)+2a_5(\mu)\}\pi^2\right] \\ D_{22} &= -\frac{1}{46080\pi^3 v^4}\left[4(1-a^2)^2 + 3(a^2-b)^2\right] \\ E_{22} &= 0. \end{aligned} \tag{3.140}$$

The tensor-isotensor channel (eq. 3.140) exhausts the list of elastic partial waves that are non-vanishing at NLO in perturbation theory, since those with angular momentum $J = 3$ and higher start at $O(s^3)$ and are NNLO in the derivative counting [19, 30, 46]. Needless to say, they would be tiny at LHC energies.

The results for the inelastic coupled channel $\omega\omega \to hh$, can be computed taking into account the results of eq. 3.46 and the factor[13] $-\sqrt{3}$ shown in eq. 3.22. Starting by the scalar channel $J = 0$,

$$\begin{aligned} K_0' &= -\frac{\sqrt{3}}{32\pi v^2}(a^2-b) \\ B_0'(\mu) &= -\frac{\sqrt{3}}{16\pi v^4}\left[d(\mu)+\frac{e(\mu)}{3}\right] + \frac{\sqrt{3}}{18432\pi^3 v^4}(a^2-b)\left[72(1-a^2)+(a^2-b)\right] \\ D_0' &= \frac{\sqrt{3}(a^2-b)^2}{9216\pi^3 v^4} \\ E_0' &= \frac{\sqrt{3}(a^2-b)(1-a^2)}{512\pi^3 v^4}. \end{aligned} \tag{3.141}$$

$I, J = 1$ is forbidden by Bose symmetry for two identical spinless particles. The tensor $J = 2$ channel will be

$$\begin{aligned} K_2' &= 0 \\ B_2'(\mu) &= \frac{e(\mu)}{160\sqrt{3}\pi v^4} + \frac{83(a^2-b)^2}{307200\sqrt{3}\pi^3 v^4} \\ D_2' &= -\frac{(a^2-b)^2}{7680\sqrt{3}\pi^3 v^4} \\ E_2' &= 0. \end{aligned} \tag{3.142}$$

Finally, the scalar partial wave of the elastic channel $hh \to hh$ amplitude, is given by the constants

$$\begin{aligned} K_0'' &= 0 \\ B_0''(\mu) &= \frac{10g(\mu)}{96\pi v^4} + \frac{(a^2-b)^2}{96\pi^3 v^4} \\ D_0'' &= -\frac{(a^2-b)^2}{512\pi^3 v^4} \\ E_0'' &= -\frac{3(a^2-b)^2}{1024\pi^3 v^4}\ , \end{aligned} \tag{3.143}$$

[12] We have found only one computation of the tensor-isotensor partial wave, in ref. [150], but within the framework of a (ruled out) Higgsless ECL model. See appendix D.4 for more details and for a comparison with our eq. 3.139.

[13] When comparing with our refs. [34, 35, 38, 39], note the change of sign in $M^{(0)}$ ($I = J = 0$) pointed out on page 28.

while the tensor T_2 requires

$$\begin{aligned} K_2'' &= 0 \\ B_2''(\mu) &= \frac{g(\mu)}{240\pi v^4} + \frac{77(a^2-b)^2}{307200\pi^3 v^4} \\ D_2'' &= -\frac{(a^2-b)^2}{5120\pi^3 v^4} \\ E_2'' &= 0. \end{aligned} \tag{3.144}$$

By using the evolution equations it is possible to check that all these partial waves are μ-independent.

Finally, note that, in the elastic $\omega\omega \to \omega\omega$ channels, the dependence of B on μ (eq. 3.135) can be explicitly written as

$$B(\mu) = B_0 + p_4 a_4(\mu) + p_5 a_5(\mu), \tag{3.145}$$

where B_0 depends on a and b, and the p_4 and p_5 coefficients can be read on the explicit computations of the partial waves (eqs. from 3.136 to 3.144). On the crossed-channels $\omega\omega \to hh$ and $hh \to hh$, we will have a dependence on μ which comes from the NLO parameters $d(\mu)$, $e(\mu)$ and $g(\mu)$.

3.3.2 $\gamma\gamma$ scattering into and out of the EWSBS

Since we deal with the polarization of photons, eq. 3.120 is needed for computing the partial waves associated to $\gamma\gamma$ scattering amplitudes (see our work [151]). Notice also that $K = 2$ in eq. 3.120 because photons are indistinguishable particles.

The scattering amplitudes are given in eqs. 3.86 and 3.89 in the required form $T_I^{\lambda_1\lambda_2}$. However, the $\gamma\gamma$ state only couples with the WBGBs (as h is chargeless), and when they are in a positive parity state. Let us remember[14] that our $|\lambda_1\lambda_2\rangle$ state is, indeed, defined as

$$|\lambda_1\lambda_2\rangle = \frac{1}{N}\left(|+k\hat{e}_z,\lambda_1;-k\hat{e}_z,\lambda_2\rangle + |-k\hat{e}_z,\lambda_2;+k\hat{e}_z,\lambda_1\rangle\right) \tag{3.146}$$

Hence, the parity operator $\mathcal{P}$ acts over $|\lambda_1\lambda_2\rangle$ according to

$$\mathcal{P}\,|\pm\pm\rangle = |\mp\mp\rangle\,, \quad \mathcal{P}\,|\pm\mp\rangle = |\pm\mp\rangle\,. \tag{3.147}$$

Thus, we have three 2-photon states with positive parity,

$$|p=+\rangle_{0,\Lambda=0} = \frac{1}{\sqrt{2}}\left(|++\rangle + |--\rangle\right), \quad |p=+\rangle_{2,\Lambda=+2} = |+-\rangle\,, \quad |p=+\rangle_{2,\Lambda=-2} = |-+\rangle\,. \tag{3.148}$$

Now, let us introduce the definition

$$P_{IJ}^i = F\left[\langle I \,|\, T \,|\, (|p=+\rangle_i)\rangle\,, IJ\right] \tag{3.149a}$$

$$R_{00}^1 = F\left[\langle hh \,|\, R \,|\, (|p=+\rangle_1)\rangle\,, IJ\right], \tag{3.149b}$$

where T is the reaction matrix $\gamma\gamma \to \omega\omega$ (whose elements are defined in eqs. 3.86) and R, the reaction matrix $\gamma\gamma \to hh$ (eq. 3.89). The operator $F[\ldots, IJ]$ stands for the computation of the corresponding partial waves (defined in eq. 3.120). It is linear

[14] See section 3.2.2 and eqs. 3.59, 3.60 and 3.67.

because, indeed, it is an integral. Thus, we can define the partial waves associated with the positive parity states (eq. 3.148),

$$P^0_{IJ} = \frac{1}{\sqrt{2}}\left(T^{++}_{IJ} + T^{--}_{IJ}\right) \tag{3.150a}$$

$$P^2_{IJ} = \frac{1}{\sqrt{2}}\left(T^{+-}_{IJ} + T^{-+}_{IJ}\right) \tag{3.150b}$$

$$R^0_{00} = \frac{1}{\sqrt{2}}\left(R^{++}_{00} + R^{--}_{00}\right). \tag{3.150c}$$

Actually, the only non-vanishing partial waves are

$$P^0_{00} = \frac{e^2 s}{32\sqrt{6}\pi}(2A_C + A_N) \qquad P^0_{20} = \frac{e^2 s}{32\sqrt{3}\pi}(A_C - A_N) \tag{3.151a}$$

$$P^2_{02} = \frac{e^2}{24\pi\sqrt{2}} \qquad P^2_{22} = \frac{e^2}{48\pi}, \tag{3.151b}$$

where A_C and A_N are defined in eqs. 3.73 and 3.76, respectively[15]. If the fine structure constant $\alpha = e^2/4\pi$ is used, eqs. 3.151 turn into

$$P_{00} = \frac{\alpha s}{8\sqrt{6}}(2A_C + A_N) \qquad P_{20} = \frac{\alpha s}{8\sqrt{3}}(A_C - A_N) \tag{3.152a}$$

$$P_{02} = \frac{\alpha}{6\sqrt{2}} \qquad P_{22} = \frac{\alpha}{12}, \tag{3.152b}$$

where be have omitted the superindices because $\omega\omega$ states with $J = 0$ only couple with $|p = +\rangle_1$ $\gamma\gamma$ ones; and $J = 2$, with $|p = +\rangle_2$.

Finally, for the crossed-channel $\gamma\gamma \to hh$ (eq. 3.89), there is only one partial wave, which corresponds to $I = J = J_z = 0$,

$$R_0 = \frac{e^2}{128\sqrt{2}\pi^3 v^2}(a^2 - b) = \frac{\alpha}{32\sqrt{2}\pi^2 v^2}(a^2 - b). \tag{3.153}$$

3.3.3 $t\bar{t}$ in the final state

In this case, if we exclude the elastic channel $t\bar{t} \to t\bar{t}$, the only non-vanishing final state is $|S = 1, S_z = 0\rangle = (|t^+\bar{t}^+\rangle - |t^-\bar{t}^-\rangle)/\sqrt{2}$ (eq. 3.117 and our ref. [136]), so that the polarized particles in the final state $t\bar{t}$ will be in the $\lambda_1 = \lambda_2 = \pm$ polarization state. That is, $\Lambda = \lambda_1 - \lambda_2 = 0$. Hence, eqs. 3.123 and its inverse 3.124 apply for the computation of the partial waves. Note that we take $K = 2$ in eq. 3.123, since the inital states $\omega\omega$ and hh are composed by indistinguishable particles.

Because of the dependence on the quark top mass, the general form of the partial waves of eq. 3.132, which was valid on the WBGBs scattering case, turns into

$$Q^{(0)}(s) = K^Q \sqrt{s} M_t \tag{3.154a}$$

$$Q^{(1)}(s) = \left(B^Q(\mu) + E^Q \log\frac{-s}{\mu^2}\right) s\sqrt{s} M_t \tag{3.154b}$$

for the

$$Q = Q^{(0)} + Q^{(1)} + \ldots \tag{3.155}$$

[15] See page 37.

expansion of the Q partial wave associated to the $\omega\omega \to t\bar{t}$ matrix element. The coefficients of eq. 3.154 are defined as

$$K^Q = \frac{\sqrt{6}}{32\pi v^2}(1 - ac_1) \tag{3.156a}$$

$$B^Q(\mu) = \frac{\sqrt{6}}{32\pi v^4}\left[\frac{g_t(\mu)}{2} + \frac{C_t}{8\pi^2}\right] \tag{3.156b}$$

$$E^Q = -\frac{\sqrt{6}}{32\pi v^4}\frac{C_t}{16\pi^2} \tag{3.156c}$$

For the expansion

$$N = N^{(0)} + N^{(1)} + \dots \tag{3.157}$$

of the N partial wave associated to the $hh \to t\bar{t}$ crossed-channel matrix element, the general form of the partial wave will be similar to eq. 3.154, that is

$$N^{(0)}(s) = K^N\sqrt{s}M_t \tag{3.158a}$$

$$N^{(1)}(s) = \left(B^N(\mu) + E^N \log\frac{-s}{\mu^2}\right) s\sqrt{s}M_t, \tag{3.158b}$$

where the constants are given by

$$K^N = -\frac{\sqrt{6}c_2}{16\pi v^2} \tag{3.159a}$$

$$B^N(\mu) = \frac{\sqrt{6}}{32\pi v^4}\left[\frac{g_t'(\mu)}{2} - \frac{3C_t'}{16\pi^2}\right] \tag{3.159b}$$

$$E^N = -\frac{3\sqrt{6}}{32\pi v^4}\frac{C_t'}{32\pi^2}. \tag{3.159c}$$

Finally, the last term in the reaction matrix $F_{J=0}$ ($\Lambda = \lambda_1 - \lambda_2 = 0$), which is the LO $t\bar{t} \to t\bar{t}$ process with $J = 0$, is vanishing. Take into account that, for initial and final states of the form $t^\pm\bar{t}^\pm$, the only allowed processes are $t^a\bar{t}^a \to t^a\bar{t}^a$, $a = \pm$ (eqs. 3.119). But, in this channel, $\mathcal{S}(t^-\bar{t}^- \to t^-\bar{t}^-) = \mathcal{S}(t^+\bar{t}^+ \to t^+\bar{t}^+)$. Thus, when we consider the elastic scattering between states $|S = 1, S_z = 0\rangle = (|t^+\bar{t}^+\rangle - |t^-\bar{t}^-\rangle)/\sqrt{2}$ (eq. 3.117), the amplitude vanishes.

To summarize, the full LO amplitude matrix which should enter the unitarization methods of sec. 4, for $IJ = 00$, is

$$F_{J=0} = \begin{pmatrix} A_{00} & M_0 & Q \\ M_0 & T_0 & N \\ Q & N & 0 \end{pmatrix}. \tag{3.160}$$

3.3.4 Validity range of the approximations

According to sec. 2.2 (page 14), if we chose $a = b = 1$ in our effective Lagrangians, and computed the LO scattering matrix elements, we should recover the SM cross sections. However, such an election of parameters leads to vanishing values for all the LO partial waves of sec. 3.3.1. The SM amplitudes are non-vanishing, leading to possible confusion.

The SM limit of our amplitudes ($a = b = 1$) undergoes a cancellation between the LO Feynman diagrams[16] which are computed for the scattering between the WBGBs, so

[16]For the elastic $\omega\omega \to \omega\omega$, the LO Feynman diagrams can be seen in fig. 3.2).

that, at the EW scale, the LO matrix element does not grow as $\mathcal{O}(s)$. This is exactly how the introduction of the SM Higgs leads to a weakly interacting theory, where unitarity is not broken at the leading order. This cancellation is critical, since each of the LO Feynman diagrams still grows as $\mathcal{O}(s)$, although their sum stabilizes.

This cancellation between LO diagrams is also a big deal in the SM when computing WBGBs scattering matrix elements numerically, since any numerical inaccuracy (for instance, in the definition of the model constants) will become dominant. In collaboration with prof. Stefano Moretti (University of Southampton), we had the opportunity to study such a problem (see page 2.1), in the scope of a numerical test of the Equivalence Theorem[17] when applied to the SM.

The reason that we obtain zero and not a finite constant is the following. On the effective Lagrangians of eqs. 2.31, 2.33, 2.34, 2.45 and 2.46, we neglect some contributions which are small well above the EW scale. For instance, the masses M_h and M_W. This is valid because $s \gg M_W^2, M_h^2$. But it is no longer true if there is a cancellation which makes these terms dominant. That is, if there are no strong interactions. In this regime, we cannot neglect the masses M_h and M_W, for instance, even if $s \gg M_h^2, M_W^2$. However, note that the Equivalence Theorem (sec. 2.1) would still be valid provided that $s \gg M_h^2, M_W^2$.

The range of parameters over which this phenomenon of cancellation which breaks our approximations takes place has been studied on our refs. [34, 35]. We focuse on $hh \to hh$ elastic scattering, because it is the elastic channel where $K = 0$ (see eq. 3.143), so that the chiral amplitude vanishes at $\mathcal{O}(s)$ and the series starts at $\mathcal{O}(s^2)$. Thus, maximum sensitivity to the correction is expected. From eqs. 3.134 and 3.143, at a simple reference point $\mu^2 = s = 1\,\mathrm{TeV}^2$, the $J = 0$ partial wave can be written as

$$T_0(s = 1\,\mathrm{TeV}^2) = \frac{1\,\mathrm{TeV}^4}{96\pi v^4}\left(10g(1\,\mathrm{TeV}) + \frac{(a^2-b)^2}{\pi^2}\right) \approx 0.905\left(10g + \frac{(a^2-b)^2}{\pi^2}\right). \tag{3.161}$$

The Higgs self-coupling potential in the SM would be

$$V^{\mathrm{self}} = \frac{M_h^2}{2}h^2 + \frac{M_h^2}{8v^2}h^4, \tag{3.162}$$

which produces a $hh \to hh$ matrix element whose scalar-isoscalar partial wave is given in eq. 3.131c,

$$T_0^{\mathrm{self}} = -\frac{3M_h^2}{32\pi v^2}\left[1 + \frac{3M_h^2}{s - M_h^2} + \frac{6M_h^2}{s - 4M_h^2}\log\left(\frac{M_h^2}{s - 3M_h^2}\right)\right]$$

For $s = 1\,\mathrm{TeV}^2$, $T_0^{\mathrm{self}} \approx -4.9 \times 10^{-3}$. If we require $T_0(s = 1\,\mathrm{TeV}^2) \gg T_0^{\mathrm{self}}$, so that the self-interaction is negligible at the TeV scale, then

$$|a^2 - b| \gg 0.23, \tag{3.163}$$

or, alternatively,

$$|g| \gg 5.9 \times 10^{-4}. \tag{3.164}$$

Thus, the analysis is safe provided that either eq. 3.163 or eq. 3.164 is satisfied.

Now, let us take $a^2 = b$ (elastic channels). We will see that this channel is also possible even if $g = 0$, that is, if both conditions 3.163 and 3.164 are violated. In this case, of course, the $hh \to hh$ amplitude will vanish in our approximations, as follows from

[17] See sec. 2.1 and eq. 2.1.

eq. 3.143. But channels $\omega\omega \to hh$ and $\omega\omega \to \omega\omega$ could still present strong interactions because of, for instance, the a_4 and a_5 NLO coefficients. In this last case, the only non-vanishing amplitudes would be the elastic $\omega\omega \to \omega\omega$, since all the contributions to the scattering amplitudes come either from the Higgs self-couplings of eq. 3.162 (neglected here) or from the 4-ω vertices. Let us analyze this case for the different channels, at a point $\mu^2 = s = 1\,\mathrm{TeV}^2$ and in the case $a^2 = b = 1$.

For the scalar-isoscalar elastic channel ($IJ = 00$, eq. 3.131b), the contribution coming from the self-interacting potential of eq. 3.162 will be $A_0^{\mathrm{self}} \approx -1.2\times10^{-2}$. From eqs. 3.134 and 3.136, the vector-isovector partial wave without the contribution from the Higgs self-couplings is

$$A_{00}(s = 1\,\mathrm{TeV}^2) = \frac{768}{9216\pi v^4}(1\,\mathrm{TeV})^2\left[7a_4(1\,\mathrm{TeV}) + 11a_5(1\,\mathrm{TeV})\right] \approx 7.2(7a_4 + 11a_5), \tag{3.165}$$

so that the Higgs self-interaction is negligible at the TeV scale when

$$|7a_4 + 11a_5| \gg 1.7 \times 10^{-3}. \tag{3.166}$$

On the contrary, for the vector-isovector elastic channel ($IJ = 11$, eq. 3.131d), the contribution coming from the self-interacting potential of eq. 3.162 will be $A_1^{\mathrm{self}} \approx 1.85\times10^{-4}$. From eqs. 3.134 and 3.137, the vector-isovector partial wave without the contribution from the Higgs self-couplings will be

$$A_{11}(s = 1\,\mathrm{TeV}^2) = \frac{4608}{110592\pi v^4}(1\,\mathrm{TeV})^2\left[a_4(1\,\mathrm{TeV}) - 2a_5(1\,\mathrm{TeV}))\right] \approx 3.62(a_4 - 2a_5). \tag{3.167}$$

Thus, for $IJ = 11$, the Higgs self-interaction is negligible at the TeV scale when

$$|a_4 - 2a_5| \gg 5.1 \times 10^{-5}. \tag{3.168}$$

Chapter 4

Analytical properties and unitarization

4.1 Unitarity condition for partial waves

The unitarity condition for the S-matrix reads

$$SS^\dagger = \mathbb{1} \tag{4.1}$$

Its analytical properties and this unitarity condition applied to partial waves can be studied in detail in Refs. [90, 137, 139, 140, 152, 153]. The transition amplitude matrix $\tilde{T}$ is defined as

$$S = \mathbb{1} + i\tilde{T}. \tag{4.2}$$

Along with eq. 4.1, such a definition implies that

$$\tilde{T} - \tilde{T}^\dagger = i\tilde{T}\tilde{T}^\dagger \tag{4.3}$$

Now, we factorize momentum conservation from the on-shell transition amplitude between states $|i\rangle$ and $|f\rangle$,

$$\left\langle f \left| \tilde{T} \right| I \right\rangle = (2\pi)^4 \delta^{(4)} \left(\sum_k p_{i,k} - \sum_l p_{f,l} \right) T(i \to f), \tag{4.4}$$

$p_{f,k}$ and $p_{i,l}$ being the 4–momenta of the final and initial state particles, respectively. If we restrict eq. 4.4 to 2-particle states,

$$\left\langle k_1 k_2 \left| \tilde{T} \right| p_1 p_2 \right\rangle = (2\pi)^4 \delta^{(4)} \left(p_1 + p_2 - k_1 - k_2 \right) T(p_1 p_2 \to k_1 k_2), \tag{4.5}$$

where p_i and k_i are 4-momenta of the particles of the initial and final state, respectively. Setting this definition into eq. 4.3, its left hand side (LHS) becomes

$$\tilde{T} - \tilde{T}^\dagger = (2\pi)^4 \left[T(p_1 p_2 \to k_1 k_2) - T(k_1 k_2 \to p_1 p_2)^* \right] \delta^{(4)} \left(p_1 + p_2 - k_1 - k_2 \right) \tag{4.6}$$

From time reversal invariance,

$$T(p_1 p_2 \to k_1 k_2) = T(k_1 k_2 \to p_1 p_2), \tag{4.7}$$

so that eq. 4.6 reduces to

$$\tilde{T} - \tilde{T}^\dagger = 2i(2\pi)^4 \,\mathrm{Im}\,[T(p_1 p_2 \to k_1 k_2)]\,\delta^{(4)}(p_1 + p_2 - k_1 - k_2) \tag{4.8}$$

The right hand side (RHS) of eq. 4.3 would be

$$i\tilde{T}\tilde{T}^\dagger = i\sum_{\{a,b\}} \int \frac{d^3\,q_{1a}}{2q^0_{1a}(2\pi)^3} \int \frac{d^3\,q_{2b}}{2q^0_{2b}(2\pi)^3}(2\pi)^8\delta^{(4)}(p_1+p_2-q_{1a}-q_{2b})\delta(k_1+k_2-q_{1a}-q_{2b})\cdot$$
$$\cdot\,[T(p_1p_2 \to q_{1a}q_{2b})][T(q_{1a}q_{2b} \to k_1k_2)]^*, \tag{4.9}$$

taking into account that all the possible transition states $\{a, b\}$ coming from S are states of two particles, so far taken as distinguishable. If they are indistinguishable, the RHS should be multiplied by a factor 1/2, in order not to count the 2-particle states twice. Hence, we need to recover the K constant which was used in eq. 3.123 in order to account for this. For a 2-particle state $\{a, b\}$, we will use the notation K_{ab} for this, with value 1 for distinguishable particles and 2 for indistinguisable ones.

Thus, the unitarity relation of eq. 4.3 turns into

$$\mathrm{Im}\,[T(p_1p_2 \to k_1k_2)] = \frac{1}{2(2\pi)^2 K_{ab}} \sum_{\{a,b\}} \int \frac{d^3\,q_{1a}}{2q^0_{1a}} \int \frac{d^3\,q_{2b}}{2q^0_{2b}}\delta^{(4)}(p_1+p_2-q_{1a}-q_{2b})\cdot$$
$$\cdot\,[T(p_1p_2 \to q_{1a}q_{2b})][T(q_{1a}q_{2b} \to k_1k_w)]^*. \tag{4.10}$$

Now, let us go to the center of mass frame, so that the relations $\vec{p_1} + \vec{p_2} = \vec{k_1} + \vec{k_2} = 0$ ($\vec{p_i}$, $\vec{k_i}$ being the 3-momenta) hold. Thus, taking into account that the masses of the two particles both in the initial and final states are the same, and that the process is on-shell, the 4-momenta are

$$p_1 = (p^0_1, \vec{p_1}),\ p_2 = (p^0_1, -\vec{p_1}),\ k_1 = (k^0_1, \vec{k_1}),\ k_2 = (k^0_1, -\vec{k_1}). \tag{4.11}$$

That is, in particular, the first components satisfy the relation $p^0_1 = p^0_2$, $k^0_1 = k^0_2$. Now, consider a change of variables in the δ distribution,

$$\int_{-\infty}^{\infty} d\,x\delta[f(x)]g(x) = \int_{-\infty}^{\infty} d\,y \frac{\delta[f^{-1}(y)]}{f'(f^{-1}(y))} g[f^{-1}(y)], \tag{4.12}$$

where $f(x)$ is a monotonically increasing function, with limits $\lim_{x\to\pm\infty} f(x) = \pm\infty$.

Provided all the intermediate states are two on-shell particles with the same mass m_q, and taking into account the appearance of the 4-vector delta-function $\delta(p_1 + p_2 - q_1 - q_2)$ in eq. 4.10,

$$\vec{q_1} = -\vec{q_2} \equiv \vec{q},\ q^0_1 = q^0_2 = \sqrt{q^2 + m_q^2} \tag{4.13}$$

$$q^0_1 + q^0_2 = 2\sqrt{q^2 + m_q^2} = p^0_1 + p^0_2 = 2p^0_1 = 2\sqrt{p^2 + m_p^2}, \tag{4.14}$$

eq. 4.10 is simplified to

$$\mathrm{Im}\,T = \sum_{\{a,b\}} \frac{1}{8\pi^2 K_{ab}} \int \frac{d^3\,\vec{q}}{4\sqrt{q^2 + m^2_{q,ab}}^2} \delta^{(4)}\left(2\sqrt{q^2 + m^2_{q,ab}} - 2\sqrt{p^2 + m_p^2}\right)\cdot$$
$$\cdot\,[T(p_1p_2 \to q_{1a}q_{2b})][T(q_{1a}q_{2b} \to k_1k_w)]^*. \tag{4.15}$$

Or equivalently, using spherical coordinates,

$$\operatorname{Im} T = \sum_{\{a,b\}} \frac{1}{8\pi^2 K_{ab}} \int d\,\Omega_{\vec{q}} \int \frac{d\,q \cdot q^2}{4(q^2 + m_{q,ab}^2)} \delta^{(4)} \left(2\sqrt{q^2 + m_{q,ab}^2} - 2\sqrt{p^2 + m_p^2} \right) \cdot$$
$$\cdot [T(p_1 p_2 \to q_{1a} q_{2b})][T(q_{1a} q_{2b} \to k_1 k_w)]^*. \quad (4.16)$$

Now, let us identify the f of eq. 4.12 with

$$f(q) = 2\sqrt{q^2 + m_q^2} - 2\sqrt{p^2 + m_p^2}, \quad (4.17)$$

so that

$$f'(q) = \frac{2q}{\sqrt{q^2 + m_q^2}},\ f(q) = 0 \to q = p\sqrt{1 + \frac{m_p^2 - m_q^2}{p^2}}, \quad (4.18)$$

with eq. 4.16 being equal to

$$\begin{aligned} \operatorname{Im} T = & \sum_{\{a,b\}} \frac{1}{8\pi^2 K_{ab}} \int d\,\Omega_{\vec{q}} \frac{q^2}{8(q^2 + m_{q,ab}^2)} \frac{\sqrt{q^2 + m_{q,ab}^2}}{q} \cdot \\ & \cdot [T(p_1 p_2 \to q_{1a} q_{2b})][T(q_{1a} q_{2b} \to k_1 k_w)]^* \\ = & \sum_{\{a,b\}} \frac{1}{64\pi^2 K_{ab}} \int d\,\Omega_{\vec{q}} \sqrt{\frac{p^2 + m_p^2 - m_{q,ab}^2}{p^2 + m_p^2}} \\ & \cdot [T(p_1 p_2 \to q_{1a} q_{2b})][T(q_{1a} q_{2b} \to k_1 k_w)]^*. \end{aligned} \quad (4.19)$$

Now, considering that $s = (p_1 + p_2)^2 = (2p^0)^2$, $p^0 = \sqrt{p^2 + m_p^2}$, then

$$\sqrt{\frac{p^2 + m_p^2 - m_q^2}{p^2 + m_p^2}} = \sqrt{1 - \frac{m_q^2}{p^2 + m_p^2}} = \sqrt{1 - \frac{4m_q^2}{s}}, \quad (4.20)$$

so that

$$\operatorname{Im}\left[T(p_1 p_2 \to k_1 k_2)\right] =$$
$$\sum_{\{a,b\}} \frac{1}{64\pi^2 K_{ab}} \sqrt{1 - \frac{4m_{q,ab}^2}{s}} \int d\,\Omega_{\vec{q}} [T(p_1 p_2 \to q_{1a} q_{2b})][T(q_{1a} q_{2b} \to k_1 k_w)]^*. \quad (4.21)$$

Note that initial, intermediate and final states are not necessarily all different. Indeed, for the so-called *elastic* channels, all of them will be the same state. Now, take eq. 3.124 relating the amplitude (in the isospin basis) with the partial waves,

$$A_I(s, x) = 16\pi K \sum_{J=0}^{\infty} (2J + 1) P_J(x) A_{IJ}(s),$$

$x = \cos\theta$ being the cosine of the angle between 3-momenta in the initial and final states, $\vec{p}_1$ and $\vec{k}_1$. Let us choose, in the center of mass frame (see fig. 4.1),

$$\hat{p}_1 = \vec{e}_z \quad (4.22)$$
$$\hat{q}_{1a} = \sin\tilde{\theta} \sin\tilde{\varphi} \vec{e}_x + \sin\tilde{\theta} \cos\tilde{\varphi} \vec{e}_y + \cos\tilde{\theta} \vec{e}_z \quad (4.23)$$
$$\hat{k}_1 = \sin\theta \vec{e}_y + \cos\theta \vec{e}_z. \quad (4.24)$$

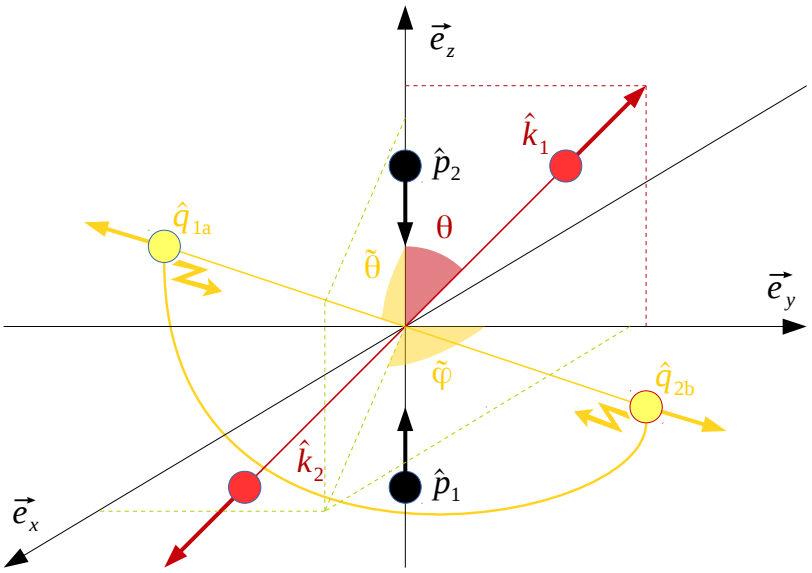

Figure 4.1: Scattering process $\{p_1, p_2\} \to \{q_{1a}, q_{2b}\} \to \{k_1, k_2\}$ in the center of mass frame. The intermediate particles $\{q_{1a}, q_{2b}\}$ are printed on dark yellow colour and the final state $\{k_1, k_2\}$ is in dark red colour. Only these last ones come out of the plane of the paper, as does $\vec{e}_x$.

Here, $\hat{a}$ stands for the unitarized vector $\hat{a} \equiv \vec{a}/\|\vec{a}\|$; θ is the angle between $\hat{p}_1$ and $\hat{k}_1$; and $(\tilde{\theta}, \tilde{\phi})$, the unitarized vector $\hat{q}_{1a}$ in spherical coordinates, ZY being the plane defined by vectors $\hat{p}_1$ and $\hat{k}_1$. With these definitions, the cosine of the angle θ' between $\hat{q}_{1a}$ and $\hat{k}_1$ can be computed as

$$\cos\theta' = \hat{q}_{1a} \cdot \hat{k}_1 = \cos\theta\cos\tilde{\theta} + \sin\theta\sin\tilde{\theta}\cos\tilde{\varphi}, \tag{4.25}$$

and the transition matrix elements can be written down as

$$T(p_1p_2 \to k_1k_2) = 16\pi K_p \sum_{J=0}^{\infty}(2J+1)P_J(\cos\theta)A_{IJ,p_i\to k_i}(s) \tag{4.26}$$

$$T(p_1p_2 \to q_{1a}q_{2b}) = 16\pi K_p \sum_{J=0}^{\infty}(2J+1)P_J(\cos\tilde{\theta})A_{IJ,p_i\to q_{i,ab}}(s) \tag{4.27}$$

$$T(q_{1a}q_{2b} \to k_1k_2) = 16\pi K_{q,ab} \sum_{J=0}^{\infty}(2J+1)P_J(\cos\tilde{\theta}\cos\theta + \cos\tilde{\varphi}\sin\tilde{\theta}\sin\theta)\cdot A_{IJ,q_{i,ab}\to k_i}(s). \tag{4.28}$$

Now, consider the property[1] of Legendre polynomials,

$$\int_0^{2\pi} d\,\tilde{\varphi} \int_0^{\pi} d\,\tilde{\theta}\cdot\sin\tilde{\theta}\cdot P_J[\cos\tilde{\theta}]\cdot P_{J'}[\cos\theta\cos\tilde{\theta} + (-1)^n\sin\theta\sin\tilde{\theta}\cos\tilde{\varphi}] = \\ = \frac{4\pi}{2J+1}\delta_{J,J'}P_J[\cos\theta], \tag{4.29}$$

[1] See appendix D.2 for the proof.

where n is an arbitrary integer. Substituting eq. 4.29 in eq. 4.21, with definitions 4.26, 4.27 and 4.28, and taking into account that transitions only happen between states with the same isospin I,

$$\mathrm{Im}\left[16\pi K_p \sum_{J=0}^{\infty}(2J+1)P_J(x)A_{IJ,p_i\to k_i}(s)\right] = \sum_{\{a,b\}} \frac{(16\pi)^2 K_p K_{q,ab}}{64\pi^2 K_{q,ab}}\sqrt{1-\frac{4m_q^2}{s}}\frac{4\pi}{2J+1}\cdot$$
$$\cdot \sum_{J=0}^{\infty}(2J+1)^2[A_{IJ,p_i\to q_{i,ab}}(s)][A_{IJ,q_{i,ab}\to k_i}(s)]^* P_J(\cos\theta), \quad (4.30)$$

so that, because of the orthonormality of Legendre polynomials,

$$\mathrm{Im}\,[A_{IJ,p_i\to k_i}(s)] = \sum_{\{a,b\}}\sqrt{1-\frac{4m_q^2}{s}}[A_{IJ,p_i\to q_{i,ab}}(s)][A_{IJ,q_{i,ab}\to k_i}(s)]^*. \quad (4.31)$$

Note that the right hand side (RHS) of eq. 4.31 is real. This is non-trivial, but it is the same difficulty which was present in eq. 4.8, whose matricial LHS has no real part. The explanation of this fact is both the unitarity relation applied to the transition amplitude matrix, $\tilde{T}-\tilde{T}^\dagger = i\tilde{T}\tilde{T}^\dagger$ (eq. 4.3), and time reversal invariance (eq. 4.7), which implies that $\tilde{T}^t = \tilde{T}$.

Finally, only if the process is *elastic*, without crossed channels, does eq. 4.31 reduce to

$$\mathrm{Im}\,[A_{IJ}(s)] = \sqrt{1-\frac{4m^2}{s}}[A_{IJ}(s)][A_{IJ}(s)]^*, \quad (4.32)$$

where $A_{IJ}(s)$ is the partial wave of the elastic scattering process and m, the invariant mass of the particle.

4.2 Poles on the analytical continuation

The result from the unitarization procedures is an analytical matrix element which will give physical values just above the real axis. That is, for $s' = s + i\epsilon$, $\epsilon \to 0^+$, $s > 0$. As shown in previous chapters, the scattering amplitude will comply with the *reflection principle*, that is, $A(s^*) = [A(s)]^*$. Thus, the analytical structure above the real axis will be reflected below it. And there can be (or not) a right cut (RC) and a left cut (LC). That is, discontinuities over the real axis.

However, as shown in fig. 4.2, an analytical continuation around a physical point $s' = s + i\epsilon$ could be done, so that we could cross the real part. This will lead to the existence of the *second Riemann sheet*. In this case, of course the reflection principle will no longer we applicable, and new singularities can appear under the real axis.

As can be seen in the literature [40], the Breit-Wigner formula for the cross section in the region of a resonance of mass m and width Γ is

$$\sigma \propto |M|^2 \propto \left|\frac{1}{p^2-(m^2-im\Gamma)}\right|^2, \quad (4.33)$$

the matrix element having a pole in $m^2 - im\Gamma$ when taking the analytical continuation to the fourth quadrant crossing the real axis $s > 0$, as shown in fig. 4.2, that is, to the second Riemann sheet. This can be generalized, so that any pole appearing on the second

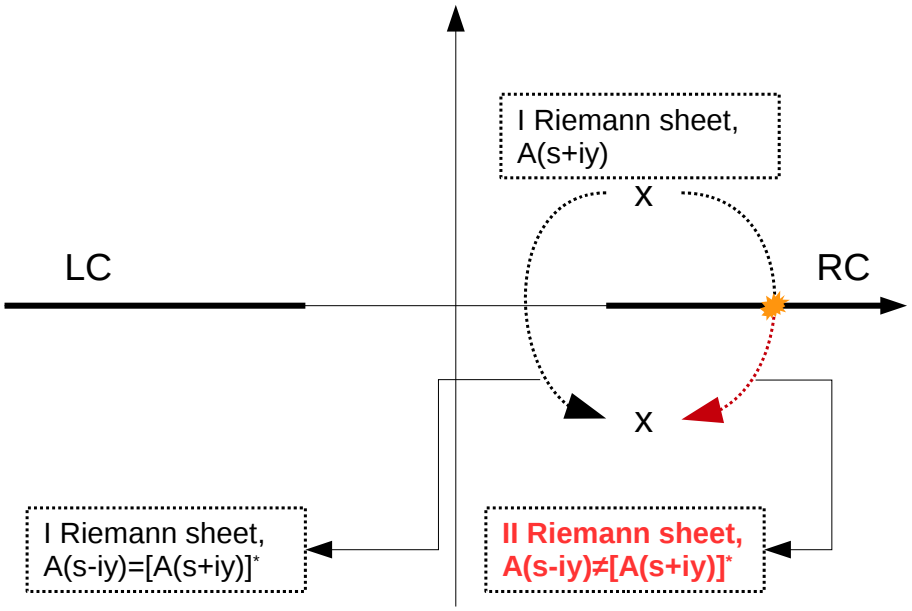

Figure 4.2: Analytical continuation to the so–called *second Riemann sheet*. Note that the trajectory of the analytical continuation has to cross the *right cut* (RC), and the *reflection principle* (eqs. 4.63 and 4.64) no longer applies. Since we are neglecting the masses of the WBGBs, the analytical segment over the real axis collapses to a point, although the analytical extension to the I Riemann sheet is still possible. See sec. 4.3.1 and fig. 4.4.

Riemann sheet at a position s_R may be equivalent to a resonance with mass m and width Γ, so that

$$s_R = \mathrm{Re}\, s_R + i\, \mathrm{Im}\, s_R \equiv m^2 - im\Gamma \tag{4.34}$$

When $\Gamma \ll m$, that is, when the pole is very close to the real axis, the cross section will look like a Breit-Wigner one. Otherwise, the shape of the resonance will become broader and broader, deviating from the Breit-Wigner shape due to the non-pole dependences in s. Anyway, the so–called pole mass (m) and width (Γ) will be defined according to eq. 4.34,

$$m \equiv \sqrt{\mathrm{Re}\, s_R} \qquad\qquad \Gamma \equiv -\frac{1}{m}\, \mathrm{Im}\, s_R, \tag{4.35}$$

where s_R is the position of the pole (on the II Riemann sheet) associated with the resonance.

Note that, if we took the first Riemann sheet, because of the reflection principle, $A(s^*) = [A(s)]^*$, so that no pole could appear since causality allows none on the upper half plane (see next section 4.2.1). Thus, our task will be performing an analytical continuation to the second Riemann sheet, as shown in fig. 4.2, and looking for poles in the fourth quadrant.

4.2.1 Spurious resonances

If we had a pole in the I Riemann sheet, that is, above the real axis, we would actually have a ghost, according to eq. 4.35. As explained in ref. [153], this would break causality,

so poles on the I Riemann sheet are not acceptable. Therefore, their appearance is interpreted as a failure of either the unitarization procedure or even the parameter set itself, in the sense that there is no underlying theory whose low energy regime is described by such a set of parameters. Sometimes, these poles on the I Riemann sheet lead to the appearance of repulsive phase shifts that vary quickly and break Wigner's bound.

However, there are authors who do speak about *negative width resonances* and *scattering amplitudes with poles in the I Riemann sheet* (see refs. [154–157]), although they use a different prescription for the Wick rotation (the so-called Lee-Wick model). These resonances simply mean that the vacuum of the theory (on which matrix elements are calculated) has not been well chosen and is unstable, decaying to another state.

Either way, we will work in the standard framework where ghosts are not allowed. But one should be aware that the parameter space which is neglected due to the presence of poles in the I Riemann sheet could be, indeed, the low energy description of an underlying theory like that of ref. [154] with a lower-energy ground state.

4.2.2 Numerical search for poles on the *s*-plane

Thus, our problem is picking the presence and position of a pole (or a set of poles) on certain region of the complex plane. To do this, first of all, we need to compute the analytical continuations to the first and second Riemann sheets which are explained in fig. 4.2. The only non-trivial functions which appear on typical partial waves such as eqs. 3.132 to 3.134 are the logarithms, $\log(s/\mu^2)$ and $\log(-s/\mu^2)$ ($\mu^2 > 0$). On the first Riemann sheet, the logarithm is written as

$$\log^I(z) = \log|z| + i\arg(z), \tag{4.36}$$

where the $\arg(z)$ cut lies along the negative real axis. Thus, the extension of $\log(s/\mu^2)$ to the second Riemann sheet is trivial [the same function as in eq. 4.36, $\log^{II}(z) = \log^I(z)$], since $\log^I(z)$ is continuous over the positive real axis. What needs examination is the extension of $\log(-s/\mu^2)$. Since the physical region where the scattering amplitudes are defined is $s' = s + i\epsilon$, $\epsilon \to 0^+$, the first Riemann sheet is defined as in eq. 4.37,

$$\log^I(-z) = \log|z| + i\arg(-z). \tag{4.37}$$

This verifies the reflection principle of eq. 4.63, $A(s+i\epsilon) - A(s-i\epsilon) = 2i\,\mathrm{Im}\,A(s+i\epsilon)$, $\epsilon \to 0^+$, since, provided that $x > 0$, $\epsilon \to 0^+$,

$$\log^I(-x-i\epsilon) - \log^I(-x+i\epsilon) \xrightarrow[\text{eq. 4.37}]{x>0,\,\epsilon\to 0^+} i\arg(-x+i\epsilon) - i\arg(-x-i\epsilon) = 2i\pi, \tag{4.38}$$

and

$$2i\,\mathrm{Im}\log^I(-x-i\epsilon) = 2i\pi, \tag{4.39}$$

thus proving that the definition of eq. 4.37 is, indeed, the first Riemann sheet of $\log^I(-z)$. Eq. 4.3 also verifies the strong version of the reflection principle $\log^I(-z^*) = [\log^I(-z)]^*$ (eq. 4.64), because

$$\begin{aligned}\log^I[-(x+iy)^*] = \log^I[-(x-iy)] &= \log(|x-iy|) + i\arg[-(x-iy)] \\ &= \log(|x-iy|) - i\arg[-(x+iy)] = \left\{\log^I[-(x+iy)]\right\}^*.\end{aligned} \tag{4.40}$$

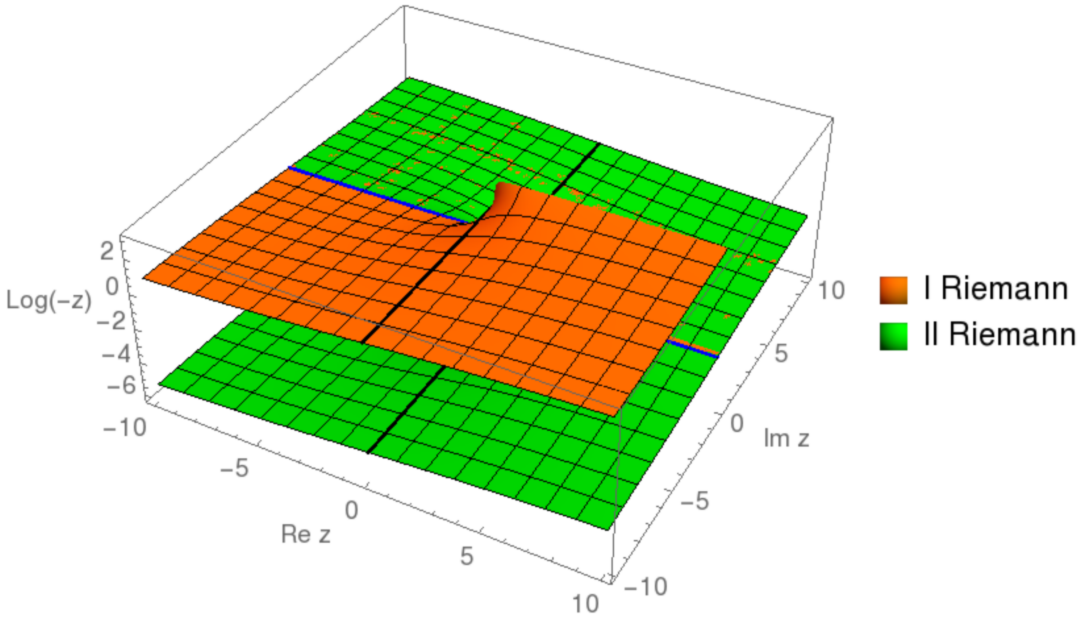

Figure 4.3: Extension to the second Riemann sheet of the function $f(z) = \log(-z)$. Only its imaginary part is shown. Note that the first Riemann sheet verifies the strong reflection principle, $f(z^*) = [f(z)]^*$ (eq. 4.64). For $\mathrm{Im}\, z > 0$, both first and second Riemann sheets coincide, as expected.

Its extension to the second Riemann sheet (see fig. 4.3) requires continuity over the positive real axis,

$$\log^{II}(-z) = \log(|z|) + i\,[\arg(z) - \pi] \tag{4.41}$$

Now we are able to extend the partial waves to the second Riemann sheet in order to look for any poles. A first approach could be looking for zeroes in the denominators, once extended to the II Riemann sheet the problematic expressions $\log(-s/\mu^2)$ by using eq. 4.41. This was the strategy that we followed in ref. [34].

Another possibility, only valid for *elastic* partial waves[2], would be using the fact that

$$A^{II}(s) = \frac{A(s)}{1 - 2iA(s)}, \tag{4.42}$$

where $A(s) = A^I(s)$ is the partial wave in the first Riemann sheet. This expression comes from the reflection principle (eq. 4.63) and the elastic version of the unitarity condition for massless particles (eq. 4.32 with $m = 0$, limit $\epsilon \to 0^+$),

$$\begin{aligned} A(s+i\epsilon) - A(s-i\epsilon) &= 2i\,\mathrm{Im}\, A(s+i\epsilon) = 2i[A(s+i\epsilon)]\cdot[A(s+i\epsilon)]^* \\ &= 2i[A(s+i\epsilon)]\cdot[A(s-i\epsilon)] \implies A(s+i\epsilon) = \frac{A(s-i\epsilon)}{1-2iA(s-i\epsilon)}. \end{aligned} \tag{4.43}$$

Because of the definition of II Riemann sheet, which requires continuity along the positive real axis, $\lim_{\epsilon\to 0^+} A^{II}(s-i\epsilon) = \lim_{\epsilon\to 0^+} A^{II}(s+i\epsilon) = \lim_{\epsilon\to 0^+} A(s+i\epsilon)$, so that eq. 4.43 indeed gives $A^{II}(s-i\epsilon)$, under the positive real axis, in terms of the values of $A^I(s-i\epsilon)$ on the I Riemann sheet under the positive real axis. The full eq. 4.42 is proven by analytical continuation of $A^{II}(s-i\epsilon)$ computed via eq. 4.43.

[2]Note that the elastic version of unitarity, eq. 4.32, is required. See ref. [153], for instance.

Note that eq. 4.42 introduces the presence of poles on the II Riemann sheet because of the annihilation of the denominator $1-2iA(s)$, so that these poles s_R can be computed by solving the resonance equation

$$A(s_R) + \frac{i}{2} = 0, \tag{4.44}$$

where $A(s)$ is evaluated on the I Riemann sheet. However, remember that this approach is valid provided that the scattering is elastic. That is, there is no contribution coming from crossed-channels.

Another approach is that used by D. Espriu et al. [158], who look for jumps on the phase shift. As in the case of eq. 4.44, this approach is no longer valid for crossed-channels, since each individual channel does not satisfy unitarity by itself, see eq. 4.32.

Finally, a third approach, which was used by us in refs. [38, 39], is using a Cauchy line integral around a closed path in the complex s-plane. This approach is the only one which is still valid for crossed-channels, along with a brute-force search for annihilations of the denominator of the partial wave extended to the II-Riemann sheet, $A^{II}(s)$.

Due to the reflection principle of eq. 4.63, every pole on the First Riemann sheet belonging to $\mathrm{Im}\, s' > 0$ will have a counterpart on $\mathrm{Im}\, s' < 0$. So that, we will consider a complex amplitude function $A(s)$ which will be defined as its II Riemann Sheet for $\mathrm{Im}\, s < 0$, that is, its analytical continuation through the real axis $s > 0$ (see Fig. 4.2). If there is any pole on the I Riemann sheet, it will apear for $\mathrm{Im}\, s > 0$. And we will be able to pick up the poles on the II Riemann Sheet.

The low-energy perturbative interactions are weak. That is, the EFT treated in perturbation theory is valid for the low-energy regime. So, we do not look for bound states and restrict ourselves to $\mathrm{Re}\, s \geq 0$. As explained before, for $\mathrm{Im}\, s > 0$ the logarithms in $A(s)$ are evaluated on the first Riemann sheet and, for $\mathrm{Im}\, s < 0$, on the second one.

Our integration contour will be a semicircle in the s-plane with radius $R = (3\,\mathrm{TeV})^2$, which is the approximate range of validity of the unitarization procedures considered, closed by a segment of the imaginary axis. This contour will be parametrized by

$$\gamma(t) = \begin{cases} R\exp\left[\frac{i\pi}{2}(2t-1)\right] & \text{for } t \in [0,\, 1] \\ iR(3-2t) & \text{for } t \in (1,\, 2] \end{cases} \tag{4.45}$$

According to Cauchy's theorem [159–161], if $A(s)$ has N poles on points s_i $(i = 1, \ldots, N)$ within the region enclosed by $\gamma(t)$ $(t \in [0,\, 2])$, then

$$I_k \equiv \int_{\gamma(t)} dt A(t) t^k = 2\pi i \sum_{i=1}^{N} s_i^k A_0(s_i). \tag{4.46}$$

Here, $A_0(s_i)$ is the pole residue corresponding to the i-th pole. Note that there is no reason to expect double poles in our NLO-based computation, although this kind of approach could deal with a number of poles as high as required at the cost of an increasing number of complex integrals to compute.

For each parameter set, the integrals I_0, I_1 and I_2 (see eq. 4.46) are evaluated. If there is no pole inside the integration contour parametrized by the function $\gamma(t)$ (eq. 4.45), then the values of all the integrals are zero. If there is only one pole at position $\tilde{s}$ then, according to eq. 4.46,

$$I_0 = A_0(\tilde{s}), \quad I_1 = \tilde{s}A_0(\tilde{s}), \quad I_2 = \tilde{s}^2 A_0(\tilde{s}) \tag{4.47}$$

So, the pole residue is $A_0(\tilde{s}) = I_0$; the pole position $\tilde{s}$,

$$\tilde{s} = \frac{I_1}{I_0}; \tag{4.48}$$

and we have the relation

$$I_1^2 = I_0 I_2 \tag{4.49}$$

that can be used as a check of the presence of a second pole. It should be exact if there is only one pole. If we had $N = 2$ poles, which is beyond the scope of this study, we could still compute both poles applying the equation

$$s_{1,2} = \frac{(I_1 I_2 - I_0 I_3) \pm \sqrt{(I_1 I_2 - I_0 I_3)^2 - 4(I_1^2 - I_0 I_2)(I_2^2 - I_1 I_3)}}{2(I_1^2 - I_0 I_2)}. \tag{4.50}$$

Even for $N = 3$ poles, the solution is still analytic. In this case, $k = 0, \ldots, 5$ integrals are needed. It is best quoted in terms of several auxiliary quantities, namely

$$\Delta = -I_3^3 + 2I_2 I_3 I_4 - I_1 I_4^2 - I_2^2 I_5 + I_1 I_3 I_5 \tag{4.51a}$$

$$\Delta \cdot \hat{A} = -I_3^2 I_4 + I_2 I_4^2 + I_2 I_3 I_5 - I_1 I_4 I_5 - I_2^2 I_6 + I_1 I_3 I_6 \tag{4.51b}$$

$$\Delta \cdot \hat{B} = -I_3 I_4^2 + I_3^2 I_5 + I_2 I_4 I_5 - I_1 I_5^2 - I_2 I_3 I_6 + I_1 I_4 I_6 \tag{4.51c}$$

$$\Delta \cdot \hat{C} = -I_4^3 + 2I_3 I_4 I_5 - I_2 I_5^2 - I_3^2 I_6 + I_2 I_4 I_6 \tag{4.51d}$$

$$\Lambda = -\hat{A}^2 \hat{B}^2 + 4\hat{B}^3 + 4\hat{A}^3 \hat{C} - 18\hat{A}\hat{B}\hat{C} + 27\hat{C}^2 \tag{4.51e}$$

$$\Gamma = \left(-2\hat{A}^3 + 9\hat{A}\hat{B} - 27\hat{C} + 3\sqrt{3\Lambda}\right)^{1/3}. \tag{4.51f}$$

Then the pole locations become

$$s_1 = \frac{\hat{A}}{3} + \frac{2^{1/3}(3\hat{B} - \hat{A}^2)}{3\Gamma} - \frac{\Gamma}{3 \cdot 2^{1/3}} \tag{4.52a}$$

$$s_2 = \frac{\hat{A}}{3} - \frac{3(1 + i\sqrt{3})(\hat{B} + \hat{A}^2)}{3 \cdot 2^{2/3}\Gamma} - \frac{(1 - i\sqrt{3})\Gamma}{6 \cdot 2^{1/3}} \tag{4.52b}$$

$$s_3 = \frac{\hat{A}}{3} - \frac{3(1 - i\sqrt{3})(\hat{B} + \hat{A}^2)}{3 \cdot 2^{2/3}\Gamma} - \frac{(1 + i\sqrt{3})\Gamma}{6 \cdot 2^{1/3}}. \tag{4.52c}$$

4.3 Unitarization procedures for $\omega\omega$ scattering

In this section we deal with the unitarization of $\omega\omega$ scattering, which we published in refs. [38, 39]. The channels $\omega\omega$ and hh are considered,

$$A_{IJ} = \mathcal{M}_{IJ}(\omega\omega \to \omega\omega) \tag{4.53a}$$

$$M_J = \mathcal{M}_{0J}(\omega\omega \to hh) = \mathcal{M}_{0J}(hh \to \omega\omega) \tag{4.53b}$$

$$T_J = \mathcal{M}_{0J}(hh \to hh), \tag{4.53c}$$

where the partial wave decomposition from sec. 3.3.1 has been used. According to eq. 4.31 (in the massless limit $s \gg M_W^2,\ M_Z^2,\ M_h^2$), the unitarity condition can be written, in terms of the partial-wave decomposition F of the reaction matrix, as

$$\operatorname{Im} F(s) = F(s)F(s)^\dagger. \tag{4.54}$$

Note that, because of T-invariance (see eq. 4.7), the matrix F is symmetric, $F(s)^t = F(s)$. Thus, the unitarity relation (eq. 4.54) implies that $\mathrm{Im}\, F(s) = F(s)F(s)^\dagger = F(s)F(s)^* \in \mathbb{R}$. Hence, $\mathrm{Im}\, F(s) = F(s)F(s)^\dagger = F(s)F(s)^* = [F(s)F(s)^*]^* = F(s)^*F(s) = F(s)^\dagger F(s)$. Thus, eq. 4.54 can also we written as

$$\mathrm{Im}\, F(s) = F(s)F(s)^\dagger = F(s)^\dagger F(s). \tag{4.55}$$

Now, the reaction matrix F, in partial-wave decomposition, will be

$$F(s) = \begin{pmatrix} F_{00}(s) & 0 & 0 & 0 & 0 \\ 0 & F_{11}(s) & 0 & 0 & 0 \\ 0 & 0 & F_{20}(s) & 0 & 0 \\ 0 & 0 & 0 & F_{02}(s) & 0 \\ 0 & 0 & 0 & 0 & F_{22}(s) \end{pmatrix}, \tag{4.56}$$

where we have used isospin symmetry. No matrix element links states with different I. Also, because of the properties of partial waves, states with different J are not connected either. However, $\omega\omega$ and hh states with the same IJ numbers can be linked by a scattering matrix element. Because of this, the channel $\omega\omega \to hh$ amplitude is zero for $I \neq 0$. Actually, the isospin of hh state is zero (h is a scalar). So,

$$F_{0J}(s) = \begin{pmatrix} A_{0J}(s) & M_J(s) \\ M_J(s) & T_J(s), \end{pmatrix},\ J = 0, 2 \tag{4.57}$$

For $I \neq 0$, the $F_{IJ}(s)$ elements are the scalars

$$F_{IJ}(s) = A_{IJ}(s)\ \forall I \neq 0. \tag{4.58}$$

To sum up, the unitarity condition 4.31, in terms of partial-waves, is written down as

$$\mathrm{Im}\, A_{0J} = |A_{0J}|^2 + |M_J|^2 \tag{4.59a}$$
$$\mathrm{Im}\, A_{IJ} = |A_{IJ}|^2 \quad \forall I \neq 0 \tag{4.59b}$$
$$\mathrm{Im}\, M_J = A_{0J}M_J^* + M_J T_J^* \tag{4.59c}$$
$$\mathrm{Im}\, T_J = |M_J|^2 + |T_J|^2 \tag{4.59d}$$

Now, take into account the partial-wave decomposition in eq. 3.132 for NLO partial waves, valid for massless particles,

$$F_{IJ}^{(0)}(s) = K_{IJ}s \tag{4.60a}$$
$$F_{IJ}^{(1)}(s) = \left(B_{IJ}(\mu) + D_{IJ}\log\frac{s}{\mu^2} + E_{IJ}\log\frac{-s}{\mu^2}\right)s^2 \tag{4.60b}$$

Applying Eqs. 4.59 in a perturbative way (expanding over s), and taking into account that the K_{IJ} are real numbers,

$$\mathrm{Im}\, F_{IJ}^{(1)} = F_{IJ}^{(0)}F_{IJ}^{(0)} \tag{4.61}$$

This relation is satisfied by any scattering partial-wave of the form of eq. 4.58. The exact form 4.58 would be satisfied by the full computation. But this sets an upper limit on the value of $|M|^2$. Consider a single-channel scattering matrix $\mathcal{M} = Me^{i\delta}$, $M \geq 0$. Then,

according to elastic unitarity in eq. 4.59a, $M^2 = M \sin\delta \leq M$, so that $M \leq 1$. This limit, if exceeded, will inform us about the validity range of the perturbative expansion.

Also, when entering an expression as eq. 4.60 on the perturbative unitary condition 4.61, which is valid on the physical region ($s' = s + i\epsilon$, $\epsilon \to 0^+$, $s > 0$), we have the additional restriction over K_{IJ} and E_{IJ},

$$E = -\frac{1}{\pi} K^2, \tag{4.62}$$

where we have used the matricial form of E and K. This expression is very useful to check the full NLO computation, and it can be seen that it is verified by the constants given on Sec. 3.3.1. Note also that eq. 3.135,

$$B(\mu) = B(\mu_0) + (D + E) \log \frac{\mu^2}{\mu_0^2},$$

is also valid for the matricial B, D and E.

4.3.1 Dispersion relations

Now, we will need the so–called *dispersion relations*. To see the full proofs, including those of the analytical properties of the S-matrix elements, see Refs. [139, 140]. Note that, because of the presence of a *left cut* due to the terms $E \log(-s/\mu^2)$ on the amplitudes[3], the so–called *forward* dispersion relations cannot be used. Fixed-t dispersion relations remain integral equations. This is the partial-wave dispersion relations that will lead to simple formulas.

The key property that we need to prove is that, on both the left and right cuts (LC and RC) of fig. 4.5,

$$A(s + i\epsilon) - A(s - i\epsilon) = 2i \,\mathrm{Im}\, A(s + i\epsilon),\ \epsilon \to 0^+, \tag{4.63}$$

or, even stronger, that

$$A\left(s^*\right) = \left[A(s)\right]^*,\ s \in \mathbb{C} \setminus \mathbb{R}, \tag{4.64}$$

the physical amplitude being

$$A(s)_{\text{phys}} = \lim_{\epsilon \to 0^+} A(s + i\epsilon),\ s > 0. \tag{4.65}$$

This last equation can be regarded as conventional, because we could take the other prescription [$A(s)_{\text{phys}} = A(s - i\epsilon)$]. But, once this chosen, let us prove eq. 4.64. First, let us suppose that there is a minimum energy threshold $\sqrt{s_{\min}}$ required for the process. Then, according to eq. 4.59, the imaginary part of the amplitude will be zero for $0 < s < s_{\min}$. But, according to the properties of analytical functions [159–161], provided that the function is analytic around a segment over the real axis, this implies that, as shown in fig. 4.4, it is possible to perform a power expansion of the form

$$A(s) = \sum_{k=0}^{\infty} \frac{1}{k!} \left.\frac{d^k\, A(s)}{d\, s^k}\right|_{s = s_{\min}/2} \left(s - \frac{s_{\min}}{2}\right)^k \equiv \sum_{k=0}^{\infty} a_k \left(s - \frac{s_{\min}}{2}\right)^k, \tag{4.66}$$

[3] See eq. 3.132 for the appearance of such a term in the $\omega\omega$ scattering amplitudes.

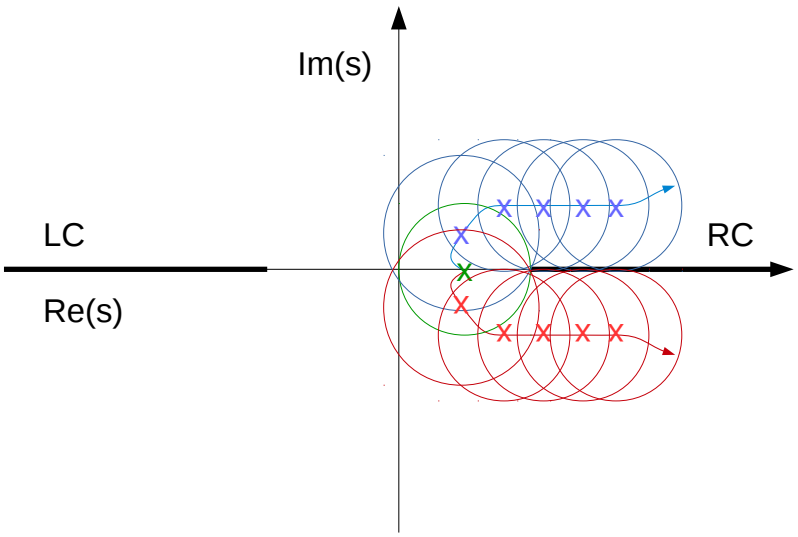

Figure 4.4: Analytic extension of a function which is real on a segment of the real axis. In general, this kind of analytical extension is also valid for every function provided that is analytic on $\mathbb{C}\setminus[(-\infty,a)\cup(b,\infty)]$, where $a<b$. Note that the real axis must be crossed through the analytic segment. In our work, we neglect the masses of the initial and final state particles, which makes this segment to collapse to a single point (the origin). However, the analytical extension is still valid. See the explanation under eq. 4.70.

being convergent on $s\in\mathbb{C}\mid|s-(s_{\min}/2)|<s_{\min}/2$. Now, because $A(s)\in\mathbb{R}\,\forall s\in(0,s_{\min})$, then $a_k\in\mathbb{R}$, so that

$$[A(s)]^*=\left[\sum_{k=0}^{\infty}a_k\left(s-\frac{s_{\min}}{2}\right)^k\right]^*=\sum_{k=0}^{\infty}a_k\left(s^*-\frac{s_{\min}}{2}\right)^k=A\left(s^*\right)$$
$$\forall\left|s-\frac{s_{\min}}{2}\right|<\frac{s_{\min}}{2},\ s\in\mathbb{C} \quad (4.67)$$

This truly defines an analytical function in the region $|s-(s_{\min}/2)|<s_{\min}/2$ of the complex plane. In any point of such a region, another analytical expansion can be carried out in the same way, the convergence area of the power expansion being a circle centered on the considered point and ending in the real axis outside the segment $0<s<s_{\min}$, beyond where the function may have the so–called *cuts* (discontinuities when crossing the real axis).

If now we perform another expansion, such as suggested in fig. 4.4. In this case,

$$A(s)=\sum_{l=0}^{\infty}\frac{1}{l!}\frac{d^l\,A(s)}{d\,s^l}\bigg|_{s=s_1}(s-s_1)^2 \quad (4.68)$$

But, because $A(s_1^*)=A(s_1)^*$, and $(s-s_1)^*=(s^*-s_1^*)$, then, again,

$$A(s^*)=\sum_{l=0}^{\infty}\frac{1}{l!}\frac{d^l\,A(s)}{d\,s^l}\bigg|_{s=s_1^*}(s^*-s_1^*)^2=\left[\sum_{l=0}^{\infty}\frac{1}{l!}\frac{d^l\,A(s)}{d\,s^l}\bigg|_{s=s_1}(s-s_1)^2\right]^*=[A(s)]^* \quad (4.69)$$

Repeating this process to reach any point in the space $\mathbb{C}\setminus\mathbb{R}$, we can prove eq. 4.64, $[A(s)]^*=A(s^*)$. Now, proving eq. 4.63 is trivial,

$$A(s+i\epsilon)-A(s-i\epsilon)=A(s+i\epsilon)-[A(s+i\epsilon)]^*=2i\,\mathrm{Im}\,A(s+i\epsilon),\ \epsilon\to0^+. \quad (4.70)$$

Note that, in our work, due to the fact that we are considering all the particles as massless, the minimum squared energy threshold $s_{\rm min}$ is zero. Thus, the finite segment $0 < s < s_{\rm min}$, which allows us to do the analytical continuation (see fig. 4.4), collapses to a point (the origin), where there is a so–called *Adler zero*. In principle, this would break the power expansion of eq. 4.66. However, we can work in the limit where $s_{\rm min} \to 0^+$. This is equivalent to keeping finite masses and taking the limit $M_W, M_h \to 0^+$ at the end. Since the analytical extension procedure (eqs. from 4.66 to 4.70) does not depend on a minimum value of $s_{\rm min}$, working in the limit $s_{\rm min} \to 0^+$ is enough to comply with the hypothesis $s_{\rm min} > 0$.

For the derivation of the unitarization procedures, it will be also very useful to take the next relations into account[4], which can be proven from eqs. 4.60:

$$\frac{1}{\pi}\int_0^{\Lambda^2} \frac{ds'\,\mathrm{Im}\,F_{IJ}^{(1)}(s')}{(s')^2(s'-s-i\epsilon)} = E_{IJ}\log\frac{-s}{\Lambda^2} \tag{4.71a}$$

$$\frac{1}{\pi}\int_{-\Lambda^2}^{0} \frac{ds'\,\mathrm{Im}\,F_{IJ}^{(1)}(s')}{(s')^2(s'-s-i\epsilon)} = D_{IJ}\log\frac{s}{\Lambda^2} \tag{4.71b}$$

$$\frac{1}{2\pi i}\int_{|s'|=\Lambda^2} \frac{ds'\,\mathrm{Im}\,F_{IJ}^{(1)}(s')}{(s')^2(s'-s-i\epsilon)} = B_{IJ}(\mu) + D_{IJ}\log\frac{\Lambda^2}{\mu^2} + E_{IJ}\log\frac{\Lambda^2}{\mu^2} \tag{4.71c}$$

To prove eq. 4.71a (eq. 4.71b is proven in a similar way), let us recall that, for $\epsilon > 0$, $s > 0$, $\mathrm{Im}[\log(-(s+i\epsilon)/\mu^2)] = -\pi$, so that

$$\begin{aligned}\int_0^{\Lambda^2} \frac{ds'\,\mathrm{Im}\,F_{IJ}^{(1)}(s')}{(s')^2(s'-s-i\epsilon)} &= \int_0^{\Lambda^2} \frac{ds'(-\pi E_{IJ})}{s'-s-i\epsilon} \\ &\overset{\epsilon\to 0^+}{=} -\pi E_{IJ}\log(s'-s)\big|_{s=0}^{\Lambda^2} \overset{\Lambda^2\gg s}{\approx} \pi E_{IJ}\log\frac{-s}{\Lambda^2}\end{aligned} \tag{4.72}$$

For eq. 4.71c, let us use polar variables $z = \Lambda^2\exp(i\phi)$,

$$\begin{aligned}&\int_{|s'|=\Lambda^2} \frac{ds'\,\mathrm{Im}\,F_{IJ}^{(1)}(s')}{(s')^2(s'-s-i\epsilon)} \\ &\qquad = \int_0^{2\pi} d\phi\cdot i\Lambda^2 e^{i\phi}\frac{B_{IJ}(\mu) + D_{IJ}\log(\Lambda^2 e^{i\phi}/\mu^2) + E_{IJ}\log(-\Lambda^2 e^{i\phi}/\mu^2)}{\Lambda^2 e^{i\phi} - s - i\epsilon}\end{aligned} \tag{4.73}$$

Now, because $\Lambda^2 \gg s$, we can approximate this integral by

$$\begin{aligned}\int_{|s'|=\Lambda^2} \frac{ds'\,\mathrm{Im}\,F_{IJ}^{(1)}(s')}{(s')^2(s'-s-i\epsilon)} &\approx i\int_0^{2\pi} d\phi\cdot\left[B_{IJ}(\mu) + D_{IJ}\log(\Lambda^2/\mu^2) + E_{IJ}\log(\Lambda^2/\mu^2)\right] \\ &\quad + \int_{-\pi}^{\pi} d\phi\, i[iD_{IJ}\phi] + \int_0^{\pi} i[iE_{IJ}\phi - i\pi] + \int_{-\pi}^{0} i[iE_{IJ}\phi + i\pi],\end{aligned} \tag{4.74}$$

where the *standard* determination for the logarithm in the I Riemann sheet, $\log(Ae^{i\phi}) = A + i\phi$, $\forall\phi \in (-\pi,\pi)$, has been used. Now, making the final integration, we have

$$\int_{|s'|=\Lambda^2} \frac{ds'\,\mathrm{Im}\,F_{IJ}^{(1)}(s')}{(s')^2(s'-s-i\epsilon)} \approx 2i\pi\left[B_{IJ}(\mu) + D_{IJ}\log(\Lambda^2/\mu^2) + E_{IJ}\log(\Lambda^2/\mu^2)\right]. \tag{4.75}$$

[4]Here, $\epsilon \to 0^+$.

Finally, taking into account that $\Lambda^2 \gg s$,

$$\int_{|s|=\Lambda^2} \frac{ds'\, F^{(0)}(s')}{(s')^2(s'-s)} \approx \int_0^{2\pi} d\phi \cdot i\Lambda^2 e^{i\phi} \frac{K_{IJ}\Lambda^2 e^{i\phi}}{(\Lambda^2 e^{i\phi})^3} = \frac{iK_{IJ}}{\Lambda^2} \int_{-\pi}^{\pi} d\phi \cdot e^{-i\phi} = 0, \tag{4.76}$$

Note that the approximations of eqs. 4.75 and 4.76 are exact in the limit $\Lambda^2 \to \infty$.

In the next sections, we will show the derivation of the unitarization procedures that will be used here: the Inverse Amplitude Method (IAM), the N/D, the *improved* K-matrix and the large-N methods.

4.3.2 Inverse Amplitude Method

An introduction to this method can be found in refs. [11, 162, 163]. This method was developed for low-energy QCD, where it was applied for ordinary ChPT for mesons (see refs. [91, 164–166]). Later, it was applied to the unitarization of the divergent NLO WBGBs scattering amplitudes of higgsless models (refs. [9–11, 167]), and has been shown (ref. [168]) that it is able to properly reproduce the channel and mass of an electroweak resonance from the footprint it leaves on the chiral parameters alone; only its width is not adequately reproduced if such resonance is very weakly coupled.

For an elastic process, unitarity implies that[5], when using partial waves,

$$\operatorname{Im} A(s) = |A(s)|^2 \Longrightarrow \operatorname{Im}\left(\frac{1}{A(s)}\right) = -\frac{\operatorname{Im} A(s)}{|A(s)|^2} = -1 \tag{4.77}$$

is exactly known, provided that $\operatorname{Im} A(s) \neq 0$. This is a remarkable result. There is an analogous expression for the matricial form of two-body partial wave amplitudes, which corresponds to non-elastic processes,

$$\operatorname{Im} F^{-1} = -\mathbb{1}. \tag{4.78}$$

Let us prove eq. 4.78. Because of T-invariance, the reaction matrix F is symmetric ($F = F^t$, $F^\dagger = F^*$). Taking also into account that

$$\operatorname{Im} F = \frac{1}{2i}[F - F^*] \tag{4.79a}$$

$$\operatorname{Im} F^{-1} = \frac{1}{2i}[F^{-1} - (F^{-1})^*] \tag{4.79b}$$

$$(F^*)^{-1} = (F^{-1})^*, \tag{4.79c}$$

we can compute

$$\begin{aligned} 0 = \mathbb{1} - [F^{-1}]^* F + (F^*)^{-1} F - \mathbb{1} &= [F^{-1} - (F^{-1})^*]F + (F^*)^{-1}(F - F^*) \\ &= [\operatorname{Im}(F^{-1})]F + (F^*)^{-1} \operatorname{Im} F = [\operatorname{Im}(F^{-1})]F + (F^\dagger)^{-1} \operatorname{Im} F, \end{aligned} \tag{4.80}$$

so that

$$\operatorname{Im}(F^{-1}) = -(F^\dagger)^{-1}(\operatorname{Im} F)(F^{-1}). \tag{4.81}$$

Because of the unitarity condition $\operatorname{Im} F = FF^\dagger = F^\dagger F$ (eq. 4.55), we can rewrite eq. 4.81 as

$$\operatorname{Im} F^{-1} = -(F^\dagger)^{-1}(\operatorname{Im} F)(F^{-1}) = -(F^\dagger)^{-1}(F^\dagger F)(F^{-1}) = -\mathbb{1}, \tag{4.82}$$

[5] See eq. 4.59 for the unitarity expressions and, for the complex variable properties, Refs. [159–161]. And take into account that $z = a\exp(i\alpha) \Longrightarrow \operatorname{Im}[1/z] = \operatorname{Im}[\exp(-i\alpha)/a] = -\operatorname{Im}(z)/|z|^2$.

thus recovering eq. 4.78.

Now, consider the generic form of our NLO processes (eq. 4.60),

$$F_{IJ}^{(0)}(s) = K_{IJ}s$$
$$F_{IJ}^{(1)}(s) = \left(B_{IJ}(\mu) + D_{IJ}\log\frac{s}{\mu^2} + E_{IJ}\log\frac{-s}{\mu^2}\right)s^2.$$

The perturbative expansion to NLO of the partial wave, valid for small s, would be

$$F_{IJ}(s) = F_{IJ}^{(0)}(s) + F_{IJ}^{(1)}(s) + \mathcal{O}(s^3). \tag{4.83}$$

Let us introduce the so–called *inverse amplitude* matrix,

$$W = F^{(0)}F^{-1}F^{(0)}. \tag{4.84}$$

Over the *physical* s (RC), where the unitarity condition of eq. 4.55 holds, we can apply eq. 4.78. Thus, using also that $\operatorname{Im}F^{(0)} = 0$ over the physical s (eq. 4.60),

$$\operatorname{Im}W = \operatorname{Im}(F^{(0)}F^{-1}F^{(0)}) = F^{(0)}\operatorname{Im}(F^{-1})F^{(0)} = -F^{(0)}(-\mathbb{1})F^{(0)} = -F^{(0)}F^{(0)}. \tag{4.85}$$

Now, applying the perturbative version of unitarity (eq. 4.61),

$$\operatorname{Im}W = -\operatorname{Im}F^{(1)} \tag{4.86}$$

This expression is *exact* over the RC. At other locations of the complex plane, it is only perturbatively correct. in particular, over the left cut (LC), it is approximate to order $\mathcal{O}(s^3)$,

$$\operatorname{Im}W = -\operatorname{Im}F^{(1)} + \mathcal{O}(s^3). \tag{4.87}$$

Let us see why. Taking into account (eq. 4.60) that $F^{(0)} \sim \mathcal{O}(s)$ and $F^{(1)} \sim \mathcal{O}(s^2)$,

$$F^{-1} = [F^{(0)} + F^{(1)} + \mathcal{O}(s^3)]^{-1} = \left[\left(\mathbb{1} + F^{(1)}(F^{(0)})^{-1} + \mathcal{O}(s^2)\right)F^{(0)}\right]^{-1}$$
$$= [F^{(0)}]^{-1}[\mathbb{1} - F^{(1)}\cdot(F^{(0)})^{-1} + \mathcal{O}(s^2)]. \tag{4.88}$$

Thus, introducing eq. 4.88 inside the definition of eq. 4.84, we obtain

$$W = F^{(0)}F^{-1}F^{(0)} = [F^{(0)}F^{(0)}]^{-1}[\mathbb{1} - F^{(1)}\cdot(F^{(0)})^{-1} + \mathcal{O}(s^2)][F^{(0)}]$$
$$= F^{(0)} - F^{(1)} + \mathcal{O}(s^3). \tag{4.89}$$

Now, we need to take into account that we are evaluating s over the LC. That is, $s = s' + i\epsilon$, where $s' < 0$ and $\epsilon \to 0^+$. Thus, the imaginary part of $F^{(0)}$ (eq. 4.60) turns into

$$\operatorname{Im}F^{(0)} = \operatorname{Im}(Ks) = \epsilon \to 0^+. \tag{4.90}$$

Thus, over the LC, eq. 4.89 can we written as $\operatorname{Im}W = -\operatorname{Im}F^{(1)} + \mathcal{O}(s^3)$, which indeed is eq. 4.87.

At this point, we will make use of the so–called *twice-subtracted* DR. Taking into account the Cauchy's Residue Theorem [159–161],

$$\int_\gamma ds' \frac{W_{IJ}(s')}{s'^2(s' - s - i\epsilon)} = 2\pi i \sum_j \operatorname{Res}\left[\frac{W_{IJ}(s')}{s'^2(s' - s - i\epsilon)}, s'_j\right], \tag{4.91}$$

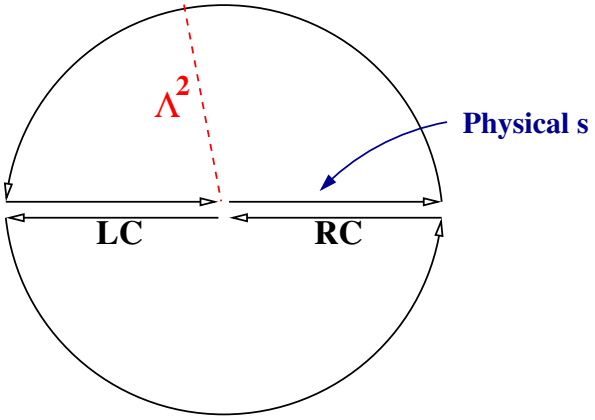

Figure 4.5: Contour for the application of Cauchy's theorem in eq. 4.91 to derive the dispersion relation in eq. 4.93. Note the presence of two cuts on the real axis (LC and RC). The *physical* values of the scattering amplitude are recovered over the right cut ($s' = s + i\epsilon$, $\epsilon \to 0^+$).

The integration contour chosen is shown in fig. 4.5, and we are using the fact that $W(s) \equiv F^{(0)}F^{-1}F^{(0)}$ (eq. 4.84) has the same analytic structure than $F(s)$ up to possible poles coming from zeros of $A(s)$. This is due to the fact that $F^{(0)} \equiv Ks$ (eq. 4.60) is analytical on $\mathbb{C}$ and only vanishes for $s = 0$. The Adler zero (on $s_{\rm Adler} = 0$) is a particular case, since the zero on $F^{(0)}$ cancels the single pole on F^{-1}. This analysis supposes that we are working in the limit where the masses of all the particles are negligible. Ref. [169] studies in more detail scattering processes with massive particles and subthreshold poles, both being a very small effect.

Now, let us evaluate the residues of $W_{IJ}(s')/s'^2(s'-s-i\epsilon)$. At lowest order, $W_{IJ}(s) \approx K_{IJ}s + \mathcal{O}(s^2)$, so that, neglecting other poles [zeroes of $F(s)$] inside the integration contour, the Cauchy integral of eq. 4.91 turns into

$$\int_\gamma ds' \frac{W_{IJ}(s')}{s'^2(s'-s-i\epsilon)} = 2\pi i \sum_j \text{Res}\left[\frac{W_{IJ}(s')}{s'^2(s'-s-i\epsilon)}, s'_j\right] = -\frac{K_{IJ}}{s+i\epsilon} + \frac{W_{IJ}(s+i\epsilon)}{(s+i\epsilon)^2}. \tag{4.92}$$

In order to carry out the actual integration over the contour of fig. 4.5, we will take different $\epsilon \to 0^+$ and $\varepsilon' \to 0^+$, the first one being the distance between the *evaluating point* $s + i\epsilon$ and the RC (in order for the point to be in the *physical region*); and the second one, the distance between the integration contour and the cuts. In order for this integration to work, it should be that $\epsilon > \varepsilon'$. That is, $s + i\epsilon$ should be over and very close to the real axis (*physical* s), but still inside the region defined by the integration contour, so Cauchy's theorem can be applied. At the end, both ϵ and ε' will be taken in the limit $\to 0^+$. Thus, the integration of the LHS of eq. 4.92 is

$$\begin{aligned}\int_\gamma ds' \frac{W_{IJ}(s')}{s'^2(s'-s-i\epsilon)} = &\int_{|s'|=\Lambda^2} \frac{ds' W_{IJ}(s')}{(s')^2(s'-s-i\epsilon)} + \int_0^\Lambda \frac{ds' W_{IJ}(s'+i\varepsilon')}{(s'+i\varepsilon')^2(s'-s-i\epsilon)} \\ &+ \int_{-\Lambda}^0 \frac{ds' W_{IJ}(s'+i\varepsilon')}{(s'+i\varepsilon')^2(s'-s-i\epsilon)} + \int_0^{-\Lambda} \frac{ds' W_{IJ}(s'-i\varepsilon')}{(s'-i\varepsilon')^2(s'-s-i\epsilon)} \\ &+ \int_\Lambda^0 \frac{ds' W_{IJ}(s'-i\varepsilon')}{(s'-i\varepsilon')^2(s'-s-i\epsilon)}\end{aligned} \tag{4.93}$$

Now, take into account eq. 4.63, $F_{IJ}(s+i\varepsilon') - F_{IJ}(s-i\varepsilon') = 2i\,\text{Im}\,F_{IJ}(s+i\varepsilon')$. Since

$W_{IJ}(s)$ has the same analytical structure, the derivation of this equation is still valid for $W_{IJ}(s)$, so that

$$W_{IJ}(s+i\epsilon) = K_{IJ}s + \frac{s^2}{2\pi i}\int_{|s'|=\Lambda^2}\frac{ds' W_{IJ}(s')}{(s')^2(s'-s-i\epsilon)} + \frac{s^2}{\pi}\int_0^{\Lambda}\frac{ds'\,\mathrm{Im}\,W_{IJ}(s'+i\varepsilon')}{(s')^2(s'-s-i\epsilon)} + \frac{s^2}{\pi}\int_{-\Lambda}^{0}\frac{ds'\,\mathrm{Im}\,W_{IJ}(s'+i\varepsilon')}{(s')^2(s'-s-i\epsilon)}, \quad (4.94)$$

and using eq. 4.86 both in the RC (exact) and the LC (approximate),

$$W_{IJ}(s+i\epsilon) \approx K_{IJ}s + \frac{s^2}{2\pi i}\int_{|s'|=\Lambda^2}\frac{ds' W_{IJ}(s')}{(s')^2(s'-s-i\epsilon)} - \frac{s^2}{\pi}\int_0^{\Lambda}\frac{ds'\,\mathrm{Im}\,F^{(1)}_{IJ}(s'+i\varepsilon')}{(s')^2(s'-s-i\epsilon)} - \frac{s^2}{\pi}\int_{-\Lambda}^{0}\frac{ds'\,\mathrm{Im}\,F^{(1)}_{IJ}(s'+i\varepsilon')}{(s')^2(s'-s-i\epsilon)}, \quad (4.95)$$

Now, taking into account eqs. 4.71,

$$W_{IJ}(s+i\epsilon) \approx K_{IJ}s - D_{IJ}s^2\log\frac{s}{\Lambda^2} - E_{IJ}s^2\log\frac{-s}{\Lambda^2} + \frac{s^2}{2\pi i}\int_{|s'|=\Lambda^2}\frac{ds'\,W_{IJ}(s')}{(s')^2(s'-s-i\epsilon)}. \quad (4.96)$$

And, using again eqs. 4.71 and 4.76, it is easily proven that this integral equation is solved by

$$W_{IJ}(s) = F^{(0)}_{IJ}(s) - F^{(1)}_{IJ}(s). \quad (4.97)$$

Now, considering the definition of the *Inverse Amplitude Matrix*, $W(s) = F^{(0)}F^{-1}F^{(0)}$ (eq. 4.84),

$$W(s) \approx F^{(0)}(s) - F^{(1)}(s) = F^{(0)}(s)F^{-1}_{\mathrm{IAM}}(s)F^{(0)}(s) \Longrightarrow F^{-1}_{\mathrm{IAM}}(s) = [F^{(0)}(s)]^{-1}[F^{(0)}(s) - F^{(1)}(s)][F^{(0)}(s)]^{-1}, \quad (4.98)$$

F_{IAM} being the *scattering partial wave* resulting from the application of the *Inverse Amplitude Method*. Thus, at the end, we arrive to the formula

$$F_{\mathrm{IAM}}(s) = [F^{(0)}(s)][F^{(0)}(s) - F^{(1)}(s)]^{-1}[F^{(0)}(s)], \quad (4.99)$$

taht reduces, for elastic scattering, to

$$A_{\mathrm{IAM}}(s) = \frac{[A^{(0)}(s)]^2}{A^{(0)}(s) - A^{(1)}(s)}. \quad (4.100)$$

4.3.3 N/D method

An introduction to this method can be found, for instance, in ref. [170]. The starting point is to consider an ansatz for the partial wave *numerator* and *denominator*,

$$A(s) = \frac{N(s)}{D(s)}, \quad (4.101)$$

$N(s)$ having only a left cut (LC) and $D(s)$ only a right cut (RC). Because of the *reflection principle* (eq. 4.63), this implies that

$$N(s), \text{ only LC} \Rightarrow N(s), \text{ continuous over the RC} \Rightarrow \mathrm{Im}\,N(s) = 0\,\forall s \in \mathrm{RC}$$

$$D(s), \text{ only RC} \Rightarrow D(s), \text{ continuous over the LC} \Rightarrow \operatorname{Im} D(s) = 0 \, \forall s \in \text{LC}$$

Now, using unitarity for elastic channels[6], the method should satisfy

$$\operatorname{Im} A(s) = |A(s)|^2 \Rightarrow \operatorname{Im} \frac{N(s)}{D(s)} = \frac{|N(s)|^2}{|D(s)|^2} \tag{4.102}$$

to be unitary. Let us study the consequences of eq. 4.102. Since, on the RC, $\operatorname{Im} N(s) = 0$, then

$$s \in \text{RC} \overset{\operatorname{Im} N(s)=0}{\Longrightarrow} \operatorname{Im} \frac{N(s)}{D(s)} = N(s) \operatorname{Im} \frac{1}{\operatorname{Re} D(s) + i \operatorname{Im} D(s)} = \frac{-N(s) \operatorname{Im} D(s)}{|D(s)|^2} = \frac{[N(s)]^2}{|D(s)|^2}$$
$$\Rightarrow \operatorname{Im} D(s) = -N(s) \tag{4.103}$$

And, on the LC, $\operatorname{Im} D(s) = 0$, then

$$s \in \text{LC} \overset{\operatorname{Im} D(s)=0}{\Longrightarrow} \operatorname{Im} A(s) = \operatorname{Im} \frac{N(s)}{D(s)} = \frac{\operatorname{Im} N(s)}{D(s)} \Rightarrow \operatorname{Im} N(s) = D(s) \operatorname{Im} A(s) \tag{4.104}$$

There is a similar (matrix) expression for coupled channels[7]. In this case, the $F(s)$ matrix is written as

$$F(s) = [D(s)]^{-1} N(s). \tag{4.105}$$

As in the elastic (non-matricial) case (see eqs. 4.102 to 4.104), we have $\operatorname{Im} N(s) = 0 \, [N(s) \text{ continuous}] \, \forall s \in \text{RC}$; and $\operatorname{Im} D(s) = 0 \, [D(s) \text{ continuous}] \, \forall s \in \text{LC}$. This allows us to recover the expressions equivalent to eqs. 4.103 and 4.104. First of all, over the right cut, $\operatorname{Im} N(s) = 0$, and taking into account the unitarity condition for coupled channels (eq. 4.55),

$$\begin{aligned} \operatorname{Im} F &= \operatorname{Im}\{[D(s)]^{-1} N(s)\} = \operatorname{Im}\{[D(s)]^{-1}\} N(s) = \frac{1}{2i}\{D^{-1}(s) - [D^{-1}(s)]^*\} N(s) \\ &= F(s) F(s)^\dagger = F F^* = [D^{-1}(s) N(s)][D^{-1}(s) N(s)]^* = D^{-1}(s) N(s) [D^{-1}(s)]^* N(s), \end{aligned} \tag{4.106}$$

where we have used the fact that $F(s)^t = F(s)$, because of the T symmetry. Now, provided that $N(s)$ is non-singular,

$$\begin{aligned} &\frac{1}{2i}\{D^{-1}(s) - [D^{-1}(s)]^*\} = D^{-1}(s) N(s) [D^{-1}(s)]^* \\ &\Rightarrow N(s) = \frac{1}{2i} D(s)\{D^{-1}(s) - [D^{-1}(s)]^*\} D^*(s) = \frac{1}{2i}\{D(s)^*(s) - D(s)\} = -\operatorname{Im} D(s), \end{aligned} \tag{4.107}$$

so that we recover eq. 4.103,

$$\operatorname{Im} D(s) = -N(s),$$

but for the matrix formalism of coupled channels. The matrix form of eq. 4.104 is easier. Just consider that, on the left cut, $\operatorname{Im} D(s) = 0$, so

$$\operatorname{Im} F(s) = \operatorname{Im}[D^{-1}(s) N(s)] = D^{-1}(s) \operatorname{Im} N(s) \Rightarrow \operatorname{Im} N(s) = D(s) \operatorname{Im} F(s) \tag{4.108}$$

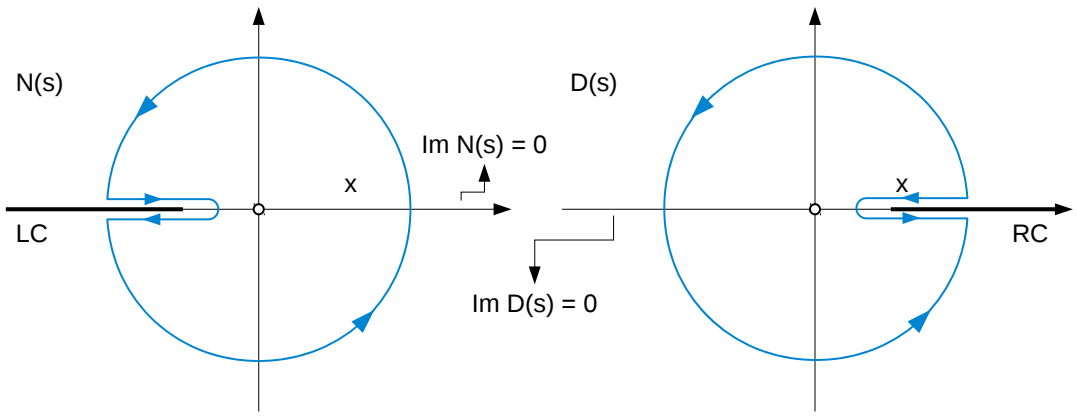

Figure 4.6: Contours for the application of Cauchy's theorem to the dispersion relations yielding the $N(s)$ and $D(s)$ functions of the N/D method. The $N(s)$ function has an Adler zero in $s = 0$ (eq. 4.110). Both $N(s)$ and $D(s)$ are analytic around $s = 0$ although, since we are neglecting the masses, this analytical region will collapse to the point $s = 0$ when the RC and LC are extended to $s = 0$. However, Cauchy's theorem can still be applied by taking the limit where this region collapses but still remains finite.

Now, the *zeroth-order* behaviour can be recovered by setting the normalization

$$D(0) = 1 \Rightarrow N(0) = A(0),\, F(0) \tag{4.109}$$

for the elastic $[A(0)]$ and cross-channel $[F(0)]$ formalisms, respectively. Because of the presence of the Adler zero in our expressions,

$$A(0),\, F(0) = 0 \implies N(0) = 0. \tag{4.110}$$

Eqs. 4.103 for $\operatorname{Im} D(s)$ [and 4.104 for $\operatorname{Im} N(s)$] will be used to compute dispersion relations. In both cases, because of their imaginary parts being zero over the LC [RC], the reflection principle 4.63 works,

$$N(s + i\epsilon) - N(s - i\epsilon) = 2i \operatorname{Im} N(s + i\epsilon),\ s > 0 \tag{4.111a}$$

$$D(s + i\epsilon) - D(s - i\epsilon) = 2i \operatorname{Im} D(s + i\epsilon),\ s < 0. \tag{4.111b}$$

Let us extract the n-subtracted dispersion relation for $N(s)$. See the left graph in fig. 4.6 for the integration contour. We will apply the Cauchy's theorem to the function

$$f(s') = \frac{N(s')}{(s')^n (s' - s - i\epsilon)}. \tag{4.112}$$

The two residues within the integration contour shown in fig. 4.6 (left plot) are

$$\left\{ \frac{N(s + i\epsilon)}{(s + i\epsilon)^n},\ \operatorname{Res}\left[\frac{N(s')}{(s')^n (s' - s - i\epsilon)}, s' = 0 \right] \right\}. \tag{4.113}$$

[6] $\operatorname{Im} A(s) = |A(s)|^2$, see sec. 4.1.

[7] We used time reversal invariance to extract the analytical structure of the partial waves (sec. 4.1). This property is exact in the perturbative expansion. However, it is not necessarily respected by the unitarization procedures. Note that the coupled channel version of N/D in this section is an example of a unitarity procedure where time reversal invariance is only approximate. Another one will be the I-K method (sec. 4.3.4). In contrast, the IAM method (sec. 4.3.2) does respect time reversal invariance exactly. Anyway, if the unitarization procedure is applied within its validity range, the violation of time reversal invariant, if there is any, should be negligible.

Now, consider that $N(s)$ is analytic around $s = 0$, and $N(0) = 0$ (Adler zero, eq. 4.110). Thus, if $n = 1$ (once-subtracted DR), we would have no pole. Otherwise, if $n > 1$,

$$N(s') = h_0 + h_1 s' + h_2 s'^2 + \cdots + h_j s'^j + \dots . \tag{4.114}$$

We have kept h_0 because we will reuse these equations for $D(s)$ ($D(0) \neq 0$). However, $h_0 = 0$ for $N(s)$. Now, $f(s')$ (in eq. 4.112) has a Laurent expansion

$$\begin{aligned} f(s') &= -\frac{N(s')}{(s')^n s[1-(s'/s)]} \\ &= -\frac{1}{(s')^n s}(h_0 + h_1 s' + h_2 s'^2 + \dots)\left[1 + \frac{s'}{s} + \left(\frac{s'}{s}\right)^2 + \left(\frac{s'}{s}\right)^3 + \dots\right]. \end{aligned} \tag{4.115}$$

Hence, the residue on $s' = 0$ is

$$\mathrm{Res}\,[f(s'), s' = 0] = -\frac{h_{n-1}}{s+i\epsilon} - \frac{h_{n-2}}{(s+i\epsilon)^2} - \cdots - \frac{h_1}{(s+i\epsilon)^{n-1}} - \frac{h_0}{(s+i\epsilon)^n}. \tag{4.116}$$

Thus, according to the Cauchy's theorem, and taking into account that $h_0 = 0$ (Adler zero, eq. 4.110),

$$\begin{aligned} 2\pi i \frac{N(s+i\epsilon)}{(s+i\epsilon)^n} = 2\pi i \sum_{j=1}^{n-1} \frac{h_j}{(s+i\epsilon)^{n-j}} &+ \int_{\Lambda^2} \frac{ds' N(s')}{(s')^n (s'-s-i\epsilon)} \\ &+ \int_{-\infty}^{0} \frac{ds' N(s'+i\varepsilon')}{(s')^n (s'-s-i\epsilon)} + \int_{0}^{-\infty} \frac{ds' N(s'-i\varepsilon')}{(s')^n (s'-s-i\epsilon)} \end{aligned} \tag{4.117}$$

Here, Λ^2 stands for the outer loop of the integrand contour ($\to \infty$). The inner arc with radius ε, which closes the integration region around the LC, gives no contribution to the integral because it is defined in a region where the integral is analytic, and its length can be taken to zero ($\varepsilon \to 0^+$), still being in a zone (between the LC and the Adler zero) where the function is continuous and bounded. Note that, provided that $N(s)/s^n \to 0$ for $s \to \infty$, the outer loop also cancels. This works when $N(s) \sim \mathcal{O}(s^d)$, $d < n$.

Now, using the reflection principle of eq. 4.111a, the relation of eq. 4.104, and taking $\epsilon \to 0^+$, $\varepsilon' \to 0^+$, $\varepsilon' > \epsilon$, eq. 4.117 turns into

$$\begin{aligned} N(s) &= \sum_{j=1}^{n} h_j s^j + \frac{s^n}{\pi} \int_{-\infty}^{0} \frac{ds' \,\mathrm{Im}\, N(s)}{(s')^n (s'-s-i\epsilon)} \\ &= \sum_{j=1}^{n} h_j s^j + \frac{s^n}{\pi} \int_{-\infty}^{0} \frac{ds' D(s) \,\mathrm{Im}\, A(s)}{(s')^n (s'-s-i\epsilon)}. \end{aligned} \tag{4.118}$$

For $D(s)$, the integration contour will be the second plot of fig. 4.6. Now, we will apply the Cauchy's theorem to a function

$$g(s') = \frac{D(s')}{(s')^n (s'-s-i\epsilon)}, \tag{4.119}$$

as we did for $N(s)$ in eq. 4.112. Now, following the same procedure that in eqs. 4.113 to 4.116, the two residues within the integration contour will be

$$\frac{D(s+i\epsilon)}{(s+i\epsilon)^n} \tag{4.120}$$

on $s' = s + i\epsilon$, and

$$\text{Res}\,[g(s'), s' = 0] = -\frac{h_{n-1}}{s+i\epsilon} - \frac{h_{n-2}}{(s+i\epsilon)^2} - \cdots - \frac{h_1}{(s+i\epsilon)^{n-1}} - \frac{h_0}{(s+i\epsilon)^n}. \tag{4.121}$$

on $s' = 0$. Note that, because of the normalization $D(0) = 1$ (see eq. 4.109), $h_0 = 1$. Now, applying the Cauchy's theorem in the same way that we did for $f(s')$ in eq. 4.117, but for $g(s')$ and using the integration contour of the right picture of fig. 4.6,

$$2\pi i \frac{D(s+i\epsilon)}{(s+i\epsilon)^n} = 1 + 2\pi i \sum_{j=1}^{n-1} \frac{h_j}{(s+i\epsilon)^{n-j}} + \int_{\Lambda^2} \frac{ds' D(s')}{(s')^n (s'-s-i\epsilon)} + \int_{\infty}^{0} \frac{ds' D(s'+i\varepsilon')}{(s')^n (s'-s-i\epsilon)} + \int_{0}^{\infty} \frac{ds' D(s'-i\varepsilon')}{(s')^n (s'-s-i\epsilon)}. \tag{4.122}$$

Therefore, using the reflection principle (eq. 4.111b) and the relation of eq. 4.103, we get the n-subtracted DR for the $D(s)$,

$$D(s) = 1 + \sum_{j=1}^{n} h_j s^j + \frac{s^n}{\pi} \int_0^\infty \frac{ds' \,\text{Im}\, D(s')}{(s')^n (s'-s-i\epsilon)} = 1 + \sum_{j=1}^{n} h_j s^j - \frac{s^n}{\pi} \int_0^\infty \frac{ds' N(s')}{(s')^n (s'-s-i\epsilon)}, \tag{4.123}$$

where we need that $D(s)/s^n \to 0$ for $s \to \infty$ in order the outer loop to cancel. This fits when $D(s) \sim \mathcal{O}(s^d)$, $d < n$.

For the one-loop Lagrangian [38, 39], a three-times subtracted version ($n = 3$) of the DR of eq. 4.123 has been used,

$$D(s) = 1 + h_1 s + h_2 s^2 - \frac{s^3}{\pi} \int_0^\infty \frac{ds' N(s')}{(s')^3 (s'-s-i\epsilon)}. \tag{4.124}$$

In order to give a first estimate of $N(s)$ and $D(s)$, we would need to split our one loop computation in two parts having one of them only a RC and the other, the LC. For the coupled channels (trivial generalization to elastic channels),

$$G(s) = \frac{1}{\pi}\left[B(\mu)(D+E)^{-1} + \log\frac{-s}{\mu^2}\right] \tag{4.125a}$$

$$F_L(s) = \left[B(\mu)(D+E)^{-1} + \log\frac{s}{\mu^2}\right] Ds^2 = \pi G(-s) D s^2 \tag{4.125b}$$

$$F_R(s) = \left[B(\mu)(D+E)^{-1} + \log\frac{-s}{\mu^2}\right] Es^2 = \pi G(s) E s^2 \tag{4.125c}$$

It can be easily proven that $F^{(1)} = F_L(s) + F_R(s)$, $F_L(s)$ having a LC and $F_R(s)$, a RC. Note that when $D + E = 0$ this will no longer work[8]. Furthermore, note that, because of eq. 4.62, eq. 4.125c turns into

$$F_R(s) = -G(s) K^2 s^2 = -G(s)[F^{(0)}(s)]^2 \tag{4.126}$$

Our estimate for $N(s)$ will be

$$N_0(s) = F^{(0)}(s) + F_L(s). \tag{4.127}$$

[8]For example, take $I = J = 1$ and $a^2 = b$.

Note that $N_0(s) \sim \mathcal{O}(s^2)$, so that using the three-times subtracted expression ensures that the outer loop integral cancels[9]. In turn, we can estimate $D_0(s)$ using eq. 4.124,

$$\begin{aligned} D_0(s) &= 1 + h_1 s + h_2 s^2 - \frac{s^3}{\pi}\int_0^\infty \frac{ds' N_0(s')}{(s')^3(s'-s-i\epsilon)} \\ &= 1 + h_1 s + h_2 s^2 - \frac{s^3}{\pi}\int_0^\infty \frac{ds'}{s'-s-i\epsilon}\left\{\frac{K}{s'^2} + \left[B(\mu)(D+E)^{-1} + \log\frac{s'}{\mu^2}\right]\frac{D}{s'}\right\} \end{aligned} \tag{4.128}$$

Thus, we will need to compute several integrals. Let us dimensionally reduce variables to $y = (s+i\epsilon)/\mu^2$, $x = s'/\mu^2$, and redefine the integration limits to be from m^2 to ∞. Later, we will take $m \to 0^+$. Thus, we have (see appendix D.3):

$$I_1 \equiv \int_{m^2}^\infty \frac{ds'}{(s')(s'-s-i\epsilon)} = -\frac{1}{s}\log\left(1-\frac{s}{m^2}\right) \tag{4.129a}$$

$$I_2 \equiv \int_{m^2}^\infty \frac{ds'}{(s')^2(s'-s-i\epsilon)} = -\frac{1}{s^2}\left[\frac{s}{m^2} + \log\left(1-\frac{s}{m^2}\right)\right] \tag{4.129b}$$

$$\begin{aligned} I_1' &\equiv \int_{m^2}^\infty \frac{ds' \log(s'/\mu^2)}{(s')(s'-s-i\epsilon)} \\ &= -\frac{1}{s}\left[\frac{1}{2}\log^2\left(\frac{-s}{\mu^2}\right) + \mathrm{Li}_2\,\frac{m^2}{s} - \frac{1}{2}\log^2\left(\frac{m^2}{\mu^2}\right) + \log\frac{m^2}{\mu^2}\log\left(1-\frac{m^2}{s}\right) + \frac{\pi^2}{6}\right]. \end{aligned} \tag{4.129c}$$

With these definitions, we can re write eq. 4.128 as

$$D_0(s) = 1 + h_1 s + h_2 s^2 - \frac{s^3}{\pi}\left[KI_2 + B(\mu)(D+E)^{-1}DI_1 + DI_1'\right]. \tag{4.130}$$

Taking into account the integrals of eqs. 4.129, and eqs. 4.127 and 4.130, and supposing that h_1 and h_2 have no imaginary part[10], we can compute, on the RC,

$$\mathrm{Im}\, D_0(s) = -F^{(0)}(s) - F_L(s) = -N_0(s), \tag{4.131}$$

thus complying with eq. 4.103, which is the condition of unitarity if we suppose $\mathrm{Im}\, N(s) = 0$ on the RC, as defined by the N/D method. Note that eq. 4.103 is also valid for crossed-channels, as explained after eq. 4.105.

Now, taking into account eqs. 4.60, 4.125, 4.105, 4.127 and 4.130,

$$\begin{aligned} F(s) = [D(s)]^{-1}N(s) \approx [D_0(s)]^{-1}N_0(s) = \\ \left[1 + h_1 s + h_2 s^2 - \frac{s^3}{\pi}T(s)\right]^{-1} \cdot \left[F^{(0)}(s) + F_L(s)\right], \end{aligned} \tag{4.132}$$

where $F^{(0)}(s)$ and $F_L(s)$ are defined in eqs. 4.60, 4.125, respectively; and

$$T(s) = KI_2 + B(\mu)(D+E)^{-1}DI_1 + DI_1'. \tag{4.133}$$

For small m, eq. 4.130 turns into

$$D_0(s) = 1 + h_1 s + \frac{F^{(0)}(s)}{\pi}\log\left(\frac{-s}{m^2}\right) + \mathcal{O}(s^2). \tag{4.134}$$

[9] See the discussions under eqs. 4.117 and 4.123.

[10] As appropriate in EFT, where the tree-level coefficients come from a real Lagrangian density.

All that remains is to fix h_1. For this, we match the N/D method to the NLO calculation. Let us write down $F(s)$ (eq. 4.132) as

$$F(s) \approx \left[1 + h_1 s + \frac{F^{(0)}(s)}{\pi} \log\left(\frac{-s}{m^2}\right) + \mathcal{O}(s^2)\right]^{-1} \cdot \left[F^{(0)}(s) + F_L(s)\right]$$
$$\approx \left[1 - h_1 s - \frac{F^{(0)}(s)}{\pi} \log\left(\frac{-s}{m^2}\right) + \dots\right] \left[F^{(0)}(s) + F_L(s)\right] + \mathcal{O}(s^3). \quad (4.135)$$

Note that we have used $F^{(0)}(s) = Ks$ (eq. 4.60) and $F_L(s) \propto s^2$ (eqs. 4.125) to compute the order $\mathcal{O}(s^3)$. In order to match N/D dispersion relation (eq. 4.132) to perturbation theory, eq. 4.132, when expanded at low s, should become

$$F(s) \approx F^{(0)}(s) + F_L(s) + F_R(s) + \mathcal{O}(s^3). \quad (4.136)$$

Let us expand eq. 4.135,

$$F(s) \approx F^{(0)}(s) + F_L(s) - \left[h_1 + \frac{F^{(0)}(s)}{\pi} \log\left(\frac{-s}{m^2}\right)\right] F^{(0)}(s)s + \mathcal{O}(s^3) \quad (4.137)$$

Thus, if we match eqs. 4.136 and 4.137,

$$F_R(s) = -\left[h_1 + \frac{F^{(0)}(s)}{\pi} \log\left(\frac{-s}{m^2}\right)\right] F^{(0)}(s)s \quad (4.138)$$

Taking into account eq. 4.125,

$$F_R(s) = \pi G(s) E s^2 = \left[B(\mu)(D+E)^{-1} + \log\frac{-s}{\mu^2}\right] E s^2, \quad (4.139)$$

If we also consider eqs. 4.62 and 4.60, the compatibility condition between eqs. 4.138 and 4.139 is written down as

$$\left[B(\mu)(D+E)^{-1} + \log\frac{-s}{\mu^2}\right] \frac{-K^2}{\pi} s^2 = -h_1 K s^2 + \frac{-K^2}{\pi} s^2 \log\left(\frac{-s}{m^2}\right), \quad (4.140)$$

so that, finally,

$$h_1 = \frac{1}{\pi}[B(\mu)](D+E)^{-1}K + \frac{1}{\pi} K \log\frac{m^2}{\mu^2}, \quad (4.141)$$

which can be written down as

$$h_1(m,\mu) = \frac{1}{\pi}[B(m,\mu)](D+E)^{-1}K. \quad (4.142)$$

Thus, according to eqs. 4.62, 4.134, 4.139 and 4.141,

$$D_0(s) = 1 + \frac{s}{\pi}\left[B(\mu)(D+E)^{-1}K + K\log\left(\frac{m^2}{\mu^2}\right) + K\log\left(\frac{-s}{m^2}\right)\right]$$
$$= 1 + \frac{s}{\pi}\left[B(\mu)(D+E)^{-1} + \log\left(\frac{-s}{\mu^2}\right)\right] K^2 + \mathcal{O}(s^2)$$
$$= 1 - [F_R(s)] \cdot [F^{(0)}]^{-1}(s) + \mathcal{O}(s^2). \quad (4.143)$$

Now, let us extend eq. 4.143 with the coefficient of order $\mathcal{O}(s^2)$. For this, we need to define

$$H(m) \equiv h_2(m)\pi + \frac{1}{m^2}K + \frac{\pi^2}{6}D, \tag{4.144}$$

so that eq. 4.130 turns into

$$\begin{aligned} D_0(s) &= 1 - [F_R(s)] \cdot [F^{(0)}(s)]^{-1} \\ &+ \frac{s^2}{\pi}\left[H(m) + B(\mu)(D+E)^{-1}D\log\frac{-s}{m^2} + \frac{1}{2}D\left(\log^2\frac{-s}{\mu^2} - \log^2\frac{m^2}{\mu^2}\right)\right] \end{aligned} \tag{4.145}$$

$H(m)$ is a renormalized parameter at the scale m. If we demand $D_0(s)$ to be independent of this scale, we find the renormalization equation

$$m^2\frac{d\,H(m)}{d\,m^2} = B(\mu)(D+E)^{-1}D + D\log\frac{m^2}{\mu^2}, \tag{4.146}$$

which leads to an evolution equation that is characteristic of an NNLO parameter in perturbation theory,

$$H(\mu) = H(\mu_0) + B(\mu_0)(D+E)^{-1}D\log\frac{\mu^2}{\mu_0^2} + \frac{1}{2}D\log^2\frac{\mu^2}{\mu_0^2} \tag{4.147}$$

This renormalized constant, $H(\mu)$, can contain contributions coming from the NNLO chiral couplings, generated by the unitarization procedure. However, we could choose

$$H(\mu) = \frac{1}{2}[B(\mu)(D+E)^{-1}]^2 D, \tag{4.148}$$

which, once we take into account eq. 3.135, $B(\mu) = B(\mu_0) + (D+E)\log(\mu^2/\mu_0^2)$, verifies eq. 4.147. With this choice, eq. 4.145 turns into

$$D_0(s) = 1 - F_R(s)[F^{(0)}(s)]^{-1} + \frac{\pi}{2}[G(s)]^2 D s^2, \tag{4.149}$$

where $F_R(s)$ and $G(s)$ are defined in eqs. 4.125. Finally, taking again into account the definitions of eqs. 4.125,

$$D_0(s) = 1 - F_R(s)[F^{(0)}(s)]^{-1} + \frac{1}{2}G(s)F_L(-s), \tag{4.150}$$

and

$$F^{\mathrm{N/D}}(s) = \left[1 - F_R(s)[F^{(0)}(s)]^{-1} + \frac{1}{2}G(s)F_L(-s)\right]^{-1} \cdot \left[F^{(0)}(s) + F_L(s)\right]. \tag{4.151}$$

Note that this method is valid even for $K = E = 0$, although it would fail in the case that the matrix $D + E$ would not have an inverse (or $D + E = 0$ for the elastic, non-matricial case), because of the appearance of a factor $(D+E)^{-1}$ in eqs. 4.125.

4.3.4 K-matrix and Improved K-matrix

The so-called K-matrix method is one of the most popular unitarization procedures. See, for instance, refs. [171–173], which develop the K-matrix theory for the low energy QCD (ChPT formalism). On the contrary, ref. [174] and the recent review [175] study the K-matrix method in the context of the EWSBS. In the single channel case, the K-matrix[11] is defined in terms of the S matrix,

$$S = \frac{1 - iK/2}{1 + iK/2}, \tag{4.152}$$

so that S is unitary if and only if K is Hermitian. In a perturbative computation, the (approximate) S matrix will be written as

$$S = 1 + S^{(1)} + S^{(2)} + \ldots, \tag{4.153}$$

the approximate S matrix not being unitary. However, the corresponding truncated expansion of K,

$$K = K^{(1)} + K^{(2)} + \ldots, \tag{4.154}$$

introduced in eq. 4.152, produces a new series of S which is exactly unitary at any order [38].

Thus, let $A_0(s)$ be a real [12] non-unitary estimation of the scattering amplitude. The K-matrix unitarized partial wave is defined as

$$A_0^K(s) = \frac{A_0(s)}{1 - iA_0(s)}, \tag{4.155}$$

which satisfies unitarity in the physical region, since, because of the fact that $\mathrm{Im}\, A_0 = 0$,

$$\mathrm{Im}\, A_0^K = \frac{\mathrm{Im}[A_0(1 + iA_0)]}{1 + A_0^2} = \frac{A_0^2}{1 + A_0^2} = |A_0^K|^2. \tag{4.156}$$

But this unitarization procedure has a problem: the unitarized partial wave has not the required analytical structure. For instance, $A^K(s)$ has no right cut (RC), so it is impossible to define a II Riemann sheet as was shown on fig. 4.2 (page 60). This definition of second Riemann sheet is crucial to recover resonances, as was exposed on sec. 4.2.

Thus, it would be expectable that the K-matrix method omits the presence of resonances which are predicted by other methods (like the N/D and the IAM). In practice, this is what happens, and most of the criticisms on the unitarization methods which appear in the literature are based on the fact that some of them can produce resonances (actually, poles on the second Riemann sheet) which are not predicted by others (tipically the K-matrix). However, this is due to the limitations of the K-matrix and, in particular, to the lack of a proper analytic structure on the K-matrix unitarized partial waves. According to the experience in unitarization methods applied to hadron physics [164–166], these resonances do appear and are well described by unitarization procedures other than the simplest K-matrix method. Actually, the $A_0^K(s)$ partial wave is defined only in the physical region, it cannot be analytically extended to the whole complex plane by following the complex integration trajectories of fig. 4.2. This is why we consider the K-matrix method less appropriate than others.

[11] See ref. [174]. Ref. [175] uses a slightly different definition (a change in the sign of K).

[12] $\mathrm{Im}[A_0(s)] = 0$ on the physical zone $s' = s + i\epsilon$, $\epsilon \to 0^+$, $s > 0$.

Hence, except otherwise indicated, we only consider an improved version of the K-matrix, which has the proper analytic structure (with a RC). Let us introduce the analytical function

$$g(s) = \frac{1}{\pi}\left(C + \log\frac{-s}{\mu^2}\right), \tag{4.157}$$

C being an arbitrary constant and μ, an arbitrary scale. At the end, we will define this $g(s)$ as in the N/D method (eq. 4.125a), taking $C = B(\mu)(D+E)^{-1}$. Anyway, in the physical region ($s' = s + i\epsilon$), $\log(-s/\mu^2) = \log(s/\mu^2) - i\pi$, so that

$$\operatorname{Im} g(s) = -1. \tag{4.158}$$

Our *heuristic* way of modifying the K-matrix method is substituting $-i \to g(s)$ in the K-matrix expression (eq. 4.155), so that

$$A^{\mathrm{IK}}(s) = \frac{A_0(s)}{1 + g(s)A_0(s)}, \quad g(s) = \frac{1}{\pi}\left(\frac{B(\mu)}{D+E} + \log\frac{-s}{\mu^2}\right), \tag{4.159}$$

this $A^{\mathrm{IK}}(s)$ being the unitarized partial wave according to the *improved* K-matrix method. Note that this is equivalent to defining

$$h_1 = h_1(\mu) = \frac{K}{\pi}\frac{B(\mu)}{D+E} \tag{4.160}$$

in eq. 4.130. When crossed-channels are included, the improved K-matrix method is defined as

$$F^{\mathrm{IK}}(s) = (1 + GN_0)^{-1}N_0 \tag{4.161a}$$

$$G = \frac{1}{\pi}\left(B(\mu)(D+E)^{-1} + \log\frac{-s}{\mu^2}\right) \tag{4.161b}$$

$$N_0(s) = F^{(0)}(s) + F_L(s). \tag{4.161c}$$

Note that G and $N_0(s)$ are defined as in the N/D method (eqs. 4.125a and 4.127, respectively).

4.3.5 Summary of the unitarization methods and their range of applicability

The detailed description of the unitarization procedures IAM, N/D and IK (improved-K matrix) is contained in secs. 4.3.2, 4.3.3 and 4.3.4, respectively. Anyway, for easy comparison, and in presence of crossed-channels, these three procedures reduce to the application of the matrix formulas

$$F^{\mathrm{IAM}}(s) = [F^{(0)}(s)]^{-1} \cdot [F^{(0)}(s) - F^{(1)}(s)] \cdot [F^{(0)}(s)]^{-1} \tag{4.162a}$$

$$F^{\mathrm{N/D}}(s) = \left[1 - F_R(s)[F^{(0)}(s)]^{-1} + \frac{1}{2}G(s)F_L(-s)\right]^{-1} \cdot N_0(s) \tag{4.162b}$$

$$F^{\mathrm{IK}}(s) = [1 + G(s)N_0(s)]^{-1} \cdot N_0(s), \tag{4.162c}$$

where $F^{(0)}(s)$ and $F^{(1)}(s)$ are the direct result of the computation of the partial waves (see eqs. 4.60) and $F_L(s)$, $F_R(s)$, $G(s)$ and $N_0(s)$ are defined in eqs. 4.125 and 4.127,

respectively. These equations, when dealing with an elastic (single channel) process, reduce to

$$A^{\mathrm{IAM}}(s) = \frac{A^{(0)}(s) + A_L(s)}{1 - \frac{A_R(s)}{A^{(0)}(s)} - \left(\frac{A_L(s)}{A^{(0)}(s)}\right)^2 + g(s)A_L(s)} = \frac{[A^{(0)}(s)]^2}{A^{(0)}(s) - A^{(1)}(s)} \tag{4.163a}$$

$$A^{\mathrm{N/D}}(s) = \frac{A^{(0)}(s) + A_L(s)}{1 - \frac{A_R(s)}{A^{(0)}(s)} + \frac{1}{2}g(s)A_L(-s)} \tag{4.163b}$$

$$A^{\mathrm{IK}}(s) = \frac{A^{(0)}(s) + A_L(s)}{1 - \frac{A_R(s)}{A^{(0)}(s)} + g(s)A_L(s)}, \tag{4.163c}$$

where $A_L(s)$, $A_R(s)$, $g(s)$ and $N_0(s)$ are defined as the scalar versions of the matricial $F_L(s)$, $F_R(s)$, $G(s)$ and $N_0(s)$. All the three methods satisfy the low energy expansion

$$A^{\mathrm{IAM}},\, A^{\mathrm{N/D}},\, A^{\mathrm{IK}} = A^{(0)}(s) + A^{(1)}(s) + \mathcal{O}(s^3), \tag{4.164}$$

and the different unitarization procedures only start differing in terms of order $\mathcal{O}(s^3)$. Anyway, from eqs. 4.163, it is clear that the conditions for the equivalence of the unitarization procedures is a small A_L ($A_L \ll A^{(0)}$), since for $A_L \to 0$ the three eqs. 4.163 collapse to a single expression $A^{(0)}(s)/[1 - (A_R(s)/A^{(0)}(s))]$.

Now, notice that the IAM method is the only one that does not require an explicit splitting of the NLO term $A^{(1)}(s)$ between two functions with a right cut (A_R) and a left cut (A_L), so that it is the only applicable method when such a splitting fails. According to eq. 4.125, such failure takes place when $(D+E)^{-1}$ is singular ($D+E$ can be vanishing for same elastic processes and consequently not invertible for coupled-channels). For $D + E \ll B$ (small $D + E$), $F_L \sim F_R$. Note that this splitting is in some way arbitrary, since we could add (and substract) terms to A_R and A_L without changing their sum, provided that such terms (actually, of the form Cs^2) are analytic. Thus, in the small $D + E$ regime, the three methods are expected to produce different results and, because of the arbitrary choice of the splitting, the IAM is preferable. This happens for the vector-isovector channel ($I = J = 1$). In this channel, for $a^2 = b$, $D + E$ is exactly zero.

On the other hand, the applicability of the IAM requires $K^2 = E \neq 0$ (which implies $A^{(0)} \neq 0$). Otherwise, the IAM gives a vanishing result: this happens for $J = 2$ channels, because they start at NLO in the effective theory. Then, the IK or N/D methods are profitably employed.

Note also that, *only for elastic scattering*, eq. 4.44 can be applied, so that the position s_R of the poles on the II Riemann sheet can be computed just by solving the equation $A(s_R) + (i/2) = 0$. Let us apply this method in eqs. 4.163. For the elastic version of the IAM method,

$$A^{(0)}(s_R) - A^{(1)}(s_R) - 2i[A^{(0)}(s_R)]^2 = 0. \tag{4.165}$$

For the N/D,

$$A^{(0)}(s_R) - A_R(s_R) + \frac{1}{2}g(s_R)A^{(0)}(s_R)A_L(-s_R) - 2iA^{(0)}(s_R)[A^{(0)}(s_R) + A_L(s_R)] = 0. \tag{4.166}$$

And, for the IK,

$$A^{(0)}(s_R) - A_R(s_R) + g(s_R)A^{(0)}(s_R)A_L(s_R) - 2iA^{(0)}(s_R)[A^{(0)}(s_R) + A_L(s_R)] = 0. \tag{4.167}$$

These are simple equations that give the resonance position and can be solved by iteration (e.g., Newton's method).

4.4 Extensions of the $\omega\omega$ unitarization

In this section, based on our works [136, 151], we will consider two possible extensions to the pure WBGBs scattering. The first one is the scattering of a 2-γ state,

$$\gamma\gamma \to \{\omega\omega, hh\}. \tag{4.168}$$

The partial waves which correspond to this process can be found in sec. 3.3.2. Since the photon is a spin-1 particle, the possible values for the total angular momentum are $J = 0, 2$ (the Landau-Yang theorem forbids $J = 1$). In each J-channel, we can have either $a^2 = b$, which implies that the $\gamma\gamma \to hh$ channel decouples (see eq. 3.87), or $a^2 \neq b$, which implies that the $\gamma\gamma \to hh$ channel contributes to the reaction matrix. These four cases will be studied from sec. 4.4.1 to sec. 4.4.4.

The second extension which we consider is a WBGBs scattering which gives a final state $t\bar{t}$,

$$\{\omega\omega, hh\} \to t\bar{t}. \tag{4.169}$$

The corresponding partial waves can be found in sec. 3.3.3. The only considered channel will be $IJ = 00$, since it is the only one which couples with the WBGBs channels at order $\mathcal{O}(M_t^2/v^2)$. Note also that, although the $t\bar{t} \to t\bar{t}$ partial wave appears in the reaction matrix, its order in M_t/v is too high, so that it does not contribute to the final unitarized partial waves $\omega\omega \to t\bar{t}$ and $hh \to t\bar{t}$. However, we have computed the matrix element $t\bar{t} \to t\bar{t}$ in sec. 3.2.4 and appendix B.2 for completeness, and because it is useful to introduce the spinor formalism in a general case.

J	0	0	2	2
Coupling with hh ($a^2 \neq b$)	no	yes	no	yes
$\gamma\gamma$ scattering	eq. 4.176	eqs. 4.190	eq. 4.194	eq. 4.197
$t\bar{t}$ in the final state	eq. 4.201	eqs. 4.215	no	no

Table 4.1: Summary of the extensions to the pure WBGBs scattering considered. In each case, the equation numbers of the final unitarization expressions are given.

4.4.1 $\gamma\gamma$ scattering without hh channel ($a^2 = b$), $J = 0$

Let us take $J = 0$ and $a^2 = b$; this implies that the $\gamma\gamma \to hh$ channel decouples (see eq. 3.87), so we omit it. In this regime, the expression for the amplitude matrix 4.57 is extended to

$$F(s) = \begin{pmatrix} A_{00}(s) & 0 & P_{00}(s) \\ 0 & A_{20}(s) & P_{20}(s) \\ P_{00}(s) & P_{20}(s) & 0 \end{pmatrix} + \mathcal{O}(\alpha^2), \tag{4.170}$$

where $A_{IJ}(s)$ are the (isospin conserving) elastic partial waves $\omega\omega \to \omega\omega$ (eqs. 3.136 and 3.138) and $P_{IJ}(s)$, the partial wave $\gamma\gamma \to \omega\omega$ (eqs. 3.152). Note that we consider only the leading order in electromagnetic α.

Partial wave unitarity $\operatorname{Im} F(s) = F(s)F(s)^\dagger$ (eq. 4.55) is applied, on the RC, to def. 4.170. We have to take into account that α is considered at leading order. With this condition, and without coupling the hh state (because we have $a^2 = b$), we recover eqs. 4.59a, 4.59c,

$$\operatorname{Im} A_{I0} = |A_{I0}|^2, \quad I = 0, 2. \tag{4.171}$$

We also obtain the new relations

$$\operatorname{Im} P_{I0} = P_{I0} A_{I0}^*, \quad I = 0, 2 \tag{4.172}$$

Note how crucial it is that α is taken at LO for checking unitarity. Namely, if we took a higher order in α, we would need to introduce corrections to the elastic A_{I0} in order to account for the rescattering $\omega\omega \to (\gamma\gamma) \to \omega\omega$.

Now, let us use the elastic IAM method (eq. 4.163a) for the unitarization of $A_{IJ}(s)$,

$$\tilde{A}(s) = \frac{A^{(0)}(s)}{1 - \frac{A^{(0)}(s)}{A^{(1)}(s)}}. \tag{4.173}$$

As usual, $A = A^{(0)} + A^{(1)} + \dots$ is a chiral expansion on s and $\tilde{A}$, the unitarized partial wave. This applies for both isospin channels, $I = 0, 2$.

For the P amplitudes, the unitarization is controled by $\omega\omega$ rescattering (Watson's Theorem). At low energies, $P \approx P^{(0)}$. Therefore, the simplest solution to the unitarity equation 4.172 with the proper analytical structure is

$$\tilde{P} = \frac{P^{(0)}}{1 - \frac{A^{(1)}}{A^{(0)}}} = \frac{P^{(0)}}{A^{(0)}} \tilde{A}. \tag{4.174}$$

Then, on the RC,

$$\operatorname{Im} \tilde{P} = \frac{P^{(0)}}{A^{(0)}} \operatorname{Im} \tilde{A} = \frac{P^{(0)}}{A^{(0)}} |\tilde{A}|^2 = \tilde{P} \tilde{A}^*, \tag{4.175}$$

which applies to the $I = J = 0$ and $I = 2$, $J = 0$ channels. Thus, our unitarized $\gamma\gamma \to \omega\omega$ matrix element, with the same phase as the elastic IAM amplitude, will be

$$\tilde{P}_{I0} = \frac{P_{I0}^{(0)}}{1 - \frac{A_{I0}^{(1)}}{A_{I0}^{(0)}}}, \quad I = 0, 2. \tag{4.176}$$

4.4.2 $\gamma\gamma$ scattering with hh channel, $J = 0$

Let us assume weak isospin conservation by the Goldstone dynamics, so that the reaction matrix is written as

$$F = \begin{pmatrix} A_{00} & M_0 & 0 & P_{00} \\ M_0 & T_0 & 0 & R_0 \\ 0 & 0 & A_{20} & P_{20} \\ P_{00} & R_0 & P_{20} & 0 \end{pmatrix} + \mathcal{O}(\alpha^2), \tag{4.177}$$

where all the elements depend on s. Here, A_{I0} are the partial waves $\omega\omega \to \omega\omega$ (eqs. 3.136 and 3.138); M_0, the $\omega\omega \to hh$ one (eq. 3.141); T_0, the $hh \to hh$ one (eq. 3.143); $P_{I0}(s)$, the $\gamma\gamma \to \omega\omega$ ones (eqs. 3.152); and $R_0(s)$, the $\gamma\gamma \to hh$ (eq. 3.153).

On the RC, perturbative unitarity (eq. 4.55) implies the same results as for WBGBs scattering (eqs. 4.59), plus the following new relations for the $\gamma\gamma$ couplings:

$$\operatorname{Im} P_{00} = P_{00} A_{00}^* + R_0 M_0^* \tag{4.178a}$$

$$\operatorname{Im} P_{20} = P_{20} A_{20}^* \tag{4.178b}$$

$$\operatorname{Im} R_0 = P_{00} M_0^* + R_0 T_0^*. \tag{4.178c}$$

Because of considering only leading order in α, the WBGBs matrix elements (A_{00}, M_0 and T_0) can be unitarized without taking into account the $\gamma\gamma$ couplings. The $IJ = 20$ channel (in eq. 4.178b) can be unitarized by following eq. 4.176 (with $I = 2$) of sec. 4.4.1, since it does not couple with $IJ = 00$ channel at this order. Regarding the $I = 0$ channel, the previous discussion of sec. 4.4.1 can be generalized by taking a matricial definition for $F(\omega\omega, hh \to \omega\omega, hh)$ (and considering only $I = 0$),

$$F = F_{00} = \begin{pmatrix} A_{00} & M_0 \\ M_0 & T_0 \end{pmatrix} = \begin{pmatrix} A & M \\ M & T \end{pmatrix}, \tag{4.179}$$

and similar definitions for $F^{(0)}$ and $F^{(1)}$,

$$F^{(i)} = \begin{pmatrix} A^{(i)} & M^{(i)} \\ M^{(i)} & T^{(i)} \end{pmatrix}, \quad i = 0, 1. \tag{4.180}$$

Following the IAM method (eq. 4.162a) for the unitarization of $\tilde{F}$, on the RC, $\tilde{F} = F^{(0)}(F^{(0)} - F^{(1)})^{-1}F^{(0)}$. Thus, if we define $(P, R) \equiv (P_{00}, R_0)$, then from eqs. 4.178,

$$\mathrm{Im}\begin{pmatrix} P \\ R \end{pmatrix} = F^* \cdot \begin{pmatrix} P \\ R \end{pmatrix}, \tag{4.181}$$

so that the following unitarized amplitude can be introduced,

$$\begin{pmatrix} \tilde{P} \\ \tilde{R} \end{pmatrix} \equiv \tilde{F}(F^{(0)})^{-1}\begin{pmatrix} P^{(0)} \\ R^{(0)} \end{pmatrix}, \tag{4.182}$$

where

$$\begin{pmatrix} \tilde{A} & \tilde{M} \\ \tilde{M} & \tilde{T} \end{pmatrix} = \tilde{F} \tag{4.183}$$

is the unitarized WBGBs reaction matrix F (eq. 4.179). The IAM method will be used for the computation of this $\tilde{F}$ (see sec. 4.3.2 and eq. 4.162a). Note that, by definition, $\tilde{F}$ satisfies the unitarity relation $\mathrm{Im}\,\tilde{F} = \tilde{F} \cdot \tilde{F}^\dagger = \tilde{F}^\dagger \cdot \tilde{F}$ (eq. 4.55).

Now, following the procedure which was used in eq. 4.175, eq. 4.182 turns into

$$\begin{aligned} \mathrm{Im}\begin{pmatrix} P \\ R \end{pmatrix} = (\mathrm{Im}\,\tilde{F}) \cdot (F^{(0)})^{-1} \cdot \begin{pmatrix} P^{(0)} \\ R^{(0)} \end{pmatrix} &= \tilde{F}^\dagger \tilde{F}(F^{(0)})^{-1}\begin{pmatrix} P^{(0)} \\ R^{(0)} \end{pmatrix} \\ &= \tilde{F}^* \tilde{F}(F^{(0)})^{-1}\begin{pmatrix} P^{(0)} \\ R^{(0)} \end{pmatrix} = \tilde{F}^*\begin{pmatrix} P \\ R \end{pmatrix}, \end{aligned} \tag{4.184}$$

so that we recover unitarity (eqs. 4.178). Note that we have used that $\mathrm{Im}\,F^{(0)} = \mathrm{Im}\,P^{(0)} = \mathrm{Im}\,R^{(0)} = 0$. Now, let us check the low-energy behaviour. Using the chiral expansion, $\tilde{F} = F^{(0)} + F^{(1)} + \ldots$, eq. 4.182 turns into

$$\begin{aligned} \begin{pmatrix} \tilde{P} \\ \tilde{R} \end{pmatrix} \equiv \tilde{F}(F^{(0)})^{-1}\begin{pmatrix} P^{(0)} \\ R^{(0)} \end{pmatrix} &= (F^{(0)} + F^{(1)} + \ldots)(F^{(0)})^{-1}\begin{pmatrix} P^{(0)} \\ R^{(0)} \end{pmatrix} \\ &= \begin{pmatrix} P^{(0)} \\ R^{(0)} \end{pmatrix} + F^{(1)}(F^{(0)})^{-1}\begin{pmatrix} P^{(0)} \\ R^{(0)} \end{pmatrix} + \ldots, \end{aligned} \tag{4.185}$$

so that the required low-energy behaviour is recovered. Note that

$$\begin{pmatrix} P^{(0)} \\ R^{(0)} \end{pmatrix} \sim \begin{pmatrix} \mathcal{O}\left(\frac{s}{v^2}\right) + \mathcal{O}(\alpha) \\ \mathcal{O}(\alpha) \end{pmatrix}, \tag{4.186}$$

as can be checked in eqs. 3.152 and 3.153. The next order of the perturbative expansion of eq. 4.185 would be

$$F^{(1)}(F^{(0)})^{-1}\begin{pmatrix} P^{(0)} \\ R^{(0)} \end{pmatrix} \sim \begin{pmatrix} \mathcal{O}\left(\frac{s^2}{v^4}\right) + \mathcal{O}(\alpha) \\ \mathcal{O}\left(\frac{s}{v^2}\right) + \mathcal{O}(\alpha) \end{pmatrix}, \tag{4.187}$$

as required. Note that P and R are computed only at lowest order in electromagnetic α at LO, $\mathcal{O}(\alpha)$, and we do not need intermediate 2-photon states. Higher order contributions come only from the WBGBs rescattering. Taking into account that the inverse of the $F^{(0)}$ amplitude matrix (eq. 4.180) is

$$(F^{(0)})^{-1} = \frac{1}{A^{(0)}T^{(0)} - (M^{(0)})^2}\begin{pmatrix} T^{(0)} & -M^{(0)} \\ -M^{(0)} & A^{(0)}, \end{pmatrix} \tag{4.188}$$

the unitarized amplitude matrix of eq. 4.182 turns into

$$\begin{pmatrix} \tilde{P} \\ \tilde{R} \end{pmatrix} \equiv \frac{1}{A^{(0)}T^{(0)} - (M^{(0)})^2}\begin{pmatrix} \tilde{A} & \tilde{M} \\ \tilde{M} & \tilde{T} \end{pmatrix}\begin{pmatrix} T^{(0)} & -M^{(0)} \\ -M^{(0)} & A^{(0)}, \end{pmatrix}\begin{pmatrix} P^{(0)} \\ R^{(0)} \end{pmatrix}. \tag{4.189}$$

Hence, eq. 4.182 is written as

$$\tilde{P} = P^{(0)}\frac{\tilde{A}T^{(0)} - \tilde{M}M^{(0)}}{A^{(0)}T^{(0)} - (M^{(0)})^2} + R^{(0)}\frac{-\tilde{A}M^{(0)} + \tilde{M}A^{(0)}}{A^{(0)}T^{(0)} - (M^{(0)})^2} \tag{4.190a}$$

$$\tilde{R} = P^{(0)}\frac{\tilde{M}T^{(0)} - \tilde{T}M^{(0)}}{A^{(0)}T^{(0)} - (M^{(0)})^2} + R^{(0)}\frac{\tilde{T}A^{(0)} - \tilde{M}M^{(0)}}{A^{(0)}T^{(0)} - (M^{(0)})^2}, \tag{4.190b}$$

where $\tilde{A}$, $\tilde{M}$ and $\tilde{T}$ are the unitarized $IJ = 00$ partial amplitudes, computed with the IAM unitarization procedure (see sec. 4.3.2 and eq. 4.162a).

4.4.3 $\gamma\gamma$ scattering without hh channel ($a^2 = b$), $J = 2$

In this case, the hh channel decouples again because $a^2 = b$ and $R = 0$. The amplitude matrix becomes

$$F = \begin{pmatrix} A_{02} & 0 & P_{02} \\ 0 & A_{22} & P_{22} \\ P_{02} & P_{22} & 0 \end{pmatrix} + \mathcal{O}(\alpha^2), \tag{4.191}$$

where A_{I2} are the elastic $\omega\omega$ partial waves (eqs. 3.138 and 3.140) and P_{I2}, the $\gamma\gamma \to \omega\omega$ ones (eqs. 3.152). Note that the P_{I2} are constant. Applying the unitarity relation (eq. 4.55) to the amplitude matrix (eq. 4.191), we recover $\operatorname{Im} A_{I2} = |A_{I2}|^2$ (eqs. 4.59a and 4.59c), and the new relations

$$\operatorname{Im} P_{I2} = P_{I2}A^*_{I2}, \quad I = 0, 2. \tag{4.192}$$

Note that, in this case, since $K = 0$, we cannot use the IAM unitarization method for the WBGBs scattering. Hence, the N/D will be used here (see eq. 4.163b with $A^{(0)} = 0$),

$$\tilde{A} = A^{\mathrm{N/D}} = \frac{A_L(s)}{1 + \frac{\pi}{2}g^2(s)Ds^2}. \tag{4.193}$$

See the discussions of sec. 4.3.3 and the summary of sec. 4.3.5 for a definition of the functions which appear in this equation.

Eqs. 4.192 are satisfied by the unitarization method

$$\tilde{P}_{I2} = \frac{P^{(0)}_{I2}}{A_{\mathrm{L},I2}}A^{\mathrm{N/D}}_{I2}, \quad I = 0, 2. \tag{4.194}$$

4.4.4 $\gamma\gamma$ scattering with hh channel, $J = 2$

Now, the reaction matrix is

$$F = \begin{pmatrix} A_{02} & M_2 & 0 & P_{02} \\ M_2 & T_2 & 0 & 0 \\ 0 & 0 & A_{22} & P_{22} \\ P_{02} & 0 & P_{22} & 0 \end{pmatrix} + \mathcal{O}(\alpha^2), \tag{4.195}$$

where A_{I2} are the partial waves $\omega\omega \to \omega\omega$ (eqs. 3.139 and 3.140); M_2, the $\omega\omega \to hh$ one (eq. 3.142); T_0, the $hh \to hh$ one (eq. 3.144); and $P_{I2}(s)$, the $\gamma\gamma \to \omega\omega$ ones (eqs. 3.152). Note also that the partial wave associated with the process $\gamma\gamma \to hh$ is zero for $J = 2$ ($R_2 = 0$), as explained around eq. 3.153.

The application of the unitarity relation (eq. 4.55) to the reaction matrix 4.195, taking into account that α is kept to leading order, gives the WBGBs scattering relations of eqs. 4.59 and the new ones

$$\mathrm{Im}\, P_{I2} = P_{I2} A_{I2}^*, \quad I = 0, 2. \tag{4.196}$$

Since $K = 0$, the N/D coupled channel method is used for the unitarization of the WBGBs scattering matrix elements (A_{02}, M_2 and T_2). This is summarized by eq. 4.163b, the discussions of sec. 4.3.3 and the summary of sec. 4.3.5. For the $IJ = 22$ channel, there is no coupling with hh, so that the single-channel N/D applies (as in the previous sec. 4.4.1). The unitarization of the P_{I2} matrix elements will be accomplished by

$$\tilde{P}_{I2} = P_{I2}^{(0)} \frac{\tilde{A}_{I2}}{A_{\mathrm{L},I2}}, \quad I = 0, 2. \tag{4.197}$$

This completes all the cases for $\gamma\gamma \to \omega\omega$, $\gamma\gamma \to hh$, $\omega\omega \to \omega\omega$, $\omega\omega \to hh$ and $hh \to hh$ scattering. We then turn to the top-antitop channel.

4.4.5 $t\bar{t}$ in the final state without hh channel ($a^2 = b$), $J = 0$

Since we are taking $a^2 = b$ and $J = 0$, the $\omega\omega \to hh$ crossed-channels decouple (see eq. 3.87). Thus, the reaction matrix can be written as

$$F = \begin{pmatrix} A_{00} & Q_0 \\ Q_0 & S_0 \end{pmatrix} \equiv \begin{pmatrix} A & Q \\ Q & S \end{pmatrix}, \tag{4.198}$$

where A_{00} (taken as $A_{00} \equiv A$ in this subsection) is the elastic partial wave $\omega\omega \to \omega\omega$ ($IJ = 00$, see eqs. 3.136); Q_0, the partial wave $\omega\omega \to t\bar{t}$ (see eq. 3.154); and S_0, the partial wave $t\bar{t} \to t\bar{t}$ (which will not be required by the unitarization procedure, since $\{\omega\omega, hh\} \to t\bar{t} \to t\bar{t}$ is a higher order correction in the M_t counting). Note that A, Q and S follow a chiral expansion

$$A = A^{(0)} + A^{(1)} + \ldots \qquad \sim \mathcal{O}\left[\left(\frac{M_t}{v}\right)^0\right] \tag{4.199a}$$

$$Q = Q^{(0)} + Q^{(1)} + \ldots \qquad \sim \mathcal{O}\left[\frac{M_t}{v}\right] \tag{4.199b}$$

$$S = S^{(0)} + \ldots \qquad \sim \mathcal{O}\left[\left(\frac{M_t}{v}\right)^2\right]. \tag{4.199c}$$

On the RC, the unitarity relation $\operatorname{Im} F = FF^\dagger$ (see eq. 4.55) applies, so that

$$\operatorname{Im} A = |A|^2 + \mathcal{O}\left(\frac{M_t^2}{v^2}\right) \tag{4.200a}$$

$$\operatorname{Im} Q = AQ^* + \mathcal{O}\left(\frac{M_t^3}{v^3}\right) \tag{4.200b}$$

$$\operatorname{Im} S = 0 + \mathcal{O}\left(\frac{M_t^2}{v^2}\right). \tag{4.200c}$$

It is not necessary to satisfy unitarity exactly here; unlike the s-expansion of the EFT that deteriorates with increasing energy, M_t is fixed and the uncertainty due to neglecting higher order terms in the unitarity relation remains controlled. M_t/v may not appear as a very good expansion parameter, but as was understood around eq. 3.154, in the unitarized regime at $E \sim$ 1-3 TeV, it is $M_t/\sqrt{s}$ that ends up controlling the size of the subleading terms, and this is small. Let us solve the unitarity eq. 4.199b by the expression

$$\tilde{Q} = Q^{(0)} + Q^{(1)}\frac{\tilde{A}}{A^{(0)}}, \tag{4.201}$$

where the unitarized partial wave $\tilde{A}$ will be computed with the IAM procedure (eq. 4.163a), $\tilde{A} = (A^{(0)})^2/(A^{(0)} - A^{(1)})]$. This ensures elastic unitarity, $\operatorname{Im}\tilde{A} = \tilde{A}\tilde{A}^*$.

Eq. 4.201 has the required low-energy behaviour (eq. 4.199b). Now, take into account that, because of unitarity and the definition of $Q^{(0)}$ and $A^{(0)}$ as real functions, $\operatorname{Im}\tilde{A} = \tilde{A}\tilde{A}^*$, $\operatorname{Im} A^{(1)} = (A^{(0)})^2$, $\operatorname{Im} Q^{(1)} = Q^{(0)}A^{(0)}$, $\operatorname{Im} Q^{(0)} = \operatorname{Im} A^{(0)} = 0$. Thus, eq. 4.201, evaluated on the RC, turns into

$$\begin{aligned}\tilde{Q}\Big|_{\text{RC}} = Q^{(0)} + Q^{(1)}\frac{\tilde{A}}{A^{(0)}} &= \left[Q^{(0)}\left(1 - \frac{A^{(1)}}{A^{(0)}}\right) + Q^{(1)}\right]\frac{A^{(0)}}{A^{(0)} - A^{(1)}} \\ &= \left[Q^{(0)} - \frac{Q^{(0)}}{A^{(0)}}\operatorname{Re} A^{(1)} + \operatorname{Re} Q^{(1)}\right]\frac{\tilde{A}}{A^{(0)}}\end{aligned} \tag{4.202}$$

Thus, we have that

$$\begin{aligned}\operatorname{Im}\tilde{Q}\Big|_{\text{RC}} &= \left[Q^{(0)} - \frac{Q^{(0)}}{A^{(0)}}\operatorname{Re} A^{(1)} + \operatorname{Re} Q^{(1)}\right]\frac{\operatorname{Im}\tilde{A}}{A^{(0)}} \\ &= \left[Q^{(0)} - \frac{Q^{(0)}}{A^{(0)}}\operatorname{Re} A^{(1)} + \operatorname{Re} Q^{(1)}\right]\frac{\tilde{A}\tilde{A}^*}{A^{(0)}} = \tilde{Q}\tilde{A}^*,\end{aligned} \tag{4.203}$$

so that we recover eq. 4.200b, proving that eq. 4.201 is a valid unitarization procedure, which we adopt for $J = 0$ and $a^2 = b$.

4.4.6 $t\bar{t}$ in the final state with hh channel, $J = 0$

If we allow $a^2 \neq b$, so that the cross-channel $\omega\omega \to hh$ is now coupled, then the reaction matrix will be

$$F = \begin{pmatrix} A_{00} & M_0 & Q \\ M_0 & T_0 & N \\ Q & N & S \end{pmatrix} \equiv \begin{pmatrix} A & M & Q \\ M & T & N \\ Q & N & S \end{pmatrix}. \tag{4.204}$$

As in sec. 4.4.5, A_{00} (note that $A_{00} \equiv A$ in this section) is the elastic partial wave $\omega\omega \to \omega\omega$ ($IJ = 00$, see eqs. 3.136); Q_0, the partial wave $\omega\omega \to t\bar{t}$ (see eq. 3.154); and S_0, the partial wave $t\bar{t} \to t\bar{t}$ (which, as in the previous $a^2 = b$ case of sec. 4.4.5, will not be required by the unitarization procedure, since $\{\omega\omega, hh\} \to t\bar{t} \to t\bar{t}$ is a higher order correction). Furthermore, since the cross-channel $\omega\omega \to hh$ is present, we need to take into account the $\omega\omega \to hh$ partial wave ($J = 0$, see eqs. 3.141), the $hh \to hh$ ($J = 0$, see eqs. 3.143), and the $hh \to t\bar{t}$ ($J = 0$, see eqs. 3.158). All the partial waves accept a chiral expansion of the form

$$F = F^{(0)} + F^{(1)} + \ldots, \quad \mathrm{Im}\, F^{(0)} \equiv 0, \tag{4.205}$$

where $F^{(n)} = \mathcal{O}(s^n)$, $n = 0, 1, \ldots$. Furthermore, the chiral expansions of Q, N and S are suppressed by M_t/v factors. In particular,

$$X = X^{(0)} + X^{(1)} + \ldots \qquad \sim 1, \quad X = A, M, T \tag{4.206a}$$

$$Q = Q^{(0)} + Q^{(1)} + \ldots \qquad \sim \mathcal{O}\left(\frac{M_t}{v}\right) \tag{4.206b}$$

$$N = N^{(0)} + N^{(1)} + \ldots \qquad \sim \mathcal{O}\left(\frac{M_t}{v}\right) \tag{4.206c}$$

$$S = S^{(0)} + \ldots \qquad \sim \mathcal{O}\left(\frac{M_t^2}{v^2}\right). \tag{4.206d}$$

On the RC, unitarity relation $\mathrm{Im}\, F = FF^\dagger$ (see eq. 4.55) is applied so that, up to order $\mathcal{O}(M_t^2/v^2)$,

$$\mathrm{Im}\, A = |A|^2 + |M|^2 + \ldots \tag{4.207a}$$

$$\mathrm{Im}\, M = AM^* + MT^* + \ldots \tag{4.207b}$$

$$\mathrm{Im}\, T = |M|^2 + |T|^2 + \ldots \tag{4.207c}$$

$$\mathrm{Im}\, Q = AQ^* + MN^* + \ldots \tag{4.207d}$$

$$\mathrm{Im}\, N = MQ^* + MN^* + \ldots \tag{4.207e}$$

$$\mathrm{Im}\, S = 0 + \ldots. \tag{4.207f}$$

This is essential in order to be able to decouple the unitarization of the WBGBs sector (partial waves A, M and T) from the $t\bar{t}$ vertices. For the unitarization of this WBGBs sector the IAM method will be used (eq. 4.162a), so that eq. 4.206a holds. Let us reuse the definition of eq. 4.179,

$$F \equiv \begin{pmatrix} A & M \\ M & T \end{pmatrix}, \tag{4.208}$$

and the corresponding definitions for the chiral expansion $F = F^{(0)} + F^{(1)} + \ldots$. The IAM unitarization (eq. 4.162a) is $\tilde{F} = F^{(0)}(F^{(0)} - F^{(1)})^{-1}F^{(0)}$, which ensures the unitarity relation $\mathrm{Im}\, \tilde{F} = \tilde{F}\tilde{F}^*$ (eq. 4.206a). Now, the rest of the unitarity condition (eqs. 4.206b, 4.206c and 4.206d) can be written as

$$\mathrm{Im} \begin{pmatrix} Q \\ N \end{pmatrix} = F \begin{pmatrix} Q \\ N \end{pmatrix}^*, \tag{4.209}$$

or, perturbatively,

$$\mathrm{Im} \begin{pmatrix} Q^{(1)} \\ N^{(1)} \end{pmatrix} = F^{(0)} \begin{pmatrix} Q^{(0)} \\ N^{(0)} \end{pmatrix}. \tag{4.210}$$

Let us introduce the unitarized amplitudes

$$\begin{pmatrix} \tilde{Q} \\ \tilde{N} \end{pmatrix} = \begin{pmatrix} Q^{(0)} \\ N^{(0)} \end{pmatrix} + \tilde{F}(F^{(0)})^{-1} \begin{pmatrix} Q^{(1)} \\ N^{(1)} \end{pmatrix}. \tag{4.211}$$

Observe that eq. 4.211 is a matricial generalization of eq. 4.201. Now, let us prove that the definition of eq. 4.211 satisfies the unitarity relations of eqs. 4.206b and 4.206c (summarized in eq. 4.209).

$$\operatorname{Im} \begin{pmatrix} \tilde{Q} \\ \tilde{N} \end{pmatrix} = \operatorname{Im} \tilde{F}(F^{(0)})^{-1} \operatorname{Re} \begin{pmatrix} Q^{(1)} \\ N^{(1)} \end{pmatrix} + \operatorname{Re} \tilde{F}(F^{(0)})^{-1} \operatorname{Im} \begin{pmatrix} Q^{(1)} \\ N^{(1)} \end{pmatrix} \tag{4.212}$$

Because of eq. 4.210, eq. 4.212 turns into

$$\begin{aligned} \operatorname{Im} \begin{pmatrix} \tilde{Q} \\ \tilde{N} \end{pmatrix} &= \operatorname{Im} \tilde{F}(F^{(0)})^{-1} \operatorname{Re} \begin{pmatrix} Q^{(1)} \\ N^{(1)} \end{pmatrix} + \operatorname{Re} \tilde{F} \begin{pmatrix} Q^{(0)} \\ N^{(0)} \end{pmatrix} \\ &= \tilde{F} \begin{pmatrix} Q^{(0)} \\ N^{(0)} \end{pmatrix} - i \operatorname{Im} \tilde{F} \begin{pmatrix} Q^{(0)} \\ N^{(0)} \end{pmatrix} + \operatorname{Im} \tilde{F}(F^{(0)})^{-1} \operatorname{Re} \begin{pmatrix} Q^{(1)} \\ N^{(1)} \end{pmatrix} \\ &= \tilde{F} \begin{pmatrix} Q^{(0)} \\ N^{(0)} \end{pmatrix} + \operatorname{Im} \tilde{F}(F^{(0)})^{-1} \operatorname{Re} \begin{pmatrix} Q^{(1)} \\ N^{(1)} \end{pmatrix} - \operatorname{Im} \tilde{F}(F^{(0)})^{-1} \operatorname{Im} \begin{pmatrix} Q^{(1)} \\ N^{(1)} \end{pmatrix} \\ &= \tilde{F} \begin{pmatrix} Q^{(0)} \\ N^{(0)} \end{pmatrix} + \tilde{F}\tilde{F}^{*}(F^{(0)})^{-1} \begin{pmatrix} Q^{(1)} \\ N^{(1)} \end{pmatrix}^{*} = \tilde{F} \begin{pmatrix} \tilde{Q} \\ \tilde{N} \end{pmatrix}^{*}, \end{aligned} \tag{4.213}$$

so that we recover eq. 4.209, as wanted. Note also that the unitarization of eq. 4.211 also recovers the correct low-energy behaviour,

$$\begin{aligned} \begin{pmatrix} \tilde{Q} \\ \tilde{N} \end{pmatrix} &= \begin{pmatrix} Q^{(0)} \\ N^{(0)} \end{pmatrix} + (F^{(0)} + F^{(1)} + \dots)(F^{(0)})^{-1} \begin{pmatrix} Q^{(1)} \\ N^{(1)} \end{pmatrix} \\ &= \begin{pmatrix} Q^{(0)} \\ N^{(0)} \end{pmatrix} + \begin{pmatrix} Q^{(1)} \\ N^{(1)} \end{pmatrix} + F^{(1)}(F^{(0)})^{-1} \begin{pmatrix} Q^{(1)} \\ N^{(1)} \end{pmatrix} + \dots \end{aligned} \tag{4.214}$$

Finally, eq. 4.211 can be written as

$$\tilde{Q} = Q^{(0)} + Q^{(1)} \frac{\tilde{A}T^{(0)} - \tilde{M}M^{(0)}}{A^{(0)}T^{(0)} - (M^{(0)})^2} + N^{(1)} \frac{\tilde{M}A^{(0)} - \tilde{A}M^{(0)}}{A^{(0)}T^{(0)} - (M^{(0)})^2} \tag{4.215a}$$

$$\tilde{N} = N^{(0)} + Q^{(1)} \frac{\tilde{M}T^{(0)} - \tilde{T}M^{(0)}}{A^{(0)}T^{(0)} - (M^{(0)})^2} + N^{(1)} \frac{\tilde{T}A^{(0)} - \tilde{M}M^{(0)}}{A^{(0)}T^{(0)} - (M^{(0)})^2}. \tag{4.215b}$$

Note that the unitarized partial waves $\tilde{A}$, $\tilde{M}$ and $\tilde{T}$, which correspond to the WBGBs sector, will be computed with the IAM procedure (eq. 4.162a).

Chapter 5

Study of the parameter space for the $\omega\omega$ scattering

The goal of this section is to study the behaviour of the three unitarization methods (IAM, N/D and improved K-matrix) when they are applied to the different channels of $\omega\omega \to \omega\omega$, $\omega\omega \to hh$ and $hh \to hh$ processes. These methods were studied on sec. 4.3. Note that the old K-matrix method is not considered here because of its bad analytic behaviour (lack of a RC), as was explained on sec. 4.3.4.

Some of the considered unitarization procedures cannot be applied to all the possible channels for all the possible parameters, due to the vanishing of some of the coefficients of the partial waves (see sec. 3.3.1). Here we will perform a detailed study of these validity conditions, although a brief summary can be found in table 5.1.

When the unitarization methods can be applied, we provide numerical results for the various situations to illustrate how the three unitarization methods work in the different channels, and whether they make predictions which are experimentally ruled out.

Finally, according to sec. 4.2.1, if poles on the first Riemann sheet appear, we will exclude the region of the parameter space where this happens. Some examples can be found in figs. 5.18, 5.23, 5.16, 5.28 and 5.30 below.

5.1 Numeric comparison of the three methods

5.1.1 Scalar-isoscalar channel, $I = J = 0$

The scalar-isoscalar channel ($I = J = 0$) is a coupled-channel with the $\omega\omega$ and hh elastic and crossed reactions forming a symmetric 2×2 matrix. We represent the two diagonal and the off-diagonal matrix elements as functions of s in fig. 5.1 for four different methods, all of which satisfy exact unitarity.

IJ	00	02	11	20	22
Method of choice	Any	N/D IK	IAM	Any	N/D IK

Table 5.1: Unitarization methods usable in each IJ channel. See section 5.1.

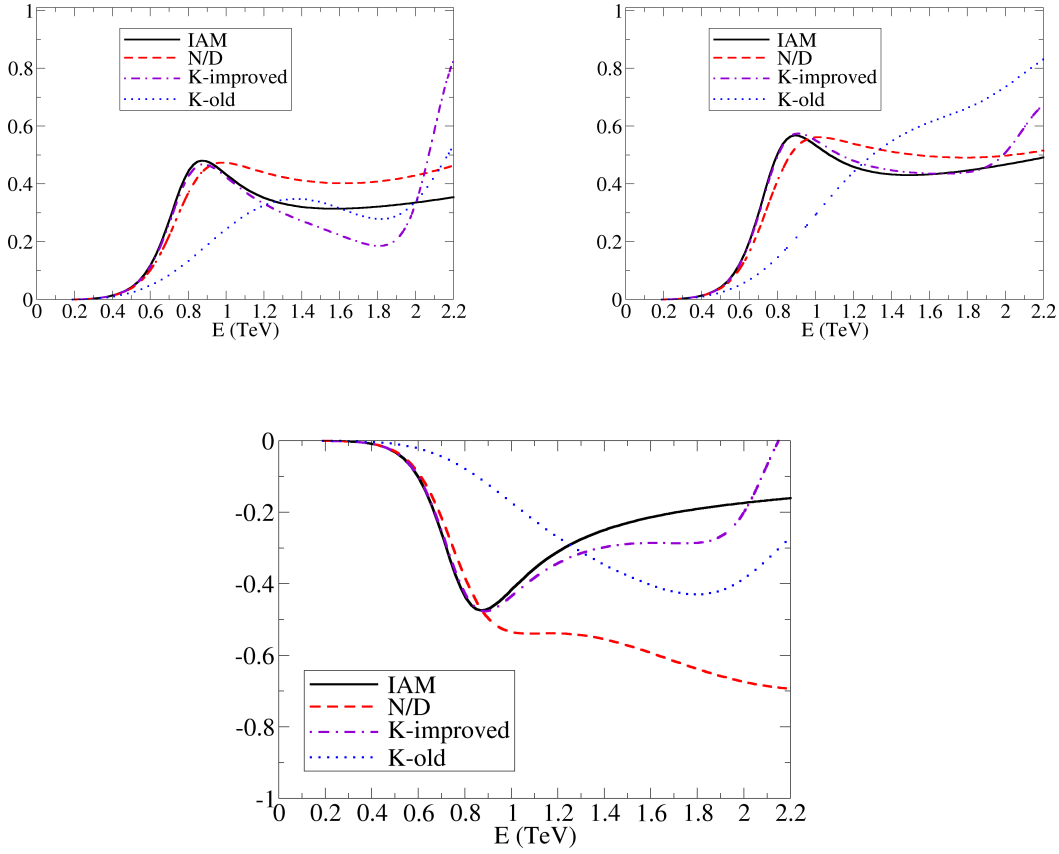

Figure 5.1: Scalar-isoscalar amplitudes, for $a = 0.88$, $b = 3$, and all NLO parameters set to 0 at a scale $\mu = 3\,\text{TeV}$. From left to right and top to bottom, elastic $\omega\omega$, elastic hh, and crossed-channels $\omega\omega \to hh$. Note that, as explained on sec. 5.1.1, the old K-matrix method gives different results because its complex-s plane analytic structure is not the correct one. It will be discarded from now on.

The three considered methods (IAM, N/D and IK) agree in predicting a scalar resonance that is visible in all the three amplitudes ($\omega\omega \to \omega\omega$, $\omega\omega \to hh$ and $hh \to hh$) between 0.8 and 0.9 TeV. As an exception, we represent in fig. 5.1 the results coming from the old K-matrix method (eq. 4.155). As explained in sec. 4.3.4, due to the fact that the analytic structure is not the correct one (there is no RC coming from eq. 4.155), it gives a different result. Thus, we discard the old K-matrix method from now on.

The other three methods are practically in perfect agreement up to the first elastic resonance and they start deviating quantitatively only for higher energies. The reason that there is good agreement between the various methods was discussed on sec. 4.3.5. Because we have set the NLO terms to 0, A_L is small, so that the three resonance equations become dominated by the tree-level and right-cut parts of the amplitude, which suggests similar resonance masses for all the methods.

Note that in ref. [39] we show that the resonance found in fig. 5.1 appears even if we set $a = 1$ (its SM value with one Higgs): it is sufficient that the coupled-channel dynamics is strong through $a^2 - b \neq 0$ for it to appear. Moreover, with the values chosen to prepare the figure this $a^2 - b$ is negative, so the crossed-channels amplitude M_J shown in the bottom plot is also negative as dictated by eq. 3.141. At last, observe that the

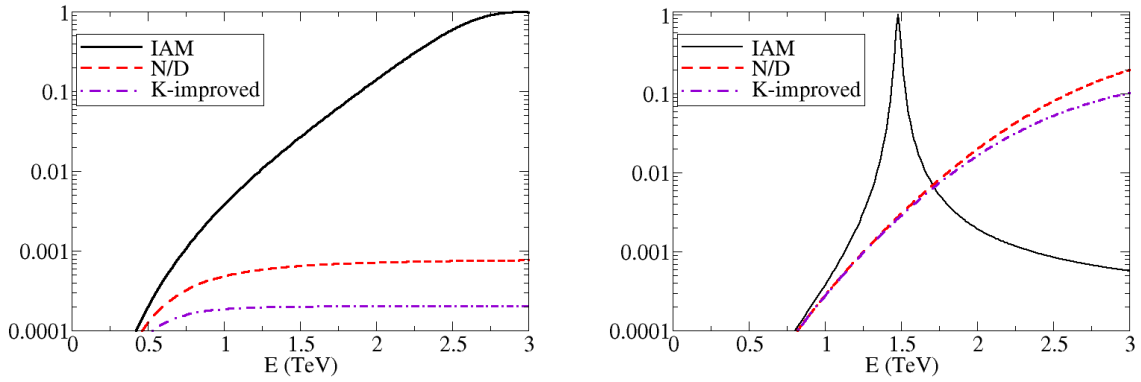

Figure 5.2: Vector-isovector partial wave. We have taken $a = 0.88$ and $b = 1.5$, but while for the left plot all the NLO parameters vanish, for the right plot we have taken $a_4 = 0.003$, known to yield an IAM resonance from the work of the Barcelona group [141]. Note that the N/D and K-improved methods are not reliable in this channel, as explained below on section 5.1.2. They are included to show the lack of agreement with the IAM.

resonance appears in all three elastic or inelastic amplitudes in the same position (though of course, with different shapes due to different backgrounds).

5.1.2 Vector-isovector channel, $I = J = 1$

The comparison between the three methods IAM, N/D and IK for the vector-isovector channel is shown in fig. 5.2. First we set all the NLO parameters to 0 (left plot). Clearly, there is no good agreement between the three methods. Moreover, if we introduce one NLO counterterm with an appropriate value to generate a resonance in the IAM, here $a_4 = 0.003$ as an example (right plot), the N/D and IK methods do not react in the same way as the former, and fail to yield a vector resonance.

In order to understand this discrepancy, which comes from an elastic channel, consider that, according to sec. 4.3.5, the definition of both the N/D and the IK methods depend on having $D + E \neq 0$. This is due to the fact that a term $(D + E)^{-1}$ appears on the definitions of $A_L(s)$, $A_R(s)$ and $g(s)$ (scalar versions of defs. 4.125). But, in the $I = J = 1$ channel,

$$D_{11} + E_{11} = \frac{3}{(96)^2\pi^3 v^4}(a^2 - b)^2, \tag{5.1}$$

which vanishes for $a^2 = b$. This is, in particular, the case of the SM, where $a = b = 1$. The SM is not very important for our discussion because it breaks the approximations used in our effective Lagrangians (see sec. 3.3.4) and, more importantly, it is a region on the parameter space where there are no strong interactions.

The condition $a^2 = b$ also applies to the Higgsless electroweak chiral perturbation theory, characterized by $a = b = 0$. This situation is already ruled out by the discovery of the light Higgs-like particle, but it is still interesting because it is equivalent to two-flavor low-energy QCD in the chiral limit with v playing the role of f_π and the WBGB being the pions.

Within $a = 0 = b$, we know that a vector resonance (the ρ) appears in the spectrum (because we can look up the answer in QCD), and know what the low-energy parameters

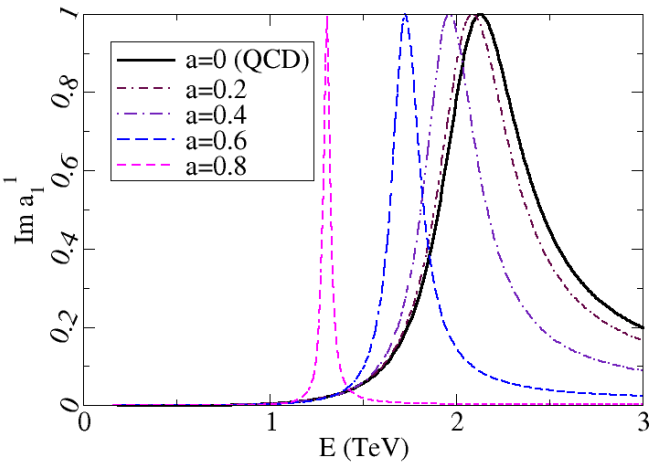

Figure 5.3: We show the vector-isovector resonance with NLO a_4, a_5 parameters taken from large-N_c QCD, $b = a^2$ and a as shown in the legend. The right-most solid line is the rescaled QCD case, towards the left we approach the EWSBS with a Higgs, where the resonance is narrow and relatively light for these a_4, a_5.

are, with good approximation. Fig. 5.3 shows the result of the calculation with the IAM (solid line). We have taken $a^2 = b = 0$ and $a_4 = -2a_5 = 3/192\pi^2$, the large-N_c prediction for these NLO constants (the other ones are set to 0). The ρ vector-isovector resonance then comes with reasonable parameters (to see it, substitute $v = 246\,\text{GeV}$ by $f = 92\,\text{MeV}$ in the scale; this amounts to $m_\rho \simeq 2.1\,\text{TeV} \to 0.79\,\text{GeV}$, just slightly above the actual $0.775\,\text{GeV}$ in the hadron spectrum).

The other lines in fig. 5.3 have been computed by increasing a towards 0.88, the value taken for fig. 5.2. One sees without doubt how the QCD-like resonance becomes narrower and lighter (this depends on the interplay of a with the NLO parameters a_4, a_5), matching the calculation of fig. 5.2. We find that the IK and N/D methods fail to provide a resonance. Therefore, the IAM is the method of choice for the vector-isovector channel, given that the other two fail at least for the $a^2 = b$ parameter election, while the IAM yields a resonance that can be continuously matched to the one we know is there for that parameter set.

The resonance may be exactly fit to data with an adequate choice of the a_4 and a_5 chiral parameters to adjust its mass and width. Beyond trial and error, an elegant method is to couple the resonance to the Chiral Lagrangian in a chiral invariant way and then integrate the resonance at tree level as done for example in ref. [176] (see also the early treatment by ref. [177] and the more formal one in ref. [178], as well as that in the context of Composite Higgs Models in ref. [80]). The tree-level chiral couplings obtained take the general form

$$a_i^{\text{tree}} = \eta_i \gamma^{\text{tree}} \left(\frac{v}{M^{\text{tree}}} \right)^4 , \tag{5.2}$$

where $i = 4, 5$, $\eta_4 = -\eta_5 = 12\pi$ and $\gamma^{\text{tree}} = \Gamma^{\text{tree}}/M^{\text{tree}}$ with M^{tree}, Γ^{tree} being the tree-level vector-resonance parameters. Thus the tree-level s^2 term induced by the resonance is

$$A_{11}^{\text{tree}}(s) = s^2 \left(p_4 a_4^{\text{tree}} + p_5 a_5^{\text{tree}} \right) , \tag{5.3}$$

where the p_4 and p_5 constants are obtained from eq. 3.145, $B_{11}(\mu) = B_0 + p_4 a_4(\mu) + p_5 a_5(\mu)$, and are given by $p_4 = 1/(24\pi v^4)$ and $p_5 = -2p_4$. Following ref. [176], we can now obtain the contribution to the renormalized chiral couplings induced by the resonance by matching the $\mathcal{O}(s^2)$ tree level amplitude with the NLO result at the point $s = M^{\text{tree }2}$, i. e.

$$A_{11}^{\text{tree}}(M^{\text{tree }2}) = \text{Re}\, A_{11}^{(1)}(M^{\text{tree }2}). \tag{5.4}$$

This identification leads us to

$$a_i(M^{\text{tree}}) = \eta_i \gamma^{\text{tree}} \left(\frac{v}{M^{\text{tree}}}\right)^4 - \frac{B_0}{p_4 + p_5} \tag{5.5}$$

for $i = 4, 5$. Therefore we get

$$A_{11}^{(1)}(s) = s^2 \left(\frac{3\gamma^{\text{tree}}}{2M^{\text{tree }4}} + D_{11} \log \frac{s}{M^{\text{tree }2}} + E_{11} \log \frac{-s}{M^{\text{tree }2}} \right). \tag{5.6}$$

Then, the IAM resonance eq. 4.165 leads us to the II Riemann sheet resonance parameters in the narrow-resonance limit $\gamma = \Gamma/M \ll 1$:

$$\left(M^{\text{IAM}}\right)^2 = \frac{K_{11}}{B_{11}(M^{\text{tree}})} \tag{5.7a}$$

$$\Gamma^{\text{IAM}} = \frac{K_{11}^2 M^{\text{IAM}}}{B_{11}(M^{\text{tree}})}, \tag{5.7b}$$

which implies the M^{tree}-independent result $\gamma^{\text{IAM}} = K_{11}\left(M^{\text{IAM}}\right)^2$, or

$$\Gamma^{\text{IAM}} = \frac{\left(M^{\text{IAM}}\right)^3}{96\pi v^2}(1 - a^2), \tag{5.8}$$

which is recognizable as a version of the so-called KSFR relation (slightly generalized to $a \neq 0$, see refs. [179, 180]). This is here a restriction arising from the constraint of exact unitarity, that has been discussed in ref. [162] and references therein and is a non-trivial relation between three observable quantities.

We also have the equation

$$M^{\text{IAM}} = M^{\text{tree}} \left(\frac{2\Gamma^{\text{IAM}}}{3\Gamma^{\text{tree}}}\right)^{1/4}, \tag{5.9}$$

which relates the resonance parameters with the tree level ones. This is a very consistent result showing that the IAM method properly predicts a vector resonance whenever $M^{\text{tree}}, \Gamma^{\text{tree}} > 0$, in which case the chiral parameters receive a contribution and may be dominated by a vector resonance. For example $M^{\text{IAM}} = M^{\text{tree}}$ implies $\Gamma^{\text{IAM}} = (3/2)\Gamma^{\text{tree}}$ which is a quite reasonable result taken into account the tree-level nature of the vector field integration performed to estimate the chiral parameters.

However, the N/D and IK unitarization methods fail to predict this resonance for the appropriate values of the chiral parameters. First of all, they are not even defined for $a = b$. For $a \neq b$, but still in the parameter region close to the SM (where $a \sim b \sim 1$), we have $D_{11} + E_{11} \sim 0$. As discussed on sec. 4.3.5, the methods are well defined in this case, but we have $A_L \sim A_R$, which means that the IAM method is very different from the N/D and IK methods. Thus, as the IAM method works pretty well in this channel according to the previous discussion, we have to give it preference over the other two methods, not appropriate to describe the vector channel.

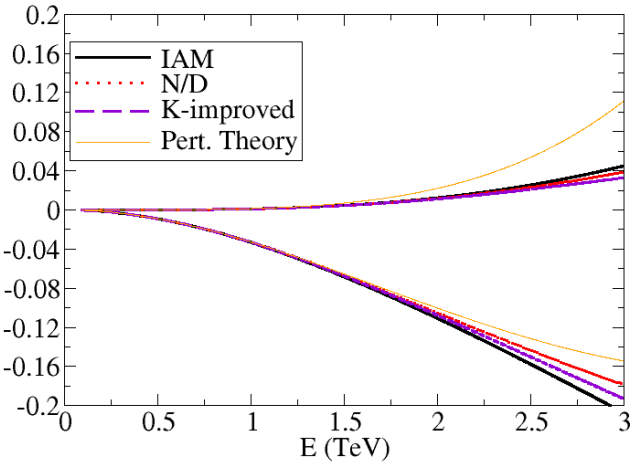

Figure 5.4: Scalar-isotensor amplitudes for $a = 0.88$, $b = a^2$, and the NLO parameters set to 0. All three unitarization methods agree qualitatively and with the perturbative amplitude too, as loop corrections are small. Here we plot both the imaginary part (top set of lines) and the real part (bottom set). That the real part is negative reflects the repulsive interaction in this channel given by $-(1 - a^2) < 0$ in eq. 3.138.

5.1.3 Scalar-isotensor channel, $J = 0$, $I = 2$

We now consider the isotensor channel, where a resonance, if there ever was one, would distinctly appear, for instance, in equal-charge $\omega^+\omega^+$ spectra. Fig. 5.4 shows the resulting amplitude for $a = 0.88$, $b = a^2$ and all NLO parameters set to 0.

We plot both the real and the imaginary parts of the three unitarized amplitudes and obtain a moderately weak, repulsive partial wave that does not bind a resonance (as seen from the negative real part). All three unitarization methods give a consistent picture: the unitarized interaction has a slightly larger real part and slightly smaller imaginary part than the (unitarity-violating) perturbative one.

In fig. 5.5 in turn we plot the same isotensor amplitude for $a = 1.15$. Now the real part has opposite sign (attractive interaction) and grows more rapidly, with all the unitarization methods agreeing and once more tracking perturbation theory until about the end of our energy interval at 3 TeV.

5.1.4 Tensor-isoscalar channel, $J = 2$, $I = 0$

In hadron physics there is a well known $f_2(1270)$ resonance that is broad and visible in $\pi^+\pi^-$ spectra. Its mass is well above the 775 MeV of the vector ρ, which is natural because the d-wave is smaller than the p-wave due to the p^l suppression factor near threshold.

In fig. 5.6 we show the tensor-isoscalar channel in perturbation theory, which is indeed small, with all the NLO parameters set to 0, and $a = 0.88$. As shown in the figure legend, b is successively taken equal to a^2 to show the elastic amplitude, and equal to $a^2/2$ to expose the other, inelastic and hh amplitudes. All are of course real and quadratic in s (because $K_{02} = 0$, the LO $O(s)$ vanishes).

Next we show, in fig. 5.7, the comparison between the N/D and IK method in unitarizing the partial wave with $I = 0$, $J = 2$. The IAM method vanishes and cannot be

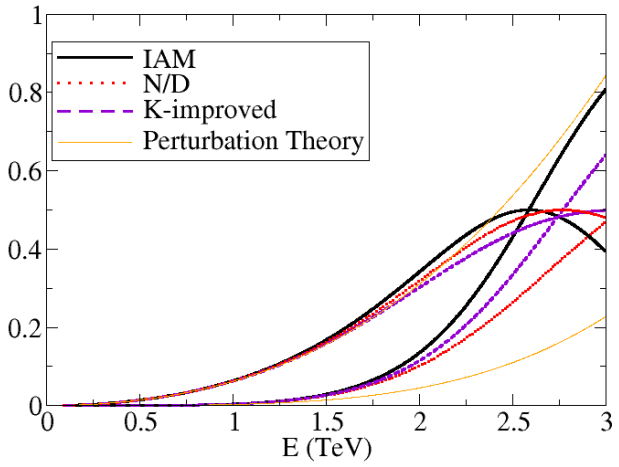

Figure 5.5: Scalar-isotensor amplitudes for $a = 1.15$, $b = a^2$, and the NLO parameters set to 0. All three unitarization methods agree qualitatively once again, even though now the amplitudes are strong. The real part (corresponding to the set of lines larger at low-E, since it receives a tree-level contribution unlike the imaginary part) is now positive because of the sign reversal of $(1 - a^2)$ respect to figure 5.4.

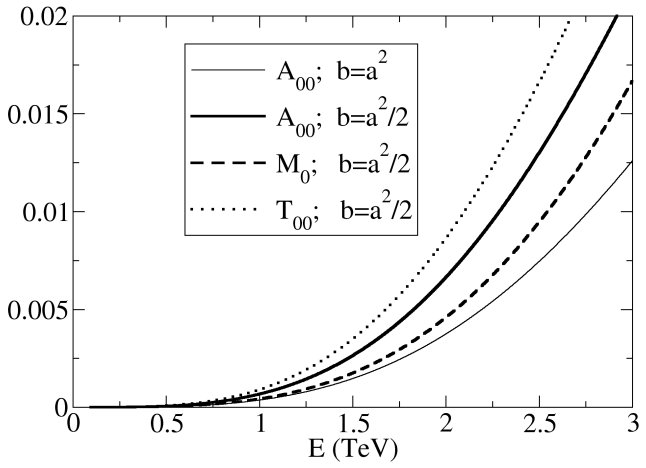

Figure 5.6: Tensor-isoscalar amplitude for $a = 0.88$, b as shown, and the NLO parameters set to 0. The amplitude is real.

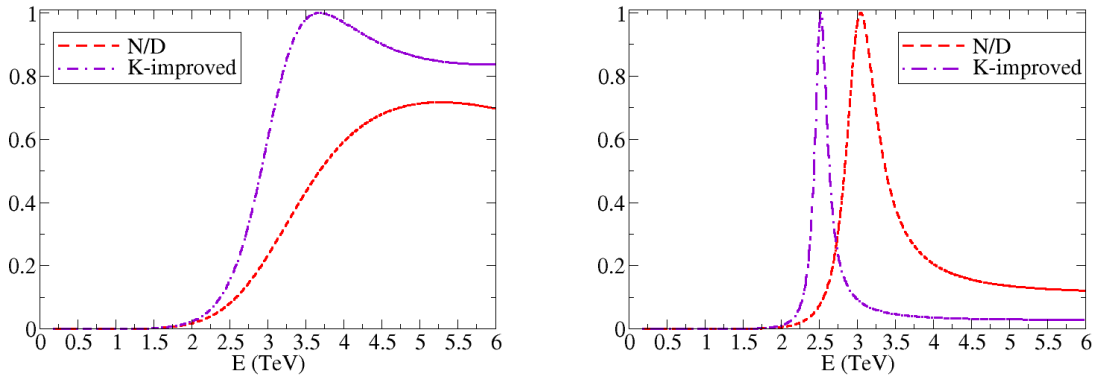

Figure 5.7: Comparison of the two available methods of unitarization for the isoscalar-tensor channel $I = 0$, $J = 2$ with $b = a^2$ (only one channel). The a_4, a_5 constants have been fixed to their values in large-N_c gauge theory, so the left plot with a=0 reproduces the QCD situation with a broad, heavy f_2-like resonance. The right plot shows how this becomes narrow for $a = 0.88$. Both N/D and IK methods agree well.

used without information from NNLO, because here the LO in perturbation theory is zero ($K_{02} = 0$).

In the left plot we have set $a = b = 0$ and $a_4 = -2a_5 = 3/192\pi^2$ as in fig. 5.3. The IK method clearly shows, and the N/D method is suggestive of, a QCD-like f_2 resonance (rescaling again $v = 246\,\text{GeV}$ to $f_\pi = 92\,\text{MeV}$, the 3.5 TeV resonance mass becomes 1.3 GeV, in very good agreement with the experimental 1.27 GeV f_2 resonance in the hadron spectrum; and this with no free NLO parameters, since they are taken from large-N_c).

In the right plot we have now increased $a = 0.88$, with $b = a^2$ still fixed to avoid the coupled-channel situation. The resonance is seen to become lighter and narrower, and both unitarization methods qualitatively agree in predicting the resonance though the mass is slightly different.

If we now lift the $b = a^2$ requirement, because this is an isoscalar channel, the hh system becomes coupled to $\omega\omega$. Then the resonance should be visible in both particle spectra, and also in the channel-coupling amplitude; all three are shown in fig. 5.8 where the now inelastic resonance is clearly visible. Its mass is very similar to the purely elastic case, and both unitarization methods continue being in qualitative agreement.

We use the opportunity to show the appearance of this resonance also as a consequence of the channel coupling induced by the parameter e of the effective Lagrangian. The IAM below does not capture the tensor channel, and the scalar one that the IAM does capture is only sensitive to the combination $d + e/3$ which does not allow to disentangle the two parameters. To see the separate effect of e we need to examine the tensor channel[1], as seen in eq. 3.142, and this can be carried out with the N/D or IK methods. The result of this analysis is shown in fig. 5.9. To prepare it, we have taken $a = 0.95$ and $b = a^2/2$. If all the NLO parameters vanish, there is no low-energy resonance in this tensor-isoscalar channel. Adding e at the level of $3 - 4 \times 10^{-3}$ or more causes a resonance to enter the low-energy region.

[1]This arises naturally because the $\partial_\mu h \partial^\mu h$ contraction that multiplies d in eq. 2.31 is a scalar, while the $\partial_\mu h \partial^\nu h$ one that accompanies e has both scalar and tensor components.

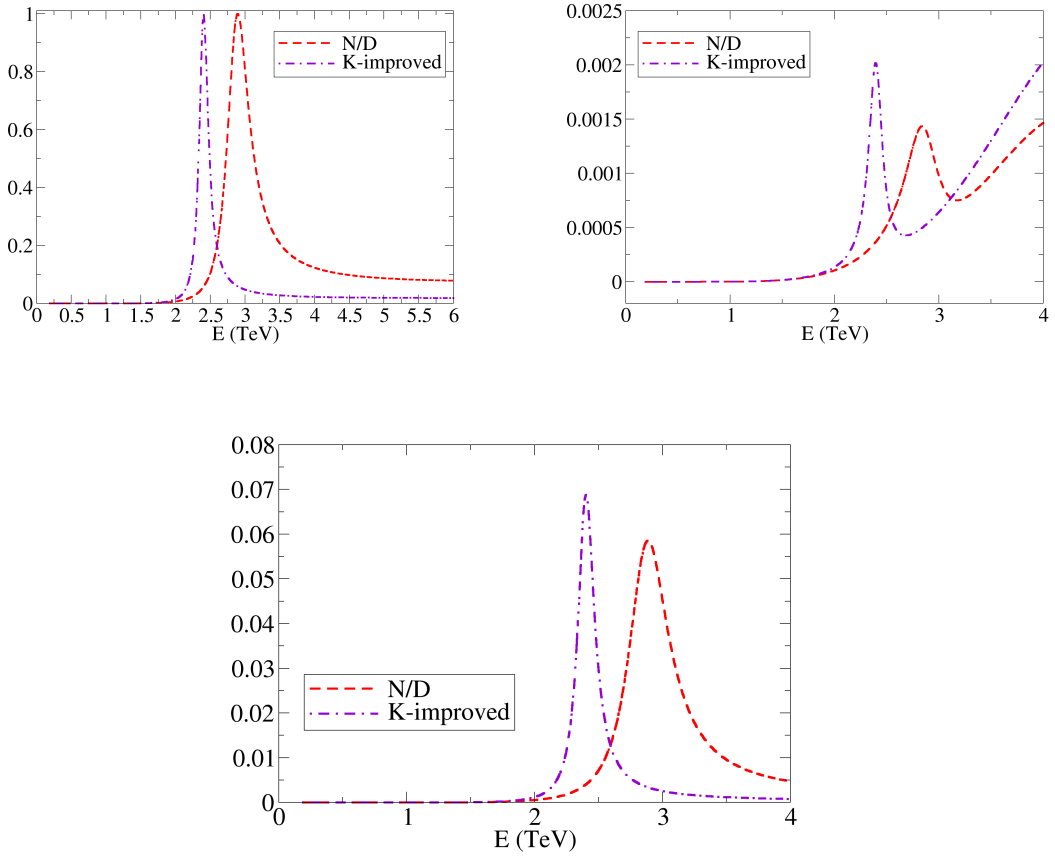

Figure 5.8: Isoscalar-tensor amplitudes (imaginary parts) for $a = 0.88$, $b = a^2/2$, and the NLO parameters set to 0. From left to right and up to down: elastic $\omega\omega$, elastic hh and crossed-channels amplitudes.

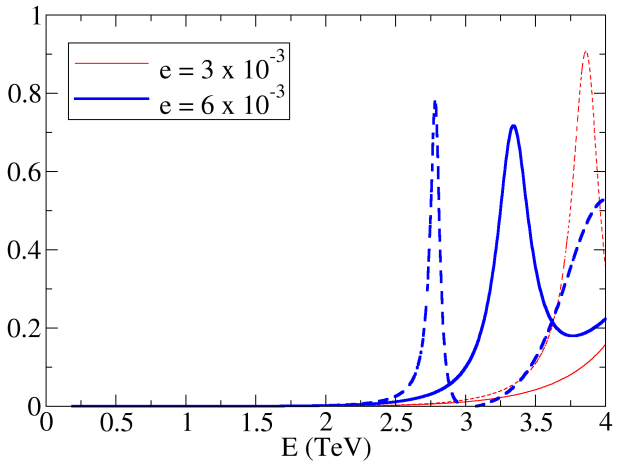

Figure 5.9: The tensor-isoscalar $J = 2$, $I = 0$ coupled channels analyzed with both IK (dashed lines) and N/D (solid line) methods can show a resonance induced by the parameter e. The line thicknesses correspond to different values of the NLO E.

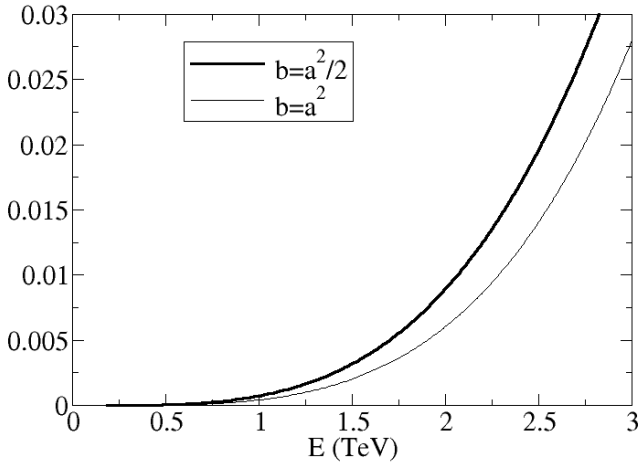

Figure 5.10: The real tensor, isotensor $I = J = 2$ amplitude in NLO perturbation theory for $a = 0.88$ and two values of b.

5.1.5 Tensor-isotensor channel, $J = 2$, $I = 2$

The last partial wave that does not vanish at NLO in perturbation theory, and that to our knowledge has not been considered in the literature except in ref. [150] in the context of the Higgsless ECL model[2], is the tensor-isotensor channel. Here again $K_{22} = E_{22} = 0$, so that the amplitude in perturbation theory is real for physical energy. The non-vanishing constants, B_{22} and D_{22} are given in eq. 3.140 below and the amplitude is drawn in fig. 5.10 in perturbation theory.

Moreover, fig. 5.11 shows this computation in perturbation theory for the case $b = a^2$ together with the isotensor-scalar one and also the two isoscalar amplitudes. Comparing those of equal I we see that larger J is suppressed below $4\pi v \sim 3\,\text{TeV}$ (more so for the scalar channel, since the scalar-isoscalar amplitude is strongly interacting). Curiously, for $J = 2$ the isotensor wave is stronger than the isoscalar one.

The unitarization of the $J = I = 2$ channel is not possible in the IAM method because $K_{22} = 0$, but both IK and N/D methods concur in the presence of a resonance, as seen in fig. 5.12, when the a_4 NLO parameter is large enough. It is worth remarking that, for a given a_4, $m_{11} < m_{22}$, so that having this resonance in the 2-3 TeV region entails the presence of the vector-isovector (ρ-like one) in the 1-2 TeV energy interval.

As we have established that the convergence of the partial wave expansion is very good by comparing the $J = 2$ and $J = 0$ amplitudes, and that the order of the spectrum of resonances is the natural one, with those of lower angular momentum appearing at lower energy, we concentrate in the following on the three cases that are accessible to the NLO-IAM, the 00, 11 and 20 channels; only the first one requires the coupled-channel treatment.

[2]See appendix D.4.

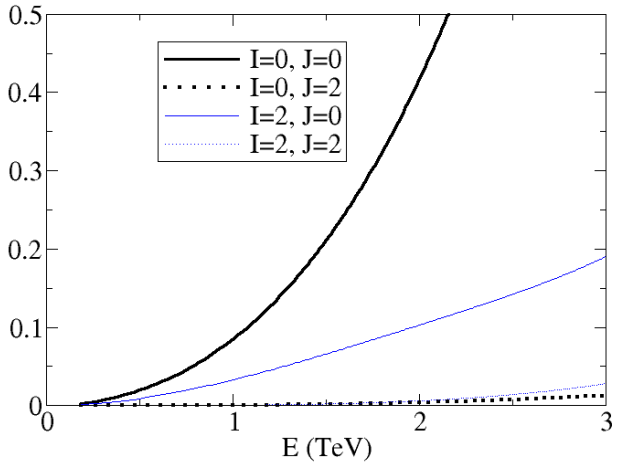

Figure 5.11: Moduli of the isoscalar and isotensor NLO perturbative amplitudes theory for $a = 0.88$ and $b = a^2$, showing good convergence of the partial wave expansion in the low energy region (the $J = 2$ waves are much smaller than the two $J = 0$ waves).

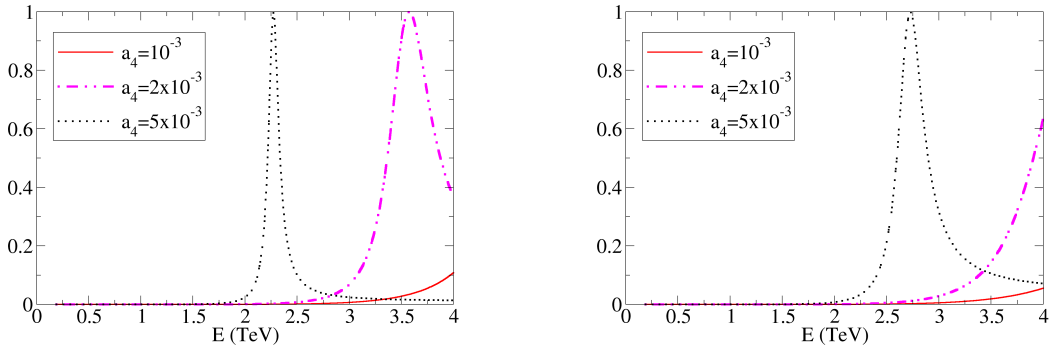

Figure 5.12: Tensor-isotensor resonance as function of the NLO a_4 parameter for the IK-matrix (left plot) and the N/D method (right plot).

5.2 Systematic numerical study of the IAM

In this section we undertake the systematic study of the IAM with the help of a computer. The calculations are very straightforward and involve simple algebraic formula (no integrations, as the dispersion relation has been analytically solved) and the inversion, at most, of dimension-two matrices. The IAM cannot handle, without NNLO information, the higher partial waves with $J = 2$ or beyond, but we have seen in fig. 5.11 that, under natural conditions, these are quite smaller in the low-energy region. For the three dominant low-energy amplitudes, the IAM based on NLO perturbation theory is reliable and powerful, so we proceed with it alone.

First, in sec. 5.2.1 we address the one-channel IAM in eq. 4.163a for the $\omega\omega$ elastic scattering. This involves setting $b = a^2$ and studying the behavior of the amplitudes upon varying each of the active parameters a, a_4 and a_5. These results are just reassuring as they are known to a large extent. Then, sec 5.2.2 addresses the coupled channels, by means of eq. 4.162a, and it is here that we make a totally new contribution.

One of our findings is a coupled-channel resonance akin to the low-energy σ meson but that can be generated by purely $ww - hh$ interactions independently of the elastic potential strength between two ωs or two hs. We have highlighted this curious object in a letter (our ref. [39]).

5.2.1 Purely elastic scattering with $b = a^2$

The current 2σ bounds on the a parameter are, from CMS (ref. [128]), $a \in (0.87, 1.14)$; and, from ATLAS (ref. [127]), $a \in (0.96 - 1.34)$. The discussion in page 14 compiles these bounds. We will take as reference a fixed value of $a = 0.95$ with NLO parameters set to 0, and later exemplify the sensitivity to each parameter (a is better chosen different from 1 because of the factor $(1 - a^2)$ that enters the leading order amplitudes). In any case, the sensitivity to a is displayed in fig. 5.13. Generally speaking, for $a < 1$ (left plot) there is a broad scalar resonance akin to the σ in hadron physics, and the other channels are nonresonant. For $a > 1$ we can see a different situation in which the scalar strength significantly diminishes, but instead the isotensor wave becomes strong and possibly resonant (because the factor $1 - a^2$ changes sign, so its normally repulsive amplitude becomes attractive). As observed by Espriu et al., in a large swath of parameter space with $a > 1$ there are violations of causality, see fig. 5.23.

We now take the top right plot in fig. 5.13 and add an NLO term proportional to either a_4 or a_5, with the outcome plotted in fig. 5.14. The effect of a_4 of order 10^{-3} (left plot) is to produce a very narrow vector-isovector resonance, and narrowing plus making the scalar-isoscalar one lighter. The effect of a_5 (right plot) at this same level of intensity is only dramatic in the scalar-isoscalar channel, while the vector one remains of moderate intensity and hardly resonant at all. This is in agreement with the independent observation in ref. [141]. The vector resonance induced by positive a_4 can also be seen in the scattering phase shift in fig. 5.15. The left plot shows the phase motion in the three lowest-E channels with all NLO parameters set to 0. No resonance is seen, in agreement with the top right plot of fig. 5.13 ($a = 0.95$). The right plot in fig. 5.15 shows clear resonant phase motion corresponding to the resonances in fig. 5.14, where we study the effect of both a_4 and a_5. The good agreement with ref. [141] is remarkable, both works agreeing on the appearance of a pole on the first Riemann sheet in the isotensor channel for negative enough values of either a_4 or a_5.

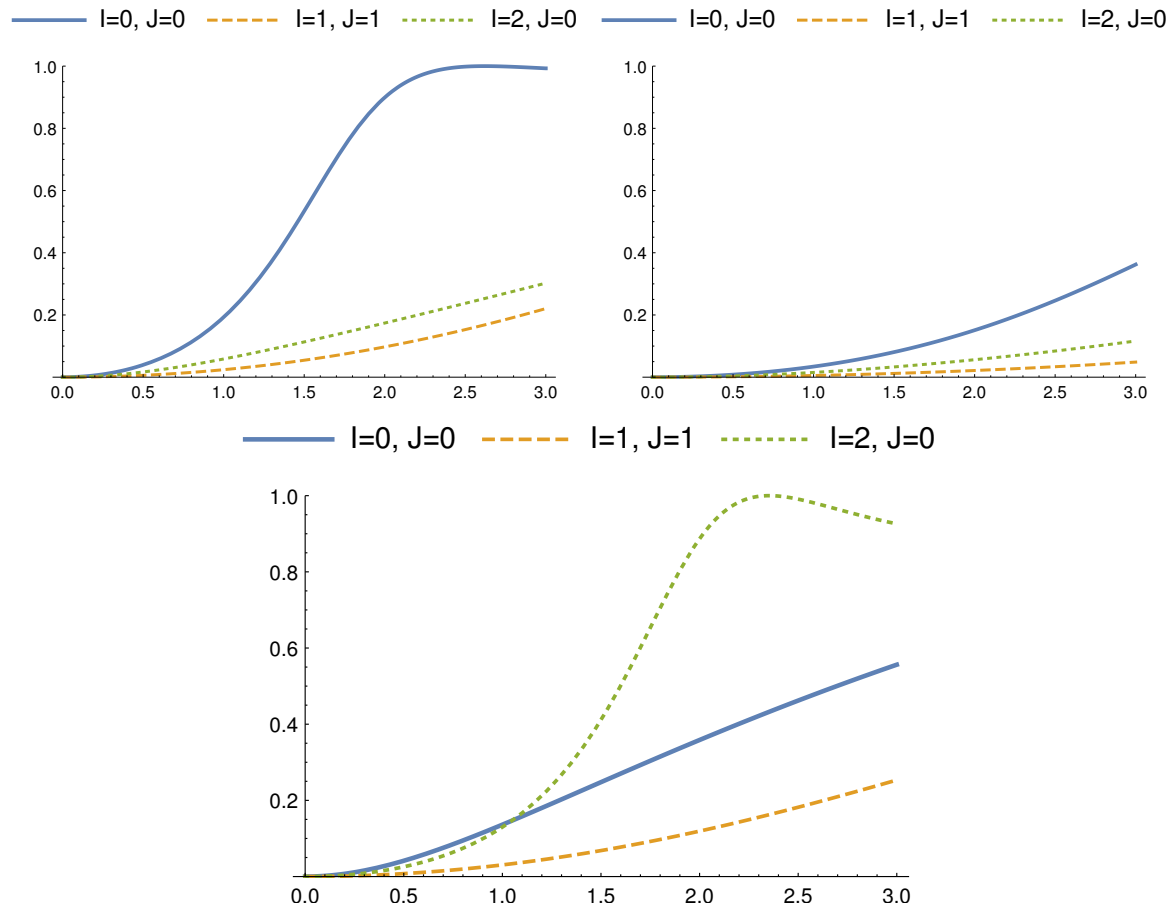

Figure 5.13: Moduli of the lowest elastic $\omega\omega \to \omega\omega$ partial waves in the IAM for $b = a^2$ (no coupled channels) as function of a. From left to right and up to down, $a = 0.75$, 0.95, 1.25. We will take the top right plot ($a = 0.95$) as reference for the parameter exploration in the next graphs.

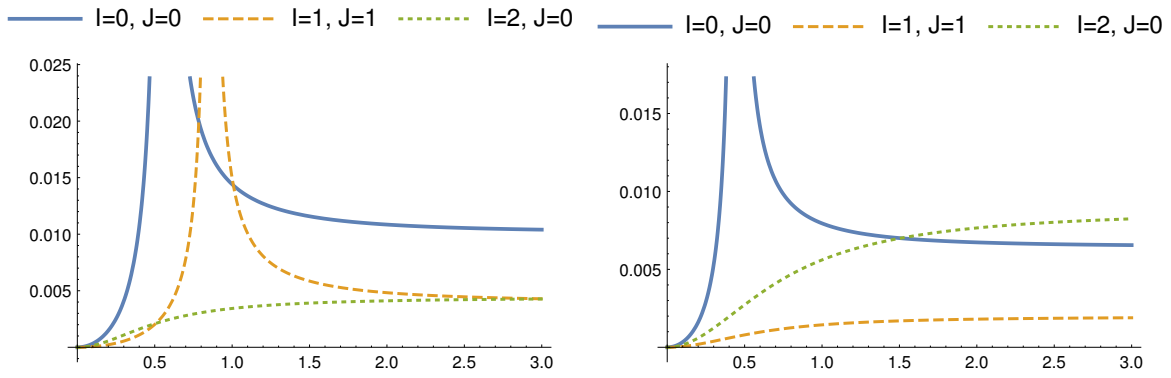

Figure 5.14: Moduli of the lowest elastic $\omega\omega \to \omega\omega$ partial waves in the IAM for $b = a^2$ (no coupled channels) showing the effect of a_4 (left) and a_5 (right) both positive and alternatively equal to 0.002. Here $a = 0.95$. We see a light scalar-isoscalar resonance, a vector-isovector resonance around a TeV in the left plot (that moves to higher masses for smaller values of the positive a_4 that induces it), and an inconspicuous isotensor amplitude.

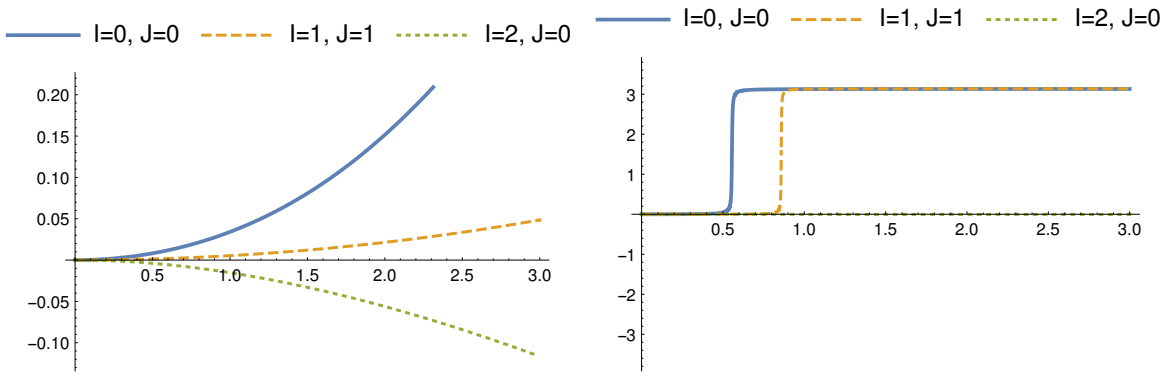

Figure 5.15: Scattering phase shift of the lowest elastic $\omega\omega \to \omega\omega$ partial waves in the IAM for $b = a^2 = 0.95^2$ (no coupled channels), $a_4 = 0$ (left plot) and $a_4 = 0.002$ (right plot). We can see how indeed the addition of an a_4 at the level of 10^{-3} generates phase motion crossing $\pi/2$ in the right plot corresponding to a resonance in both the scalar and vector channels.

This feature is shown in fig. 5.16, is in full agreement with the results of ref. [141] and, as discussed in sec. 4.2.1, excludes this parameter space within the IAM. In order to produce this and the following maps in parameter space, we use the numerical method, described in sec. 4.2.2, which involves the computation of numerical Cauchy integrals.

In fig. 5.16 we call the *experimentally disfavored* regions so because poles appear with $|s| \leq (837\,\text{GeV})^2$ (scalar-isoscalar and isotensor channels) and $(1.22\,\text{TeV})^2$ (vector-isovector channel), and this is at odds with absence of LHC signals.

The vector-isovector channel is here exceptional in that the two variables enter with opposite signs, in the combination $a_4 - 2a_5$, [see eq. 3.137], whereas in all other four NLO amplitudes they come with equal sign. Thus, the slant in the middle plot is opposite to the other two.

For broad swipes of a_4–a_5 parameter space the IAM predicts either isoscalar or isovector resonances or both. In fig. 5.17 we show an example of a pole in the second Riemann sheet of elastic $\omega\omega$ scattering in $l = 0$, the A_{00} partial wave for one channel only ($b = a^2$).

Therein, the continuation to the II Riemann sheet has been obtained with eq. 4.42 and the resonance appears as appropriate below the real, physical s-axis (bright yellow line). This pole corresponds to the scalar IAM resonance shown for physical s in fig. 5.14 (blue solid line there) though a_4 is somewhat smaller here. This serves as illustration of the pole structures in the complex plane (unstable particles or resonances) that accompany our resonant shapes for physical s.

A lot of the a_4–a_5 parameter space represented in ref. [141] is experimentally disfavored because the mass-range where the resonances appear is being covered by LHC data (see refs. [59–61]), with none found yet, though such experimental bounds are not very strong because the couplings between the new resonances and the detected SM leptons are quite arbitrary (from the effective theory point of view), so it is difficult to interpret the bounds beyond particular models.

In fig. 5.18 the simultaneous effect of a (with $a^2 = b$) and a_4 is shown, again swiping the parameter space looking for resonances. Note the presence of a resonance on the first Riemann sheet in the isotensor channel even for $a < 1$ and sufficiently negative values of a_4. For $a > 1$ (and $b = a^2$), there is no resonance on the first Riemann sheet. For $a < 1$, we can find a pole in both the isoscalar and isovector channels. For $a > 1$, only

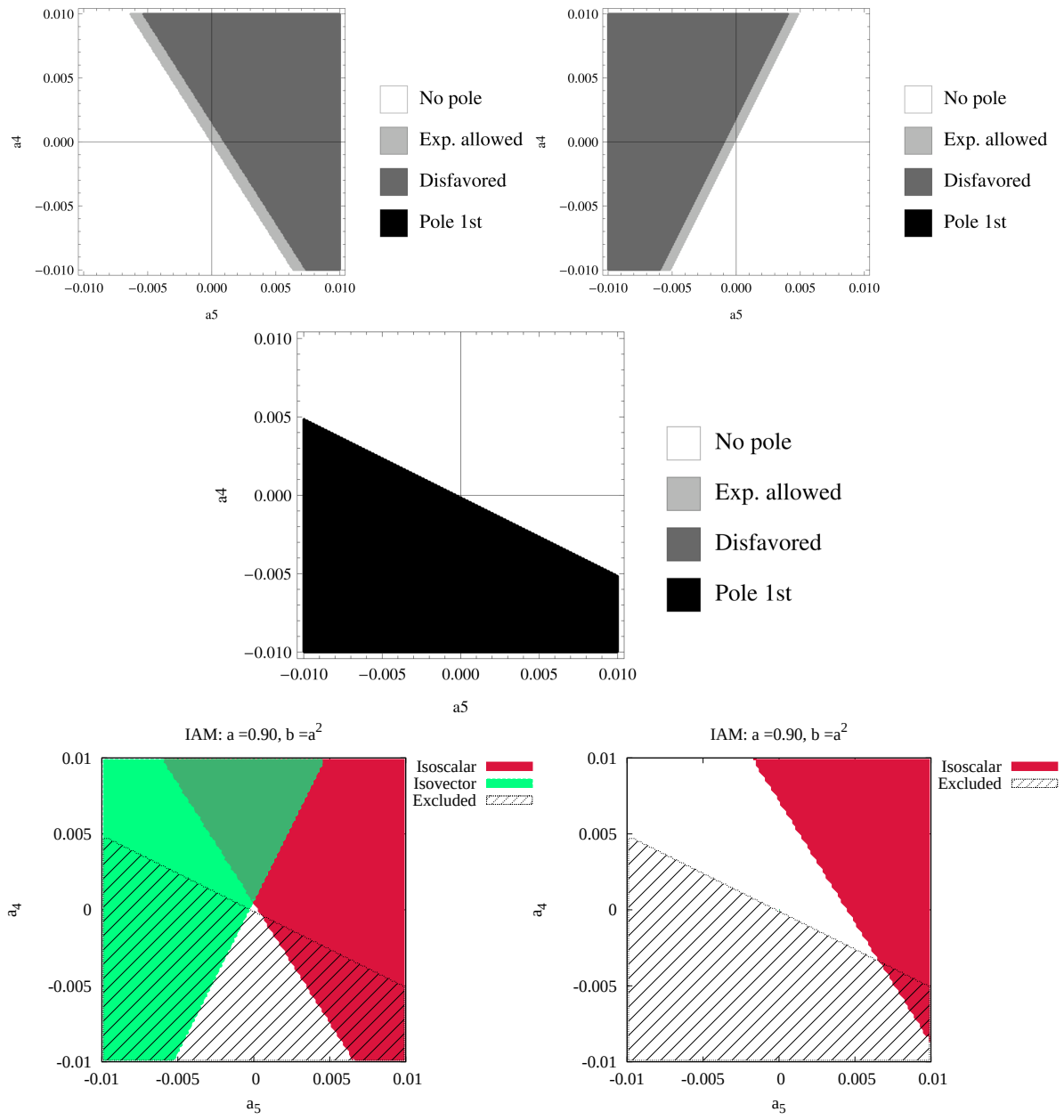

Figure 5.16: From left to right and top to middle, isoscalar ($IJ = 00$), isovector ($IJ = 11$) and isotensor ($IJ = 20$) channels in elastic $\omega\omega \to \omega\omega$ scattering. For $a = 0.90$ (different from our base scenario so we may compare with Espriu *et al.* [141]), $b = a^2$, we show the a_4-a_5 parameter map, setting the other NLO parameters to zero. Note the appearance of a pole on the first Riemann sheet for $IJ = 20$ and negative enough values of both a_4 and a_5.

Bottom: same parameter space, reprinted Fig. 6 with permission from ref. ([158], Domenec Espriu, Federico Mescia, Physical Review D, **90**, 015035, 2014). Copyright 2014 by the American Physical Society.

The bottom left plot shows the presence of resonances. Note that the comparison with our plots is very satisfactory. The botom right plot only shows isoscalar/isovector resonances with $M_{S,V} < 600\,\text{GeV}$, which are experimentally disfavoured [158].

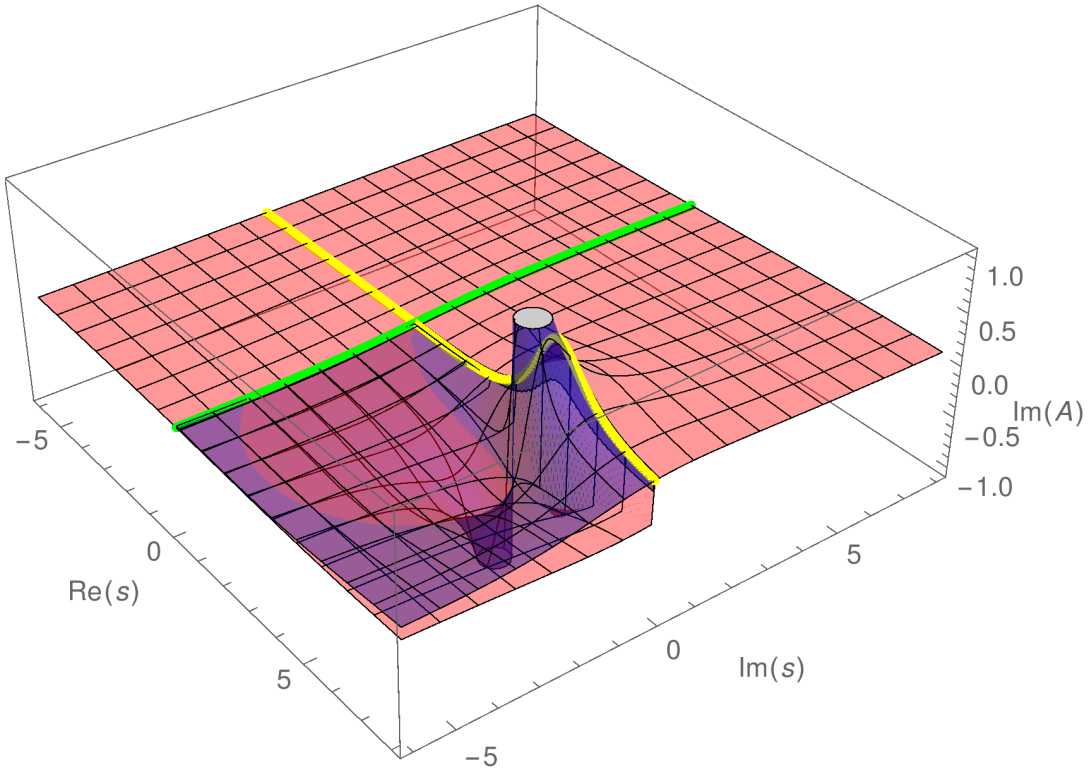

Figure 5.17: Example pole of the isoscalar elastic amplitude with $b = a^2$ (only the $\omega\omega \to \omega\omega$ channel is active), $a = 0.95$, $a_4 = 10^{-4}$, and all other NLO parameters set to 0. Pole in the second Riemann sheet (below the physical, real-s axis highlighted in bright yellow online). The lower (salmon online) and upper (blue online) surfaces are, respectively, the first and second Riemann sheets.

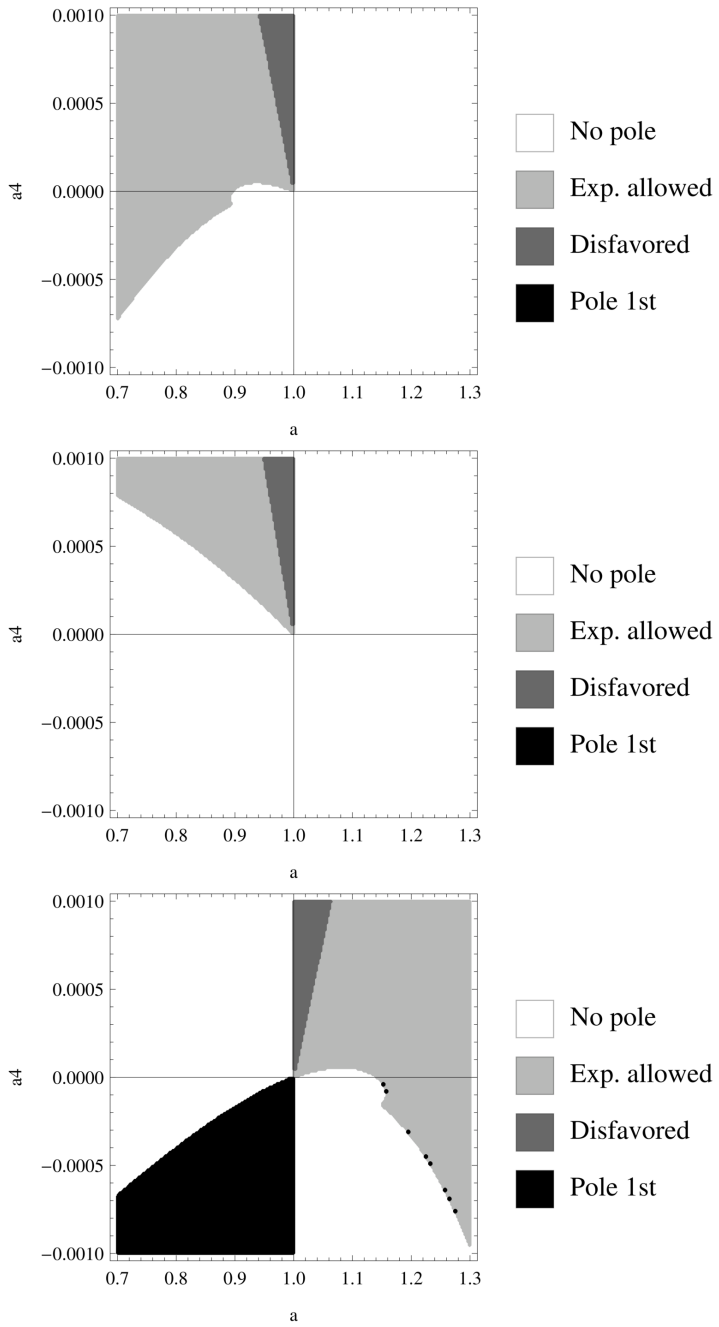

Figure 5.18: From top to bottom, isoscalar ($IJ = 00$), isovector ($IJ = 11$) and isotensor ($IJ = 20$) channels. $a^2 = b$ vs. a_4. Note the presence of poles on the I Riemann sheet for certain region of the $a > 1$, $a_4 < 0$ parameter space.

an isotensor resonance is to be found.

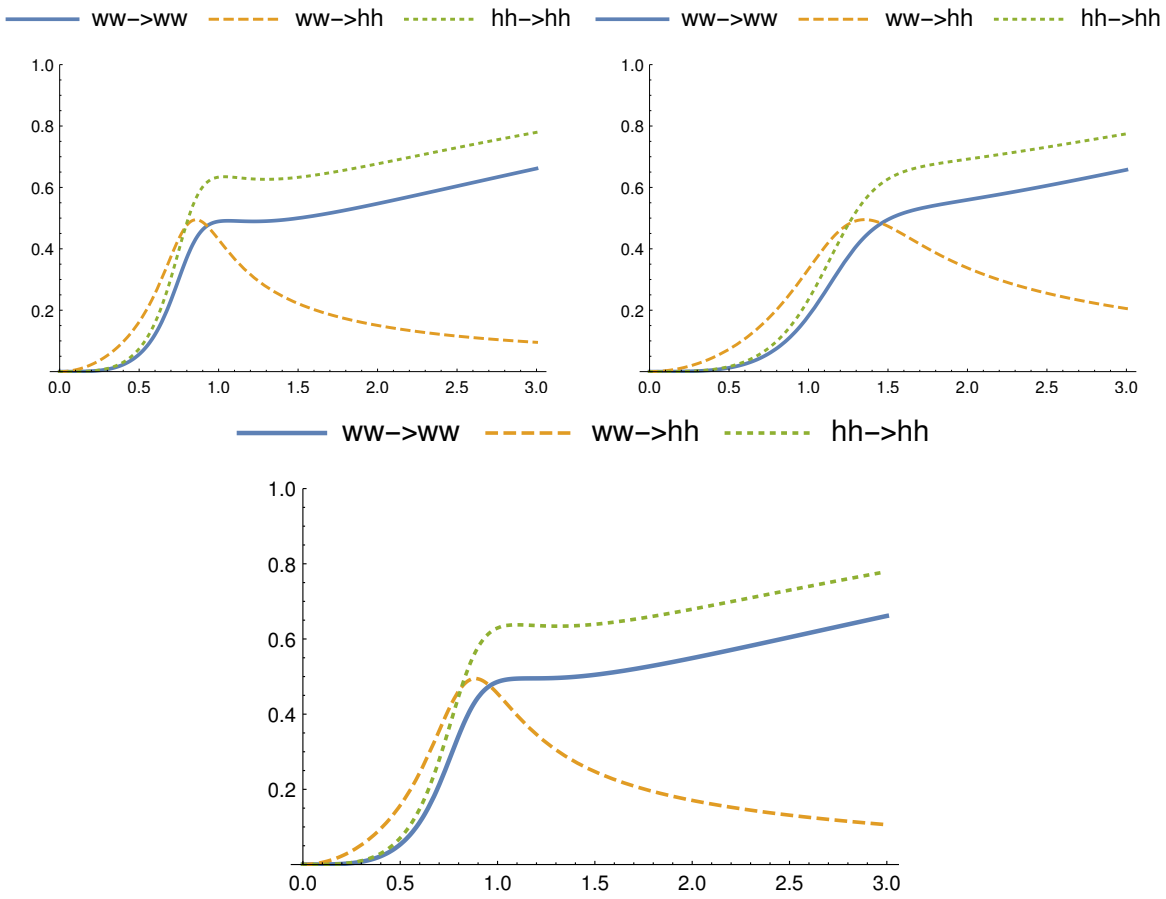

Figure 5.19: Moduli of the lowest ($I = J = 0$) partial waves in the IAM for $b \neq a^2 = 1$ (all the strong dynamics comes from the coupled channels). From left to right and top to bottom, $b = -1$, $b = 2$, $b = 3$ (the first and third are almost equal since they are symmetric respect to $b = 1$). A scalar resonant structure is apparent for $s = 1\,\mathrm{TeV}^2$; because more extreme values of b lower its mass, we are able to give a bound on the value of b, that must be roughly contained in $(-1, 3)$, as explained in our ref. [39]. We will take the middle plot as reference for the parameter exploration in several of the following graphs.

5.2.2 Scattering $\omega\omega$ in the presence of $b \neq a^2$

Setting $b \neq a^2 = 1$ opens the inelastic scattering $\omega\omega \to hh$ channel in the absence of elastic strength. Figs. 5.19 and 5.20 show the dependence on b. Almost all our computed perturbative amplitudes are symmetric around $b = a^2 = 1$, as can be seen on sec. 3.3.1. The only exception is the scalar-isoscalar $\omega\omega \to hh$ channel-mixing M_0 partial wave in eq. 3.141. Note that this asymmetry then appears in other channels due to the unitarization (which can be thought of as resumming perturbation theory), but the effect is small, so that the left and right plots are quite similar. The scalar-isoscalar resonance shown is very interesting and the object of focuse of our letter [39].

Fig. 5.21 shows a comparison between the three unitarization procedures (IAM, N/D and Improved K-matrix) which are valid in the scalar-isoscalar $IJ = 00$ channel. The IAM is within 2% on the Improved K-matrix and within 10% of the N/D[3]. Anyway, the

[3]For a short review of these unitarization procedures, and more information about the validity ranges

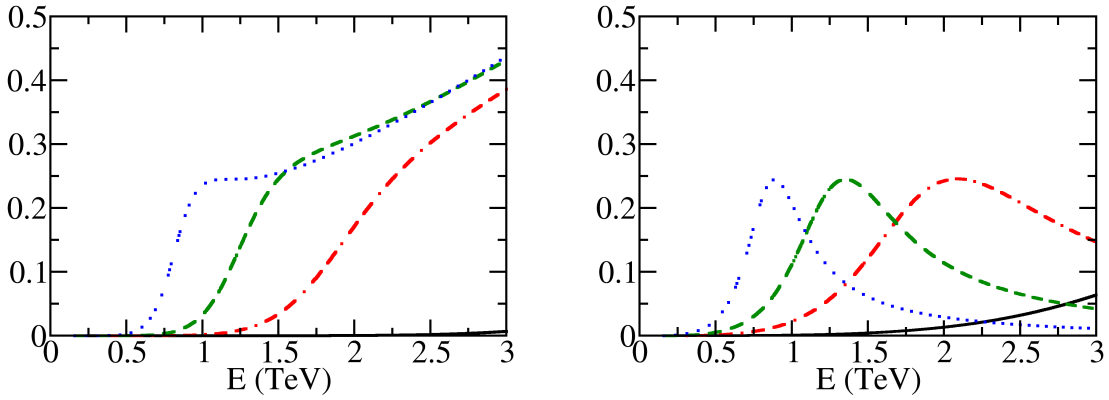

Figure 5.20: Squared moduli of the lowest ($I = J = 0$) partial waves in the IAM for $b \neq a^2 = 1$. Left: $|A|^2$ (elastic channel $\omega\omega \to \omega\omega$). Right: $|M|^2$ (crossed-channels $\omega\omega \to hh$). We show $b = 1.1$ (lowest, solid black line), $b = 1.5$ (dot-dashed, red online) and $b = 3$ (dotted, blue online).

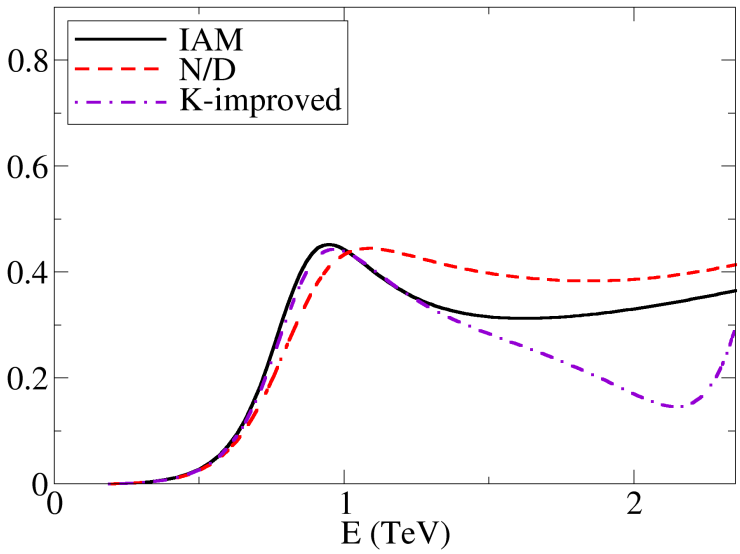

Figure 5.21: Comparison of the three unitarization methods that we consider (IAM, N/D and K-improved) in the presence of coupled $\omega\omega$, hh channels, for $IJ = 00$. $\mathrm{Im}\, A = |A|^2 + |M|^2$ is shown.

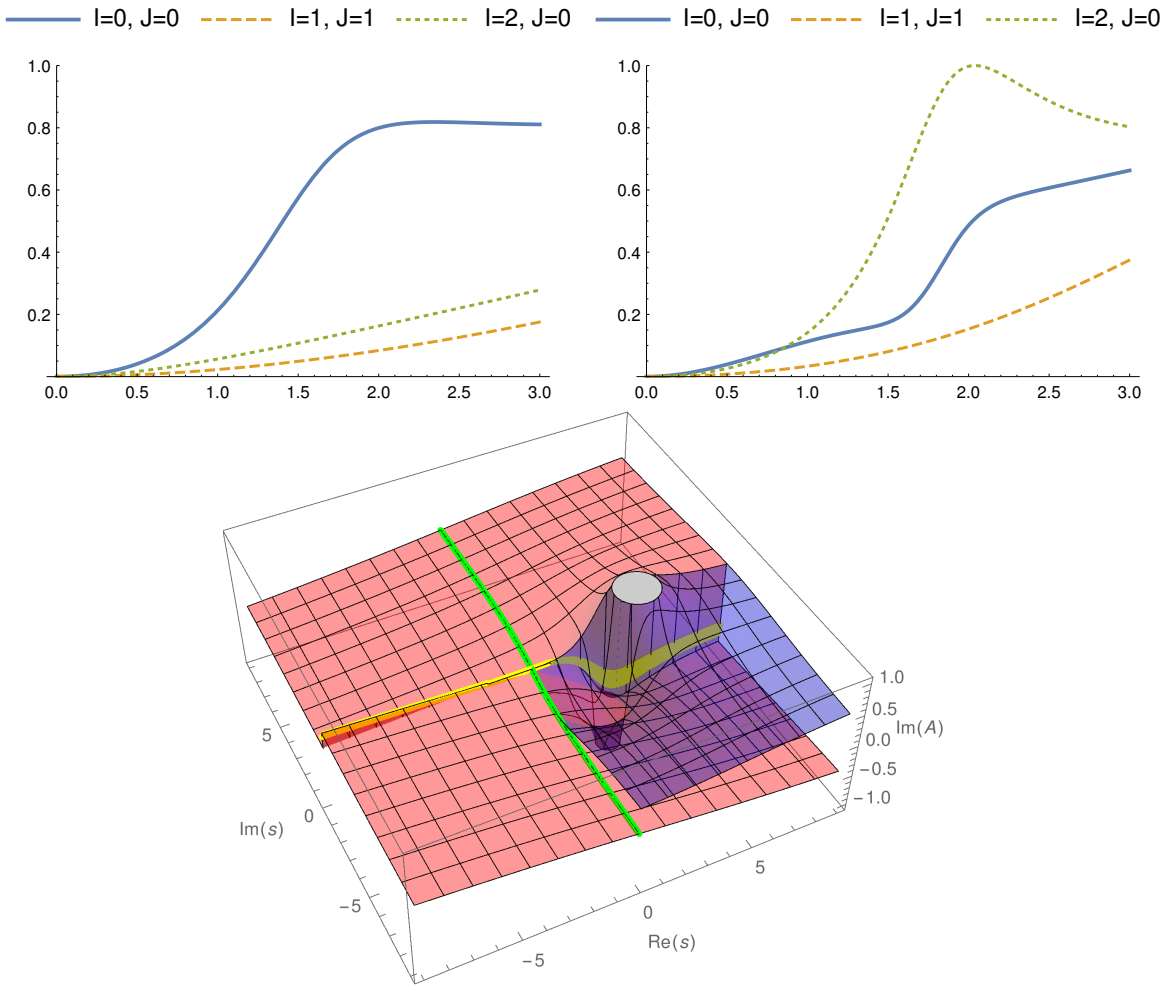

Figure 5.22: Top: moduli of the lowest elastic $\omega\omega \to \omega\omega$ partial waves in the IAM for $b \neq a^2 \neq 1$ (strength from both elastic and coupled-channel dynamics). Top left plot: $a = 0.75$, $b = 0.9$, showing much strength in the scalar channel, presumably due to a σ resonance. Top right plot: $a = 1.25$, $b = 1.1$, showing a pole on the second Riemann sheet in the isotensor channel, clearly seen also on the bottom plot imaginary part of the amplitude in the complex s-plane.

three methods are valid because, for $a^2 \neq 1$, we have that the LO term does not vanish ($K \neq 0$) for all the three channels ($\omega\omega \to \omega\omega$, $\omega\omega \to hh$ and $hh \to hh$), thus ensuring the validity of the IAM. And $D + E \neq 0$, so that the decomposition of the NLO part of the partial waves between a sum of two functions, one with a right cut (RC) and another with a left cut (LC), does work.

Figs. 5.22 shows the lowest elastic $\omega\omega \to \omega\omega$ partial waves in the presence of $a \neq 1$ (as well as $b \neq a^2$), so there is both elastic and inelastic potential strength. The scalar resonance is then more similar to the standard QCD σ resonance.

A novelty is the appearance of a pole on the second Riemann sheet of the isotensor channel for $a = 1.25$, $b = 1.1$. This is very much unlike QCD, where the isotensor channel is weak and repulsive; while there is no $\pi^+\pi^+$ resonance in the hadron spectrum, this is still allowed by current constraints on the W^+W^+ one.

and the differences between the methods, see sec. 4.3.5.

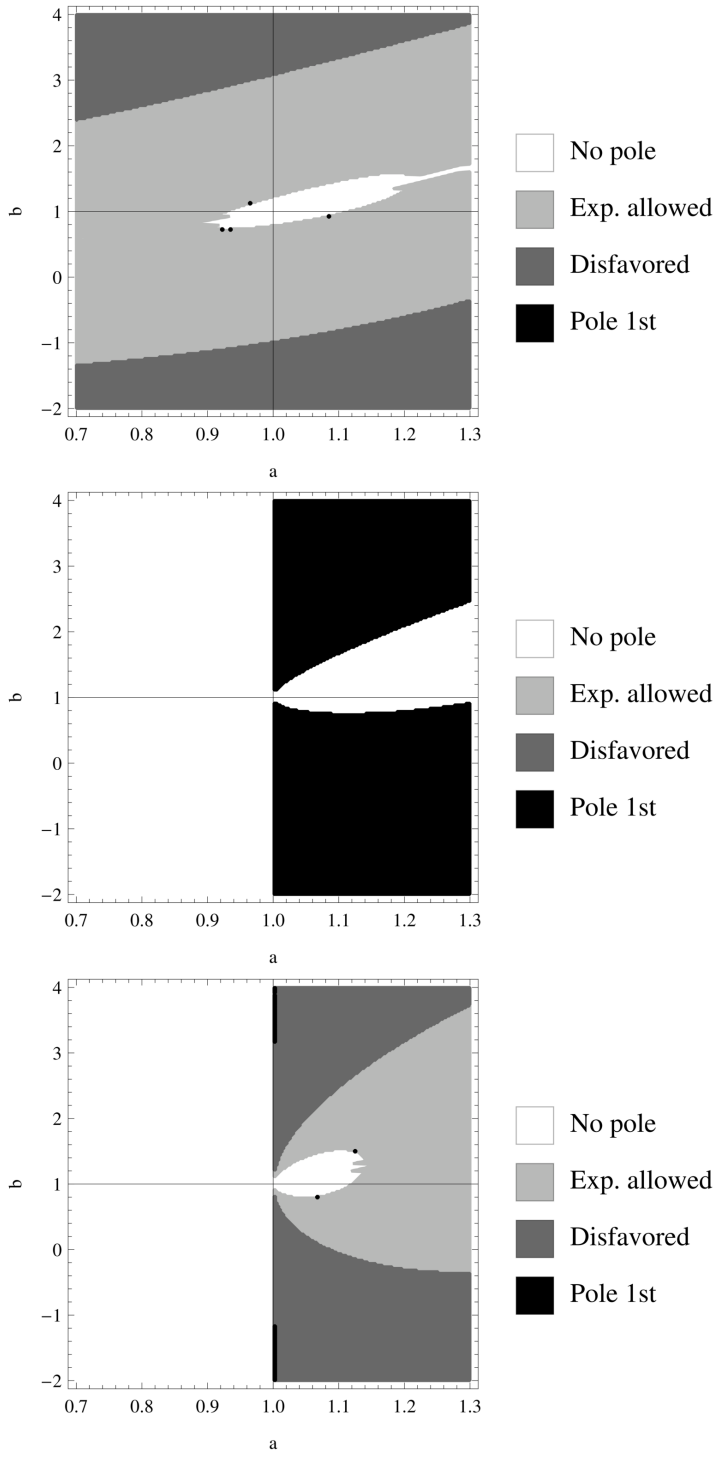

Figure 5.23: From top to bottom, isoscalar ($IJ = 00$, isovector ($IJ = 11$) and isotensor ($IJ = 20$) channels. Note the presence of a pole in the first Riemann sheet of the isovector channel in quite some of the parameter space with $a > 1$. All the NLO parameters are set to zero.

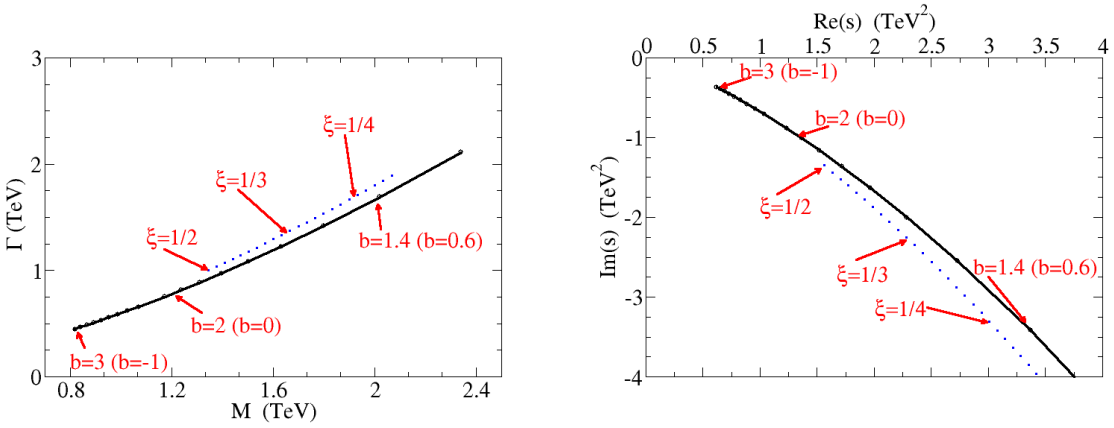

Figure 5.24: Dependence of the pole position for $a^2 = 1$ (lower curve) and $a = \sqrt{1-\xi}$, $b = 1-\xi$, $\xi = v^2/f^2$ (upper curve, blue online). The IAM is used here. Left: resonant mass and width (defined as in eq. 4.35). Right: real and imaginary part of the pole position in terms of the Mandelstam variable s.

However, as we show in fig. 5.23, this case with $a > 1$ is quite critical, because most of the parameter space features an isovector pole on the first Riemann sheet, so that much of this parameter region must be ruled out or declared beyond our validity range. Only a small part of the $a > 1$ parameter space shows an isotensor pole on the second Riemann sheet while excluding an isovector pole on the first one, and simultaneously remains out of experimentally disfavored values of a.

On the other hand, the behaviour for $a < 1$ is more standard, showing a resonance on the second Riemann sheet only in the isoscalar channel. This resonance is quite broad, and only becomes experimentally disfavored for relatively large values of $a^2 - b$.

In fig. 5.24 we study the position of a resonance in the scalar-isoscalar channel ($IJ = 00$) for both $a^2 = 1$ and $a = \sqrt{1-\xi}$ ($b = 1-\xi$, $\xi = v^2/f^2$). In the first case, $a^2 = 1$, the strong interaction comes from the $\omega\omega hh$ vertex, that is, from the crossed-channels $\omega\omega \to hh$. However, a resonance which appears in this crossed-channels also re-enters in the elastic one because of a rescattering process $\omega\omega \to hh \to \omega\omega$. But it enters in the same position of the II Riemann sheet in both channels (elastic and cross-coupled), as shown in fig. 5.25. The $a = \sqrt{1-\xi}$, $b = 1-\xi$, $\xi = v^2/f^2$ corresponds to the Minimal Composite Higgs Models, which introduce a symmetry breaking $SO(5) \to SO(4)$. See refs. [78–81]) for further detail.

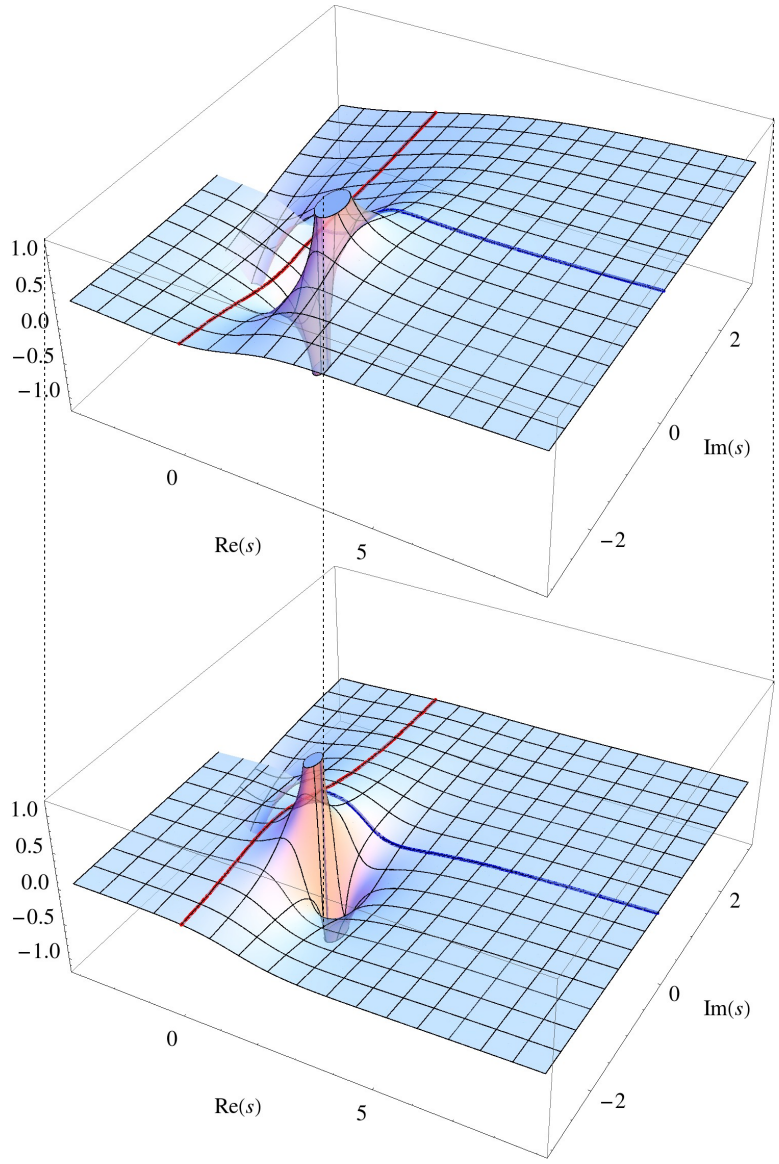

Figure 5.25: Imaginary part of the unitarized partial waves in the II Riemann sheet. $a = 1$, $b = 2$ and all the NLO parameters set to zero. The IAM is used here. Top: elastic channel $\omega\omega \to \omega\omega$ ($\mathrm{Im}\, A$). Bottom: crossed-channels $\omega\omega \to hh$ ($\mathrm{Im}\, M$). Note that, although the amplitudes are different, the pole appear at the same point of the II Riemann sheet.

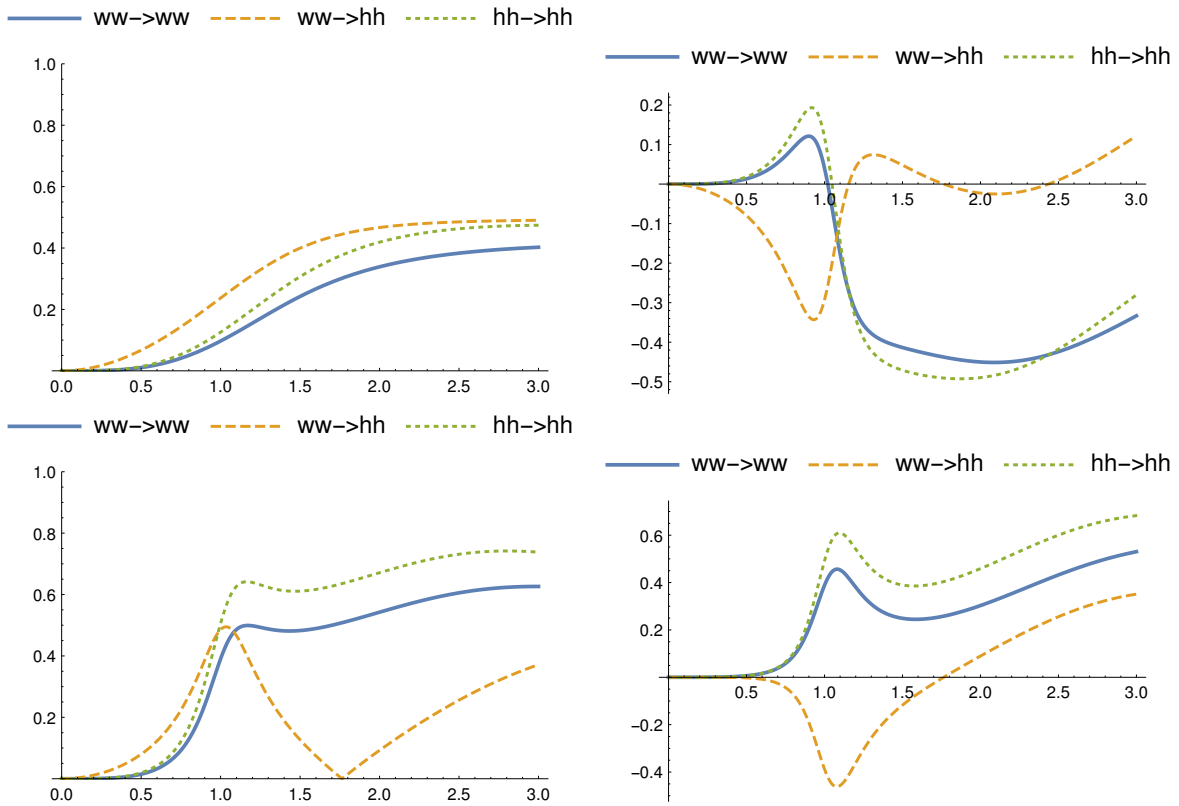

Figure 5.26: Sensitivity to d. We depict the lowest ($I = J = 0$) partial wave in the IAM for $b = 2 \neq a^2 = 1$. Left: moduli of the amplitudes with $d = 0.01$ (top) and $d = -0.01$ (bottom). Right: real (top) and imaginary (bottom) value of that partial wave for $d = -0.01$, where we see that the channel-coupling partial wave is analytic but has a zero.

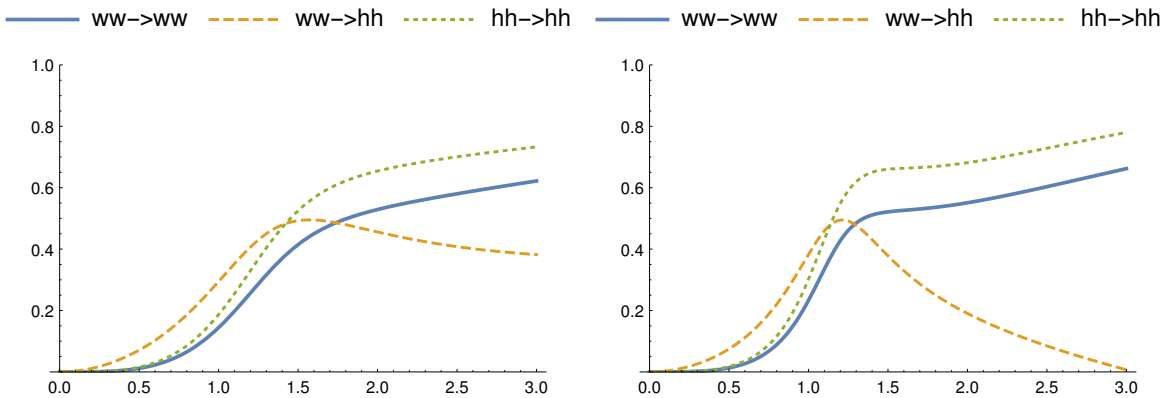

Figure 5.27: Moduli of the lowest ($I = J = 0$) partial waves in the IAM for $b = 2 \neq a^2 = 1$. Left plot: $e = 0.01$. Right plot: $e = -0.01$. The result is similar to fig. 5.26. because, of course, this channel depends only on the parameter combination $d + (e/3)$, which serves as a check.

The d and e parameters are studied in figures 5.26 and 5.27, respectively. However, note that they appear in the combination $d+(e/3)$ on the lowest partial wave ($IJ = 00$), so the IAM applied to any future strongly coupled resonance would be insufficient to separate them and one would need to resort to the $J = 2$, $I = 0$ resonance in fig. 5.9 above to obtain e independently of d.

We concentrate now on the $I = J = 0$, $a = 1$, $b = 2$ case, which has an isoscalar pole on the second Riemann sheet. A peak on $\omega\omega \to hh$ is shown in figs. 5.26 (right) and 5.27. This is expected, since d and e accompany four-particle operators $\omega\omega hh$.

In fig. 5.28 we see that for positive values of d or e, the isoscalar pole weakens and then disappears. But for negative values, a pole on the first Riemann sheet emerges. The case of $d = -0.01$ shown in fig. 5.26 is curious because there is no pole on the first Riemann sheet *below* 3 TeV so we should not a priori reject all that structure in the corresponding plots of fig. 5.26, including a zero of the amplitude at high energies. Of course, we should be cautious: perhaps, for these small negative values of d the pole simply moves to higher energies and we should not trust the computation (or discard negative d altogether).

Finally, we study the dependence of all amplitudes on the g parameter (the only one that we have kept from the pure Higgs scattering sector, as needed to renormalize our amplitudes). It most directly produces an enhancement of $hh \to hh$ scattering that starts at NLO, as can be seen in fig. 5.29, since it comes from a $(\partial_\mu h \partial^\mu h)^2$ term in the effective Lagrangian.

In fig. 5.30 we study the parameter combination $a = 1$ and $b > 1.5$ together with a varying g, so we see the interplay of the channel coupling with the Higgs-sector dynamics. We find a proper isoscalar pole on the II Riemann sheet for positive g. If either g or b are somewhat large, the isoscalar resonance enters the experimentally disfavored zone where LHC data are having an impact. On the contrary, negative values of g introduce a pole on the first Riemann sheet, so we must exclude those.

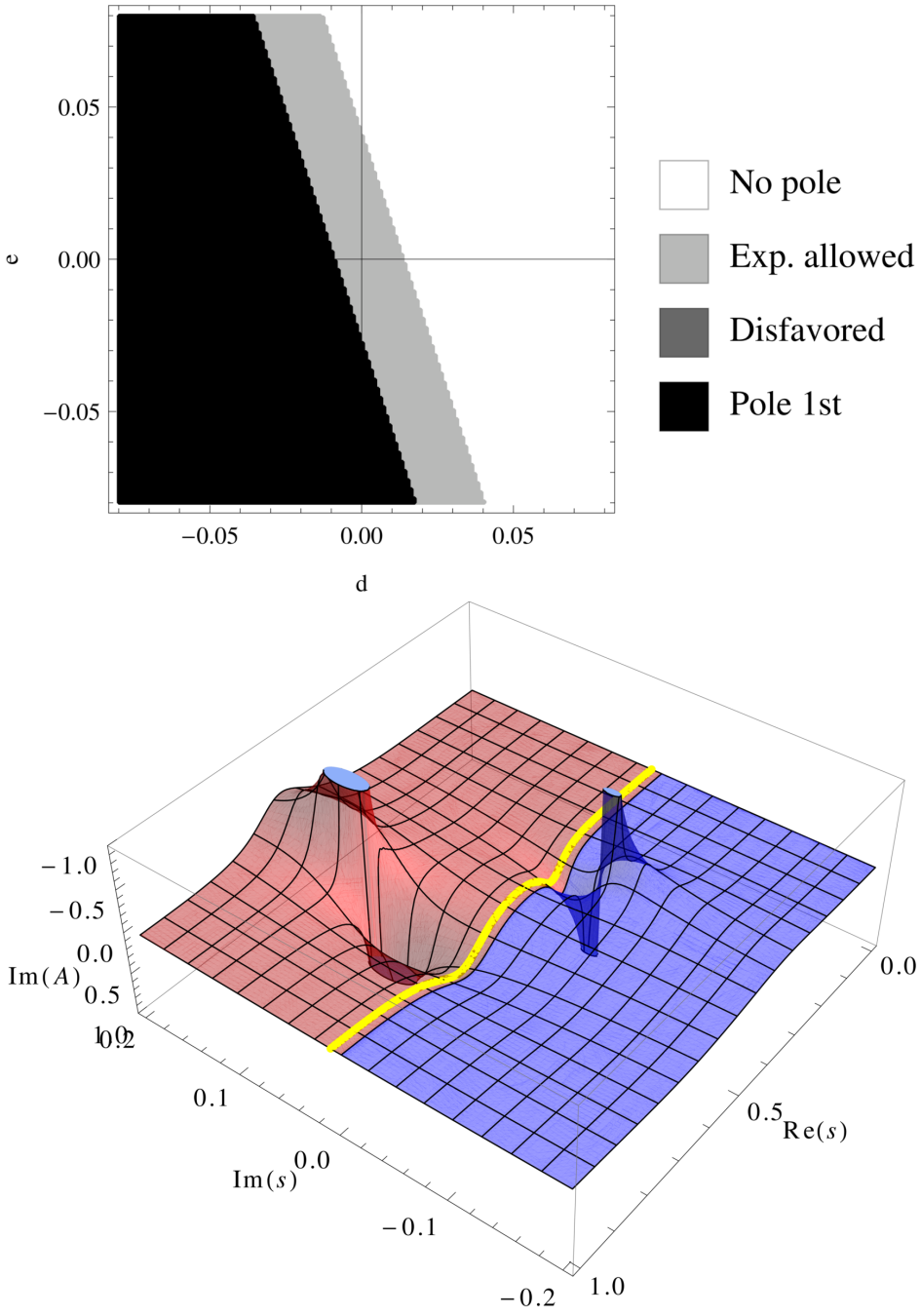

Figure 5.28: Scalar-isoscalar channel ($IJ = 00$), with $a = 1$, $b = 2$. Top: d-e parameter map looking for poles. Bottom: imaginary part of the elastic $\omega\omega$ scattering ($d = e = -0.005$). The isovector and isotensor channels, not shown, have no poles in the region of interest [$|s| < (3\,\mathrm{TeV})^2$]. As discussed above in sec. 4.2.1, the black region contains a pole on the first Riemann sheet (and a conjugate pole that is outside our circuit).

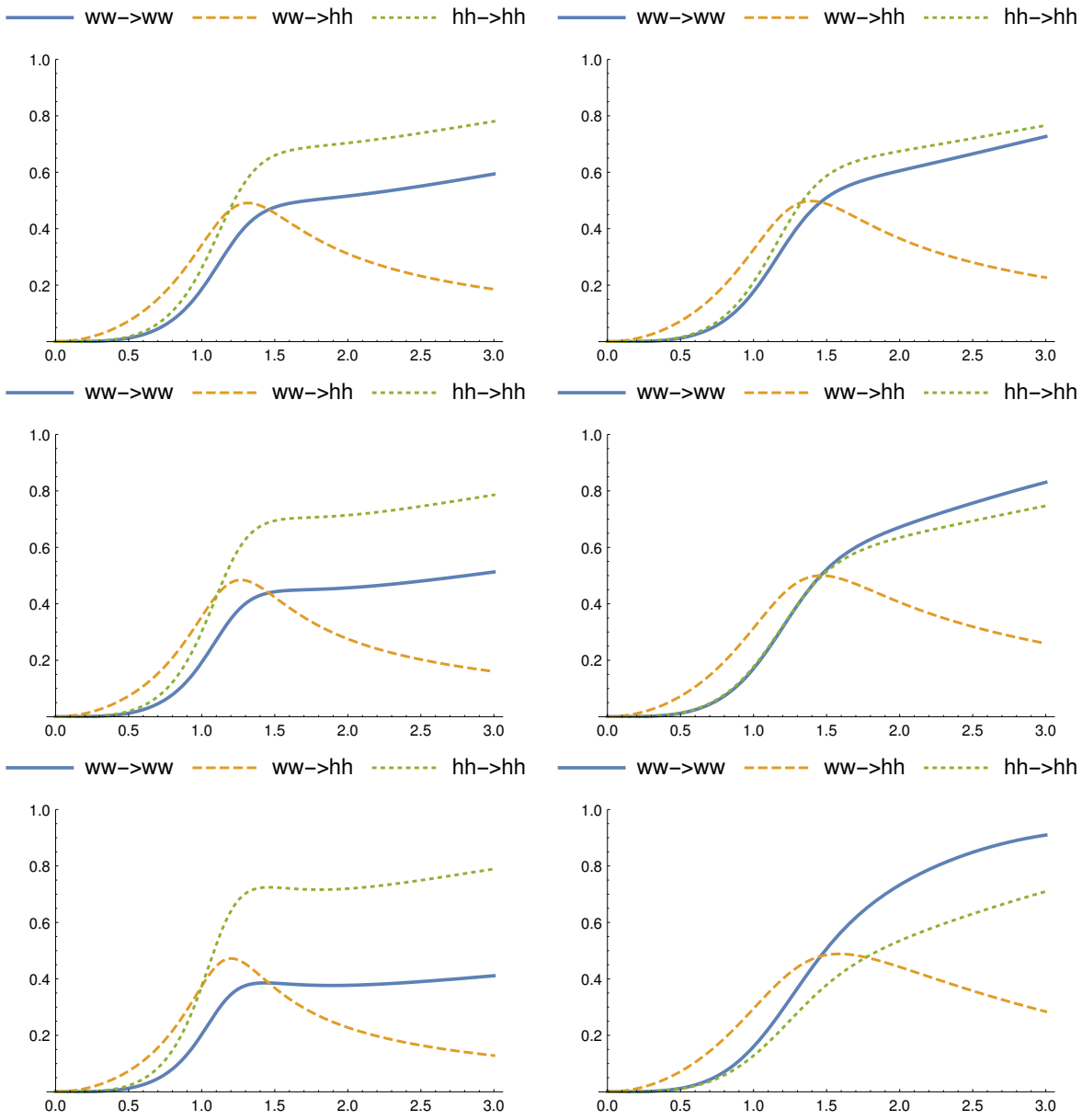

Figure 5.29: Dependence on g, that we find weak for natural values thereof. Displayed are the moduli of the lowest ($I = J = 0$) IAM partial waves for $b = 2 \neq a^2 = 1$. Left panel: from top to bottom, $g = 0.002$, $g = 0.005$, $g = 0.01$. Right panel: negative g values of equal magnitude.

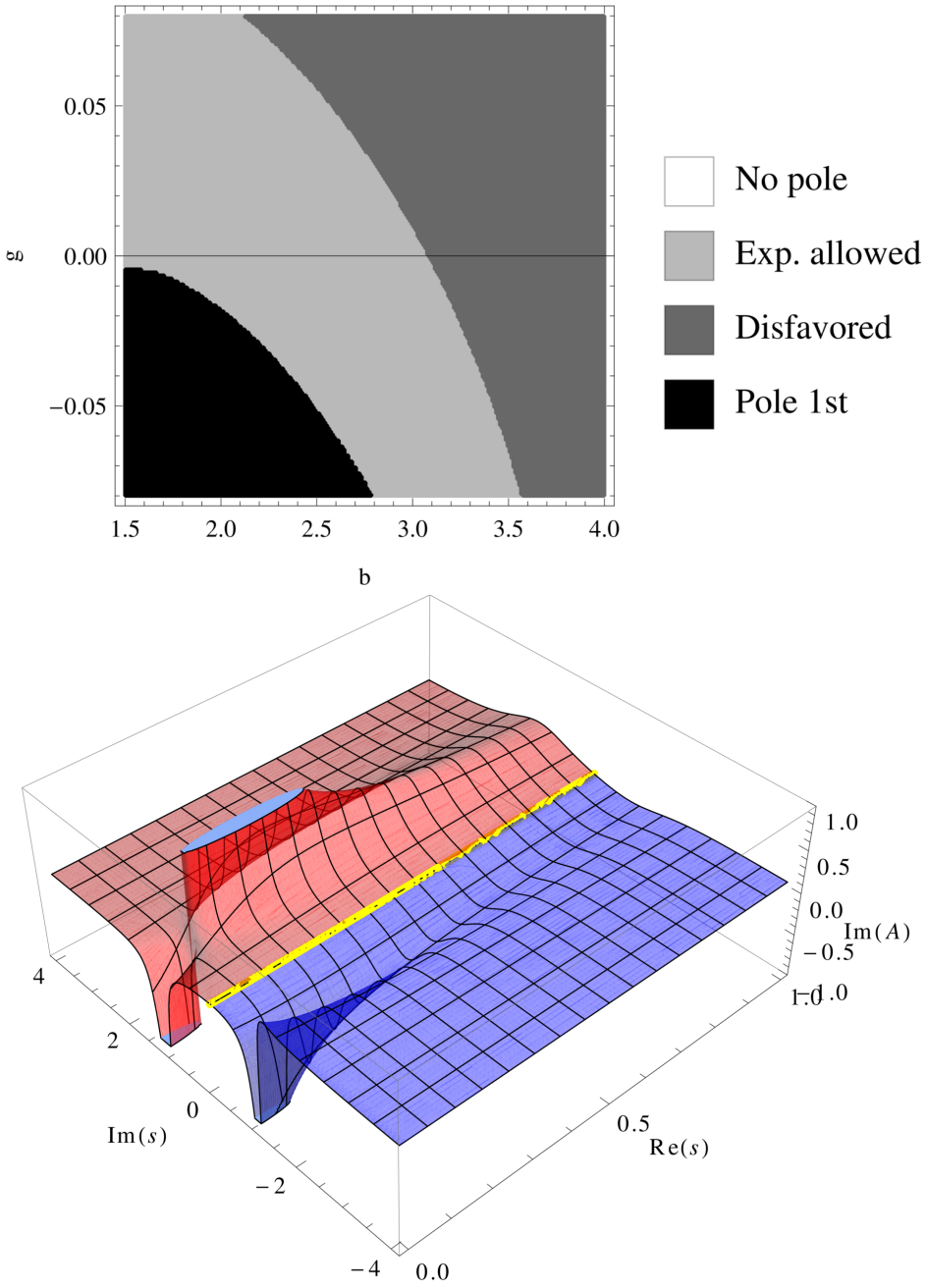

Figure 5.30: Top: map of the b–g parameter space, seeking poles in the isoscalar channel ($IJ = 00$), with $a = 1$ fixed and the remaining NLO parameters set to zero. The isovector and isotensor channels have no poles in the region of interest, $|s| < (3\,\mathrm{TeV})^2$. In the black regions there are two poles above and below the real axis on the I Riemann sheet, and we capture at least one with Cauchy's theorem, excluding the corresponding parameter swath. Bottom: explicit plot of these two poles for fixed parameter values $b = 2.4$, $g = -0.08$ (plotting again the imaginary part of the elastic $\omega\omega$ scattering).

Chapter 6

Conclusions

In this work we have performed a comprehensive study of the unitarized amplitudes obtained from the the Effective Chiral Lagrangian which describes the Electroweak Symmetry Breaking Sector (EWSBS) in the TeV region. A next-to-leading order (NLO) computation has been performed within a (massless) Effective Field Theory (EFT) to obtain the one-loop scattering amplitudes. The (weak) coupling with $\gamma\gamma$ and $t\bar{t}$ states has also been considered. Table 6.1 summarizes the applicability range of each unitarization procedure, and could be used as a guide for developers of Monte Carlo simulation programs. The Inverse Amplitude Method (IAM), N/D and improved K-matrix (I-K) methods are considered. The couplings with $\gamma\gamma$ and $t\bar{t}$ use extended versions of the IAM and the N/D.

The first kind of process which has been studied is the scattering between the EWSBS constituents themselves. Under the assumptions of the Equivalence Theorem, they are the 3 would-be Goldstone bosons, whose scattering cross sections are equivalent to those of the longitudinal modes of $W^{\pm}$ and Z gauge bosons[1], and the Higgs-like particle h. The processes considered are the elastic channel $\omega\omega \to \omega\omega$, and the cross-channels $\omega\omega \to hh$ and $hh \to hh$.

The Effective Lagrangian in the massless limit (eq. 2.31) has seven free parameters if one considers only those needed for absorbing the one-loop divergencies. Those named a and b, respectively provide elastic $\omega\omega \to \omega\omega$ and cross-channel $\omega\omega \to hh$ strength at LO. The other 5 parameters are the NLO counterterms: the elastic a_4 and a_5 (inherited from the old Electroweak Chiral Lagrangian), d and e (that couple the two channels at NLO) and g (in the pure $hh \to hh$ sector). This is the minimum number of parameters necessary to obtain a renormalized theory at NLO for massless ω and h bosons. The parameter set, the combinations in which they appear[2], and the experimental reactions useful to extract them, are all summarized in table 6.2.

Some parts of the computation have been succesfully cross-checked with the literature. For instance, in appendix D.4, we have compared the elastic NLO partial waves with the ECL (Higgs-less) model of ref. [150], when $a = b = 0$. And the work of Espriu et al. [158] is also a good check of the unitarized parameter space of the a_4 and a_5 NLO coefficients (see fig. 5.16 above).

Five unitarization methods have been described, aiming at classifying their respective strengths and weaknesses. From them, we argued that the three mentioned in the previous page satisfy all desirable properties (describe several IJ channels, produce unitary

[1] See sec. 2.1.

[2] At the level of NLO partial waves without unitarization.

IJ	00	02	11	20	22
Only EWSBS	Any	N/D IK	IAM	Any	N/D IK
Coupling with $\gamma\gamma$ ($a^2 = b$)	IAM + eq. 4.176	N/D + eq. 4.194	–	IAM + eq. 4.176	N/D + eq. 4.194
Coupling with $\gamma\gamma$ ($a^2 \neq b$)	crs. IAM + eqs. 4.190	crs. N/D + eq. 4.197	–	IAM + eqs. 4.176	N/D + eq. 4.197
Coupling with $t\bar{t}$ ($a^2 = b$)	IAM + eq. 4.201	–	–	–	–
Coupling with $t\bar{t}$ ($a^2 \neq b$)	crs. IAM + eqs. 4.215	–	–	–	–

Table 6.1: Unitarization methods usable in each IJ channel, both for the EWSBS itself and the couplings to $\gamma\gamma$ and $t\bar{t}$ states. "*crs.*" refers to the usage of the matricial version of the corresponding unitarization procedure in the presence of crossed channels, and it is shown only for the couplings with $\gamma\gamma$ and $t\bar{t}$. Data taken from tables 5.1 and 4.1.

Parm.	Combination	Simplest reactions	Expt. extraction	Reson. type
a	$1-a^2$	$A_{00}, A_{11}, A_{20} \propto (1-a^2)s$	Low-E W_LW_L s-wave	σ-like
b	a^2-b	$M_0 \propto (a^2-b)s$	Low-E hh s-wave	Coupl. chann. f_0
	$2a_4+a_5$	$A_{02} \propto [(\dots)+(\dots)(2a_4+a_5)]s^2$	Low-E W_LW_L d-wave	f_2-like
		$A_{20} \propto (\dots)s+[(\dots)+(\dots)(2a_4+a_5)]s^2$		Exotic W^+W^+
a_4, a_5	a_4+2a_5	$A_{22} \propto [(\dots)+(\dots)(a_4+2a_5)]s^2$		
	$7a_4+11a_5$	$A_{00} \propto (\dots)s+[(\dots)+(\dots)(7a_4+11a_5)]s^2$		
	a_4-2a_5	$A_{11} \propto (\dots)s+[(\dots)+(\dots)(a_4-2a_5)]s^2$	Low-E W_LW_L d-wave	ρ-like
d, e	$d+\frac{e}{3}$	$M_0 \propto (\dots)\ s+[(\dots)+(\dots)(d+\frac{e}{3})]s^2$	Low-E W_LW_L s-wave	
	e	$M_2 \propto [(\dots)+(\dots)e]s^2$	Low-E W_LW_L d-wave	Coupl. chann. f_2
g	g	T_0, $T_2 \propto [(\dots)+(\dots)g]s^2$		Elastic hh-f_0
c_γ	c_γ	$\mathcal{M}(\gamma\gamma \to W_L^+W_L^-) \propto [(\dots)+c_\gamma]s$	Low-E $\gamma\gamma \to W_L^+W_L^-$	
$a_1, a_2,$ a_3	$a_1-a_2+a_3$ $+(a\cdot c_\gamma/4)$	$\mathcal{M}(\gamma\gamma \to ZZ) \propto [(\dots)+4(a_1-a_2+a_3)+a\cdot c_\gamma]s$	Low-E $\gamma\gamma \to Z_LZ_L$	
c_1	$1-ac_1$	$Q \propto (1-ac_1)M_t\sqrt{s}$	Low-E $\omega\omega \to t\bar{t}$	
g_t	g_t	$Q \propto (\dots)\sqrt{s}+[g_t(\dots)+(\dots)]M_ts\sqrt{s}$	Low-E $\omega\omega \to t\bar{t}$	
C_t	C_t	$Q \propto (\dots)\sqrt{s}+[(\dots)+C_t(\dots)]M_ts\sqrt{s}$	Low-E $\omega\omega \to t\bar{t}$	
c_2	c_2	$N \propto c_2M_t\sqrt{s}$	Low-E $hh \to t\bar{t}$	
g'_t	g'_t	$N \propto (\dots)\sqrt{s}+[g'_t(\dots)+(\dots)]M_ts\sqrt{s}$	Low-E $hh \to t\bar{t}$	
C'_t	C'_t	$N \propto (\dots)\sqrt{s}+[(\dots)+C'_t(\dots)]M_ts\sqrt{s}$	Low-E $hh \to t\bar{t}$	

Table 6.2: Relevant combination of the free parameters a, b, a_4, a_5, d, e and g, besides the photon couplings c_γ^r, a_1, a_2 and a_3. We have included some useful reactions to extract them from the lowest order terms (i.e., s and s^2) in a derivative expansion, without considering unitarization (as well as a few selected resonances with the appropriate quantum numbers for each channel). The numeric coefficients can be found in secs. 3.3.1 (EWSBS alone) and 3.2.2 (coupling with $\gamma\gamma$), so we gloss them over with ellipsis.

Note that the only combination of a_1, a_2 and a_3 parameters that contributes to the $\gamma\gamma$ partial waves of sec. 3.3.2 is $a_1-a_2+a_3$. In order to separate these parameters, the usage other observables would be necessary. On ref. [36], the S-paramter and several photon transitions are quoted.

and analytic amplitudes, are independent of the renormalization scale, and agree with perturbation theory at low energy) and provided explicit constructions for them based on exact (elastic) dispersion relations. These are the IAM, that we have studied at length, the N/D and the I-K (those appearing in table 6.2). All three have been compared.

The inclusion of the cross-channels $\omega\omega \to hh$ and $hh \to hh$ in the unitarization is a novelty of this work. Because of this, we made the case for an interesting potential phenomenon to be sought at the LHC run II and beyond[3] (see our ref. [39]): a possible new f_0-like scalar-isoscalar resonance in the $W_LW_L - hh$ coupled channels, caused by the channel-mixing interaction even when direct elastic interactions in both channels are weak ($a \simeq 1$), as long as b is large enough (to provide coupled-channel strength). Note that, though the LHC starts imposing relatively significant constraints on the a parameter, it has not made much progress of substance in constraining b, so this coupled-channel resonance is one of the most interesting strongly interacting objects that can be sought for at the LHC run-II and beyond, because it may appear at relatively low-energies of 1 TeV or less (because of its somewhat large width, it can easily have escaped detection so far).

The alternative, weakly coupled resonances that do not saturate unitarity, imply parameters fine-tuned to be very close to $a = b = 1$, those of the Standard Model (that also remains a viable theory with current data). We do not have a strong reason to *predict* this f_0-like resonance, rather observe that it features in the largest part of parameter space of the Effective Lagrangian with the known particle content, that supports strong channel coupling. The alternative, weakly coupled resonances that do not saturate unitarity, imply parameters fine-tuned to be very close to those of the SM, $a = b = 1$.

The three *best* methods (IAM, N/D and I-K) are all applicable to the $I = J = 0$ coupled-channel partial wave, and to the exotic $I = 2$, $J = 0$ $\omega\omega$ channel. For any given set of parameters in the Lagrangian, the three methods are in qualitative agreement. In particular, they all produce a σ-like resonance when the interactions become strong, and the mass values obtained agree to within a few percent, which is quite remarkable and means that the model dependence is well controlled by imposing all the necessary theory constraints.

In the $I = 1 = J$ channel (covering for example the W' and Z' bosons associated to Composite Higgs Models, as long as they are strongly coupled to $\omega\omega$) the IAM is the method of choice because the other two cannot be constructed in a renormalization-scale invariant way. Provided that there is no coupling with hh states, the KFSR relation in eq. 5.8 holds. If we require $a \approx 1$, as suggested by the LHC bounds, this leads to small widths for the resonances appearing in this channel (always for $a^2 = b$), like in the study of the a_4 and a_5 parameter space by Espriu et al. [158].

Finally, for the two channels with $J = 2$ (where in particular f_2-like resonances might appear, as well as exotic ones in W^+W^+ same-charge combinations) the IAM cannot be constructed with NLO amplitudes (because the lowest order is s^2 for these), but the other two methods do work and are in qualitative agreement.

In fig. 6.1, we have compared, in the Standard Model, the total production of W^+W^- versus those produced with longitudinal polarization. We conclude from it that, within

[3]Even more, outside particle physics one can find strongly coupled channels with small elastic interaction (see also ref. [39]). For instance, $C_2 + O_2 \to C_2 + O_2$ or $CO + CO \to CO + CO$ elastic scattering is negligible against the coupled-channel $C_2 + O_2 \to 2CO$, a strong exothermic oxidation reaction, freeing almost 11 eV, driven by the large phase space. What is perhaps distinctive in our mechanism is that the *coupled-channel* is large, with no phase space advantage (all particles being approximately massless).

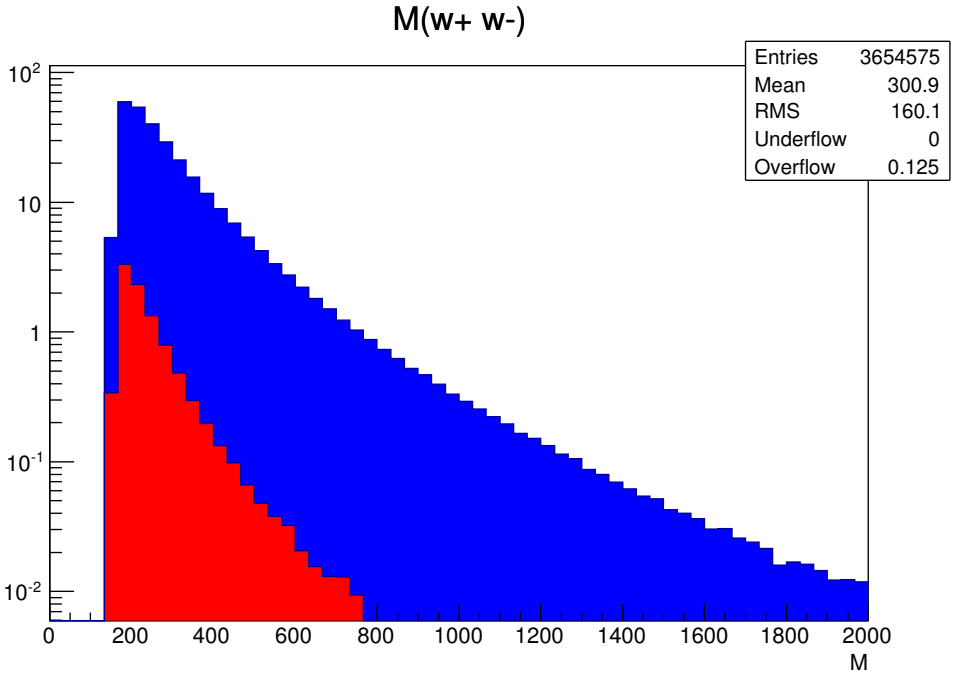

Figure 6.1: Production of W^+W^- (dark gray, blue online) versus longitudinal modes $W_L^+W_L^-$ (light gray, red online) in the SM. x–axis in GeV and y–axis in events / 33.3 GeV. $\sqrt{s} = 13\,\text{TeV}$, $L = 10\,\text{fb}^{-1}$. MadGraph v5 [126] has been used.

the SM, $\omega_L\omega_L$ is a rare process at energies above a TeV. The developing of a Monte Carlo simulation for the unitarized partial waves with strong interactions is still work in progress.

Once the presumed strongly interacting sector has been studied, we have coupled it to two other channels to identify promising final states as well as interesting production mechanisms. One of them is the coupling of the EWSBS with the two photon state; we have studied, in our ref. [36] and here in sec. 3.2.2, the scattering amplitudes

$$\gamma\gamma \to \omega\omega, \qquad\qquad \gamma\gamma \to hh. \tag{6.1}$$

The corresponding partial waves for $\omega\omega \to \gamma\gamma$ scattering can be found on sec. 3.3.2, and we have developed a new *perturbative* (in electromagnetic α) unitarization procedure on sec. 4.4. Basically, such a procedure supposes that the WBGBs follow a strongly coupled dynamics and the photons are weakly coupled to the WBGB sector. As an additional product we are preparing a study of the processes

$$\gamma\gamma \to \{W^+W^-,\, ZZ,\, hh\} \tag{6.2}$$

as an optimal tool to discern possible new physics related to the EWSB in future collider data. The hh in the final state is necessary for unitarization, since it could enter the other channels via rescattering processes like $\gamma\gamma \to hh \to W^+W^-$. Both in CMS and ATLAS there are Forward Detector Facilities for detecting events with $\gamma\gamma$ as initial state at the TeV range: AFP in ATLAS [105] and TOTEM in CMS [106, 107]. Even without such forward detectors, there is a study from CMS (ref. [108]) reporting a search for (deep inelastic) $\gamma\gamma \to \omega\omega$ scattering processes. Although only 2 events are found, since they consider the $\sqrt{s} = 7\,\text{TeV}$ series of data (with an integrated luminosity of $5.05\,\text{fb}^{-1}$), this study shows that there is interest in $\gamma\gamma$ scattering at the LHC.

Moreover, independently of the data coming from the $\gamma\gamma$ scattering at the LHC, the matrix elements of the scattering processes of eq. 6.2 are interesting because they can be inverted, by applying T-invariance, in order to recover a two photon state as a final one coming from a strongly interacting EWSBS.

Thus, we have presented a full one-loop computation of the related amplitudes, by means of the Equivalence Theorem, for the scattering processes $\gamma\gamma \to w^+w^-$ and $\gamma\gamma \to zz$, which should provide a good description of the physical processes of interest if the EWSBS is strongly interacting, in the kinematic regime $m_{W,Z,h} \ll E \ll 4\pi v$.

The computation has been performed up to NLO, which in this chiral Lagrangian context means taking into account all contributing one-loop diagrams generated from $\mathcal{L}_2$ in addition to the tree level contributions from both $\mathcal{L}_2$ and $\mathcal{L}_4$. That means that we have computed for the first time the quantum effects introduced by the light Higgs-like scalar and the would-be-Goldstone bosons $w^\pm$ and z altogether as dynamical fields in the loops of these radiative processes. As part of this computation we have also set clearly here the proper 'chiral counting rules' that are needed to reach a complete NLO result in the massless limit[4] and we have also illustrated the details of the renormalization procedure involved.

For a further check (this, highly non trivial) of our computation we have done the same exercise with two different parametrizations of the $SU(2)_L \times SU(2)_R/SU(2)_{L+R}$ coset, the exponential and the spherical ones[5], and we have found the same results, as expected.

Our final matrix elements for the $\gamma\gamma$ scattering, summarized in sec. 3.2.2, are surprisingly very short and extremely simple. The case $\gamma\gamma \to zz$ depends just on a and c_γ, and these ECLh parameters appear in the simple form given in eq. 3.55. The case $\gamma\gamma \to w^+w^-$ depends on a, c_γ, a_1, a_2 and a_3, and they also enter in a very simple way given in eq. 3.57. In our opinion, one of the most relevant features in these simple results, is the fact that these two amplitudes are found to be given by ECLh parameters or combinations of them that are renormalization-group invariant. This is very interesting and a consequence of our findings in the computation of all the one-loop diagrams from the ECLh that when added together yield a total contribution that is ultraviolet finite, in both $\gamma\gamma \to zz$ and $\gamma\gamma \to w^+w^-$ cases. Specifically, we have found our results are expressable in terms of a, c_γ and the combination $(a_1 - a_2 + a_3)$, none of which is renormalized, as it happens in the Higgsless ECL case.

Finally, our last study concerns the presence of $t\bar{t}$ in the final state[6]. The channels considered are

$$\{\omega\omega,\, hh,\, t\bar{t}\} \to t\bar{t}. \tag{6.3}$$

In secs. 3.2.3 and 3.2.4, we give the matrix elements. In appendix B, the spinor chain computations are given in detail. The partial waves are given in sec. 3.3.3 and the unitarization procedure, on sec. 4.4.

The unitarization is perturbative in $M_t/\sqrt{s}$. That is, we suppose that the WBGB dynamics is strongly interacting, while considering the couplings with the top quark as weak. Note that, in the end, the elastic $t\bar{t} \to t\bar{t}$ amplitude does not enter the unitarization procedure. As in the case of the $\gamma\gamma$ scattering, the study of the parameter space is work in progress.

[4] See sec. 2.2 and refs. [19, 30, 46].

[5] See sec. 2.2 for an definition of the different parameterizations.

[6] This work has been carried out in collaboration with our visitor from the Universidad Nacional de Colombia, Andrés Fernando Castillo.

To conclude, we believe that we have made a substantive contribution to the discussion of possible strongly-interacting extensions of the Standard Model, which are currently the most natural scenario with the particles W, Z and h in the Electroweak Symmetry Breaking sector. Thus we have extended previous works prepared long before the discovery of the 125 GeV Higgs like boson, that did not include it, as for example those in [12].

Furthermore, to consider as many experimental channels as possible, we are introducing couplings with $\gamma\gamma$ and $t\bar{t}$ states.

We hope that the results of table 6.2 will be useful for the developers of Monte Carlo simulation programs, since it is a comprehensive study of the validity of each unitarization procedure depending on the channel.

Of course, it can still be that the SM exhausts TeV-scale physics, in which case the parameters of the effective Lagrangian become $a = b = 1$ (all the NLO ones vanishing). Or it can also be that some of them only slightly deviate from the SM values; this could be suggestive of weakly coupled resonances, and the theory would be unitary far from saturation. But the strongly interacting regime remains the bulk of the parameter space to be explored by the LHC run-II.

Appendix A

Mandelstam variables

Take a $(p_1, p_2) \to (p_3, p_4)$ scattering processes, where $p_{1,2}$ and $p_{3,4}$ are, respectively, the 4–momentum of the incoming and outcoming particles. Because of 4–momentum conservation,

$$p_1 + p_2 = p_3 + p_4 \tag{A.1}$$

If the invariant mass of i particle is m_i, then

$$p_i^2 = (p_{i0}, p_{i1}, p_{i2}, p_{i3})^2 = p_{i0}^2 - p_{i1}^2 - p_{i2}^2 - p_{i3}^2 = m_i^2 \tag{A.2}$$

So, we have, for the four cases (E_i, $i = 1, 2, 3, 4$),

$$E_i^2 = p_i'^2 + m_i^2 \tag{A.3}$$

Without loss of generality, for a scattering process in the center of mass (CM) frame, we can take

$$p_1 = (E_1, 0, 0, p_1') \tag{A.4}$$
$$p_2 = (E_2, 0, 0, -p_1') \tag{A.5}$$
$$p_3 = (E_3, 0, p_3' \sin\theta, p_3' \cos\theta) \tag{A.6}$$
$$P_4 = (E_4, 0, -p_3' \sin\theta, -p_3' \cos\theta) \tag{A.7}$$

where θ is the angle between particles 1 and 3 in the CM. The Mandelstam variables[1] s, t and u are defined as

$$s = (p_1 + p_2)^2 = (p_3 + p_4)^2 \tag{A.8}$$
$$t = (p_1 - p_3)^2 = (p_2 - p_4)^2 \tag{A.9}$$
$$u = (p_1 - p_4)^2 = (p_2 - p_3)^2 \tag{A.10}$$

So, using momentum conservation (A.1) and rel. (A.2),

$$s + t + u = p_1^2 + p_2^2 + p_3^2 + p_4^2 = m_1^2 + m_2^2 + m_3^2 + m_4^2 \tag{A.11}$$

With eq. (A.3) and defs. (A.4) to (A.10),

$$p_{1,3}'^2 = \frac{\left(s - m_{1,3}^2 - m_{2,4}^2\right)^2 - 4m_{1,3}^2 m_{2,4}^2}{4s} \tag{A.12a}$$

$$\begin{aligned} t = (p_1 - p_3)^2 &= (E_1 - E_3)^2 - p_3'^2 - p_1'^2 + 2p_1'p_2' \cos\theta \\ &= m_1^2 + m_3^2 - 2\sqrt{m_1^2 + p_1'^2}\sqrt{m_3^2 + p_3'^2} + 2p_1'p_3' \cos\theta \end{aligned} \tag{A.12b}$$

$$u = m_1^2 + m_2^2 + m_3^2 + m_4^2 - s - t \tag{A.12c}$$

[1] See, for example, ref. [40].

Now, if we take the particular case $m_1 = m_2$ and $m_3 = m_4$ (both incoming and outgoing particle pairs have the same mass), these last expressions simplify to

$$p'^2_{1,3} = \frac{s}{4} - m^2_{1,3} \rightarrow p'_{1,3} = \frac{\sqrt{s}}{2}\sqrt{1 - \frac{4m^2_{1,3}}{s}} \tag{A.13}$$

$$t = m_1^2 + m_3^2 - \frac{s}{2}\left(1 - \sqrt{1 - \frac{4m_1^2}{s}}\sqrt{1 - \frac{4m_3^2}{s}}\cos\theta\right) \tag{A.14}$$

The scattering angle θ can be expressed as

$$\cos\theta = \frac{1}{\sqrt{1 - \frac{4m_1^2}{s}}\sqrt{1 - \frac{4m_3^2}{s}}}\left(1 + \frac{2(t - m_1^2 - m_2^2)}{s}\right) \tag{A.15}$$

Finally, if all the masses are zero,

$$t = -\frac{s}{2}(1 - \cos\theta) \tag{A.16}$$

$$u = -\frac{s}{2}(1 + \cos\theta) \tag{A.17}$$

$$\cos\theta = 1 + \frac{2t}{s} \tag{A.18}$$

Appendix B

Spinor computation

B.1 $t\bar{t}$ in the final state

The goal of this appendix is to prove eqs. 3.104,

$$\bar{u}^{+}(p_1)\, v^{+}(p_2) = +\sqrt{s - 4M_t^2} = +\sqrt{s} + \mathcal{O}\left(\frac{M_t^2}{s}\right). \tag{B.1a}$$

$$\bar{u}^{+}(p_1)\, v^{-}(p_1) = 0. \tag{B.1b}$$

$$\bar{u}^{-}(p_1)\, v^{+}(p_2) = 0. \tag{B.1c}$$

$$\bar{u}^{-}(p_1)\, v^{-}(p_2) = -\sqrt{s - 4M_t^2} = -\sqrt{s} + \mathcal{O}\left(\frac{M_t^2}{s}\right), \tag{B.1d}$$

where u and v are the spinors associated with the $t\bar{t}$ final state in $\omega\omega \to t\bar{t}$ and $hh \to t\bar{t}$ processes. These spinors are defined as[1]

$$u(p_1, \xi, \lambda_1) = \begin{pmatrix} \sqrt{(p_1 \cdot \sigma)}\xi \\ \sqrt{(p_1 \cdot \bar{\sigma})}\xi \end{pmatrix}, \qquad v(p_2, \eta, \lambda_2) = \begin{pmatrix} \sqrt{(p_2 \cdot \sigma)}\eta \\ -\sqrt{(p_2 \cdot \bar{\sigma})}\eta, \end{pmatrix} \tag{B.2a}$$

where u and v are, respectively, a particle (the top quark, t) and antiparticle (the anti-top quark, $\bar{t}$); p, the 4-momentum of the final state particles referred to the center of mass frame; and ξ, η, the corresponding 2-component spinors. These spinors are normalized (see refs. [40–42]) by

$$\xi^{\dagger}\xi = \eta^{\dagger}\eta = 1. \tag{B.3}$$

Note that the square roots of eqs. B.2 are defined for complex 2×2 matrices. The square root of a matricial operator, in its diagonal form, is defined as the diagonal matrix of the square root of its eigenvalues. Note that the positive determination is used here (at the end, the eigenvalues will be real and positive). If the operator is not in a diagonal form, then it will be rotated in order to compute the square root matrix. Note that, in general, this definition of a square root does not verify the property $\sqrt{AB} = \sqrt{A}\sqrt{B}$, only applicable when A and B have a common eigenbasis.

[1] See, for instance, refs. [40–42].

Now, let us use the Weyl basis (see refs. [40–42]), where

$$\gamma^0 = \begin{pmatrix} 0 & \mathbb{1}_{2\times 2} \\ \mathbb{1}_{2\times 2} & 0 \end{pmatrix} \tag{B.4a}$$

$$\sigma \equiv (\mathbb{1}_{2\times 2}, \hat{\sigma}) \tag{B.4b}$$

$$\bar{\sigma} \equiv (\mathbb{1}_{2\times 2}, -\hat{\sigma}) \tag{B.4c}$$

$$\hat{\sigma} \equiv (\sigma_1, \sigma_2, \sigma_3), \tag{B.4d}$$

σ_i $(i = 1, 2, 3)$ being the Pauli matrices. Furthermore, since we are in the center of mass frame,

$$p_1 = (E, \vec{p}), \quad p_2 = (E, -\vec{p}) \tag{B.5a}$$

$$\vec{p} = p(\sin\theta\cos\phi, \sin\theta\sin\phi, \cos\theta). \tag{B.5b}$$

We could have taken $\theta = \phi = 0$, without loss of generality. However, let us keep the complete computation, which will be illustrative for the more general case of sec. B.2. Note that, because of eq. B.4 and B.5,

$$(p_1 \cdot \sigma) = \begin{pmatrix} E - p\cos\theta & -pe^{-i\phi}\sin\theta \\ -pe^{i\phi}\sin\theta & E + p\cos\theta \end{pmatrix}, \quad (p_1 \cdot \bar{\sigma}) = \begin{pmatrix} E + p\cos\theta & -pe^{-i\phi}\sin\theta \\ -pe^{i\phi}\sin\theta & E - p\cos\theta \end{pmatrix}. \tag{B.6}$$

Note that both $(p_1 \cdot \sigma)$ and $(p_1 \cdot \bar{\sigma})$ are 2×2 hermitian matrices, so that they are diagonalizable by an orthonormal basis of eigenvectors with real eigenvalues. Indeed, the eigenvalues of $(p_1 \cdot \sigma)$ are $E - p$ and $E + p$, with the corresponding eigenvectors v_λ,

$$v_{E-p} = \begin{pmatrix} \cos\frac{\theta}{2} \\ e^{i\phi}\sin\frac{\theta}{2} \end{pmatrix}, \qquad v_{E+p} = \begin{pmatrix} e^{-i\phi}\sin\frac{\theta}{2} \\ -\cos\frac{\theta}{2} \end{pmatrix}. \tag{B.7}$$

For $(p_1 \cdot \bar{\sigma})$, the eigenvalues and eigenvectors (v'_λ) are obtained by swapping $p \to -p$ on those for $(p_1 \cdot \sigma)$,

$$v'_{E+p} = v_{E-p} = \begin{pmatrix} \cos\frac{\theta}{2} \\ e^{i\phi}\sin\frac{\theta}{2} \end{pmatrix}, \qquad v'_{E-p} = v_{E+p} = \begin{pmatrix} e^{-i\phi}\sin\frac{\theta}{2} \\ -\cos\frac{\theta}{2} \end{pmatrix}. \tag{B.8}$$

And, finally, the definition of $\bar{k}$ is $\bar{k} \equiv k^\dagger\gamma^0$ for any 4-vector k, where the matrix γ^0 is defined in eq. B.4a. Hence, the expression we are trying to compute, $\bar{u}_1^\lambda v_2^\lambda$ (eq. B.1), turns into

$$\bar{u}_1^\lambda v_2^\lambda \equiv (u^{\lambda_1})^\dagger\gamma^0 v^{\lambda_2} = \left(\xi^\dagger\sqrt{(p_1\cdot\sigma)}^\dagger, \xi^\dagger\sqrt{(p_1\cdot\bar{\sigma})}^\dagger\right)\cdot\gamma^0\cdot\begin{pmatrix} \sqrt{(p_2\cdot\sigma)}\eta \\ -\sqrt{(p_2\cdot\bar{\sigma})}\eta, \end{pmatrix} \tag{B.9}$$

Now, taking into account the definitions of eqs. B.4 and B.5, eq. B.9 becomes

$$\bar{u}_1^\lambda v_2^\lambda = \xi^\dagger\left[-\sqrt{(p_1\cdot\sigma)}^\dagger\sqrt{(p_1\cdot\sigma)} + \sqrt{(p_1\cdot\bar{\sigma})}^\dagger\sqrt{(p_1\cdot\bar{\sigma})}\right]\eta. \tag{B.10}$$

Now, consider that both $(p_1\cdot\sigma)$ and $(p_1\cdot\bar{\sigma})$ are hermitian matrices with positive eigenvalues ($\sqrt{E-p}$ and $\sqrt{E+p}$). Then, the matricial square roots will also be hermitian, so that eq. B.10 reduces to

$$\bar{u}^{\lambda_1}v^{\lambda_2} = \xi^\dagger[-(p_1\cdot\sigma) + (p_1\cdot\bar{\sigma})]\eta = 2p[\xi^\dagger(\hat{p}\cdot\hat{\sigma})\eta], \tag{B.11}$$

where $\vec{p} \equiv p\hat{p}$ is a 3-vector. Now, because the helicity operator Σ for a particle with 3-momenta $\vec{p}$ is

$$\hat{h} = \hat{p} \cdot \hat{\sigma}. \tag{B.12}$$

Let us introduce the notation η^{λ_i} and ξ^{λ_i} for the spinors ($i = 1, 2$), where the $\lambda_i = \pm$ superindex stands for the helicity state $h = \pm 1$ of the particle i. Because changing particle by anti-particle changes the helicity sign, as does changing $\vec{p}$ by $-\vec{p}$, eq. B.11 turns into

$$\bar{u}^{\lambda_1} v^{\lambda_2} = 2ph^{\lambda_2} (\xi^{\lambda_1})^\dagger \xi^{\lambda_2}. \tag{B.13}$$

Finally, according to the orthonormality of helicity states (eq. B.3 and $\eta^\pm \cdot \eta^\mp = \xi^\pm \cdot \xi^\mp = 0$), and to the definition of s Mandelstam variable (eq. A.8), we recover eqs. 3.104 (quoted in eqs. B.1),

$$\bar{u}^{\lambda_1} v^{\lambda_2} = 2ph^{\lambda_1} \delta_{\lambda_1,\lambda_2} = 2h^{\lambda_1} \sqrt{E^2 - M_t^2} \delta_{\lambda_1,\lambda_2} = h^{\lambda_1} \sqrt{s - 4M_t^2} \delta_{\lambda_1,\lambda_2}, \tag{B.14}$$

where $h^\pm = \pm 1$.

B.2 Analysis of the spinors of the $t\bar{t} \to t\bar{t}$ process

The goal of this appendix is the computation of the spinor chains which appear on the $t\bar{t} \to t\bar{t}$ scattering amplitude in eq. 3.118. First of us, let us define the notation

$$[t(p_1, u_1, \xi_1, \lambda_1), \bar{t}(p_2, v_2, \eta_2, \lambda_2)] \to [t(p_3, u_3, \xi_3, \lambda_3), \bar{t}(p_4, v_4, \eta_4, \lambda_4)]. \tag{B.15}$$

Here, p_i ($i = 1, 2, 3, 4$) stands for the 4-momentum of the initial and final state particles; u_i ($i = 1, 3$) and v_i ($i = 2, 4$), for the spinors of the top quarks and antiquarks, respectively; ξ_i ($i = 1, 3$) and η_i ($i = 2, 4$), for the polarization vectors of the quarks and antiquarks; and λ_i ($i = 1, 2, 3, 4$), for the helicities of the particles.

Now, in the center of mass frame, and taking into account that all the particles and antiparticles have the same mass (the top quark one, M_t) and the 4-momenta conservation ($p_1 + p_2 = p_3 + p_4$), the 4-momenta may be chosen as

$$p_1 = (E, 0, 0, p) \qquad p_2 = (E, 0, 0, -p) \tag{B.16a}$$

$$p_3 = (E, \vec{p}) \qquad p_4 = (E, -\vec{p}), \tag{B.16b}$$

where $\vec{p}$ is defined in spherical coordinates,

$$\vec{p} = p(\sin\theta\cos\phi, \sin\theta\sin\phi, \cos\theta). \tag{B.16c}$$

As in the case of the previous appendix B.1, we will work in the Weyl basis. See refs. [40–42] for an introduction to Dirac spinors in such a basis. The spinors are defined as

$$u(p_i, \xi, \lambda) = \begin{pmatrix} \sqrt{(p_i \cdot \sigma)}\xi \\ \sqrt{(p_i \cdot \bar{\sigma})}\xi \end{pmatrix}, \quad v(p_i, \eta, \lambda) = \begin{pmatrix} \sqrt{(p_i \cdot \sigma)}\eta \\ -\sqrt{(p_i \cdot \bar{\sigma})}\eta, \end{pmatrix} \tag{B.17a}$$

$$\gamma^0 = \begin{pmatrix} 0 & \mathbb{1}_{2\times2} \\ \mathbb{1}_{2\times2} & 0 \end{pmatrix}, \qquad \gamma^5 = \begin{pmatrix} -\mathbb{1}_{2\times2} & 0 \\ 0 & \mathbb{1}_{2\times2} \end{pmatrix} \tag{B.17b}$$

$$u_i^{\lambda_i} = \begin{pmatrix} \sqrt{p_i \cdot \sigma}\xi^{\lambda_i} \\ \sqrt{p_i \cdot \bar{\sigma}}\xi^{\lambda_i} \end{pmatrix}, \qquad v_j^{\lambda_j} = \begin{pmatrix} \sqrt{p_j \cdot \sigma}\eta^{\lambda_j} \\ -\sqrt{p_j \cdot \bar{\sigma}}\eta^{\lambda_j} \end{pmatrix}, \quad i = 1, 3,\ j = 2, 4 \tag{B.17c}$$

$$\sigma = (\mathbb{1}_{2\times2}, \hat{\sigma}), \qquad \bar{\sigma} = (\mathbb{1}_{2\times2}, -\hat{\sigma}), \qquad \hat{\sigma} = (\sigma_1, \sigma_2, \sigma_3), \tag{B.17d}$$

and $\bar{k} \equiv k^\dagger \gamma^0$ for any 4-vector k. Note that σ_i $(i = 1, 2, 3)$ are the Pauli matrices[2], and that we are making the same definitions in eqs. B.17d that in eqs. B.4 in the previous appendix B.1.

Now, eq. B.12 defines the helicity operator for particles,

$$\hat{h_i} = \hat{p_i} \cdot \hat{\sigma} = \begin{pmatrix} \cos\theta_i & e^{-i\phi_i}\sin\theta_i \\ e^{i\phi_i}\sin\theta_i & -\cos\theta_i \end{pmatrix}, \quad i = 1, 3 \tag{B.18}$$

where $\vec{p} = p\hat{p}$. Note that, by definition (eqs. B.16), $\theta_1 = \phi_1 = 0$ for the p_1 initial state 4-momentum. For antiparticles, there is a change of sign,

$$\hat{h}'_i = -\hat{p_i} \cdot \hat{\sigma}, \quad i = 2, 4. \tag{B.19}$$

The polarization vectors will be the corresponding eigenvectors of operators B.18 and B.19, so that

$$\xi_i^+ = [\cos(\theta/2), e^{i\phi}\sin(\theta/2)] \qquad \xi_i^- = [e^{-i\phi}\sin(\theta/2), -\cos(\theta/2)] \tag{B.20a}$$

$$\eta_i^+ = [\sin(\theta/2), -e^{i\phi}\cos(\theta/2)] \qquad \eta_i^- = [e^{-i\phi}\cos(\theta/2), \sin(\theta/2)] \tag{B.20b}$$

These definitions verify the closure relations

$$(\xi_i^{\lambda_1})^\dagger \cdot \xi_i^{\lambda_2} = \delta_{\lambda_1,\lambda_2} \tag{B.21a}$$

$$(\eta_i^{\lambda_1})^\dagger \cdot \eta_i^{\lambda_2} = \delta_{\lambda_1,\lambda_2} \tag{B.21b}$$

$$(\xi_i^{\lambda_1})^\dagger \cdot \eta_i^{\lambda_1} = 0 \quad \forall\lambda_1 = \pm \tag{B.21c}$$

Indeed, $\eta_i^\pm = \xi_i^\pm|_{\vec{p}\to-\vec{p}}$. Note also that $\xi_i^\pm$ and $\eta_i^\pm$ are eigenvectors of the corresponding helicity operator, $\hat{h_i}\xi_i^\pm = (\pm 1)\xi_i^\pm$ $(i = 1, 3)$, $\hat{h}'_i\eta_i^\pm = (\pm 1)\eta_i^\pm$ $(i = 2, 4)$. Note that the correct 3-momentum $\vec{p}$ should enter the definitions of $\hat{h}$, $\hat{h}'$ (eqs. B.18 and B.19).

Now, consider that, according to eq. B.8 a generic $(p_i \cdot \sigma)$ operator will be hermitian and diagonalizable by

$$(p_i \cdot \sigma) = \begin{pmatrix} \cos\frac{\theta_i}{2} & e^{-i\phi_i}\sin\frac{\theta_i}{2} \\ e^{i\phi_i}\sin\frac{\theta_i}{2} & -\cos\frac{\theta_i}{2} \end{pmatrix} \cdot \begin{pmatrix} E_i - p_i & 0 \\ 0 & E_i + p_i \end{pmatrix} \cdot \begin{pmatrix} \cos\frac{\theta}{2} & e^{-i\phi_i}\sin\frac{\theta_i}{2} \\ e^{i\phi_i}\sin\frac{\theta_i}{2} & -\cos\frac{\theta_i}{2} \end{pmatrix}^\dagger . \tag{B.22}$$

The corresponding square root will be defined by

$$\sqrt{(p_i \cdot \sigma)} = \\ = \begin{pmatrix} \cos\frac{\theta}{2} & e^{-i\phi_i}\sin\frac{\theta_i}{2} \\ e^{i\phi_i}\sin\frac{\theta_i}{2} & -\cos\frac{\theta_i}{2} \end{pmatrix} \cdot \begin{pmatrix} \sqrt{E_i - p_i} & 0 \\ 0 & \sqrt{E_i + p_i} \end{pmatrix} \cdot \begin{pmatrix} \cos\frac{\theta}{2} & e^{-i\phi_i}\sin\frac{\theta_i}{2} \\ e^{i\phi_i}\sin\frac{\theta_i}{2} & -\cos\frac{\theta_i}{2} \end{pmatrix}^\dagger . \tag{B.23}$$

If, on the other hand, we considered $(p_i \cdot \bar{\sigma})$ and $\sqrt{(p_i \cdot \bar{\sigma})}$, then we would recover the diagonalization just by swapping $[(E_i - p_i) \leftrightarrow (E_i + p_i)]$ on the diagonal matrices of eqs. B.22 and B.23 (see the discussion after eq. B.7).

Note also that, if $i = 1$ in eqs. B.22 and B.23, that is, if we had $\theta_1 = 0$ and $\phi_1 = 0$, then the change of basis matrix which diagonalized $(p_1 \cdot \sigma)$ and $(p_1 \cdot \bar{\sigma})$ would be the identity. That is, $(p_1 \cdot \sigma)$ and $(p_1 \cdot \bar{\sigma})$ would be diagonal matrices. Furthermore, note

[2]Defined, for instance, in refs. [40–42].

that, because of the definitions of the 4-momenta (eqs. B.16) and the $(\sigma, \bar{\sigma})$ matrices (eqs. B.17), we have that

$$(p_i \cdot \sigma) = (p_{i+1} \cdot \bar{\sigma}), \qquad (p_i \cdot \bar{\sigma}) = (p_{i+1} \cdot \sigma), \qquad i = 1, 3 \tag{B.24}$$

Now, taking into account all the definitions introduced in this section until now, we can evaluate the fermion chains of eq. 3.118 for the $\mathcal{S}(t\bar{t} \to t\bar{t})$. This, indeed, is the goal of the present section.

To sum up, our definitions are: eqs. B.16, for the momenta; eqs. B.17, for the spinors and γ-matrices[3]; eq. B.20, for the helicity vectors, which correspond to the different polarizations; and eq. B.23 for the definition of the square roots of matrices which appear in eqs. B.17. The results can be found on table B.1

$\lambda\lambda'$	$++$	$+-$	$-+$	$--$
$\bar{u_1}^{\lambda}(p_1)v_2^{\lambda'}(p_2)$	$2p$	0	0	$-2p$
$\bar{u_3}^{\lambda}(p_3)v_4^{\lambda'}(p_4)$	$2p$	0	0	$-2p$
$\bar{v_2}^{\lambda}(p_2)u_1^{\lambda'}(p_1)$	$2p$	0	0	$-2p$
$\bar{u_3}^{\lambda}(p_3)u_1^{\lambda'}(p_1)$	$2m\cos\frac{\theta}{2}$	$2e^{-i\phi}E\sin\frac{\theta}{2}$	$-2e^{i\phi}E\sin\frac{\theta}{2}$	$2m\cos\frac{\theta}{2}$
$\bar{v_2}^{\lambda}(p_2)v_4^{\lambda'}(p_4)$	$-2m\cos\frac{\theta}{2}$	$2e^{-i\phi}E\sin\frac{\theta}{2}$	$-2e^{i\phi}E\sin\frac{\theta}{2}$	$-2m\cos\frac{\theta}{2}$
$\bar{u_3}^{\lambda}(p_3)\gamma^5 v_4^{\lambda'}(p_4)$	$-2E$	0	0	$-2E$
$\bar{v_2}^{\lambda}(p_2)\gamma^5 u_1^{\lambda'}(p_1)$	$2E$	0	0	$2E$
$\bar{u_3}^{\lambda}(p_3)\gamma^5 u_1^{\lambda'}(p_1)$	0	$-2e^{-i\phi}p\sin\frac{\theta}{2}$	$-2e^{i\phi}p\sin\frac{\theta}{2}$	0
$\bar{v_2}^{\lambda}(p_2)\gamma^5 v_4^{\lambda'}(p_4)$	0	$2e^{-i\phi}p\sin\frac{\theta}{2}$	$2e^{i\phi}p\sin\frac{\theta}{2}$	0

Table B.1: Fermion bilinears which appear in eq. 3.118, and whose computation is the goal of this appendix B.2. Note that, as expected in the previous appendix B.1, $\bar{u_1}^{\lambda}(p_1)v_2^{\lambda'}(p_2) = \bar{u_3}^{\lambda}(p_3)v_4^{\lambda'}(p_4) = 2ph^{\lambda}\delta_{\lambda,\lambda'}$.

[3]Remember that $\bar{k} \equiv k^{\dagger}\gamma^0$ for any 4-vector k.

Appendix C

Dimensional regularization and Passarino-Veltman functions

For computing the amplitudes at NLO, the set of programs FeynRules [142], FeynArts [143] and FormCalc [144, 145] has been used. These programs take as input a Lagrangian and a wanted scattering process, and give as output its matrix element. FeynRules could also give a so-called UFO file [181], which is useful to use as input for Monte Carlo (MC) simulation programs.

The multi-loop computation requires to integrate over all the possible 4-momenta (including off-shellness) of the particles inside the loop. For 1-loop computation, there is only one 4-momentum which has to be integrated. This integration can lead both to ultraviolet (UV, limit $k \to \infty$) and infrared (IR, limit $k \to 0$) singularities.

To deal with the UV divergences, FormCalc uses the *dimensional regularization* and expresses the total amplitudes in terms of the so–called *Passarino-Veltman functions*. FormCalc defines them in the following way:

$$A_0^{(r)}(m) = \frac{\mu^{4-D}}{i\pi^2} \int \frac{d^D\, k}{(2\pi)^{D-4}} \frac{1}{(k^2 - m^2 + i\varepsilon)^r},\ r \geq 1 \tag{C.1a}$$

$$B_0(p^2; m_1, m_2) = \frac{(2\pi\mu)^{4-D}}{i\pi^2} \int \frac{d^D\, k}{[k^2 - m_1^2][(k+p)^2 - m_2^2]} \tag{C.1b}$$

$$C_0(p_1^2, p_2^2, p_3^2; m_1, m_2, m_3) = \\ = \frac{1}{i\pi^2} \int \frac{d^4\, k}{[k^2 - m_1^2][(k+p_1)^2 - m_2^2][(k+p_1+p_2)^2 - m_3^2]} \tag{C.1c}$$

$$D_0[p_1^2, p_2^2, p_3^2, p_4^2; (p_2+p_3)^2, (p_1+p_2)^2; m_1, m_2, m_3, m_4] = \\ = \frac{1}{i\pi^2} \int \frac{d^4\, k}{[k^2 - m_1^2][(k+p_1)^2 - m_2^2][(k+p_1+p_2)^2 - m_3^2][(k+p_1+p_2+p_3)^2 - m_4^2]} \tag{C.1d}$$

Usually, refs. [182, 183] are credited in this context, since Passarino and Veltman introduced this notation. However, Veltman used a slightly different convention in several places, like in the definition of the 4-momenta. This introduces multiplicative constants in the defition of the Passarino-Veltman functions. There is even a notation change between refs. [182] and [183]. So, the notation actually used by FormCalc is that given by ref. [184], which refers to [185] for the details of the dimensional regularization.

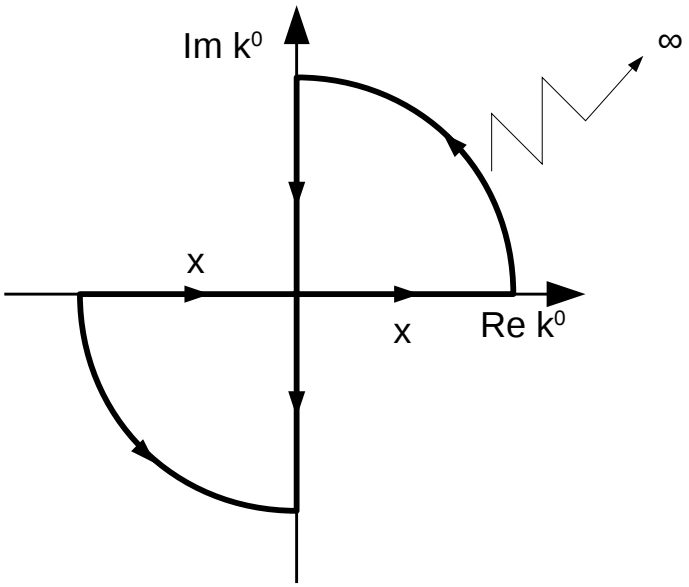

Figure C.1: Position of the poles appearing in the integrand of Passarino-Veltman functions, and integration contour choosen to perform the Wick rotation.

The basic idea is to substitute the 4-dimensional integration by an integration over $D = 4 - 2\epsilon$ dimensions. The UV divergences will appear as poles on $\epsilon \to 0$, but we will be able to reabsorb them in the counter-terms. By definition of dimensional regularization [185], integrals that do not depend on any scale will vanish,

$$\int d^D\, k \cdot (k^2)^\alpha = 0. \tag{C.2}$$

In contrast, this integral does not exist in the Riemann sense, diverging with the volume $\forall D \in \mathbb{Z}$, $\alpha \in \mathbb{R}$. The integrations rely on a so–called *Wick rotation*, which transforms the integral over Minkowski space to another one over Euclidean space. The trick is making an analytical extension to the complex plane of the *temporal component*, $k^0 = ik^0_E$, and maintaining the *spatial componentes*, $\vec{k} = \vec{k}_E$.

So, we are dealing with a real $D-1$ dimensional vector $\vec{k}$ in *space coordinates*, and a *complex* 1-dimensional vector k^0 in time. The Minkowski metric works as expected, $k^2 = (k^0)^2 - \|\vec{k}\|^2$, whose equivalent is $k^2_E = (k^0_E)^2 + \|k\|^2$ in Euler space. As shown in fig. C.1, because of Cauchy's Theorem, the Wick rotation requires that no pole is present inside the integration region shown in fig. C.1, and that the contribution of the arcs vanishes in the limit $|k^0| \to \infty$.

Let us first think about the poles. All interactions in EFT are polynomial at tree level, so the poles can only be due to the denominators of propagating particles. If we take the Feynman prescription for these denominators

$$D_n = \left(k + \sum_{i=1}^{n-1} p_i\right)^2 - m_n^2 + i\varepsilon,\ \varepsilon \to 0^+ \tag{C.3}$$

with k, p_i being 4-momenta, then,

$$\mathrm{Re}\, D_n = \left(\mathrm{Re}\, k^0 + \sum_{i=1}^{n-1} p_i^0\right)^2 - \left(\mathrm{Im}\, k^0\right)^2 - \left(\vec{k} + \sum_{i=1}^{n-1} \vec{p_i}\right)^2 - m_n^2 \tag{C.4}$$

$$\mathrm{Im}\, D_n = 2\,\mathrm{Im}\, k^0 \left(\mathrm{Re}\, k^0 + \sum_{i=1}^{n-1} p_i^0\right) + \varepsilon,\ \varepsilon \to 0^+. \tag{C.5}$$

The zero condition for D_n, which will lead to a pole on the Passarino-Veltman integrand coming from $(1/D_n)$, is $\mathrm{Re}\, D_n = \mathrm{Im}\, D_n = 0$. Because they correspond to external (physical, not virtual) particles, they must by on the mass shell, $p_i^0 \geq 0\,\forall i$, so that $\mathrm{Im}\, k^0 \cdot \mathrm{Re}\, k^0 \leq 0$. $\mathrm{Re}\, D_n = 0$ means that

$$\left(\mathrm{Re}\, k^0 + \sum_{i=1}^{n-1} p_i^0\right)^2 = \left(\mathrm{Im}\, k^0\right)^2 + \left(\vec{k} + \sum_{i=1}^{n-1} \vec{p_i}\right)^2 + m_n^2, \tag{C.6}$$

and there will be *two* solutions, one with $\mathrm{Re}\, k^0 > 0$ and another one with $\mathrm{Re}\, k^0 < 0$. So, if simultaneously $\mathrm{Im}\, D_n = 0$, we extract the value of $\mathrm{Im}\, k^0$ which, as just shown, will have opposite sign to $\mathrm{Re}\, k^0$, thus recovering a couple of zeroes (poles of the integrand) marked in fig. C.1. They always appear in pairs, in the second and fourth quadrant.

The second condition is that the contribution of the arcs shown in fig. C.1 vanishes in the limit $|k^0| \to \infty$. Because of the fact that we keep the spatial component $\vec{k}$ finite, the divergence would come from the limit

$$\lim_{|k^0|\to\infty} \int_\gamma d\, k^0 \frac{1}{(k^0)^{2n}}, \tag{C.7}$$

where n is the number of denominators D_n. But this does vanish for $n \geq 1$. Take $z = k^0 e^{i\theta}$, with $\theta \in [0, \pi/2]$,

$$\int_\gamma d\, z \cdot \frac{1}{z^2} = \int_0^{\pi/2} d(k^0 e^{i\theta}) \frac{1}{(k^0 e^{i\theta})^{2n}} = \int_0^{\pi/2} d\theta\, \frac{i e^{i(1-2n)\theta}}{(k^0)^{2n-1}} \xrightarrow[n\geq 1]{k^0\to\infty} 0. \tag{C.8}$$

Thus, we have proven the two conditions which are necessary for the Wick rotation. Namely, absence of pole contributions in the domain through which the axes are rotated, and convergence to zero of the arch integrals. Now, once in Euclidean space, and using the spherical symmetry of the problem, the integration can be decomposed as

$$\int d^D k_E f(\|k_E\|^2) = \int d\, k_E \cdot k_E^{D-1} \int d\,\Omega_D f(k_E^2) = \int d\,\Omega_D \int d(k_E^2) \cdot \frac{1}{2} (k_E^2)^{(D-4)/2} f(k_E^2), \tag{C.9}$$

where we have used the integral over the surface of the full D-dimensional sphere,

$$\int d\,\Omega_D = \frac{2\pi^{D/2}}{\Gamma(D/2)}, \tag{C.10}$$

whose proof can be found in appendix D.1. $\Gamma(x)$ is the Euler's Gamma function, whose properties can be found, for instance, on Ref. [186].

Furthermore, to maintain consistency while changing the dimension of the integral over the 4-momentum, the integral in eq. C.9 will be multiplied by a constant μ^{4-D},

where μ has dimensions of momentum k. The divergent Passarino-Veltman functions A_0 and B_0 (eqs. C.1a and C.1b) already include this constant. Anyway, this will lead to the appearance of an energy scale μ on the final result.

Once all the substitutions completed with the help of the efficient symbolic computations software FORM [183], FormCalc express all the matrix elements as function of the *scalar Passarino-Veltman functions* defined in the four eqs. C.1. Note that, although C_0 and D_0 in eqs. C.1c and C.1d have very tricky analytical expressions, they are finite. So, no regularization is needed for them. Because $A_0^{(1)}(m)$ and $B_0(p,0,0)$ functions in eqs. C.1a and C.1b are the ones appearing in our computations, we will show here how to compute them. Let us start with $A_0^{(1)}(m)$. By definition,

$$A_0^{(1)}(m) = \frac{\mu^{4-D}}{i\pi^2}\int \frac{d^D\,k}{(2\pi)^{D-4}}\frac{1}{k^2-m^2+i\varepsilon}. \tag{C.11}$$

Doing the Wick rotation, we substitute $k^0 \to ik_E^0$, $\vec{k} \to \vec{k}_E$. So,

$$k^2 = (k^0)^2 - \|\vec{k}\|^2 = -(k_E^0)^2 - \|\vec{k}_E\|^2 = -k_E^2, \tag{C.12}$$

and

$$d^D\,k = dk^0 \cdot d^{D-1}\vec{k} = i\,dk_E^0 \cdot d^{D-1}\vec{k}_E. \tag{C.13}$$

Thus, taking also into account that $\varepsilon \to 0^+$, Eq. C.11 transforms to

$$A_0^{(1)}(m) = \frac{\mu^{4-D}}{i\pi^2}\int \frac{i\,d^D\,k_E}{(2\pi)^{D-4}}\frac{1}{-k_E^2-m^2} = -\frac{\mu^{4-D}}{(2\pi)^{D-4}\pi^2}\frac{2\pi^{D/2}}{\Gamma(D/2)}\int_0^\infty d\,k_E\frac{k_E^{D-1}}{k_E^2+m^2} \tag{C.14}$$

Making the change of variables $k_e = mx$, $dk_e = m\,dx$,

$$\begin{aligned} A_0^{(1)}(m) &= -\frac{(2\pi\mu)^{4-D}}{\Gamma(D/2)}2\pi^{(D-4)/2}\frac{m\cdot m^{D-1}}{m^2}\int_0^\infty dx\frac{x^{D-1}}{x^2+1} \\ &= -2\pi^{(D-4)/2}m^{D-2}\frac{(2\pi\mu)^{4-D}}{\Gamma(D/2)}\int_0^\infty dx\frac{x^{D-1}}{x^2+1} \end{aligned} \tag{C.15}$$

Now, provided that $D \in (0,2)$,

$$\int_0^\infty dx\frac{x^{D-1}}{x^2+1} = \frac{\pi}{2}\csc\frac{D\pi}{2} = \frac{1}{2}\Gamma\left(1-\frac{D}{2}\right)\Gamma\left(\frac{D}{2}\right), \tag{C.16}$$

thus we find the result

$$A_0^{(1)}(m) = -m^2\left(\frac{m^2}{4\pi\mu}\right)^{(D-4)/2}\Gamma\left(1-\frac{D}{2}\right). \tag{C.17}$$

Now, let us substitute $D = 4-2\epsilon$. Take into account that the integral is convergent for $D \in (0,2)$, which means $\epsilon \in (1,2)$.

$$A_0^{(1)}(m) = -m^2\left(\frac{4\pi\mu^2}{m^2}\right)^{\epsilon}\Gamma(\epsilon-1) \tag{C.18}$$

It can be seen that this is not well defined for $\epsilon < 1$. However, let us see what happens when we force a Laurent expansion near $\epsilon = 0$,

$$\Gamma(\epsilon-1) = -\frac{1}{\epsilon} - 1 + \gamma + \mathcal{O}(\epsilon) \tag{C.19}$$

$$A^\epsilon = e^{\epsilon\log A} = 1 + \epsilon\log A + \mathcal{O}(\epsilon^2), \tag{C.20}$$

where $1/\epsilon$ stands for the divergent behaviour near $D = 4$ and $\gamma \approx 0.5772\ldots$ is the so–called Euler's constant. So,

$$A_0^{(1)}(m) = m^2\left(\frac{1}{\epsilon} + 1 - \gamma + \log\frac{4\pi\mu^2}{m^2}\right) = m^2\left(\Delta - \log\frac{m^2}{\mu^2} + 1\right), \tag{C.21}$$

where $\Delta = (1/\epsilon) - \gamma + \log 4\pi$ is the Δ variable used by FormCalc [144].

For the function $B_0(p^2; 0, 0)$, which appears in the NLO computation, we take the definition C.1b (particularized to $m_1 = m_2 = 0$),

$$B_0(p^2; 0, 0) = \frac{(2\pi\mu)^{4-D}}{i\pi^2}\int \frac{d^D\, k}{[k^2 + i\varepsilon][(k+p)^2 + i\varepsilon]}. \tag{C.22}$$

In order to apply eq. C.9, we need an integrand which only depends on k_E^2 after the Wick rotation. Note that, in the end, the only operation that we have defined over D-dimensional vectors (with D non-integer, $D \in \mathbb{R} \setminus \mathbb{Z}$) is the integration over the surface of the D-dimensional sphere (appendix D.1). Here, we do not have a definition of D-dimensional vectors which allows us to explicitly sum them. Thus, we cannot sum $k + p$ and integrate over k on $D \in \mathbb{R} \setminus \mathbb{Z}$ dimensions. Even worse, whatever *D-dimensional* means, p is a 4-dimensional vector whose components are fixed by external kinematics. To deal with this problem let us assume that, although we are not able to explicitly define such an operation as $k+p$, it is well defined and verify the corresponding algebraic properties. We introduce the *Feynman parametrization* [184], which for the product $1/(D_1 D_2)$ is

$$\frac{1}{D_1 D_2} = \int_0^1 \frac{dx}{[(1-x)D_1 + xD_2]^2}. \tag{C.23}$$

Hence, $B_0(p^2; 0, 0)$ defined in eq. C.22 is turned into

$$\begin{aligned} B_0(p^2; 0, 0) = \frac{(2\pi\mu)^{4-D}}{i\pi^2}\int_0^1 dx \int \frac{d^D k}{[(1-x)k^2 + (k+p)^2 x + i\varepsilon]^2} = \\ = \frac{(2\pi\mu)^{4-D}}{i\pi^2}\int_0^1 dx \int \frac{d^D k}{[k^2 + 2x(kp) + x(p)^2 + i\varepsilon]^2} \end{aligned} \tag{C.24}$$

Now, let us perform the change of variables $k \to k - xp$, so that

$$k^2 + 2x(kp) + x(p)^2 \xrightarrow{k\to k-xp} (k-xp)^2 + 2xp(k-xp) + p^2 x = k^2 + x(1-x)p^2 \tag{C.25}$$

When substituting in eq. C.24,

$$B_0(p^2; 0, 0) = \frac{(2\pi\mu)^{4-D}}{i\pi^2}\int_0^1 dx \int \frac{d^D k}{[k^2 + x(1-x)p^2 + i\varepsilon]^2}, \tag{C.26}$$

where linear combinations of D-dimensional vectors (like $k+p$ in eq. C.22) do not appear. Next, perform the Wick rotation and change to generalized spherical coordinates in D-dimensions,

$$B_0(p^2; 0, 0) = \frac{(2\pi\mu)^{4-D}}{\pi^2}\frac{2\pi^{D/2}}{\Gamma(D/2)}\int_0^1 dx \int \frac{dk_e \cdot k_e^{D-1}}{[-k^2 + x(1-x)p^2 + i\varepsilon]^2}. \tag{C.27}$$

Let us sustitute $D = 4-2\epsilon$, and note that we are keeping $\epsilon \neq \varepsilon$. Now, provided $0 < D < 4$ and $\varepsilon > 0$ being small enough ($\varepsilon < x(1-x)p^2$),

$$B_0(p^2;0,0) = (4\pi\mu^2)^\epsilon \Gamma(\epsilon) \int_0^1 dx \, [-x(1-x)p^2 - i\varepsilon]^{-\epsilon}, \tag{C.28}$$

where the integrand is extended to the complex plane by

$$[-x(1-x)p^2 - i\varepsilon]^{-\epsilon} = \exp\left[-\epsilon \log\left(-x(1-x)p^2 - i\varepsilon\right)\right]. \tag{C.29}$$

This is defined because the logarithm is a complex function with a cut on the left axis. For the sake of simplicity, since $0 \leq x(1-x) \leq 1 \, \forall x \in [0,1]$, we redefine ε so that

$$-x(1-x)p^2 - i\varepsilon \to x(1-x)(-p^2 - i\varepsilon) \tag{C.30}$$

without changing the Riemann sheet where $F(x) = x^{-\epsilon} = e^{-\epsilon \log x}$ is evaluated. Thus, eq. C.28 turns into

$$\begin{aligned} B_0(p^2;0,0) = (4\pi\mu^2)^\epsilon (-p^2 - i\varepsilon)^{-\epsilon} \Gamma(\epsilon) \int_0^1 dx \, [x(1-x)]^{-\epsilon} \\ = \left(\frac{-p^2 - i\varepsilon}{4\pi\mu^2}\right)^{-\epsilon} \frac{\Gamma(\epsilon) \cdot [\Gamma(1-\epsilon)]^2}{\Gamma(2-2\epsilon)} \end{aligned} \tag{C.31}$$

And carrying out a power expansion around $\epsilon = 0$,

$$B_0(p^2;0,0) = \Delta + 2 - \log \frac{-p^2 - i\varepsilon}{\mu^2} + \mathcal{O}(\epsilon), \tag{C.32}$$

with Δ being $(1/\varepsilon) - \gamma + \log 4\pi$, as it was the case of A_0.

Appendix D

Several proofs and explanations

D.1 Integral over the surface of a D-dimensional sphere

The integral over the surface of the D-dimensional sphere is

$$\int d\,\Omega_D = \frac{2\pi^{D/2}}{\Gamma(D/2)}, \tag{D.1}$$

where $\Gamma(x)$ is the Euler Gamma function, whose properties can be found in ref. [186]. Eq. D.1 can be extended to D to the real (and positive) axis, $D \in \mathbb{R}^+$. Let us prove this. Using the identity

$$\int_{-\infty}^{\infty} dx\, e^{-x^2} = \sqrt{\pi}, \tag{D.2}$$

following ref. [40], and provided that $D \in \mathbb{N}$ ($D \geq 1$),

$$\pi^{D/2} = \left[\int_{-\infty}^{\infty} dx\, e^{-x^2}\right]^D = \int d^D\vec{x}\cdot\, e^{-\|\vec{x}\|^2} = \int d\,\Omega_D \int_0^{\infty} dx\, x^{D-1} e^{-x^2}$$
$$= \left(\int d\,\Omega_D\right)\cdot \frac{\Gamma(D/2)}{2}, \tag{D.3}$$

thus recovering eq. D.1 only for natural values of D. However, the function $2\pi^{D/2}/\Gamma(D/2)$ is defined also in $D \notin \mathbb{N}$, because it is a composition of analytic functions in the complex plane[1]. Thus, the analytic extension of eq. D.1 to the complex plane is trivial.

D.2 Integration of Legendre Polynomials

Eq. 4.29,

$$\int_0^{2\pi} d\,\tilde{\varphi} \int_0^{\pi} d\,\tilde{\theta}\cdot \sin\tilde{\theta}\cdot P_J[\cos\tilde{\theta}]\cdot P_{J'}[\cos\theta\cos\tilde{\theta} + (-1)^n \sin\theta\sin\tilde{\theta}\cos\tilde{\varphi}] =$$
$$= \frac{4\pi}{2J+1}\delta_{J,J'} P_J[\cos\theta], \tag{D.4}$$

[1] See ref. [186] for more details. Special care should be taken for $n = 0, -1, -2, \ldots$ ($D = 0, -1/2, -1/3, \ldots$), where $\Gamma(n)$ has single poles. However, this does not affect our computations, since we always have real and positive values of D.

can be easily proven taking into account the *Addition Theorem for Spherical Harmonics*[2],

$$\cos\gamma \equiv \cos\theta_1\cos\theta_2 + \sin\theta_1\sin\theta_2\cos(\varphi_1-\varphi_2) \tag{D.5}$$

$$P_J(\cos\gamma) = \frac{4\pi}{2J+1}\sum_{m=-J}^{J}(-1)^m Y_J^m(\theta_1,\varphi_1)Y_J^{-m}(\theta_2,\varphi_2) \tag{D.6}$$

$$= P_J(\cos\theta_1)P_J(\cos\theta_2) + 2\sum_{m=1}^{J}\frac{(J-m)!}{(J+m)!}P_J^m(\cos\theta_1)P_J^m(\cos\theta_2)\cos[m(\varphi_1-\varphi_2)] \tag{D.7}$$

Just take $\theta_1 \to \tilde{\theta}$, $\theta_2 \to \theta$, $\varphi_1 \to \tilde{\varphi}$, $\varphi_2 \to n\pi$, considering that $\cos(\tilde{\varphi}-n\pi) = (-1)^n\cos\tilde{\varphi}\,\forall n\in\mathbb{Z}$. Now,

$$\int_0^{2\pi} d\,\tilde{\varphi}\cos[m(\tilde{\varphi}-n\pi)] = \frac{1}{m}\sin[m(\tilde{\varphi}-n\pi)]\Big|_{\tilde{\varphi}=0}^{2\pi} = 0\,\forall m\in\mathbb{Z}, \tag{D.8}$$

so that the integration of eq. 4.29 reduces to

$$2\pi\int_0^{\pi} d\cdot\tilde{\theta}\cdot P_J[\cos\tilde{\theta}]P_{J'}(\cos\tilde{\theta})P_J(\cos\theta) \tag{D.9}$$

And now, because of the orthonormality of Legendre polynomials [186],

$$\int_{-1}^{1} d\,x\cdot P_J(x)P_{J'}(x) = \frac{2}{2J+1}\delta_{J,J'}, \tag{D.10}$$

we recover trivially eq. 4.29 when integrating over $\tilde{\theta}$.

D.3 Integrals for the N/D method

In order to compute the integrals of eqs. 4.129, let us first consider the following ones,

$$I_1(y,y_1,y_2) = \int_{y_1}^{y_2}\frac{dx}{x(x-y)} = \int_{y_1}^{y_2} dx\frac{1}{y}\left[\frac{1}{x-y}-\frac{1}{x}\right] = \frac{1}{y}\log\left(1-\frac{y}{x}\right)\Big|_{x=y_1}^{y_2} \tag{D.11a}$$

$$I_2(y,y_1,y_2) = \int_{y_1}^{y_2}\frac{dx}{x^2(x-y)} = \frac{1}{y^2}\left[\log\left(1-\frac{y}{x}\right)+\frac{y}{x}\right]\Big|_{x=y_1}^{y_2} \tag{D.11b}$$

$$\tilde{I}_1'(y,y_1,y_2) = \int_{y_1}^{y_2}\frac{dx\,\log x}{x(x-y)} = 2\log x\log\left(1-\frac{x}{y}\right)+\log^2 x+2\,\mathrm{Li}_2\left(\frac{x}{y}\right)\Big|_{x=y_1}^{y_2}, \tag{D.11c}$$

where $\mathrm{Li}_2(\eta)$ is the dilogarithm function[3], defined as

$$\mathrm{Li}_2(x) \equiv \sum_{n=1}^{\infty}\frac{x^n}{n^2},\ |x|\le 1. \tag{D.12}$$

For $|x|>1$, the dilogarithm is defined by an analytic continuation. Anyway, according to refs. [148, 187], this analytic continuation can be embodied in an integrate form

$$\mathrm{Li}_2(x) = -\int_0^x\frac{\log(1-t)}{t}dt, \tag{D.13}$$

[2]For a proof of this theorem refer, for example, to [186].

[3]See, for example, refs. [148, 187].

and its asymptotic form for large values of x, necessary in order to compute the limit $\Lambda \to \infty$ in eq. D.11c,

$$\mathrm{Li}_2(z) \xrightarrow[\mathrm{Im}\, z \to 0^+]{z\to\infty} \frac{\pi^2}{3} - \frac{1}{2}\log^2 z + i\pi \log z, \tag{D.14}$$

provided that $z = \mathrm{Re}(z) + i\epsilon$, where $\epsilon \to 0^+$. If, on the other had, we had $z = \mathrm{Re}(z) - i\epsilon$ ($\epsilon \to 0^+$), then the correct asymptotic form would be

$$\mathrm{Li}_2(z) \xrightarrow[\mathrm{Im}\, z \to 0^-]{z\to\infty} \frac{\pi^2}{3} - \frac{1}{2}\log^2 z - i\pi \log z. \tag{D.15}$$

Note that this last case ($z = \mathrm{Re}(z) - i\epsilon$, $\epsilon \to 0^+$) is the one which, indeed, appears in eq. D.11c. Take into account that $y_2 \to \infty$, and $y \equiv (s+i\epsilon)/\mu^2$ (with $\mathrm{Im}\, y \to 0^+$) appears on the denominator, so that $\mathrm{Im}(y_2/y) \to 0^-$.

If the limits $y_2 \to \infty$ are computed in eqs. D.11, then those expressions turn into

$$I_1(y, y_1, \infty) = -\frac{1}{y}\log\left(1 - \frac{y}{y_1}\right) \tag{D.16a}$$

$$I_2(y, y_1, \infty) = -\frac{1}{y^2}\left[\frac{y}{y_1} + \log\left(1 - \frac{y}{y_1}\right)\right] \tag{D.16b}$$

$$I_1'(y, y_1, \infty) = -\frac{1}{y}\left[\frac{1}{2}\log^2(-y) + \mathrm{Li}_2\,\frac{y_1}{y} - \frac{1}{2}\log^2(y_1) + \log y_1 \log\left(1 - \frac{y_1}{y}\right) + \frac{\pi^2}{6}\right], \tag{D.16c}$$

Now, let us effect the change of variables $y = (s + i\epsilon)/\mu^2$, $x = s'/\mu^2$, $y_1 = m^2/\mu^2$, $y_2 = \Lambda^2/\mu^2$. The integrals of eqs. D.11 and their solutions when $\Lambda^2 \to \infty$ and $\epsilon \to 0^+$ (eqs. D.16) turn into

$$\frac{1}{\mu^2} I_1(y, y_1, y_2) = \frac{1}{\mu^2}\int_{y_1}^{y_2} \frac{dx}{x(x-y)} = \int_{m^2}^{\Lambda^2} \frac{ds'}{s'(s'-s-i\epsilon)} \xrightarrow[y_2\to\infty]{\Lambda^2\to\infty} -\frac{1}{s}\log\left(1 - \frac{s}{m^2}\right) \tag{D.17a}$$

$$\frac{1}{\mu^4} I_2(y, y_1, y_2) = \frac{1}{\mu^2}\int_{y_1}^{y_2} \frac{dx}{x^2(x-y)} = \frac{1}{\mu^4}\int_{\mu^2}^{\Lambda^2} \frac{ds'}{(s')^2(s'-s-i\epsilon)} \xrightarrow[y_2\to\infty]{\Lambda^2\to\infty} -\frac{1}{s^2}\left[\frac{s}{m^2} + \log\left(1 - \frac{s}{m^2}\right)\right] \tag{D.17b}$$

$$\frac{1}{\mu^2} I_1'(y, y_1, y_2) = \frac{1}{\mu^2}\int_{y_1}^{y_2} \frac{dx \log x}{x(x-y)} = \int_{m^2}^{\Lambda^2} \frac{ds' \log \frac{s'}{\mu^2}}{s'(s'-s-i\epsilon))} \xrightarrow[y_2\to\infty]{\Lambda^2\to\infty} -\frac{1}{s}\left[\frac{1}{2}\log^2\left(\frac{-s}{\mu^2}\right) + \mathrm{Li}_2\,\frac{m^2}{s} - \frac{1}{2}\log^2\left(\frac{m^2}{\mu^2}\right) + \log\frac{m^2}{\mu^2}\log\left(1 - \frac{m^2}{s}\right) + \frac{\pi^2}{6}\right]. \tag{D.17c}$$

These expressions allow us to recover eqs. 4.129, as expected.

D.4 Comparison of our elastic $\omega\omega$ partial waves with a Higgsless ECL model

Before the discovery of the Higgs boson at the LHC, several authors ([4, 6, 7]) motivated a strongly interacting regime for the dynamics of the EWSBS to solve some of the problems for which the Higgs boson was postulated. In particular, we will quote ref. [150] since, although they worked in the Higgsless ECL model, they have computed the real part of the NLO partial waves (including the tensor-isotensor channel $IJ = 22$), and their results can be used to check our elastic WBGBs partial waves of eqs. 3.136 to 3.140, taking $a = b = 0$ in our expressions.

Furthermore, ref. [150] (and its extension [175]) are particularly encouraging since they are interested in the implementation of strongly interacting theories into their own MonteCarlo program, WHIZARD [188, 189].

However, while we take the non-linear electroweak chiral Lagrangian with an arbitrary function for the couplings of the Higgs-like particle with the EWSBS[4],

$$\mathcal{L}_2 = \frac{v^2}{4}\left(1 + 2a\frac{h}{v} + b\left(\frac{h}{v}\right)^2 + \dots\right)\mathrm{Tr}[(D_\mu U)^\dagger D^\mu U] + \dots, \tag{D.18}$$

ref. [150] takes the Higgsless regime $a = b = 0$,

$$\mathcal{L}_2 = \frac{v^2}{4}\mathrm{Tr}[(D_\mu U)^\dagger D^\mu U]. \tag{D.19}$$

Note that the work of ref. [150] has been extended (see ref. [175] for example), but apparently a non-linear chiral Lagrangian of the form of eq. 2.31, has not been considered. In particular, ref. [150] introduces the Higgs-like particle through their eq. 1,

$$\mathbf{H} \to \frac{1}{2}(v + h)\Sigma \tag{D.20}$$

where Σ is the non-linear Goldstone-boson representation. Apparently, they are not considering a more general coupling with the Higgs-like boson, with a factor like (a, b) (see this work, eq. 2.6; and some other works like ref. [158]), the c_W (see ref. [31]), the $F_U(h)$ (see ref. [29] and their their eq. 5),...

Anyway, we are interested in eqs. 4.13 and 4.14 from ref. [150]. They should be compatible with the real part of our $\omega\omega \to \omega\omega$ partial waves (eqs. 3.136 to 3.140, see also the definition of eq. 3.132). Provided that we define $a = b = 0$, in our equations, and consider that the definition of partial wave of ref. [150] (see their eqs. 4.11 and 4.12) should be multiplied by $1/(32\pi)$ to match the definition of partial wave which we use ($K = 2$ in eqs. 3.123 and 3.124). This is an independent check of our NLO and partial waves computation.

Note that, when the real part of our amplitudes is taken, because we are working over the RC (physical zone, $s' = s + i\epsilon$, $s > 0$, $\epsilon \to 0^+$), we have $\mathrm{Re}\log(s/\mu^2) = \log(s/\mu^2)$, $\mathrm{Re}\log(-s/\mu^2) = \log(s/\mu^2)$. Thus, once we define $a = b = 0$, in our equations (eqs. 3.136

[4]See our eq. 2.4 and the phenomenological Lagrangian of eq. 2.31.

to 3.140), and we multiply them by 32π, we find that

$$A_{00}^{(0)} = 32\pi K_{00} s|_{a=b=0} = \frac{3s}{v^2} \tag{D.21a}$$

$$A_{11}^{(0)} = \frac{s}{3v^2} \tag{D.21b}$$

$$A_{20}^{(0)} = -\frac{s}{v^2} \tag{D.21c}$$

$$A_{02}^{(0)} = A_{22}^{(0)} = 0, \tag{D.21d}$$

thus being compatible with eq. 4.13 from ref. [150]. Now, let us compute the real part of our NLO results, (with $a = b = 0$, $a_4 = \alpha_4$, $a_5 = \alpha_5$)

$$\mathrm{Re}\, A_{00}^{(1)} = \left[\frac{8}{3}(7a_4(\mu) + 11a_5(\mu)) - \frac{25}{144\pi^2}\log\frac{s}{\mu^2} + \frac{101}{288\pi^2}\right]\frac{s^2}{v^4} \tag{D.22a}$$

$$\mathrm{Re}\, A_{11}^{(1)} = \left[\frac{4}{3}(a_4(\mu) - 2a_5(\mu)) + \frac{1}{432\pi^2}\right]\frac{s^2}{v^4} \tag{D.22b}$$

$$\mathrm{Re}\, A_{20}^{(1)} = \left[\frac{16}{3}(2a_4(\mu) + a_5(\mu)) - \frac{5}{72\pi^2}\log\frac{s}{\mu^2} + \frac{91}{576\pi^2}\right]\frac{s^2}{v^4} \tag{D.22c}$$

$$\mathrm{Re}\, A_{02}^{(1)} = \left[\frac{8}{15}(2a_4(\mu) + a_5(\mu)) - \frac{1}{144\pi^2}\log\frac{s}{\mu^2} + \frac{1}{90\pi^2}\right]\frac{s^2}{v^4} \tag{D.22d}$$

$$\mathrm{Re}\, A_{22}^{(1)} = \left[\frac{4}{15}(a_4(\mu) + 2a_5(\mu)) - \frac{1}{360\pi^2}\log\frac{s}{\mu^2} + \frac{71}{28800\pi^2}\right]\frac{s^2}{v^4}. \tag{D.22e}$$

Our computations (eqs. D.22) coincide with ref. [150]. The LO, NLO logarithm terms and the coefficients of the NLO parameters $\alpha_4(\mu)$ and $\alpha_5(\mu)$ (our a_4 and a_5) are the same. The non-logarithm term which is $\propto s^2/v^4$ appears to be incompatible, but note that this is due to a different renormalization of the $\alpha_4(\mu)$ and $\alpha_5(\mu)$ parameters. Our running equations for $a_4^r(\mu)$ and $a_5^r(\mu)$ (eqs. 3.42a and 3.42b), taking $a = b = 0$, are compatible with those for $\alpha_4(\mu)$ and $\alpha_5(\mu)$ (eq. 4.6 from ref. [150]). But we have taken different values for $a_4(\mu_0)$ and $a_5(\mu_0)$. Thus, in order to have full agreement, it is necessary to introduce

$$a_4(\mu) - \alpha_4(\mu) = a_4(\mu_0) - \alpha_4(\mu_0) = \frac{13}{1152\pi^2} \tag{D.23a}$$

$$a_5(\mu) - \alpha_5(\mu) = a_5(\mu_0) - \alpha_5(\mu_0) = \frac{5}{1152\pi^2}. \tag{D.23b}$$

This is an additional check to our expressions (eqs. D.22). Note that, when comparing with the results from other works, it is necessary to take into account possible differences in the definition of $a_4(\mu_0)$ and $a_5(\mu_0)$, as in eq. D.23.

D.5 Concerns about the aplicability conditions of the ET

Many references from the 90's studied the limits of applicability of the equivalence theorem [124, 190–196], arriving to the conclusion that it is valid also for the particular case of the chiral Lagrangian. This allows us to use the ET in this dissertation.

As an instance of a suggested counterexample of the ET, ref. [197] claimed that, for certain kind of technicolor models, the ET would be violated. Such a violation would come from a *global anomaly* through the triangle fermion loop. That is, from the vertex $Z_L^0 - \gamma - \gamma^*$, γ^* being a virtual photon. As clarified in ref. [198], the key point is that the $\pi^0 \to \gamma\gamma$ amplitude violates the ET only in the zero momentum limit due to its low energy nature, but not in the high energy limit case ($E \gg M_W$). This is a very important concern, since any computation of low-energy events like the decay of a SM-like Higgs boson cannot be computed with techniques that involve the usage of the ET. Only hard scattering events, like scattering of gauge bosons can. Hence, ref. [198] restated the validity of the ET for the particular case of chiral Lagrangians at sufficient energy.

Appendix E

Feynman diagrams for the Effective Lagrangian

All the necessary vertices have been computed both by hand and by using the program FeynRules [142], as explained in page 31. The FeynRules convention is followed, thus our vertices correspond to $i\mathcal{M}$, where $\mathcal{M}$ is the scattering amplitude.

E.1 $\omega\omega$ scattering, isospin basis, LO coefficients

Vertex	Feynman diagram
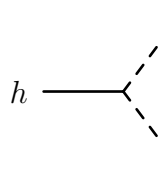	$-\frac{2ia}{v}(p_1p_2)\delta_{a,b}$
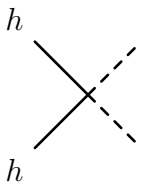	$-\frac{2ib}{v^2}(p_3p_4)\delta_{a,b}$
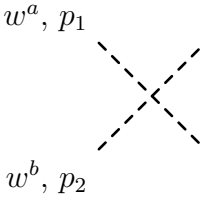	$-\frac{i}{v^2}\big\{[p_1p_3+p_1p_4+p_2p_3+p_2p_4]\delta_{a,b}\delta_{c,d}$ $+[p_1p_2+p_1p_4+p_3p_2+p_3p_4]\delta_{a,c}\delta_{b,d}$ $+[p_1p_2+p_1p_3+p_4p_2+p_4p_3]\delta_{a,d}\delta_{b,c}\big\}$

Vertex	Feynman diagram
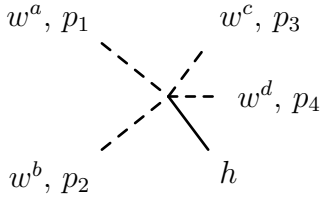	$-\frac{2ia}{v^3}\{[p_1p_3+p_1p_4+p_2p_3+p_2p_4]\delta_{a,b}\delta_{c,d}$ $+[p_1p_2+p_1p_4+p_3p_2+p_3p_4]\delta_{a,c}\delta_{b,d}$ $+[p_1p_2+p_1p_3+p_4p_2+p_4p_3]\delta_{a,d}\delta_{b,c}\}$
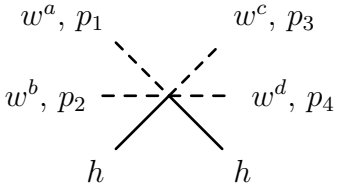	$-\frac{2ib}{v^4}\big[(p_1p_3+p_1p_4+p_2p_3+p_2p_4)\delta_{a,b}\delta_{c,d}$ $+(p_1p_2+p_1p_4+p_3p_2+p_3p_4)\delta_{a,c}\delta_{b,d}$ $+(p_1p_2+p_1p_3+p_4p_2+p_4p_3)\delta_{a,d}\delta_{b,c}\big]$

These vertices correspond to the effective Lagrangian of eq. 2.31. The vertices where the NLO counterterms a_4, a_5, d, e and g appear will be given in the next subsection.

E.2 $\omega\omega$ scattering, isospin basis, NLO coefficients

Vertex	Feynman diagram
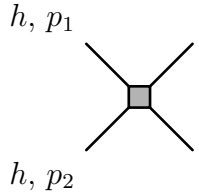	$\frac{8ig}{v^4}[(p_1p_2)(p_3p_4)+(p_1p_3)(p_2p_4)+(p_1p_4)(p_2p_3)]$
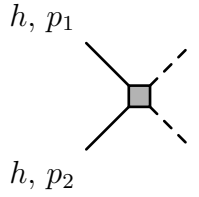	$\frac{4ie}{v^4}[(p_1p_4)(p_2p_3)+(p_1p_3)(p_2p_4)]\delta_{a,b}$ $+\frac{8id}{v^4}[(p_1p_2)(p_3p_4)]\delta_{a,b}$
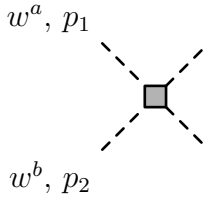	$\frac{16ia_4}{v^4}\{[(p_1p_3)(p_2p_4)+(p_1p_4)(p_2p_3)]\delta_{a,b}\delta_{c,d}$ $+[(p_1p_2)(p_3p_4)+(p_1p_4)(p_2p_3)]\delta_{a,c}\delta_{b,d}$ $+[(p_1p_2)(p_3p_4)+(p_1p_3)(p_2p_4)]\delta_{a,d}\delta_{b,c}\}$ $+\frac{32ia_5}{v^4}\{[(p_1p_2)(p_3p_4)]\delta_{a,b}\delta_{c,d}$ $+[(p_1p_3)(p_2p_4)]\delta_{a,c}\delta_{b,d}+[(p_1p_4)(p_2p_3)]\delta_{a,d}\delta_{b,c}\}$

The shown vertices correspond to the effective Lagrangian of eq. 2.31. We include only the vertices where the NLO counterterms a_4, a_5, d, e and g appear.

E.3 $\gamma\gamma$ scattering, charge basis, LO

Vertex	Exponential	Spherical
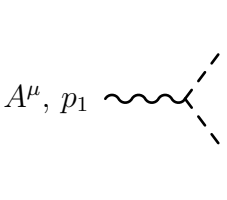	$ie(p_{2\mu} - p_{3\mu})$	$ie(p_{2\mu} - p_{3\mu})$
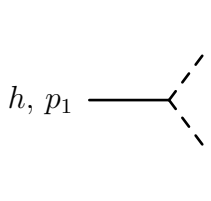	$-\frac{2ia}{v}(p_2 p_3)$	$-\frac{2ia}{v}(p_2 p_3)$
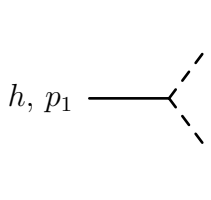	$-\frac{2ia}{v} p_2 p_3$	$-\frac{2ia}{v} p_2 p_3$
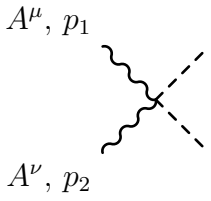	$2ie^2 g_{\mu\nu}$	$2ie^2 g_{\mu\nu}$
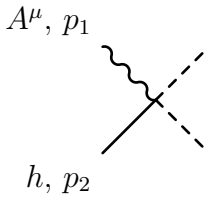	$\frac{2iae}{v}(p_{3\mu} - p_{4\mu})$	$\frac{2iae}{v}(p_{3\mu} - p_{4\mu})$
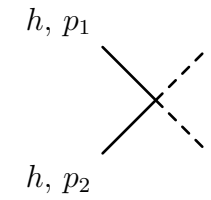	$-\frac{2ib}{v^2} p_3 p_4$	$-\frac{2ib}{v^2} p_3 p_4$

Vertex	Exponential	Spherical
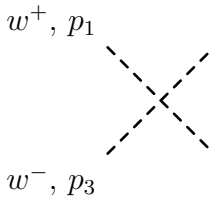	$-\frac{i}{3v^2}[2(p_1p_2+p_3p_4)+(p_1+p_2)^2]$	$-\frac{i}{v^2}[2(p_1p_2+p_3p_4)-(p_1+p_2)^2]$
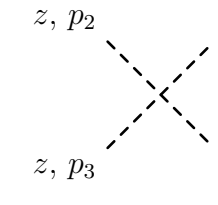	$\frac{i}{3v^2}[2(p_1p_4+p_2p_3)+(p_1+p_4)^2]$	$\frac{i}{v^2}(p_1+p_4)^2$
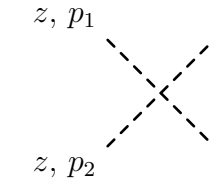	0	$-\frac{2i}{v^2}[p_1p_4+p_2p_3-(p_1+p_4)^2]$
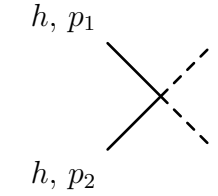	$-\frac{2ib}{v^2}p_3p_4$	$-\frac{2ib}{v^2}p_3p_4$
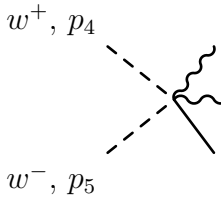	$\frac{4iae^2}{v}g_{\mu\nu}$	$\frac{4iae^2}{v}g_{\mu\nu}$
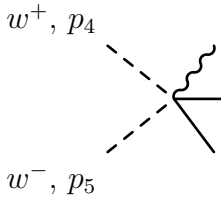	$\frac{2ibe}{v^2}(p_{4\mu}-p_{5\mu})$	$\frac{2ibe}{v^2}(p_{4\mu}-p_{5\mu})$

Vertex	Exponential	Spherical
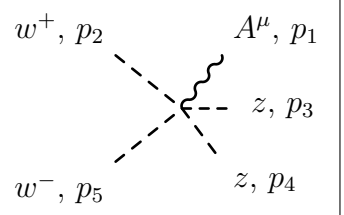	$\frac{2ie}{3v^2}(p_{5\mu} - p_{2\mu})$	0
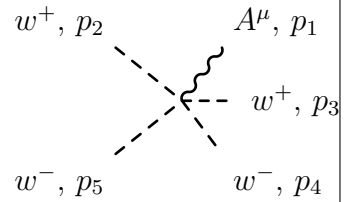	$\frac{4ie}{3v^2}(p_{5\mu} + p_{4\mu} - p_{3\mu} - p_{2\mu})$	0
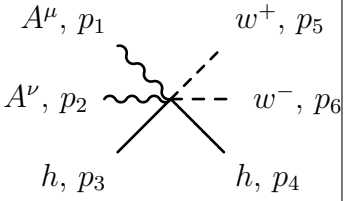	$\frac{4ibe^2}{v^2}g_{\mu\nu}$	$\frac{4ibe^2}{v^2}g_{\mu\nu}$

These vertices correspond to the effective Lagrangian of eqs. 2.33 (for the exponential parametrization) and 2.34 (for the spherical parametrization). The vertices where the NLO counterterms a_1, a_2, a_3 and c_γ appear will be given in the next subsection. Note that, on the contrary, the NLO counterterms which do not contain any photons (d, e and g) do appear in this table. Some diagrams are very similar to those listed on appendix E.1, but note the change of basis (from isospin to charge one). We also omit the diagramas which are not necessary for $\gamma\gamma$ scattering.

E.4 $\gamma\gamma$ scattering, charge basis, NLO

Vertex	Exponential	Spherical
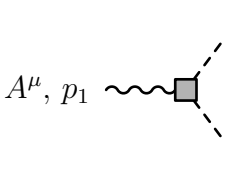	$-\frac{4ie(a_3-a_2)}{v^2}\left[(p_1p_3)p_{2\,\mu} - (p_1p_2)p_{3\,\mu}\right]$	Same than Expon.
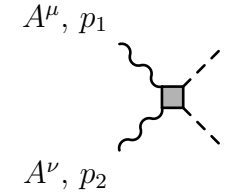	$\frac{8ie^2a_1}{v^2}\left[(p_1p_2)g_{\mu\nu} - p_{2\,\mu}p_{1\,\nu}\right]$ $+\frac{4ie^2(a_3-a_2)}{v^2}\left[(p_1+p_2)^2 g_{\mu\nu}\right.$ $\left. - (p_{1\,\mu} + p_{2\,\mu})p_{1\,\nu}\right.$ $\left. - p_{2\,\mu}(p_{1\,\nu} + p_{2\,\nu})\right]$	Same than Expon.

Vertex	Exponential	Spherical
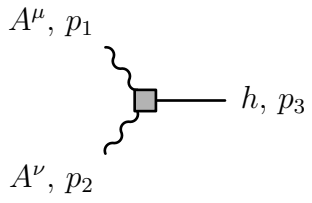	$\frac{2ic_\gamma}{v}\left[(p_1p_2)g_{\mu\nu} - p_{2\,\mu}p_{1\,\nu}\right]$	Same than Expon.

These vertices correspond to the effective Lagrangian of eqs. 2.33 (for the exponential parametrization) and 2.34 (for the spherical parametrization). We include only the vertices where the NLO counterterms a_1, a_2, a_3 and c_γ appear.

E.5 $t\bar{t}$ in the final state, isospin basis

Vertex	Feynman diagram	Vertex	Feynman diagram
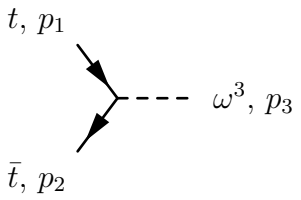	$\frac{M_t}{v}\gamma^5$	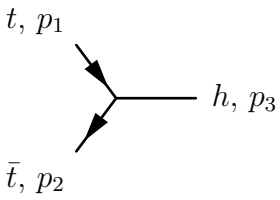	$-i\frac{c_1 M_t}{v}$
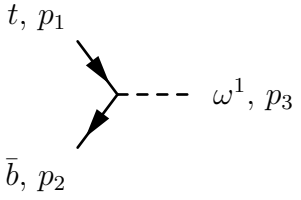	$\frac{M_t}{v}P_R$	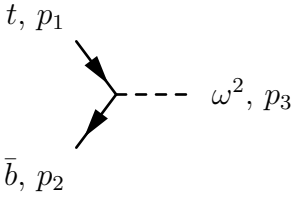	$\frac{iM_t}{v}P_R$
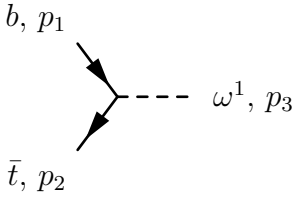	$-\frac{M_t}{v}P_L$	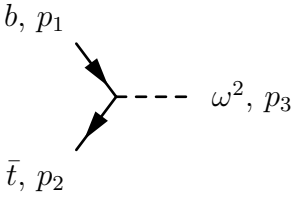	$\frac{iM_t}{v}P_L$
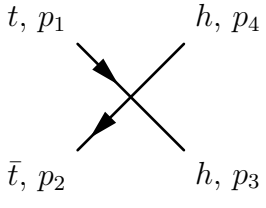	$-\frac{2iM_t c_2}{v^2}$	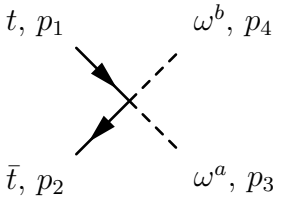	$\frac{iM_t}{v^2}\delta_{a,b}$

Vertex	Feynman diagram	Vertex	Feynman diagram
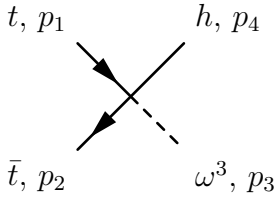	$\frac{M_t c_1}{v^2}\gamma^5$		
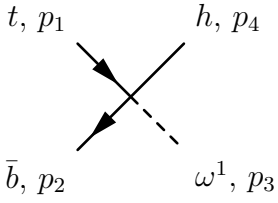	$\frac{M_t c_1}{v^2}P_R$	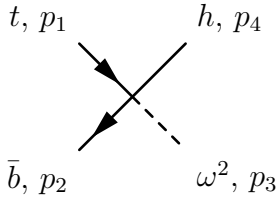	$\frac{iM_t c_1}{v^2}P_R$
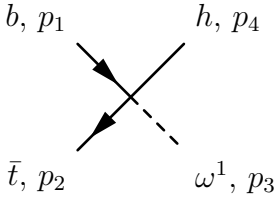	$-\frac{M_t c_1}{v^2}P_L$	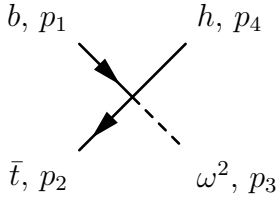	$\frac{iM_t c_1}{v^2}P_L$
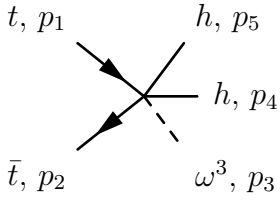	$\frac{2M_t c_2}{v^3}\gamma^5$	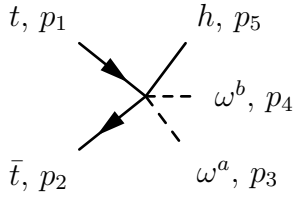	$\frac{iM_t c_1}{v^3}\delta_{a,b}$
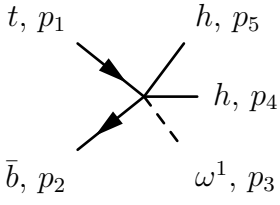	$\frac{2M_t c_2}{v^3}P_R$	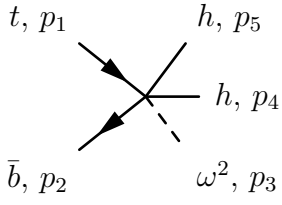	$\frac{2iM_t c_2}{v^3}P_R$
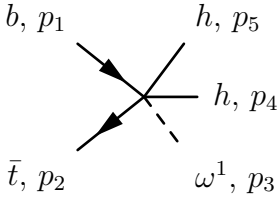	$-\frac{2M_t c_2}{v^3}P_L$	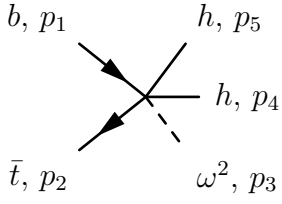	$\frac{2iM_t c_2}{v^3}P_L$

Vertex	Feynman diagram	Vertex	Feynman diagram
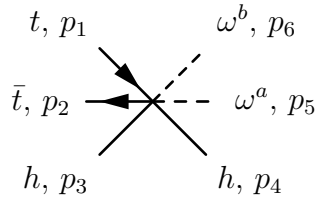	$\frac{2iM_t c_2}{v^4}\delta_{a,b}$		

Appendix F

One-loop Feynman diagrams

This Appendix contains all the NLO Feynman diagrams which enter in the computations. All the tadpoles have been omitted, since we are neglecting all the masses of particles inside the loops and lacking a scale, they vanish because of eq. C.2. These diagrams have been drawn with FeynArts [143] and generated with FeynRules [142], FeynArts [143] and FormCalc [144, 145], as explained in page 31.

F.1 $\omega\omega$

These computations are based on the spherical parameterization and the isospin basis is used. See eq. 2.31 for the Lagrangian and appendices E.1 and E.2 for the Feynman rules.

F.1.1 $\omega\omega \to \omega\omega$

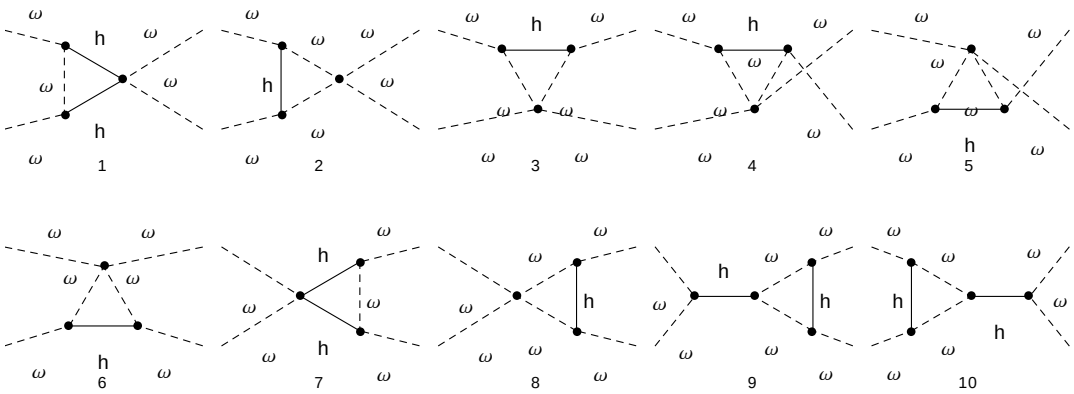

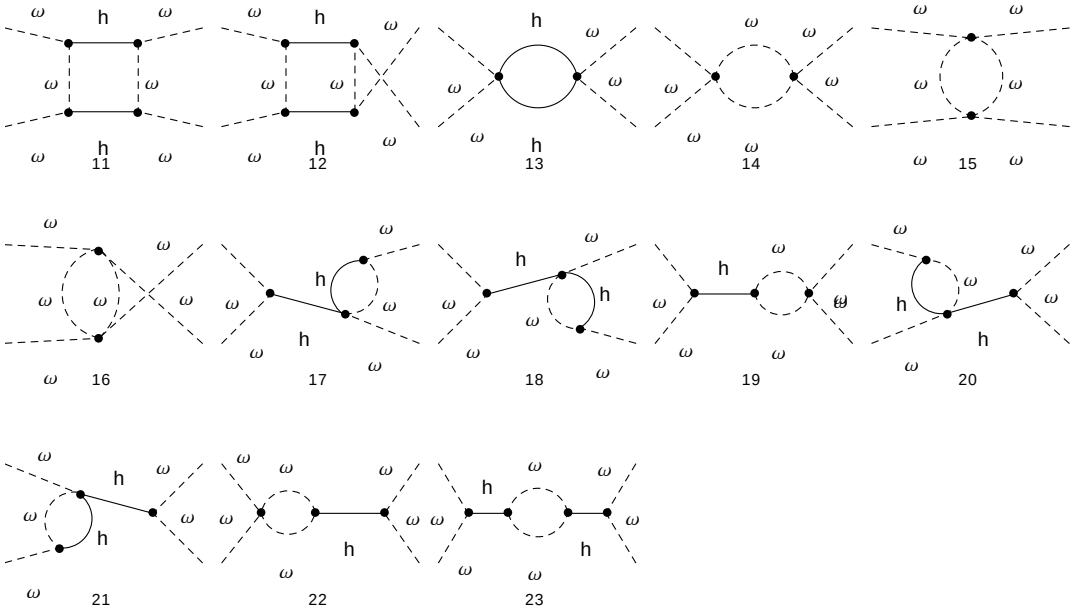

Diagrams used to obtain the amplitude of eq. 3.32.

F.1.2 $\omega\omega \to hh$

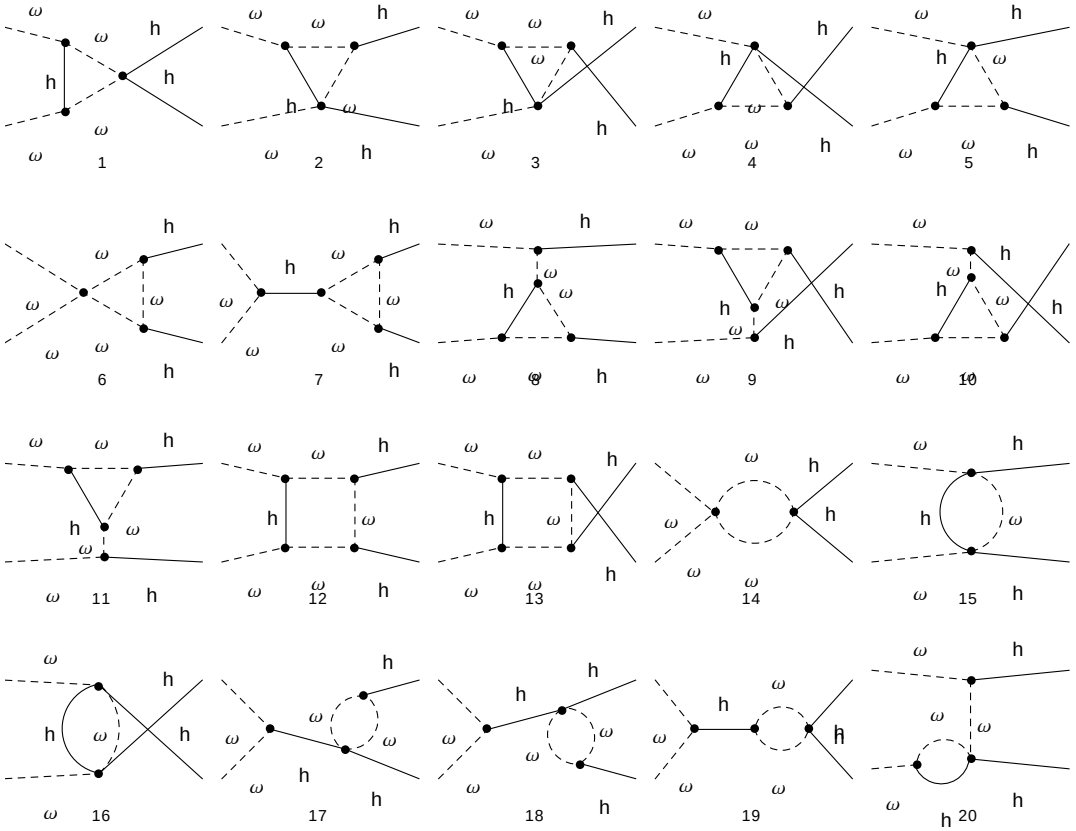

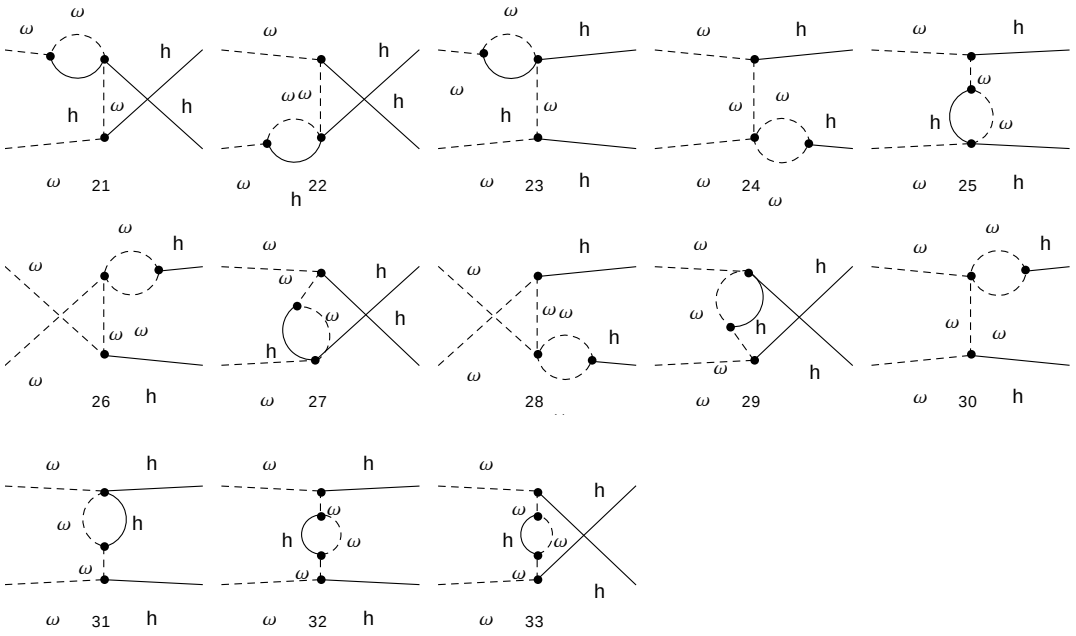

Diagrams used to obtain the amplitude of eq. 3.37.

F.1.3 $hh \to hh$

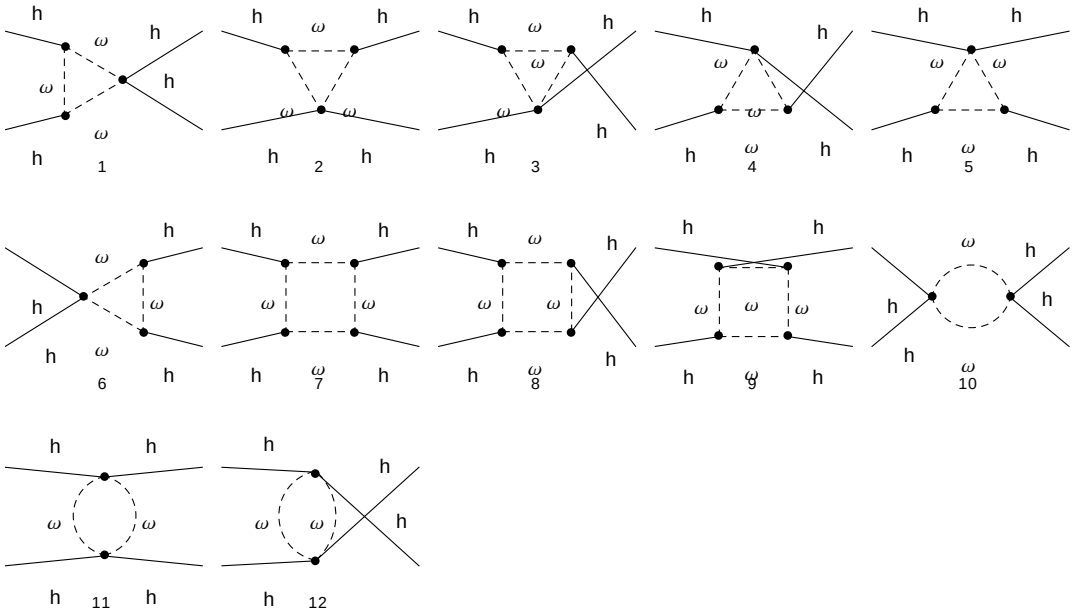

Diagrams used to obtain the amplitude of eq. 3.41.

F.2 $\gamma\gamma$ scattering

Both the spherical and exponential parameterization are used here. See eqs. 2.33 and 2.34; and appendices E.3 and E.4 for the Feynman rules. Note the usage of the charge basis

for the description of the ω WBGBs. By definition, the w particle (antiparticle) that appears in the next figures is defined as ω^+ (ω^-).

F.2.1 $\gamma\gamma \to w^+w^-$

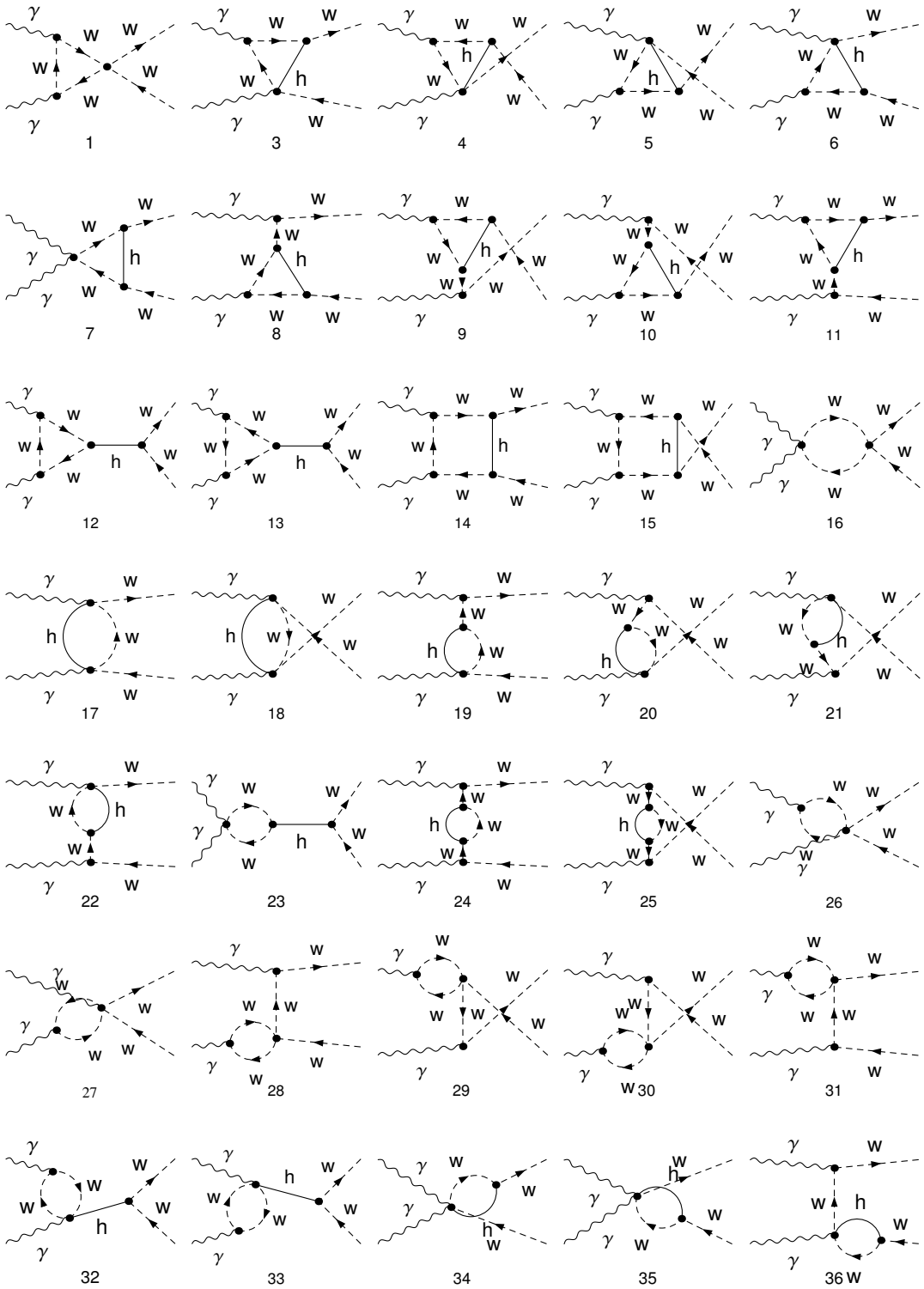

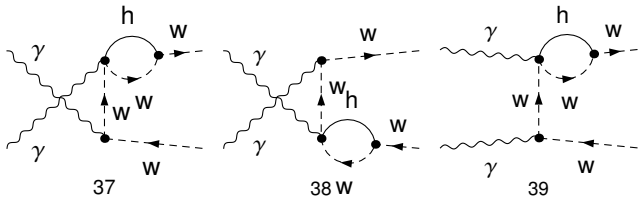

Diagrams used to obtain the amplitude of eq. 3.57 (Lorentz structure in eq. 3.51).

F.2.2 $\gamma\gamma \to zz$

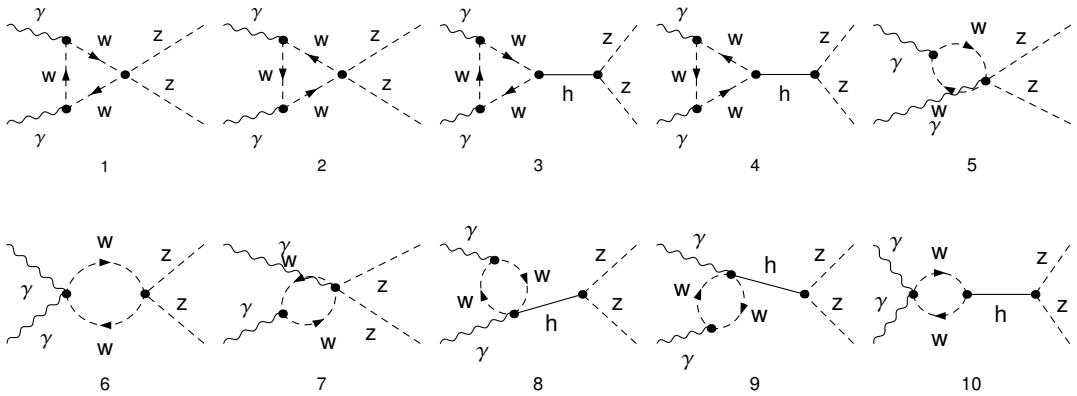

Diagrams used to obtain the amplitude of eq. 3.55 (Lorentz struct. in eq. 3.51).

F.2.3 $\gamma\gamma \to hh$

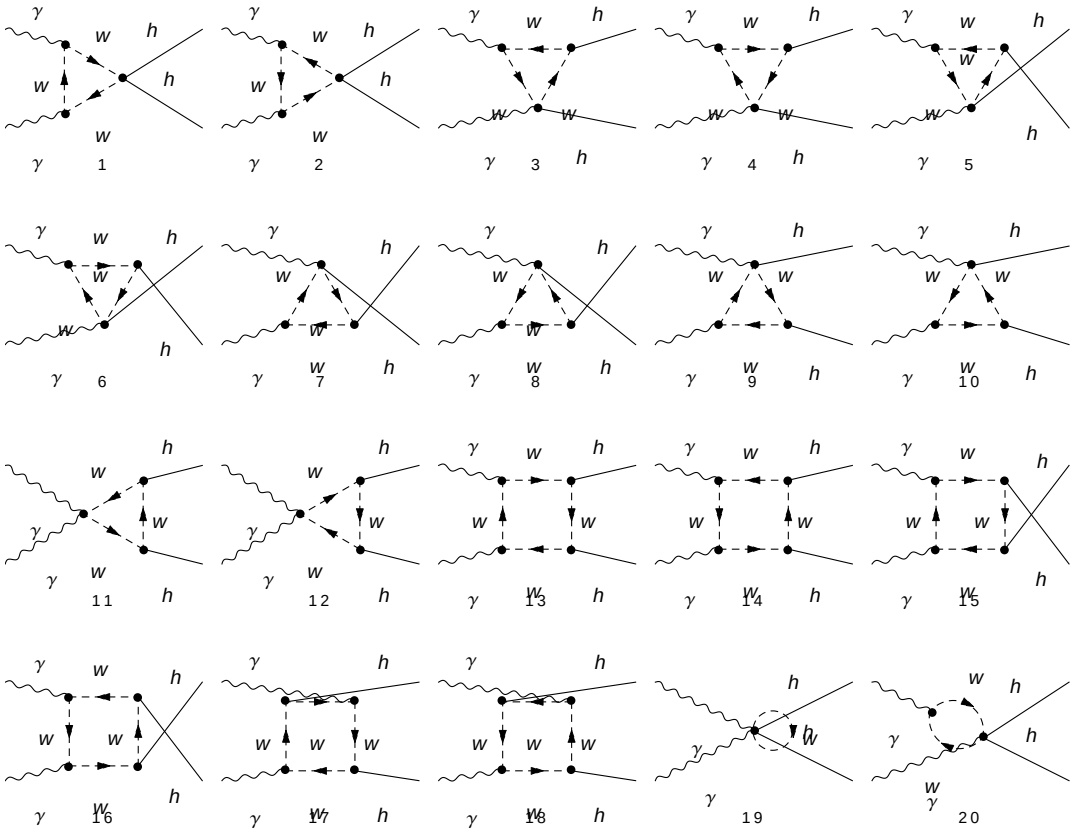

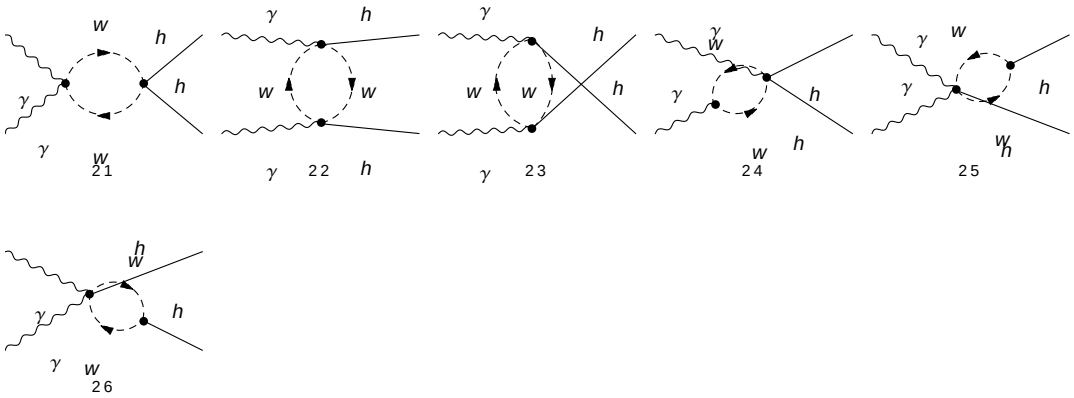

Diagrams used to obtain the amplitude of eq. 3.87.

F.3 Scattering involving $t\bar{t}$ states

The exponential parameterization is used here. See eqs. 2.45 and 2.46 for the considered Lagrangian; and appendix E.5 for the Feynman rules. Note that we are using the isospin basis, although due to the appearance of terms which break the isospin symmetry we have to consider separately the ω^1, ω^2 and ω^3 bosons. At the end, all the possible scattering processes $\omega^i\omega^i \to t\bar{t}$, where $i = 1, 2, 3$, have the same diagrams and matrix element. That is, the isospin symmetry is restored. So, we only paint the diagramas associated with the process $\omega^1\omega^1 \to t\bar{t}$.

F.3.1 $\omega\omega \to t\bar{t}$

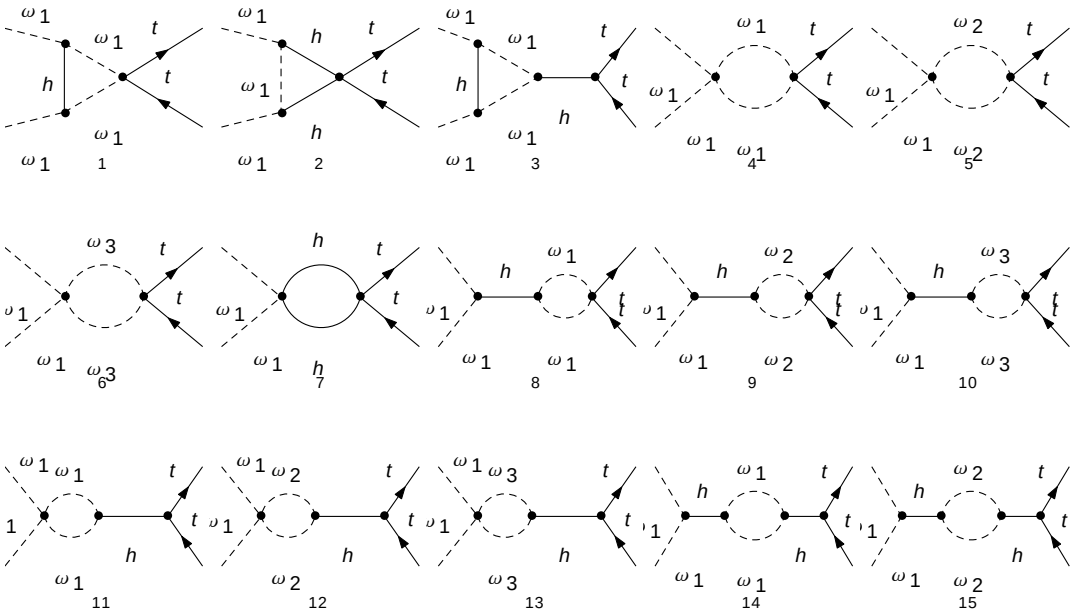

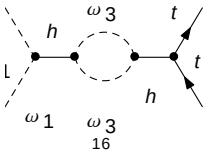

Diagrams used to obtain the amplitude of eq. 3.97.

F.3.2 $hh \to t\bar{t}$

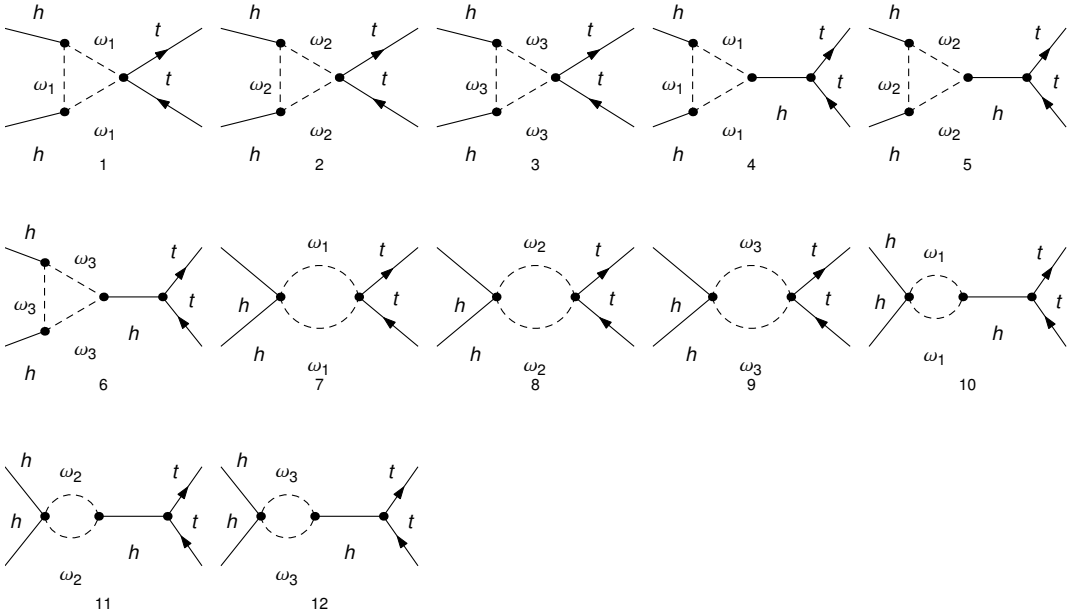

Diagrams used to obtain the amplitude of eq. 3.108.

Bibliography

[1]ATLAS Collaboration, "Observation and study of the Higgs boson candidate in the two photon decay channel with the ATLAS detector at the LHC", ATLAS-CONF-2012-168, ATLAS-COM-CONF-2012-203 (2012).

[2]CMS Collaboration, "Evidence for a new state decaying into two photons in the search for the standard model Higgs boson in pp collisions", CMS-PAS-HIG-12-015 (2012).

[3]S. Chatrchyan et al., "Observation of a new boson at a mass of 125 GeV with the CMS experiment at the LHC", Phys. Lett. **B716**, 30–61 (2012).

[4]T. Appelquist and C. W. Bernard, "Strongly Interacting Higgs Bosons", Phys. Rev. **D22**, 200 (1980).

[5]T. Appelquist, M. J. Bowick, E. Cohler, and A. I. Hauser, "The Breaking of Isospin Symmetry in Theories With a Dynamical Higgs Mechanism", Phys. Rev. **D31**, 1676 (1985).

[6]A. C. Longhitano, "Low-Energy Impact of a Heavy Higgs Boson Sector", Nucl. Phys. **B188**, 118 (1981).

[7]A. C. Longhitano, "Heavy Higgs Bosons in the Weinberg-Salam Model", Phys. Rev. **D22**, 1166 (1980).

[8]G. Cvetic and R. Kogerler, "Fermionic Couplings in an Electroweak Theory With Nonlinear Spontaneous Symmetry Breaking", Nucl. Phys. **B328**, 342 (1989).

[9]A. Dobado and M. J. Herrero, "Phenomenological Lagrangian Approach to the Symmetry Breaking Sector of the Standard Model", Phys. Lett. **B228**, 495 (1989).

[10]A. Dobado and M. J. Herrero, "Testing the Hypothesis of Strongly Interacting Longitudinal Weak Bosons in Electron - Positron Collisions at Tev Energies", Phys. Lett. **B233**, 505 (1989).

[11]A. Dobado, M. J. Herrero, and T. N. Truong, "Study of the Strongly Interacting Higgs Sector", Phys. Lett. **B235**, 129 (1990).

[12]A. Dobado, M. J. Herrero, and J. Terron, "The Role of Chiral Lagrangians in Strongly Interacting $W(\mathrm{l})$ $W(\mathrm{l})$ Signals at pp Supercolliders", Z. Phys. **C50**, 205–220 (1991).

[13]A. Dobado, D. Espriu, and M. J. Herrero, "Chiral Lagrangians as a tool to probe the symmetry breaking sector of the SM at LEP", Phys. Lett. **B255**, 405–414 (1991).

[14]A. Dobado, M. J. Herrero, J. R. Pelaez, E. Ruiz Morales, and M. T. Urdiales, "Learning about the strongly interacting symmetry breaking sector at LHC", Phys. Lett. **B352**, 400–410 (1995).

[15]A. Dobado, M. J. Herrero, J. R. Pelaez, and E. Ruiz Morales, "CERN LHC sensitivity to the resonance spectrum of a minimal strongly interacting electroweak symmetry breaking sector", Phys. Rev. **D62**, 055011 (2000).

[16]B. Holdom and J. Terning, "Large corrections to electroweak parameters in technicolor theories", Phys. Lett. **B247**, 88–92 (1990).

[17]M. Golden and L. Randall, "Radiative Corrections to Electroweak Parameters in Technicolor Theories", Nucl. Phys. **B361**, 3–23 (1991).

[18]D. Espriu and J. Manzano, "CP violation and family mixing in the effective electroweak Lagrangian", Phys. Rev. **D63**, 073008 (2001).

[19]G. Buchalla and O. Cata, "Effective Theory of a Dynamically Broken Electroweak Standard Model at NLO", JHEP **07**, 101 (2012).

[20]G. Buchalla, O. Cata, R. Rahn, and M. Schlaffer, "Effective Field Theory Analysis of New Physics in e+e- → W+W- at a Linear Collider", Eur. Phys. J. **C73**, 2589 (2013).

[21]R. Alonso, M. B. Gavela, L. Merlo, S. Rigolin, and J. Yepes, "Minimal Flavour Violation with Strong Higgs Dynamics", JHEP **06**, 076 (2012).

[22]F. Feruglio, "The Chiral approach to the electroweak interactions", Int. J. Mod. Phys. **A8**, 4937–4972 (1993).

[23]J. Bagger, V. D. Barger, K.-m. Cheung, J. F. Gunion, T. Han, G. A. Ladinsky, R. Rosenfeld, and C. P. Yuan, "The Strongly interacting W W system: Gold plated modes", Phys. Rev. **D49**, 1246–1264 (1994).

[24]V. Koulovassilopoulos and R. S. Chivukula, "The Phenomenology of a nonstandard Higgs boson in W(L) W(L) scattering", Phys. Rev. **D50**, 3218–3234 (1994).

[25]C. P. Burgess, J. Matias, and M. Pospelov, "A Higgs or not a Higgs? What to do if you discover a new scalar particle", Int. J. Mod. Phys. **A17**, 1841–1918 (2002).

[26]L.-M. Wang and Q. Wang, "Electroweak chiral Lagrangian for neutral Higgs boson", Chin. Phys. Lett. **25**, 1984 (2008).

[27]B. Grinstein and M. Trott, "A Higgs-Higgs bound state due to new physics at a TeV", Phys. Rev. **D76**, 073002 (2007).

[28]R. Alonso, M. B. Gavela, L. Merlo, S. Rigolin, and J. Yepes, "The Effective Chiral Lagrangian for a Light Dynamical "Higgs Particle"", Phys. Lett. **B722**, [Erratum: Phys. Lett. **B726**, 926 (2013)], 330–335 (2013).

[29]G. Buchalla, O. Catà, and C. Krause, "Complete Electroweak Chiral Lagrangian with a Light Higgs at NLO", Nucl. Phys. **B880**, 552–573 (2014).

[30]G. Buchalla, O. Catá, and C. Krause, "On the Power Counting in Effective Field Theories", Phys. Lett. **B731**, 80–86 (2014).

[31]R. Contino, M. Ghezzi, C. Grojean, M. Muhlleitner, and M. Spira, "Effective Lagrangian for a light Higgs-like scalar", JHEP **07**, 035 (2013).

[32]I. Brivio, O. J. P. Éboli, M. B. Gavela, M. C. Gonzalez-Garcia, L. Merlo, and S. Rigolin, "Higgs ultraviolet softening", JHEP **12**, 004 (2014).

[33]M. B. Gavela, J. Gonzalez-Fraile, M. C. Gonzalez-Garcia, L. Merlo, S. Rigolin, and J. Yepes, "CP violation with a dynamical Higgs", JHEP **10**, 44 (2014).

[34]R. L. Delgado, A. Dobado, and F. J. Llanes-Estrada, "Light 'Higgs', yet strong interactions", J.Phys. **G41**, 025002 (2014).

[35]R. L. Delgado, A. Dobado, and F. J. Llanes-Estrada, "One-loop W_LW_L and Z_LZ_L scattering from the electroweak Chiral Lagrangian with a light Higgs-like scalar", JHEP **1402**, 121 (2014).

[36]R. Delgado, A. Dobado, M. Herrero, and J. Sanz-Cillero, "One-loop $\gamma\gamma \to \mathrm{W}_L^+ \mathrm{W}_L^-$ and $\gamma\gamma \to \mathrm{Z}_L \mathrm{Z}_L$ from the Electroweak Chiral Lagrangian with a light Higgs-like scalar", JHEP **1407**, 149 (2014).

[37]R. L. Delgado, A. Dobado, M. J. Herrero, and J. J. Sanz-Cillero, "Electroweak Chiral Lagrangians and $\gamma\gamma \to Z_LZ_L$, $W_L^+W_L^-$ at One Loop", in Proceedings, 2nd Conference on Large Hadron Collider Physics Conference (LHCP 2014) (2014), arXiv:1409.3983 [hep-ph].

[38]R. L. Delgado, A. Dobado, and F. J. Llanes-Estrada, "Unitarity, analyticity, dispersion relations, and resonances in strongly interacting W_LW_L, Z_LZ_L, and hh scattering", Phys. Rev. **D91**, 075017 (2015).

[39]R. L. Delgado, A. Dobado, and F. J. Llanes-Estrada, "Possible new resonance from W_LW_L-hh interchannel coupling", Phys. Rev. Lett. **114**, 221803 (2015).

[40]M. E. Peskin and D. V. Schroeder, *An Introduction to Quantum Field Theory; 1995 ed.* (Westview, Boulder, CO, 1995).

[41]J. F. Donoghue, E. Golowich, and B. R. Holstein, *Dynamics of the Standard Model*, Cambridge monographs on particle physics, nuclear physics, and cosmology (Cambridge Univ. Press, Cambridge, 1992).

[42]P. Ramond, *Field Theory: A Modern Primer*, Frontiers in Physics (Westview Press, New York, 1997).

[43]K. Olive et al., "Review of Particle Physics", Chin.Phys. **C38**, 090001 (2014).

[44]M. Creutz, *Quarks, gluons and lattices; 2nd ed.* (Cambridge Univ. Press, Cambridge, 1985).

[45]S. Weinberg, "Nonlinear realizations of chiral symmetry", Phys. Rev. **166**, 1568–1577 (1968).

[46]S. Weinberg, "Phenomenological Lagrangians", Physica **A96**, 327 (1979).

[47]J. Gasser and H. Leutwyler, "Chiral Perturbation Theory to One Loop", Annals Phys. **158**, 142 (1984).

[48]J. Gasser and H. Leutwyler, "Chiral Perturbation Theory: Expansions in the Mass of the Strange Quark", Nucl. Phys. **B250**, 465 (1985).

[49]J. Gasser and H. Leutwyler, "Low-Energy Expansion of Meson Form-Factors", Nucl. Phys. **B250**, 517–538 (1985).

[50]R. L. Delgado, C. Hidalgo-Duque, and F. J. Llanes-Estrada, "To What Extent is Gluon Confinement an Empirical Fact?", Few Body Syst. **54**, 1705–1717 (2013).

[51]S. De Curtis, S. Moretti, K. Yagyu, and E. Yildirim, "Perturbative Unitarity Bounds in Composite 2-Higgs Doublet Models", (2016), arXiv:1602.06437 [hep-ph].

[52]P. W. Anderson, "Plasmons, Gauge Invariance, and Mass", Phys.Rev. **130**, 439–442 (1963).

[53]F. Englert and R. Brout, "Broken Symmetry and the Mass of Gauge Vector Mesons", Phys.Rev.Lett. **13**, 321–323 (1964).

[54]P. W. Higgs, "Broken Symmetries and the Masses of Gauge Bosons", Phys.Rev.Lett. **13**, 508–509 (1964).

[55]P. W. Higgs, "Spontaneous Symmetry Breakdown without Massless Bosons", Phys.Rev. **145**, 1156–1163 (1966).

[56]G. Guralnik, C. Hagen, and T. Kibble, "Global Conservation Laws and Massless Particles", Phys.Rev.Lett. **13**, 585–587 (1964).

[57]R. Barate et al., "Search for the standard model Higgs boson at LEP", Phys. Lett. **B565**, 61–75 (2003).

[58]"A Combination of preliminary electroweak measurements and constraints on the standard model", (2002), arXiv:`hep-ex/0212036 [hep-ex]`.

[59]G. Aad et al., "Search for heavy vector-like quarks coupling to light quarks in proton-proton collisions at $\sqrt{s} = 7$ TeV with the ATLAS detector", Phys.Lett. **B712**, 22–39 (2012).

[60]G. Aad et al., "Search for long-lived, multi-charged particles in pp collisions at $\sqrt{s}$=7 TeV using the ATLAS detector", Phys.Lett. **B722**, 305–323 (2013).

[61]S. Chatrchyan et al., "Search for Resonances in the Dijet Mass Spectrum from 7 TeV pp Collisions at CMS", Phys.Lett. **B704**, 123–142 (2011).

[62]A. Liddle, *An Introduction to Modern Cosmology* (Wiley, 2002).

[63]P. Schneider, *Extragalactic Astronomy and Cosmology. An Introduction*, Extraterrestrial Physics, Space Sciences (Springer-Verlag Berlin Heidelberg, 2006).

[64]R. P. Kirshner, *The Extravagant Universe: Exploding Stars, Dark Energy, and the Accelerating Cosmos* (Princeton University Press, Princeton, 2002).

[65]D. O. B.W. Carroll, *An Introduction to Modern Astrophysics* (Pearson-Addison Wesley, 2007).

[66]M. Sher, "Electroweak Higgs Potentials and Vacuum Stability", Phys. Rept. **179**, 273–418 (1989).

[67]C. Ford, D. R. T. Jones, P. W. Stephenson, and M. B. Einhorn, "The Effective potential and the renormalization group", Nucl. Phys. **B395**, 17–34 (1993).

[68]F. Bezrukov, M. Yu. Kalmykov, B. A. Kniehl, and M. Shaposhnikov, "Higgs Boson Mass and New Physics", JHEP **10**, 140 (2012).

[69]J. R. Espinosa and C. Grojean, "Implications of the Higgs boson discovery", Comptes Rendus Physique **16**, 394–406 (2015).

[70]J. Elias-Miro, J. R. Espinosa, G. F. Giudice, G. Isidori, A. Riotto, and A. Strumia, "Higgs mass implications on the stability of the electroweak vacuum", Phys. Lett. **B709**, 222–228 (2012).

[71]G. Isidori, G. Ridolfi, and A. Strumia, "On the metastability of the standard model vacuum", Nucl. Phys. **B609**, 387–409 (2001).

[72]J. A. Casas, J. R. Espinosa, and M. Quiros, "Standard model stability bounds for new physics within LHC reach", Phys. Lett. **B382**, 374–382 (1996).

[73]S. Baum, "On the metastability of the Standard Model", MA thesis (Uppsala U., 2015).

[74]G. Degrassi, "The role of the top quark in the stability of the SM Higgs potential", Nuovo Cim. **C037**, 47–53 (2014).

[75]D. Buttazzo, G. Degrassi, P. P. Giardino, G. F. Giudice, F. Sala, A. Salvio, and A. Strumia, "Investigating the near-criticality of the Higgs boson", JHEP **12**, 089 (2013).

[76]J. Goldstone, "Field Theories with Superconductor Solutions", Nuovo Cim. **19**, 154–164 (1961).

[77]J. Goldstone, A. Salam, and S. Weinberg, "Broken Symmetries", Phys.Rev. **127**, 965–970 (1962).

[78]K. Agashe, R. Contino, and A. Pomarol, "The Minimal composite Higgs model", Nucl. Phys. **B719**, 165–187 (2005).

[79]R. Contino, L. Da Rold, and A. Pomarol, "Light custodians in natural composite Higgs models", Phys. Rev. **D75**, 055014 (2007).

[80]R. Contino, D. Marzocca, D. Pappadopulo, and R. Rattazzi, "On the effect of resonances in composite Higgs phenomenology", JHEP **10**, 081 (2011).

[81]D. Barducci, A. Belyaev, M. S. Brown, S. De Curtis, S. Moretti, and G. M. Pruna, "The 4-Dimensional Composite Higgs Model (4DCHM) and the 125 GeV Higgs-like signals at the LHC", JHEP **09**, 047 (2013).

[82]E. Halyo, "Technidilaton or Higgs?", Mod. Phys. Lett. **A8**, 275–284 (1993).

[83]W. D. Goldberger, B. Grinstein, and W. Skiba, "Distinguishing the Higgs boson from the dilaton at the Large Hadron Collider", Phys. Rev. Lett. **100**, 111802 (2008).

[84]A. Dobado, R. L. Delgado, and F. J. Llanes-Estrada, "Strongly Interacting Electroweak Symmetry Breaking Sector with a Higgs-like light scalar", AIP Conf.Proc. **1606**, 151–158 (2014).

[85]R. L. Delgado, A. Dobado, and F. J. Llanes-Estrada, "Strongly interacting W_LW_L, Z_LZ_L and hh from unitarized one-loop computations", Nucl. Part. Phys. Proc. **273-275**, 2436–2438 (2016).

[86]R. L. Delgado, A. Dobado, M. J. Herrero, and J. J. Sanz-Cillero, "Electroweak chiral Lagrangian with a light Higgs and $\gamma\gamma \to Z_LZ_L, W_L^+W_L^-$ scattering at one loop", Nucl. Part. Phys. Proc. **273-275**, 703–709 (2016).

[87]R. L. Delgado, A. Dobado, and F. J. Llanes–Estrada, "A Strongly Interacting Electroweak Symmetry Breaking Sector with a Higgs-like light scalar", AIP Conf. Proc. **1701**, 090003 (2016).

[88]A. Dobado, R. L. Delgado, and F. J. Llanes-Estrada, "Resonances in W_LW_L, Z_LZ_L and hh scattering from dispersive analysis of the non-linear Electroweak+Higgs Effective Theory", PoS **EPS-HEP2015**, 173 (2015).

[89]F. J. Llanes-Estrada, A. Dobado, and R. L. Delgado, "Describing 2-TeV scale W_LW_L resonances with Unitarized Effective Theory", in 18th Workshop on What Comes Beyond the Standard Models? Bled, Slovenia, July 11-19, 2015 (2015), arXiv:`1509.00441 [hep-ph]`.

[90]A. Dobado, A. Gómez-Nicola, A. L. Maroto, and J. R. Peláez, *Effective lagrangians for the standard model*, Texts and monographs in physics (Springer, Berlin, 1997).

[91]A. Dobado and J. R. Pelaez, "The Inverse amplitude method in chiral perturbation theory", Phys. Rev. **D56**, 3057–3073 (1997).

[92]S. D. Protopopescu, M. Alston-Garnjost, A. Barbaro-Galtieri, S. M. Flatte, J. H. Friedman, T. A. Lasinski, G. R. Lynch, M. S. Rabin, and F. T. Solmitz, "Pi pi Partial Wave Analysis from Reactions pi+ p → pi+ pi- Delta++ and pi+ p → K+ K- Delta++ at 7.1-GeV/c", Phys. Rev. **D7**, 1279 (1973).

[93]G. Grayer et al., "High Statistics Study of the Reaction pi- p → pi- pi+ n: Apparatus, Method of Analysis, and General Features of Results at 17-GeV/c", Nucl. Phys. **B75**, 189–245 (1974).

[94]M. J. Losty, V. Chaloupka, A. Ferrando, L. Montanet, E. Paul, D. Yaffe, A. Zieminski, J. Alitti, B. Gandois, and J. Louie, "A Study of pi- pi- scattering from pi- p interactions at 3.93-GeV/c", Nucl. Phys. **B69**, 185–204 (1974).

[95]P. Estabrooks and A. D. Martin, "pi pi Phase Shift Analysis Below the K anti-K Threshold", Nucl. Phys. **B79**, 301–316 (1974).

[96]V. Srinivasan et al., "Pi- pi+ → pi- pi+ Interactions Below 0.7-GeV from pi- p → pi- pi+ n Data at 5-GeV/c", Phys. Rev. **D12**, 681 (1975).

[97]L. Rosselet et al., "Experimental Study of 30,000 K(e4) Decays", Phys. Rev. **D15**, 574 (1977).

[98]W. Hoogland et al., "Measurement and Analysis of the pi+ pi+ System Produced at Small Momentum Transfer in the Reaction pi+ p → pi+ pi+ n at 12.5-GeV", Nucl. Phys. **B126**, 109 (1977).

[99]R. Mercer et al., "K pi scattering phase shifts determined from the reactions k+ p → k+ pi- delta++ and k+ p → k0 pi0 delta++", Nucl. Phys. **B32**, 381–414 (1971).

[100]H. H. Bingham et al., "A New analysis of K pi scattering as observed in K+ p → K+ pi0 DELTA++ from 3-GeV/c to 13-GeV/c", Nucl. Phys. **B41**, 1–34 (1972).

[101]D. Linglin et al., "K- pi- elastic scattering cross-section measured in 14.3 gev/c k- p interactions", Nucl. Phys. **B57**, 64–76 (1973).

[102]M. J. Matison, A. Barbaro-Galtieri, M. Alston-Garnjost, S. M. Flatte, J. H. Friedman, G. R. Lynch, M. S. Rabin, and F. T. Solmitz, "Study of K+ pi- Scattering in the Reaction K+ p → K+ pi- Delta++ at 12-GeV/c", Phys. Rev. **D9**, 1872 (1974).

[103]S. L. Baker et al., "A Study of K+ pi- Elastic Scattering in the Reaction K+ n → K+ pi- p Between 2.0-GeV/c and 3.0-GeV/c", Nucl. Phys. **B99**, 211 (1975).

[104]P. Estabrooks, R. K. Carnegie, A. D. Martin, W. M. Dunwoodie, T. A. Lasinski, and D. W. G. S. Leith, "Study of K pi Scattering Using the Reactions $K^{\pm}$ p → $K^{\pm}$ pi+ n and $K^{\pm}$ p → $K^{\pm}$ pi- Delta++ at 13-GeV/c", Nucl. Phys. **B133**, 490–524 (1978).

[105]M. Taševský, "Status of the AFP project in the ATLAS experiment", AIP Conf. Proc. **1654**, 090001 (2015).

[106]M. Albrow et al., *CMS-TOTEM Precision Proton Spectrometer*, tech. rep. CERN-LHCC-2014-021. TOTEM-TDR-003. CMS-TDR-13 (CERN, Geneva, Sept. 2014).

[107]V. Berardi et al., *Total cross-section, elastic scattering and diffraction dissociation at the Large Hadron Collider at CERN: Addendum to the TOTEM Technical Design Report*, TOTEM-TDR-001-add-1, Submitted on 18 Jun 2004 (CERN, Geneva, 2004).

[108]S. Chatrchyan et al., "Study of exclusive two-photon production of W^+W^- in *pp* collisions at $\sqrt{s} = 7$ TeV and constraints on anomalous quartic gauge couplings", JHEP **07**, 116 (2013).

[109]G. Aad et al., "Measurements of Higgs boson production and couplings in diboson final states with the ATLAS detector at the LHC", Phys. Lett. **B726**, [Erratum: Phys. Lett. **B734**, 406 (2014)], 88–119 (2013).

[110]S. Chatrchyan et al., "Observation of a new boson with mass near 125 GeV in pp collisions at $\sqrt{s} = 7$ and 8 TeV", JHEP **06**, 081 (2013).

[111]D. B. Kaplan and H. Georgi, "SU(2) x U(1) Breaking by Vacuum Misalignment", Phys. Lett. **B136**, 183 (1984).

[112]S. Dimopoulos and J. Preskill, "Massless Composites With Massive Constituents", Nucl. Phys. **B199**, 206 (1982).

[113]T. Banks, Nucl. Phys. **B243**, 125 (1984).

[114]D. B. Kaplan, H. Georgi, and S. Dimopoulos, "Composite Higgs Scalars", Phys. Lett. **B136**, 187 (1984).

[115]H. Georgi, D. B. Kaplan, and P. Galison, "Calculation of the Composite Higgs Mass", Phys. Lett. **B143**, 152 (1984).

[116]H. Georgi and D. B. Kaplan, "Composite Higgs and Custodial SU(2)", Phys. Lett. **B145**, 216 (1984).

[117]M. J. Dugan, H. Georgi, and D. B. Kaplan, "Anatomy of a Composite Higgs Model", Nucl. Phys. **B254**, 299 (1985).

[118]G. F. Giudice, C. Grojean, A. Pomarol, and R. Rattazzi, "The Strongly-Interacting Light Higgs", JHEP **06**, 045 (2007).

[119]R. Contino, "The Higgs as a Composite Nambu-Goldstone Boson", in Physics of the large and the small, TASI 09, proceedings of the Theoretical Advanced Study Institute in Elementary Particle Physics, Boulder, Colorado, USA, 1-26 June 2009 (2011), pp. 235–306, arXiv:1005.4269 [hep-ph].

[120]J. M. Cornwall, D. N. Levin, and G. Tiktopoulos, "Derivation of Gauge Invariance from High-Energy Unitarity Bounds on the s Matrix", Phys. Rev. **D10**, [Erratum: Phys. Rev. **D11**, 972 (1975)], 1145 (1974).

[121]C. E. Vayonakis, "Born Helicity Amplitudes and Cross-Sections in Nonabelian Gauge Theories", Lett. Nuovo Cim. **17**, 383 (1976).

[122]B. W. Lee, C. Quigg, and H. B. Thacker, "Weak Interactions at Very High-Energies: The Role of the Higgs Boson Mass", Phys. Rev. **D16**, 1519 (1977).

[123]M. S. Chanowitz and M. K. Gaillard, "The TeV Physics of Strongly Interacting W's and Z's", Nucl. Phys. **B261**, 379 (1985).

[124]P. B. Pal, "What is the equivalence theorem really?", (1994), arXiv:hep-ph/9405362 [hep-ph].

[125]D. Espriu and J. Matias, "Renormalization and the equivalence theorem: On-shell scheme", Phys. Rev. **D52**, 6530–6552 (1995).

[126]J. Alwall et al., "The automated computation of tree-level and next-to-leading order differential cross sections, and their matching to parton shower simulations", JHEP **07**, 079 (2014).

[127]The ATLAS collaboration, "Updated coupling measurements of the Higgs boson with the ATLAS detector using up to 25 fb^{-1} of proton-proton collision data", ATLAS-CONF-2014-009 (2014).

[128]V. Khachatryan et al., "Precise determination of the mass of the Higgs boson and tests of compatibility of its couplings with the standard model predictions using proton collisions at 7 and 8 TeV", Eur. Phys. J. **C75**, 212 (2015).

[129]G. Buchalla, O. Cata, A. Celis, and C. Krause, "Fitting Higgs Data with Nonlinear Effective Theory", Eur. Phys. J. **C76**, 233 (2016).

[130]J. Bernon and B. Dumont, "Lilith: a tool for constraining new physics from Higgs measurements", Eur. Phys. J. **C75**, 440 (2015).

[131]P. P. Giardino, "Aspects of LHC phenomenology", PhD thesis (Pisa U., 2013).

[132]G. Aad et al., "Evidence for Electroweak Production of $W^{\pm}W^{\pm}jj$ in pp Collisions at $\sqrt{s} = 8$ TeV with the ATLAS Detector", Phys. Rev. Lett. **113**, 141803 (2014).

[133]V. Khachatryan et al., "Study of vector boson scattering and search for new physics in events with two same-sign leptons and two jets", Phys. Rev. Lett. **114**, 051801 (2015).

[134]M. Baak et al., "Working Group Report: Precision Study of Electroweak Interactions", in Community Summer Study 2013: Snowmass on the Mississippi (CSS2013) Minneapolis, MN, USA, July 29-August 6, 2013 (2013), arXiv:1310.6708 [hep-ph].

[135]M. Fabbrichesi, M. Pinamonti, A. Tonero, and A. Urbano, "Vector boson scattering at the LHC: A study of the WW $\to$ WW channels with the Warsaw cut", Phys. Rev. **D93**, 015004 (2016).

[136]A. Castillo, R. L. Delgado, A. Dobado, and F. J. Llanes-Estrada, "Top-antitop production from $W_L^+W_L^-$ and Z_LZ_L scattering under a strongly-interacting symmetry-breaking sector", (2016), arXiv:1607.01158 [hep-ph].

[137]B. R. Martin, D. Morgan, and G. Shaw, *Pion-pion interactions in particle physics* (Academic Press, London, 1976).

[138]M. E. Rose, *Elementary theory of angular momentum*, Also as a reprint ed.: New York, Dover, 1995 (Wiley, New York, NY, 1957).

[139]J. R. Taylor, *Scattering theory: the quantum theory of nonrelativistic collisions*, Dover Books on Engineering (Dover Publ., Newburyport, MA, 2012).

[140]R. J. Eden, P. V. Landshoff, D. I. Olive, and J. C. Polkinghorne, *The analytic S-matrix* (Cambridge Univ. Press, Cambridge, 1966).

[141]D. Espriu, F. Mescia, and B. Yencho, "Radiative corrections to WL WL scattering in composite Higgs models", Phys.Rev. **D88**, 055002 (2013).

[142]A. Alloul, N. D. Christensen, C. Degrande, C. Duhr, and B. Fuks, "FeynRules 2.0 - A complete toolbox for tree-level phenomenology", Comput. Phys. Commun. **185**, 2250–2300 (2014).

[143]T. Hahn, "Generating Feynman diagrams and amplitudes with FeynArts 3", Comput. Phys. Commun. **140**, 418–431 (2001).

[144]T. Hahn and M. Perez-Victoria, "Automatized one loop calculations in four-dimensions and D-dimensions", Comput. Phys. Commun. **118**, 153–165 (1999).

[145]J. A. M. Vermaseren, "New features of FORM", (2000), arXiv:math-ph/0010025 [math-ph].

[146]J. Elias-Miro, J. R. Espinosa, and A. Pomarol, "One-loop non-renormalization results in EFTs", Phys. Lett. **B747**, 272–280 (2015).

[147]E. T. Whittaker and G. N. Watson, *A course of modern analysis; 4th ed.* Cambridge Mathematical Library (Cambridge University Press, Cambridge, 1996).

[148]G. E. Andrews, R. A. Askey, and R. Roy, *Special functions; 2nd ed.* Encyclopaedia of mathematics and its applications (Cambridge Univ. Press, Cambridge, 2001).

[149]M. Jacob and G. C. Wick, "On the general theory of collisions for particles with spin", Annals Phys. **7**, [Annals Phys.281,774(2000)], 404–428 (1959).

[150]A. Alboteanu, W. Kilian, and J. Reuter, "Resonances and Unitarity in Weak Boson Scattering at the LHC", JHEP **11**, 010 (2008).

[151]R. L. Delgado, A. Dobado, and F. J. Llanes-Estrada, "Coupling WW, ZZ unitarized amplitudes to $\gamma\gamma$ in the TeV region", Eur. Phys. J. **C77**, 205 (2017).

[152]M. Chaichian, C. Montonen, and A. Tureanu, "Tree unitarity and partial wave expansion in noncommutative quantum field theory", Phys. Lett. **B566**, 263–270 (2003).

[153]V. Gribov, *Strong interactions of hadrons at high energies: Gribov lectures on theoretical physics*, Cambridge monographs on particle physics, nuclear physics, and cosmology (Cambridge Univ. Press, Cambridge, 2008).

[154]R. E. Cutkosky, P. V. Landshoff, D. I. Olive, and J. C. Polkinghorne, "A non-analytic S matrix", Nucl. Phys. **B12**, 281–300 (1969).

[155]B. Grinstein, D. O'Connell, and M. B. Wise, "Causality as an emergent macroscopic phenomenon: The Lee-Wick O(N) model", Phys. Rev. **D79**, 105019 (2009).

[156]T. Figy and R. Zwicky, "The other Higgses, at resonance, in the Lee-Wick extension of the Standard Model", JHEP **10**, 145 (2011).

[157]T. G. Rizzo, "Searching for Lee-Wick gauge bosons at the LHC", JHEP **06**, 070 (2007).

[158]D. Espriu and F. Mescia, "Unitarity and causality constraints in composite Higgs models", Phys. Rev. **D90**, 015035 (2014).

[159]S. G. Krantz, *Handbook of complex variables* (Birkhäuser, Basel, 1999).

[160]J. E. Marsden, M. Buchner, M. Hoffman, and C. Risk, *Basic complex analysis* (Freeman, San Francisco, CA, 1973).

[161]R. V. Churchill and J. W. Brown, *Complex variables and applications; 4th ed.* (McGraw-Hill, New York, NY, 1984).

[162]T. N. Truong, "Chiral Perturbation Theory and Final State Theorem", Phys. Rev. Lett. **61**, 2526 (1988).

[163]A. Dobado, M. J. Herrero, and T. N. Truong, "Unitarized Chiral Perturbation Theory for Elastic Pion-Pion Scattering", Phys. Lett. **B235**, 134 (1990).

[164]A. Dobado and J. R. Pelaez, "A Global fit of pi pi and pi K elastic scattering in ChPT with dispersion relations", Phys. Rev. **D47**, 4883–4888 (1993).

[165]J. A. Oller, E. Oset, and J. R. Pelaez, "Nonperturbative approach to effective chiral Lagrangians and meson interactions", Phys. Rev. Lett. **80**, 3452–3455 (1998).

[166]A. Gomez Nicola and J. R. Pelaez, "Meson meson scattering within one loop chiral perturbation theory and its unitarization", Phys. Rev. **D65**, 054009 (2002).

[167]J. F. Donoghue and C. Ramirez, "Symmetry Breaking Schemes and WW Scattering", Phys. Lett. **B234**, 361 (1990).

[168]T. Corbett, O. J. P. Éboli, and M. C. Gonzalez-Garcia, "Inverse amplitude method for the perturbative electroweak symmetry breaking sector: The singlet Higgs portal as a study case", Phys. Rev. **D93**, 015005 (2016).

[169]A. Gomez Nicola, J. R. Pelaez, and G. Rios, "The Inverse Amplitude Method and Adler Zeros", Phys. Rev. **D77**, 056006 (2008).

[170]J. D. Bjorken, "Construction of Coupled Scattering and Production Amplitudes Satisfying Analyticity and Unitarity", Phys. Rev. Lett. **4**, 473–474 (1960).

[171]W. Heitler, "The influence of radiation damping on the scattering of light and mesons by free particles. i", Mathematical Proceedings of the Cambridge Philosophical Society **37**, 291–300 (1941).

[172]J. S. Schwinger, "Quantum electrodynamics. I A covariant formulation", Phys. Rev. **74**, 1439 (1948).

[173]S. N. Gupta, *Quantum electrodynamics* (Gordon and Breach, New York, NY, 1977).

[174]S. N. Gupta, J. M. Johnson, and W. W. Repko, "W, Z and Higgs scattering at SSC energies", Phys. Rev. **D48**, 2083–2096 (1993).

[175]W. Kilian, T. Ohl, J. Reuter, and M. Sekulla, "High-Energy Vector Boson Scattering after the Higgs Discovery", Phys. Rev. **D91**, 096007 (2015).

[176]J. F. Donoghue, C. Ramirez, and G. Valencia, "The Spectrum of QCD and Chiral Lagrangians of the Strong and Weak Interactions", Phys. Rev. **D39**, 1947 (1989).

[177]T. N. Pham and T. N. Truong, "Evaluation of the Derivative Quartic Terms of the Meson Chiral Lagrangian From Forward Dispersion Relation", Phys. Rev. **D31**, 3027 (1985).

[178]G. Ecker, J. Gasser, A. Pich, and E. de Rafael, "The Role of Resonances in Chiral Perturbation Theory", Nucl. Phys. **B321**, 311 (1989).

[179]K. Kawarabayashi and M. Suzuki, "Partially conserved axial vector current and the decays of vector mesons", Phys. Rev. Lett. **16**, 255 (1966).

[180]Riazuddin and Fayyazuddin, "Algebra of current components and decay widths of rho and K* mesons", Phys. Rev. **147**, 1071–1073 (1966).

[181]C. Degrande, C. Duhr, B. Fuks, D. Grellscheid, O. Mattelaer, and T. Reiter, "UFO - The Universal FeynRules Output", Comput. Phys. Commun. **183**, 1201–1214 (2012).

[182]G. Passarino and M. J. G. Veltman, "One Loop Corrections for e+ e- Annihilation Into mu+ mu- in the Weinberg Model", Nucl. Phys. **B160**, 151 (1979).

[183]G. 't Hooft and M. J. G. Veltman, "Scalar One Loop Integrals", Nucl. Phys. **B153**, 365–401 (1979).

[184]M. Böhm, A. Denner, and H. Joos, *Gauge theories of strong and electroweak interactions; 3rd ed.* Trans. of 3rd ed.: Eichtheorien der starken und elektroschwachen Wechselwirkung. Stuttgart, Teubner, 2001 (B. G. Teubner, Stuttgart, 2001).

[185]J. C. Collins, *Renormalization: an introduction to renormalization, the renormalization group, and the operator-product expansion*, Cambridge monographs on mathematical physics (Cambridge Univ. Press, Cambridge, 1984).

[186]G. B. Arfken and H. J. Weber, *Mathematical methods for physicists; 6th ed.* (Academic Press, New York, NY, 2005).

[187]L. Lewin, *Polylogarithms and associated functions* (North-Holland, New York, NY, 1981).

[188]W. Kilian, T. Ohl, and J. Reuter, "WHIZARD: Simulating Multi-Particle Processes at LHC and ILC", Eur. Phys. J. **C71**, 1742 (2011).

[189]M. Moretti, T. Ohl, and J. Reuter, "O'Mega: An Optimizing matrix element generator", 1981–2009 (2001), arXiv:`hep-ph/0102195 [hep-ph]`.

[190]W. B. Kilgore, "Anomalous condensates and the equivalence theorem", Phys. Lett. **B323**, 161–168 (1994).

[191]P. B. Pal, "Equivalence theorem and dynamical symmetry breaking", Phys. Lett. **B321**, 229–233 (1994).

[192]X. Zhang, "A Remark on the Yukawa sector of the standard model", Phys. Rev. **D43**, 3768–3770 (1991).

[193]A. Dobado, J. R. Pelaez, and M. T. Urdiales, "Applicability constraints of the equivalence theorem", Phys. Rev. **D56**, 7133–7142 (1997).

[194]A. Dobado, J. R. Pelaez, and M. T. Urdiales, "The Applicability of the equivalence theorem in chi(PT)", in 27th International Conference on High-energy Physics (ICHEP 94) Glasgow, Scotland, July 20-27, 1994 (1994), arXiv:`hep-ph/9407384 [hep-ph]`.

[195]A. Dobado and J. R. Pelaez, "On The Equivalence theorem in the chiral perturbation theory description of the symmetry breaking sector of the standard model", Nucl. Phys. **B425**, [Erratum: Nucl. Phys. **B434**, 475 (1995)], 110–136 (1994).

[196]A. Dobado and J. R. Pelaez, "The Equivalence theorem for chiral lagrangians", Phys. Lett. **B329**, [Addendum: Phys. Lett. **B335**, 554 (1994)], 469–478 (1994).

[197]J. F. Donoghue and J. Tandean, "The Equivalence theorem and global anomalies", Phys. Lett. **B301**, 372–375 (1993).

[198]H.-J. He, Y.-P. Kuang, and X.-y. Li, "Proof of the equivalence theorem in the chiral Lagrangian formalism", Phys. Lett. **B329**, 278–284 (1994).